Université catholique de Louvain

Faculté des bioingénieurs

Process disturbances in anaerobic digestion: biogas-based detection and chemically induced recovery strategies assessed through metabolic and microbial monitoring

Sébastien LEMAIGRE

Doctoral thesis in
agronomic sciences and biological engineering

Jury:
Prof. Stephan DECLERCK, UCLouvain (president)
Prof. Patrick GERIN, UCLouvain (supervisor)
Dr. Phillippe DELFOSSE, University of Luxembourg (supervisor)
Prof. Benoît STENUIT, UCLouvain
Dr. Magdalena CALUSINSKA, LIST
Prof. Thomas UDELHOVEN, Trier University

Executive summary

Anaerobic digestion (AD) is a multi-stage microbial process that breaks down organic matter into gases (including methane, an energy carrier) and a residual fraction used as fertiliser, all in the absence of oxygen. Agricultural biogas production through the AD of organic materials such as animal manures, crop residues, and agri-food wastes holds promise for mitigating climate change and recycling essential nutrients back into the food production system. However, the AD process is prone to disturbances that can lead to significant economic losses for biogas plant operators. The two primary disturbances affecting anaerobic microbial populations are (1) free volatile fatty acid (FVFA) intoxication due to organic overload, and (2) free ammonia nitrogen (FAN) intoxication due to nitrogen overload. These disturbances often alter methane production in agricultural anaerobic digesters due to the lack of robust and cost-effective online process monitoring techniques. Additionally, current bioaugmentation methods for restoring functional processes in severely intoxicated AD reactors are not easily scalable from the laboratory to full-scale biogas plants.

This thesis explores methods to (I) detect FVFA and FAN intoxications cost-effectively and (II) restore a functional AD process in biogas production reactors that ceased producing methane due to the most critical form of these two process disturbances. To achieve these objectives, four continuously stirred tank bioreactors (100 litres each) and automated gas monitoring tools were constructed. Across two successive experiments, three test reactors were progressively subjected to either organic or nitrogen overload, leading to the development of FVFA and FAN intoxication, respectively. The fourth reactor was maintained in a steady state as a reference. Once methane production ceased in the test reactors, chemical strategies were developed and tested to restore AD process functionality. Additionally, various multivariate statistical process control (MSPC) models were developed, using a post-experimental modelling approach, and compared for their efficiency in detecting disturbances during the overload phases of each experiment. Both metabolic (in biogas and slurry) and microbial monitoring were employed to assess the MSPC models and process recovery strategies throughout the experiments.

Our findings demonstrate that MSPC models based on the main biogas components can deliver warning signals announcing early signs of the two main process disturbances in pilot-scale reactors. Through out-of-control values of statistical indices, static PCA-MSPC models based primarily on biogas composition

allowed to detect FVFA intoxication, while recursively updated PCA-MSPC models, relying on biogas composition only, allowed to detect early symptoms of FAN intoxication. Notably, when approaching FAN intoxication, out-of-control values of the Hotelling's T_A^2 statistics were concomitant with significant shifts in the bacterial and archaeal communities, suggesting that biogas composition dynamics reflects microbial response to stress in AD reactors. Both static and recursively updated models based on biogas composition could potentially enable online monitoring of full-scale AD reactors using a relatively low-cost biogas analyser as the sole analytical tool. However, monitoring the biogas composition of a steady reference reactor remains essential for generation of in-control process data, which could be accomplished at full-scale with a post-digester, the latter being generally less exposed to disturbances. In contrast, microbial ecological indices monitored during the FVFA intoxication experiment failed to detect the process disturbance.

We also demonstrated that a chemical-based strategy involving pH neutralisation with NaOH and $NaHCO_3$ supplementation to rebuild the buffer capacity, can restore the AD process functionality after critical FVFA intoxication without microbial re-inoculation. Recovery in our reactors was significantly faster than what has been previously observed using bioaugmentation with microbial cultures exposed to propionate. Using potassium-based chemicals instead of sodium may help minimise potential harm to agricultural soils. These results are promising, especially considering they were achieved under particularly severe intoxication conditions.

Similarly, we successfully restored AD process functionality after critical FAN intoxication using a multi-step strategy, including acetic acid supplementation to lower the pH and to shift free ammonia into ammonium (less toxic for microorganisms), dilution with water, and re-inoculation with effluents from a low-nitrogen input reactor. After this initial reconditioning stage, restored feeding combined with ongoing re-inoculation, reestablished methane production in the intoxicated reactors. Re-inoculation proved essential for maintaining process stability during recovery. Ten weeks after initiating this strategy, a functional AD process was restored, producing methane from the feedstock, even after re-inoculation was discontinued. Given residual symptoms of instability, prolonged re-inoculation with an active microbiome is recommended for sustained recovery of critically FAN-

intoxicated reactors. Interestingly, effluents from a reactor not acclimatised to ammonia were effective for this purpose. This is a more practical solution than alternatives proposed in the literature, based on maintaining an additional digester to produce large volumes of ammonia-acclimatised inoculum for bioaugmentation.

Our results suggest that the presence of *Methanosarcina* archaea provided resilience and played a crucial role in avoiding the need for acclimatised inoculum to restore AD process functionality after both types of disturbance. We attribute the pivotal role of *Methanosarcina* spp. in the recovery to their fast growth, robustness, and versatility, which enable methane production via all known methanogenesis pathways under a wide range of environmental conditions, including extreme ones.

While our multivariate monitoring approach based on biogas composition requires further laboratory evaluation in real-time monitoring conditions, it could pave the way for low-cost and online process monitoring in biogas plants equipped with biogas analysers. Moreover, our findings provide evidence that specific chemical supplementations can contribute to restore AD functionality in reactors exposed to process disturbances, even in their most critical forms, by reestablishing favourable conditions for microbial growth. The process monitoring and recovery methods developed here could enable biogas plant operators to maximise digester capacity with reduced concern for potential disturbances.

Acknowledgements

Defending this doctoral thesis marks the culmination of a journey that began a decade ago. This path, sometimes chaotic, punctuated by doubts but also by achievements and moments of pride, has been a significant chapter in my life, both professionally and personally.

Of course, this work has not been a solitary journey. It has allowed me to appreciate the value of a multidisciplinary approach to research and, in doing so, to learn to temper my own character in order to adapt to the diversity of those around me. Over the past ten years, I have had the privilege of meeting many inspiring people, and I would like to take this opportunity to express my sincere gratitude to those who come to mind.

First and foremost, I would like to thank Dr Philippe Delfosse for his trust and support, not only for guiding me through this thesis but also for giving me a chance to join his emerging research team right after university. Philippe, your supervision, insightful advice, and unwavering support throughout this thesis have been invaluable. I am also deeply grateful to Professor Patrick Gerin for co-supervising this thesis at UCLouvain. Patrick, your scientific rigour, availability, and constructive criticism have been a constant source of inspiration.

I also extend my sincere thanks to the members of my jury, Prof. Benoît Stenuit, Prof. Stephan Declerck, Prof. Thomas Udelhoven and Dr Magdalena Calusinska for agreeing to evaluate this work, for the time and attention they devoted to its review, and for the constructive exchanges during the defence.

My gratitude also goes to the members of my advisory committee, Prof. Michel Focant and Dr Gilles Adam, for their availability, valuable insights, and continuous support throughout my research. I would particularly like to thank Gilles Adam for his guidance in statistical data processing, his contagious enthusiasm, and his natural kindness.

I am also grateful to my colleagues at LIST, past and present, and especially to Bénédicte De Vos and Élodie Boland for their technical support. Thank you for your invaluable assistance and for putting up with my occasionally moody temperament.

A special thanks goes to the biogas plant operators in the Greater Luxembourg Region, particularly Jean Kessler, Mélody Kessler, and Ludovic Peters from Ferme du Faascht. Your dedication, despite the many administrative constraints

imposed on you, is truly admirable. Your practical expertise and common sense have, I hope, helped to ground this thesis in the realities of your sector.

Finally, my deepest gratitude goes to my parents and my brother Régis, who have always believed in me and supported me unwaveringly throughout this journey. I am also immensely grateful to my friends Julien, Aurélie, and Marti for their encouragement and for doing their best (often successfully) to distract me during the more difficult moments. And last but not least, a heartfelt thank you to my cat, Arya, whose mere presence provided comfort and companionship throughout the long hours of writing.

Foreword

This thesis was initiated in 2013, in anticipation of the merger between two former institutions that created the Luxembourg Institute of Sciences and Technology (LIST). The work was conducted under an internal funding program aimed at engineers aspiring to earn a Ph.D. degree. The institute imposed a tight timeline, requiring the thesis to be completed in three years while working part-time. Thus, we decided to utilise datasets that I generated during previous projects (Interreg IVA 2007 project OPTIBIOGAZ 001/GR/2/3/003) and advanced projects (FNR CORE 2011 project GASPOP CO11/SR/1280949) to support the thesis. Consequently, the process monitoring part of this work (**Chapter 3** and **Chapter 4**) focused on post-experimental modelling rather than real-time AD process monitoring.

Although this work addressed practical issues faced by agricultural biogas plants, full-scale experimentation was beyond its scope, so the experiments were conducted in a laboratory setting. However, to closely mimic the conditions encountered in full-scale digesters, we used pilot-scale reactors with a substantial working volume and supplied them with feedstocks in the same form as those used on-farm.

To conduct the research for my thesis, I designed and built several bioreactors and monitoring instruments with my teammates. These tools were used to track the progress of biogas production and its composition over time, and to automate the measurement of the biochemical methane potential of organic matrices. Some of this engineering work contributed to publications and patents that are not included in this thesis. A condensed and graphical description of these tools is provided in **Chapter 10** (Annex 1).

Note: Except for papers written in American English, this work has been prepared in British English

Scientific publications and communications

- **Scientific publications in peer-reviewed journals**[1]

Goux, X., Calusinska, M., Lemaigre, S., Marynowska, M., Klocke, M., Udelhoven, T., Benizri, E., & Delfosse, P. (2015). Microbial community dynamics in replicate anaerobic digesters exposed sequentially to increasing organic loading rate, acidosis, and process recovery. *Biotechnology for Biofuels*, *8*(1), 122. doi:10.1186/s13068-015-0309-9

Lemaigre, S., Adam, G., Goux, X., Noo, A., De Vos, B., Gerin, P. A., & Delfosse, P. (2016). Transfer of a static PCA-MSPC model from a steady-state anaerobic reactor to an independent anaerobic reactor exposed to organic overload. *Chemometrics and Intelligent Laboratory Systems*, *159*, 20–30. doi:10.1016/j.chemolab.2016.09.010

Lemaigre, S., Adam, G., Gerin, P. A., Noo, A., De Vos, B., Klimek, D., Goux, X., Calusinska, M., & Delfosse, P. (2018). Potential of multivariate statistical process monitoring based on the biogas composition to detect free ammonia intoxication in anaerobic reactors. *Biochemical Engineering Journal*, *140*, 17–28. doi:10.1016/j.bej.2018.08.018

Lemaigre, S., Gerin, P. A., Adam, G., Klimek, D., Goux, X., Herold, M., Frkova, Z., Calusinska, M., & Delfosse, P. (2023). Potential of acetic acid to restore methane production in anaerobic reactors critically intoxicated by ammonia as evidenced by metabolic and microbial monitoring. *Biotechnology for Biofuels and Bioproducts*, *16*(1), 1–20. doi:10.1186/s13068-023-02438-5

- **Oral presentations in international conferences**[1]

Lemaigre, S., Adam, G., Goux, X., & Delfosse, P. (2015). Multivariate process control charts based on reputed process indicators as an alternative to univariate control charts for the monitoring of anaerobic reactors submitted to acidosis. *11th international conference on renewable resources & biorefineries*, York (United Kingdom).

[1] Limited to the outcomes directly resulting from the thesis work.

Lemaigre, S., Adam, G., Gerin, P. A., Noo, A., De Vos, B., Klimek, D., Goux, X., Calusinska, M., & Delfosse, P. (2019). Potential of multivariate statistical process monitoring based on the biogas composition to detect free ammonia intoxication in anaerobic reactors. *3rd international biotechnology congress,* Singapore (Singapore).

- **Poster presentations in international conferences**

Lemaigre, S., Adam, G., Goux, X., & Delfosse, P. (2014). A multivariate statistic approach to detect process imbalance in lab scale continuously stirred tank anaerobic reactors submitted to inadequate organic loading rate. *17th World Congress on Anaerobic Digestion*, Valladolid (Spain).

Lemaigre, S., Adam, G., Goux, X., & Delfosse, P. (2015). Multivariate process control charts based on reputed process indicators as an alternative to univariate control charts for the monitoring of anaerobic reactors submitted to acidosis. *2nd international conference on monitoring & process control of anaerobic digestion*, Leipzig, Germany.

Lemaigre, S., Adam, G., Goux, X., Noo, A., De Vos, B., Gerin, P. A., & Delfosse, P. (2016). Multivariate control charts based on the biogas composition for the monitoring of anaerobic reactors submitted to VFA intoxication and ammonia intoxication. *3rd international conference on renewable energy gas technology*, Malmö, Sweden.

Table of contents

Acronyms

A: number of principal components retained in a PCA-MSPC model

ABR: anaerobic biofilm reactor

AD: anaerobic digestion

ATP: adenosine triphosphate

BMP: biochemical methane potential

CCA: canonical correspondence analysis

CHP: combined heat and power

CL: control limit of a control chart

COD: chemical oxygen demand

CSTR: continuously stirred tank reactor

DIET: direct interspecies electron transfer

DNA: deoxyribonucleic acid

$\Delta G^{\circ\prime}$: standard free enthalpy change (or Gibbs free energy) under biochemical standard conditions (pressure = 1 atm, temperature = 25°C, pH = 7)

EU: European Union

e-nose: electronic nose

FAN: free ammonia nitrogen

FM: fresh matter

FVFA: free volatile fatty acids

GC: gas chromatography

H': Shannon–Weaver index

HDS: historical data set

HNR: high nitrogen input reactor

HRT: hydraulic retention time

HTS: high-throughput amplicon sequencing

IET: interspecies electron transfer

IFT: interspecies formate transfer

IHT: interspecies hydrogen transfer

IPV: individual process variable

J: Pielou (evenness) index

LCL: lower control limit of a control chart

LMM: linear mixed-effect model

L_N: litre of gas normalised to normal conditions of temperature and pressure (0°C; 1013 hPa)

LNR: low nitrogen input reactor

MOS: metal oxide semiconductor

nano SIMS: nanometer-scale secondary ion mass spectrometry

NIR: near infrared spectroscopy

NMDS: non-metric multidimensional scaling

OLR: organic loading rate

OR: overfed reactor

OTU: operational taxonomic unit

PCA: principal component analysis

PC: principal component

PCA-MSPC: multivariate statistical process control based on PCA

MSPC: multivariate statistical process control

rRNA: ribosomal ribonucleic acid

RU-PCA-MSPC: recursively updated PCA-MSPC

SCADA: supervisory control and data acquisition

SAO: syntrophic acetate oxidation (or oxidiser)

SAOB: syntrophic acetate-oxidising bacteria

SPC: statistical process control

SPE: squared prediction error index that complements the T_A^2 index in PCA-MSPC

SPE_{lim}: control limit of a SPE control chart

SPO: syntrophic propionate oxidation (or oxidiser)

SSR: steady-state reactor

T^2: Hotelling's T^2 (statistical) index

T_A^2: Hotelling's T^2 index computed with the scores obtained for the *A* dominant principal components retained in a PCA-MSPC model

TAN: total ammonia nitrogen

TIC: total inorganic carbon

T-RF: terminal restriction fragment

T-RFLP: terminal restriction fragment length polymorphism

TS: total solids

TVFA: total volatile fatty acids

UCL: upper control limit of a control chart, especially used in T^2 (or T_A^2) control charts

VFA: volatile fatty acid(s)

VS: volatile solids

WWTP: wastewater treatment plant

Definitions

(Heterotrophic) Acetogenesis: The third step of the anaerobic digestion (AD) process, where acetogenic bacteria convert volatile fatty acids longer than acetate into direct precursors of methane, including acetate, dihydrogen, and carbon dioxide.

Acidogenesis: The second step of the AD process, wherein fermentative bacteria ferment simple soluble compounds from the hydrolysis step into volatile fatty acids, other organic acids, alcohols, methylamines, dihydrogen, and carbon dioxide.

Anaerobic digestion (AD): A bioprocess where microbial communities decompose and convert complex organic molecules into biogas in the absence of oxygen.

Bioaugmentation: In the thesis context, the addition of specialised microorganisms to a bioprocess to prevent or correct a process disturbance.

Biogas: A gaseous mixture produced by the AD process, exploitable as a renewable fuel due to its high content in methane (CH_4) and its high calorific value. Biogas contains also carbon dioxide and trace concentrations of hydrogen sulphide, hydrogen and ammonia. If air is injected in the anaerobic digester as a desulfurisation measure, biogas contains also traces of oxygen and dinitrogen.

Biogas upgrading: The operation of concentrating methane in biogas to meet natural gas standards.

Biomethane: Purified methane obtained from biogas upgrading.

Common-cause variation: In statistical process control (SPC), the total process variation attributable to many small, unavoidable sources of variability inherent to the process itself.

Contribution plot: In static PCA-MSPC, a visual tool indicating the individual process variables that mostly contributed to out-of-control values of the T_A^2 or SPE indices.

Control chart: In SPC, a visual tool where a statistical index characterising the process is plotted over time for each sample and compared to control limits that delimit the in-control process region.

Control limit: In SPC, a horizontal line representing one of the limits of the in-control process region on a control chart, calculated based on a given statistical distribution for a certain confidence level.

Digester: An industrial-scale bioreactor where an AD process is operated.

Digestate: Solid, semi-solid, or liquid material that remains at the end of the AD process and possesses high fertilising value.

Electronic nose (e-nose): An array of non-specific gas sensors used for bioprocess monitoring.

Feedstock: Any material containing an organic fraction that can be converted to biogas through the AD process.

Free ammonia nitrogen (FAN): The portion of nitrogen present as un-ionised ammonia (NH_3) within the slurry of an AD reactor. Unlike its ionised form, ammonium (NH_4^+), free ammonia readily diffuses across cell membranes, making it the primary toxic form.

FAN intoxication: One of the two main AD process disturbances, where toxic free ammonia inhibits methanogens, causing intracellular disruptions that alter or completely halt their CH_4 production. In this thesis, *critical* FAN intoxication refers to the advanced stage characterised by the cessation of feedstock conversion to CH_4.

Free volatile fatty acids (FVFA): The un-ionised, protonated form of short-chain fatty acids. This "free" form is the primary agent of VFA toxicity in AD reactors, because it can passively diffuse across microbial cell membranes.

FVFA intoxication: One of the two main AD process disturbances, where toxic free VFAs inhibit methanogens, causing detrimental intracellular acidification, and altering their CH_4 production. In this thesis, critical FVFA intoxication refers to the advanced stage characterised by the cessation of feedstock conversion to CH_4.

Historical data set (HDS): In SPC, a data set collected during an initial period when the process is suspected to express only common-cause variation (Phase I). The HDS is used to estimate model parameters and define control limits for control charts used with new samples for actual process control (Phase II).

Homo-acetogenesis: The biochemical reaction where homo-acetogenic bacteria convert carbon dioxide to acetate, using H_2 as an electron donor (also referred to as "autotrophic acetogenesis" in literature).

In-control process: In SPC, a process exhibiting only common-cause variability.

Individual process variable (IPV): In SPC, a process characteristic expressed by a numerical measurement.

Interspecies hydrogen transfer: The direct transfer of dihydrogen from acetogenic bacteria to hydrogenotrophic methanogens in AD reactors, necessary to maintain acetogenesis.

Hydrolysis: The first step of the AD process, where fermentative bacteria and other microorganisms break down extracellularly large biopolymers to soluble oligo- and mono-mers.

Mahalanobis distance: See (Hotelling's) T^2 index.

Methanogens: The only microorganisms capable of producing CH_4. They are strictly anaerobic microbes belonging to the domain *Archaea*.

Methanogenesis: The fourth and final step of the AD process, where methane is produced from its direct precursors.

Mesophilic temperature range: One of the three temperature ranges in which microorganisms preferentially grow, characterised by values of 30-40°C.

Microbial community: The collection of microorganisms (or microbiota), interacting in an environment and their relationships (Berg et al., 2020).

Microbiome: A characteristic microbial community occupying a reasonable well-defined habitat which has distinct physio-chemical properties (Berg et al., 2020). The microbiome not only refers to the microorganisms involved but also encompass their theatre of activity, which results in the formation of specific ecological niches.

Multivariate statistical process control (MSPC): A mode of SPC that examines measured IPVs as a group, considering their correlation.

Multicollinearity: A statistical issue that occurs when two or more independent variables are highly correlated with one another, meaning one can be linearly predicted from the others (Alin, 2010).

PCA-MSPC: A mode of MSPC that separates the main signal space from stochastic variation ("noise") by performing PCA on the raw dataset.

Offline (Bio)process monitoring: A mode of process monitoring where samples are manually taken from the process stream and analysed later in a remote laboratory.

Online (Bio)process monitoring: A mode of process monitoring where samples are automatically taken from the process stream and carried to an analyser located in close proximity for almost immediate analysis.

Organic overload: The most common cause of free VFA intoxication in AD reactors, where the feeding rate of biodegradable material exceeds the microbial community's total degradation capacity.

Out-of-control process: In SPC, process exhibiting special-cause variability (i.e. becoming unstable and unpredictable).

Phase I: In SPC, the initial period when the historical data set is collected to define model parameters and control limits for control charts.

Phase II: In SPC, the period following Phase I, during which statistical indices calculated for new samples are plotted in their control charts for actual process control.

Post-digester: The downstream, secondary digester of a two-stage AD plant.

Principal component analysis (PCA): A linear dimensionality reduction technique used to extract important information from a multivariate dataset and express it as a set of few new variables, called principal components (PCs).

Process monitoring: The use of sensors and/or analytical methods to diagnose the status of a process over time and evaluate its risk of disturbance.

Process disturbance: In the thesis context, refers to any causal event (e.g. protonated VFA or FAN intoxication) that disrupts microbial activity within an AD reactor and impairs the stability or efficiency of biogas production. C*ritical* process disturbance

refers to the advanced stage characterised by the cessation of feedstock conversion to CH_4.

Process stability indicator: In the thesis context, a process parameter monitored to assess the adequacy of MSPC models by comparing the alarm signals provided by the models with the microbiome's ability to convert the introduced feedstock into CH_4. Note: These indicators are not used as IPVs to build MSPC models.

Recursively updated PCA-MSPC (RU-PCA-MSPC): A mode of PCA-MSPC involving the recursive update of model parameters after Phase I to reduce false alarm rates due to time-varying process conditions during Phase II.

Shewhart control chart: In univariate SPC, a basic control chart displaying values of individual observations (x-charts) or averages of subgroups of observations ($\bar{x}$-charts). A Shewhart control chart includes two control limits calculated assuming the monitored IPV follows a normal distribution when the process is statistically in-control.

Special-cause variability: In SPC, the part of total process variability attributable to occasional sources that force an otherwise in-control process to become unstable and unpredictable.

Squared prediction error (SPE): In PCA-MSPC, a statistical index complementing the T_A^2 index that quantifies model residuals (or "noise"). Values exceeding control limits on an SPE control chart indicate observations breaking the PCA model's correlation structure.

Static PCA-MSPC: The basic way to implement PCA-MSPC, where model parameters remain unchanged after Phase I.

Statistical process control (SPC): A set of methods for monitoring and ideally improving process performance through statistical analysis.

Substrate: Any specific molecule (e.g. propionate, acetate, CO_2, H_2) that can be directly consumed and transformed by individual microbial groups as part of their metabolic processes for energy and growth. In the broader AD literature, this term is often used incorrectly to refer to feedstocks.

Syntrophic acetate oxidation (SAO): A biochemical reaction where specialised bacteria oxidise the carbon of acetate to produce carbon dioxide in the slurry of an AD reactor while releasing the electrons as dihydrogen. This reaction only occurs if these products are subsequently utilised by hydrogenotrophic methanogens.

Syntrophic propionate oxidation (SPO): Crucial form of heterotrophic acetogenesis where propionate, which is particularly difficult to eliminate, is broken down into acetate, CO_2, and H_2/formate by specialised bacteria, a reaction only made possible by the simultaneous consumption of H_2/formate by other microbes, especially hydrogenotrophic methanogens.

(Hotelling's) T^2 statistics: The basic statistical index used in MSPC to monitor divergences of a multivariate process from an in-control situation. In PCA-MSPC, the T^2 index is called T_A^2 because it is computed using the scores obtained for a limited number (A) of principal components retained in the model.

Total ammonia nitrogen (TAN) Content: The nitrogen content present as ammonium (NH_4^+) or free ammonia in the slurry (NH_3) of an anaerobic digestion reactor.

Thermophilic temperature range: One of the three temperature ranges in which microorganisms preferentially grow, characterised by values of 50-60°C.

Univariate statistical process control: An SPC mode that monitors measured individual process variables on independent control charts, without considering their potential correlation.

Wet fermentation: An implementation mode for the AD process characterised by a low total solid content in the reactor slurry (< 0.1 g. g_slurry^{-1}).

Chapter 1

General introduction

1.1. Agricultural biogas production via the anaerobic digestion process

Anaerobic digestion[2] (AD) is a bioprocess wherein microbial communities cultured in bioreactors decompose complex organic molecules in the absence of oxygen (O_2). Through the AD process, the carbon content of organic *feedstocks* is converted to the most reduced and oxidized forms of monoatomic carbon: methane (CH_4) and carbon dioxide (CO_2), respectively. These two products are the main components of *biogas*, which can be exploited as a renewable fuel due to the high calorific value of its CH_4 content. Furthermore, effluents from the AD process are by-products that have a significant fertiliser value. Indeed, the three primary nutrients plants need to grow, namely nitrogen (N), phosphorus (P), and potassium (K), accumulate in AD residues, vernacularly referred to as *digestate*.

In the European Union (EU), biogas production via the AD process can help accelerate the transition towards net-zero global greenhouse gas emissions by 2050 (IPCC, 2022). Moreover, biogas production increases European energy security by reducing dependence on imported fossil fuels and can alleviate the burden of energy costs on households and industries (Xue et al., 2022).

In the EU, most AD plants belong to the agricultural category (EBA, 2022), meaning they co-digest manure with other organic feedstocks, many of which are also of agricultural origin. Farms are ideal environments to implement the AD process, especially those involving cattle breeding in their agricultural systems. Firstly, using fresh ruminant manure as a feedstock ensures the permanent reseeding of relevant microorganisms in the AD process. The digestive tract of ruminants naturally hosts a fully functional anaerobic microbial consortium (Cholewińska et al., 2021). Secondly, conventional agricultural equipment allows for the harvest and storage of vegetal feedstocks and manure to feed the reactors and apply their effluents on the fields. Finally, fertilising farmlands with AD effluents helps mitigate the loss of N, P, and K from the food production chain. This nutrient cycle completion could reduce the industrial synthesis of nitrogen-based fertilisers, which consumes massive amounts of fossil fuels and contributes to global warming (Razon, 2014). It could also slow down

[2] In this introduction, italicised terms are defined in the list of definitions provided at the beginning of the manuscript, with the exception of microbial taxa.

the mining of phosphates and potash, two dwindling fossil resources (Al Rawashdeh, 2020; Reijnders, 2014).

1.2. Common practices for the agricultural implementation of the AD process in Europe

In the EU, *wet fermentation* is by far the most adopted model in agricultural AD plants. Wet fermentation is characterised by a low total solids (TS) content in the reactor slurry (< 0.1g.g_slurry^{-1}), allowing the continuous digestion of a wide variety of liquid, pasty, and solid feedstocks (Weiland, 2006).

Typical agricultural AD plants based on wet fermentation are schematised in **Figure 1.1**. In such plants, the bioreactors are often called *digesters*, their liquid content is the *slurry*, and the effluents they produce are commonly referred to as the *digestate*. The vertical continuously stirred tank reactor (CSTR) is the most widespread design for digesters (Weiland, 2010). Nowadays, most newly built AD plants are designed with two digesters placed in series, resulting in a higher biogas yield compared to AD plants operating with only one stage (Weiland, 2006). In these two-stage AD plants, the secondary digester is often called a *post-digester*. Digesters and post-digesters should be operated at a temperature range that allows optimal microbial activity. In practice, this temperature range is either *mesophilic* (30–40 °C) or *thermophilic* (50–60 °C). In Europe, to reach and maintain these temperature conditions, the digesters are heated, insulated, and thermally regulated. The produced biogas is usually collected in the digester headspace, which is covered with an inflatable plastic membrane.

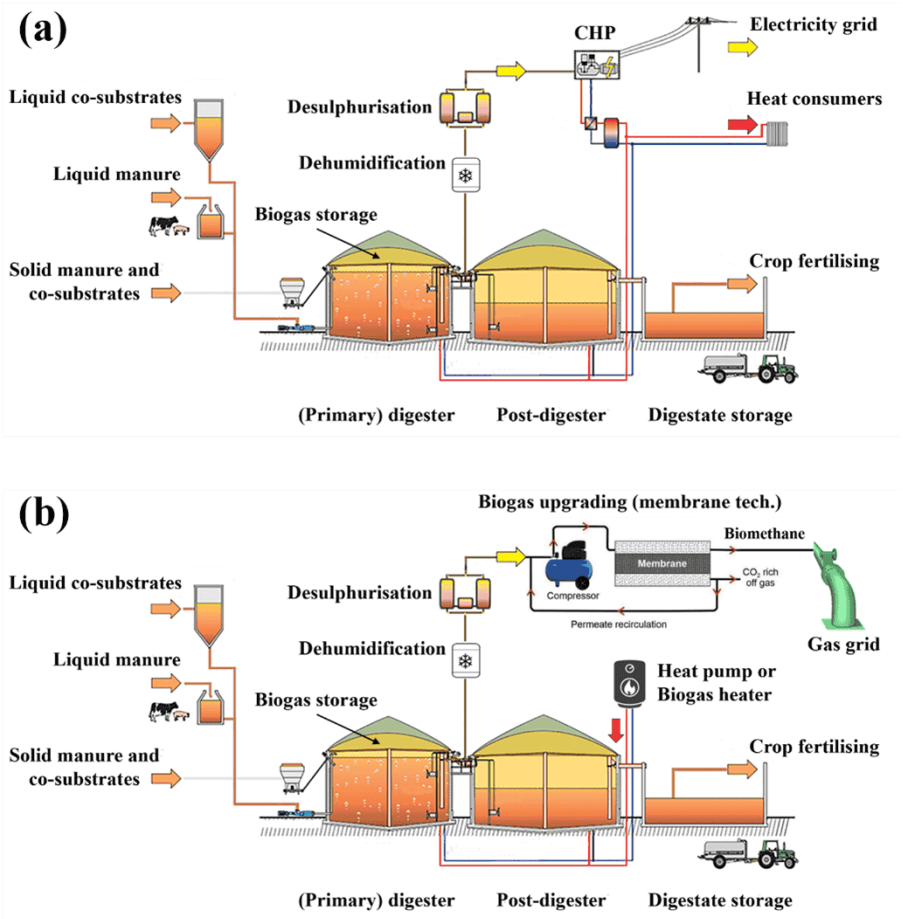

Figure 1.1. Typical agricultural AD plants using wet fermentation that generate revenue from (a) electricity and heat production; (b) biomethane production. Adapted from http://www.silicasolar.com/bio-digester-technology-and-substrates/. CHP: combined heat and power unit.

In the EU, the most common way to valorise biogas is through the local production of electricity and heat via CH_4 combustion in combined heat and power (CHP) units (EBA, 2022). The produced electricity is fed into the public grid (ensuring financial income), while the thermal energy is used to heat the digesters and for other local use (**Figure 1.1**a). Alternatively, biogas can be valorised by concentrating its CH_4 content to produce *biomethane* via a process called *biogas upgrading*. AD plants that upgrade biogas generate revenue from injecting biomethane into the natural gas grid (**Figure 1.1**b). Currently, more and more European countries are shifting incentives from biogas production to biomethane

production, leading to the rapid growth of the biomethane industry (EBA, 2022). Unlike biogas, biomethane can be used for a variety of applications, as it can replace all the end-uses of natural gas.

1.3. AD process disturbances hamper the development of the agricultural biogas production sector

While agricultural production of biogas and biomethane has strong potential, AD is a fragile bioprocess that can suffer from instability. Given the complex interactions within microbial communities and the high diversity of potential AD feedstocks, biogas production digesters are highly susceptible to *process disturbances*[3].

To guarantee stable biogas production, agricultural biogas production digesters are usually operated at an organic loading rate (OLR) significantly lower than their design specification. This precautionary strategy results in considerable oversizing and underutilisation of the digesters, leading to low specific biogas yields and unfavourable cost-to-income ratios (Kleyböcker et al., 2014; Spanjers & van Lier, 2006).

[3] In this work, the term *(process) disturbance* refers to any causal event that disrupts microbial activity within an AD reactor and impairs the stability or efficiency of its biogas production. The term *critical (process) disturbance* refers to the advanced stage characterised by the cessation of feedstock conversion to methane. In microbial ecology, a disturbance is defined as a discrete, often unpredictable event that can cause direct removal of living biomass (Plante, 2017) within a microbiome. It refers to a causal event that can trigger a microbial response, such as shifts in community structure, provided the disturbance is of sufficient magnitude (Glasby & Underwood, 1996).

1.4. Free volatile fatty acids and free ammonia nitrogen intoxications

The two main process disturbances in biogas production digesters are *free volatile fatty acids (FVFA) intoxication* caused by organic overload, and *free ammonia nitrogen (FAN) intoxication* resulting from nitrogen overload (L. Li et al., 2018). These two disturbances are therefore the primary focus of this work. Here, a general introduction to the main biochemical mechanisms underlying the AD process is provided, then the mechanisms behind FVFA and FAN intoxications are presented.

1.4.1. AD fundamentals

The AD process occurs in aqueous solution with an optimal pH range close to neutrality ($6.8 < pH < 7.2$; Cioabla et al., 2012). The degradation of organic matter is commonly summarised in four main steps (**Figure 1.2**): (1) *hydrolysis*, (2) *acidogenesis*, (3) *acetogenesis*, and (4) *methanogenesis*. These steps are performed by a complex *microbial community*, a consortium of different microbes (**Table 1.1** and **Table 1.2**) that interact through syntrophic relationships. These microorganisms act as biocatalysts (**Table 1.3**), and their metabolic activity is intimately linked to the physicochemical conditions of their environment. Together, the community and its surrounding environment form the AD *microbiome*, where factors like pH, temperature, and the presence of inhibitory compounds are critical.

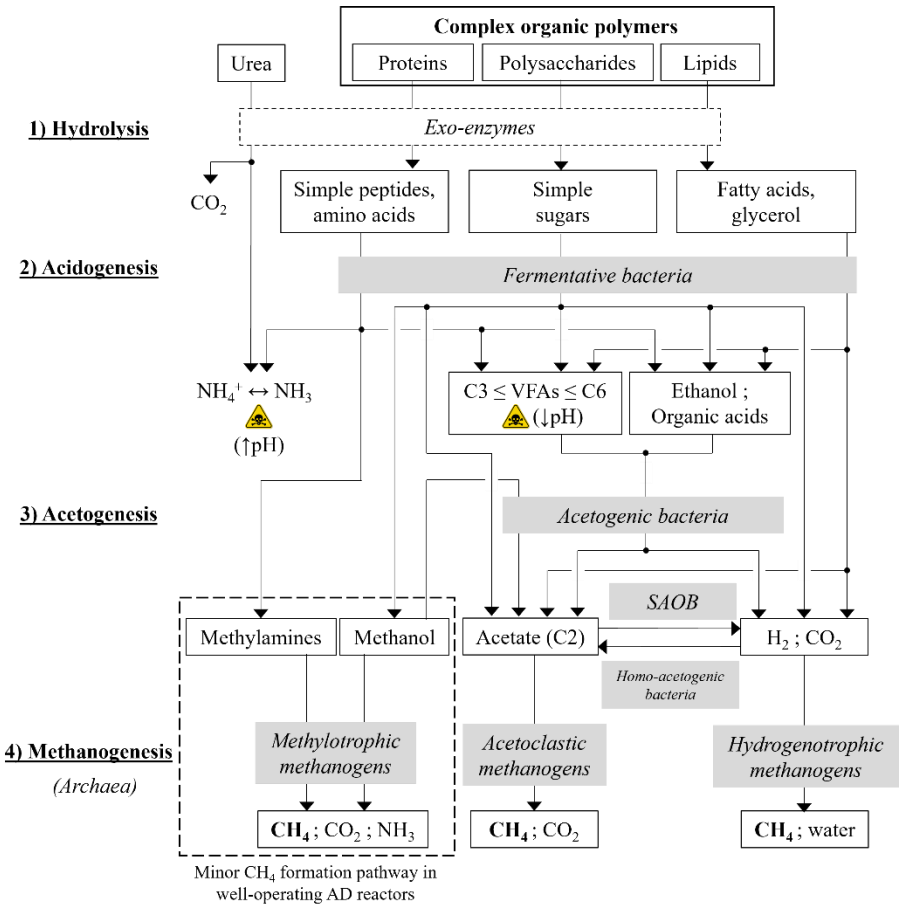

Figure 1.2. The four steps of the AD process. Adapted from Görish & Helm (2008). AD: anaerobic digestion, IET: interspecies electron transfer, VFA: volatile fatty acid, SAOB: syntrophic acetate-oxidising bacteria.

Table 1.1. Typical bacterial phyla involved in the anaerobic digestion process and potential function of their members.

Phylum (Current Name)	Previous Nomenclature	Hydrolysis	Acidogenesis	Heterotrophic acetogenesis	Homo-acetogenesis	SAO
Bacillota	*Firmicutes*	X	X	X	X	X
Bacteroidota	*Bacteroidetes*	X	X			
Chloroflexi	Unchanged	X	X	X		
Pseudomonadota	Part of *Proteobacteria*	X	X	X		
Thermodesulfobacteriota	Part of *Proteobacteria*			X		
Actinobacteriota	*Actinobacteria*	X	X			
Synergistota	*Synergistetes*		X			
Acidobacteriota	*Acidobacteria*		X		X	
Thermotogota	*Thermotogae*		X			X
Cloacimonadota	*Cloacimonetes* (*WWE1*)			X		X

Compiled from data presented by X. Zhang et al. (2024) and Lyu & Liu (2018).
The presence of an X indicates that the phylum includes key players. SAO: syntrophic acetate oxidation.

Table 1.2. Typical archaeal genera involved in the anaerobic digestion process, function of their members and key physiological traits.

Genus	Doubling time (h)	Particularities
Hydrogenotrophic methanogenesis from H_2 + CO_2 (or formate for some species)		
Methanobacterium	5-14	
Methanobrevibacter	13-40	High tolerance to VFAs and ammonia
Hydrogenotrophic methanogenesis from H_2 + CO_2 (or formate for most species)		
Methanoculleus	6-46	
Methanospirillum	11-40	High ammonia tolerance
Methanolinea	29	
Stricly acetoclastic methanogenesis		
Methanosaeta	28-65	Slow growth, high sensitivity to VFAs and ammonia
Methylotrophic methanogenesis		
Methanomethylovorans	12	High ammonia tolerance
H_2-dependent methylotrophic methanogenesis		
Methanomassilicoccus	ND	High ammonia tolerance
Hydrogenotrophic, acetoclastic and methylotrophic methanogenesis		
Methanosarcina	4-9	Metabolic versatility, fast growth, high tolerance to VFAs, ammonia and salts

Compiled from data presented by Lyu et al. (2018). ND: not determined, VFAs: volatile fatty acids.

Table 1.3. Key biochemical reactions driving the anaerobic digestion process.

AD process step	Substrate(s)	Reaction	ΔG°'
(Heterotrophic) acetogenesis			[kJ per mol substrate]
	Propionate	$CH_3CH_2COO^- + 3H_2O \rightarrow CH_3COO^- + HCO_3^- + H^+ + 3H_2$	+76.1
	Butyrate	$CH_3[CH_2]_2COO^- + 2H_2O \rightarrow 2CH_3COO^- + H^+ + 2H_2$	+48.5
	Valerate*	$CH_3[CH_2]_3COO^- + 2H_2O \rightarrow CH_3COO^- + CH_3CH_2COO^- + H^+ + 2H_2$	+48.5
	Caproate*	$CH_3[CH_2]_4COO^- + 2H_2O \rightarrow CH_3COO^- + CH_3[CH_2]_2COO^- + H^+ + 2H_2$	+48.5
Methanogenesis			[kJ per mol CH_4]
Acetoclastic pathway	Acetate	$CH_3COO^- + H_2O \rightarrow CH_4 + HCO_3^-$	-31.0
Hydrogenotrophic pathway	$H_2 + CO_2$	$4H_2 + HCO_3^- + H^+ \rightarrow CH_4 + 3H_2O$	-135.6
	Formate	$HCOO^- + 3H_2 + H^+ \rightarrow CH_4 + 2H_2O$	-134.3
Methylotrophic pathway (methyl dismutation)	Methanol	$4CH_3OH \rightarrow 3CH_4 + HCO_3^- + H^+ + H_2O$	-104.8
	Monomethylamine	$4CH_3NH_2 + 3H_2O \rightarrow 3CH_4 + HCO_3^- + H^+ + 4NH_3$	-57.7
H_2-dependent methylotrophic pathway	Methanol	$CH_3OH + H_2 \rightarrow CH_4 + H_2O$	-112.5
	Monomethylamine	$CH_3NH_2 + H_2 \rightarrow CH_4 + NH_3$	-77.2
Interconversion between acetate and $H_2 + CO_2$			[kJ per mol acetate]
Homo-acetogenesis (autotrophic acetogenesis)	$H_2 + CO_2$	$4H_2 + 2HCO_3^- + H^+ \rightarrow CH_3COO^- + 4H_2O$	-104.6
Acetate oxidation	Acetate	$CH_3COO^- + 4H_2O \rightarrow 2HCO_3^- + 4H_2 + H^+$	+104.6
Syntrophic acetate oxidation	Acetate	$CH_3COO^- + H_2O \rightarrow CH_4 + HCO_3^-$	-31.0

Compiled from data presented by Thauer et al. (1977).
ΔG°': standard free enthalpy change under biochemical standard conditions (pressure = 1 atm, temperature = 25°C, pH = 7)
A negative value of ΔG°' indicates an exergonic (spontaneous) reaction, while a positive value indicates an endergonic (non-spontaneous) reaction.
* The reaction and its ΔG°' correspond to the first β-oxidation step.

1.4.1.1. Hydrolysis

During the hydrolysis step, also known as the liquefaction or solubilisation phase, large organic polymers such as starch, cellulose, proteins, and fats are broken down into soluble mono- and oligomers like simple sugars, amino acids, non-volatile fatty acids (i.e. long-chain and medium-chain fatty acids with more than 6 carbon atoms), and glycerol. This initial step is crucial for the overall degradation process because microbes cannot absorb complex organic polymers. Additionally, the hydrolysis of simpler molecules also takes place, leading to the release of ammonia (NH_3) and ammonium (NH_4^+) from urea degradation in agricultural reactors fed with livestock effluents or in wastewater treatment reactors processing human urine. NH_3 is a microbial toxicant causing free ammonia intoxication in AD reactors (see § 1.4.3).

Hydrolysis is an extracellular process catalysed by exoenzymes excreted by fermentative bacteria and other organisms. Typical bacterial phyla including members capable of hydrolysis are listed in **Table 1.1**.

1.4.1.2. Acidogenesis

During the acidogenesis step, also known as the first fermentation step, fermentative bacteria convert the simple soluble compounds resulting from hydrolysis into volatile fatty acids (short-chain VFAs, or VFAs in the thesis context: C1 ≤ chain length ≤ C6), other organic acids (e.g. lactate), alcohols (ethanol and methanol), methylamines, dihydrogen (H_2), and CO_2. Among these products, acetate (C2 VFA), CO_2, H_2 and formate (C1 VFA) are direct precursors of CH_4. To a lesser extent, methylated compounds such as methanol and methylamines can also be directly converted to CH_4. NH_3 (and NH_4^+) is also released during the acidogenesis step through deamination of peptides and amino acids resulting from protein hydrolysis.

Hydrolysis and acidogenesis were sometimes associated to distinct functional groups of microbes since certain fermentative bacteria are not capable of hydrolysis (**Table 1.1**; Lim et al., 2020). However, all hydrolytic bacteria derive their energy from fermentation, while the enzymes and metabolic pathways involved in each process are distinct (Sikora et al., 2019). This dual functionality of fermentative bacteria has led other authors to classify hydrolytic and fermentative bacteria within a single functional group (fermentative-hydrolytic bacteria; Munisamy et al., 2017).

In this work, we have chosen to attribute the hydrolysis and acidogenesis processes to fermentative bacteria.

Fermentative bacteria are strict or facultative anaerobes that grow fast, with a generation time of the order of hours, and are highly resistant to changes in their growing environment. Acidogenesis can be 30 to 40 times faster than hydrolysis (Godon, 1998).

1.4.1.3. Acetogenesis

In a well-operating AD reactor, most of the fed biodegradable carbon is converted into direct precursors of CH_4 during the first fermentation step (Ahring, 2003; Murphy & Thanasit Thamsiriroj, 2013). However, fermentation products such as short-chain VFAs longer than acetate (i.e. C3 ≤ chain length ≤ C6: propionate, butyrate, valerate, caproate) require secondary fermentation to be converted to direct precursors of CH_4 (acetate, formate, H_2 and CO_2). This step, called *(heterotrophic) acetogenesis*, is crucial for AD process stability since VFAs are toxic to microbes, especially in acidic conditions (see § 1.4.2).

Heterotrophic acetogenic bacteria (also known as acetogens) derive their energy by oxidising substrates, such as C3-to-C6 VFAs and ethanol, producing acetate as a result. During this oxidation process, electrons are released and must be transferred to maintain the cell redox balance. Acetogens typically transfer these electrons to protons (H^+) or CO_2, releasing H_2 and/or formate as byproducts (De Bok et al., 2004). However, substrate oxidation is thermodynamically unfavourable under standard biochemical conditions (**Table 1.3**), unless the concentrations of H_2 or formate in the environment are kept very low. Therefore, in AD reactors, acetogenic bacteria exhibit obligate syntrophic behaviour, relying on H_2- or formate-utilising microbes to sustain growth (Sieber et al., 2018).

This syntrophic relationship is supported by hydrogenotrophic methanogens, which use H_2 and/or formate as electron donors (Baek et al., 2018) and CO_2 as an electron acceptor, producing methane. The syntrophy between acetogens and hydrogenotrophic methanogens is essential for maintaining energy flow in the AD process and is facilitated by *interspecies electron transfer* (IET). Electrons can be exchanged between species via hydrogen (*interspecies hydrogen transfer*, IHT),

formate (*interspecies formate transfer*, IFT), or directly through conductive structures such as nanowires (*direct interspecies electron transfer*, DIET; Reguera et al., 2005).

The preferred electron carrier, whether H_2 or formate, has been the subject of research for decades (Schink et al., 2017; Thiele & Zeikus, 1988). Factors influencing this preference include the distance between microbes (Harirchi et al., 2022), the process temperature, and the concentration of trace elements in the environment (Westerholm et al., 2022). In this work, we consider H_2 as the primary vector for interspecies electron transfer, as not all hydrogenotrophic microorganisms can utilise formate as an electron donor (Ahring, 2003; Murphy & Thanasit Thamsiriroj, 2013).

Syntrophic VFA oxidisers are found in several bacterial phyla (A. Singh & Schnürer, 2022), such as *Bacillota* (e.g., *Syntrophomonas*), *Pseudomonadota* (e.g., *Syntrophobacterium*) and *Desulfobacteriota* (e.g., *Syntrophobacter*). S*yntrophic propionate oxidation* (SPO) represents a thermodynamic bottleneck in the AD process (A. Singh et al., 2021; Westerholm et al., 2022) , as the conversion of propionate to acetate involves a single, energetically demanding step ($\Delta G^{\circ\prime}$ = +76.1 kJ/mol, **Table 1.3**). This contrasts with other VFAs, whose degradation begins with a more thermodynamically favourable β-oxidation step ($\Delta G^{\circ\prime}$ = +48.5 kJ/mol). Recent studies have highlighted members of the phylum *Cloacimonadota* (formerly *Cloacimonetes* or *WWE1*) as possible syntrophic propionate oxidisers in AD reactors (Westerholm et al., 2022).

1.4.1.4. Methanogenesis

During the methanogenesis step, CH_4 is finally produced from its direct precursors.

CH_4 can be produced exclusively by strictly anaerobic microbes belonging to the domain *Archaea*, known as *methanogens*. Although archaea and bacteria may appear similar morphologically, archaea are not bacteria; organisms in these two groups are phylogenetically different. Methanogens are primitive organisms that are widely considered sensitive to changes in their growing environment. In the AD environment, their optimal growing conditions are met within a very narrow pH range close to neutrality, whereas most fermentative bacteria are tolerant to acidic conditions (Pind et al., 2003).

Methanogens can produce CH_4 from three primary metabolic pathways: (1) acetoclastic methanogenesis, (2) hydrogenotrophic methanogenesis, and (3) methylotrophic methanogenesis.

1.4.1.4.1. Acetoclastic methanogenesis

The acetoclastic (syn. aceticlastic) pathway involves the cleavage of acetate into CH_4 and CO_2.

The archaea capable of this pathway are referred to as acetoclastic methanogens. In AD reactors, they primarily belong to the genera *Methanosaeta* and *Methanosarcina* (**Table 1.2**). Unlike the metabolically versatile *Methanosarcina* spp., which can utilise multiple methanogenic pathways, *Methanosaeta* spp. are obligate acetotrophs, relying exclusively on the acetoclastic pathway.

Members of *Methanosaeta* are considered more sensitive to high concentrations of free ammonia than hydrogenotrophic methanogens. In full-scale AD reactors operating at low ammonia level (< 1.21 g_TAN L^{-1}), obligatory acetoclastic methanogenesis by *Methanosaeta* spp. was reported as the dominant pathway (Fotidis et al., 2014).

1.4.1.4.2. Hydrogenotrophic methanogenesis

The hydrogenotrophic pathway involves the use of H_2 as an electron donor and CO_2 as an electron acceptor to produce CH_4 and water. The role of hydrogenotrophic methanogenesis is fundamental in maintaining low partial pressures of H_2, which is essential for the thermodynamics of heterotrophic acetogenesis.

The archaea capable of this pathway are known as hydrogenotrophic methanogens. In AD reactors, they are distributed among the following primary orders: *Methanobacteriales* (genera *Methanobacterium* and *Methanobrevibacter*), *Methanomicrobiales* (genera *Methanoculleus*, *Methanospirillum* an *Methanolinea*) and *Methanosarcinales* (genus *Methanosarcina*). Certain hydrogenotrophic methanogens can also use formate as major electron donor. While only some species within the *Methanobacteriales* can utilise formate, it is a substrate used by most cultured species of the *Methanomicrobiales* (**Table 1.2**).

Many hydrogenotrophic methanogens grow fast (doubling time on the order of hours), especially compared to obligate acetoclastic methanogens from the

Methanosaeta genus, which have a doubling time on the order of days (Murphy & Thanasit Thamsiriroj, 2013). In addition, hydrogenotrophic methanogens are more tolerant to high ammonia concentrations than *Methanosaeta*. Several studies have indicated that in agricultural AD reactors, hydrogenotrophic methanogenesis is the dominant pathway for methane production (Klocke et al., 2008; Nettmann et al., 2008), with ammonia playing a key role in promoting hydrogenotrophic methanogenesis (Yang et al., 2018).

1.4.1.4.3. Methylotrophic methanogenesis

The methylotrophic pathway involves the use of methyl groups from methylated compounds, such as methanol and methylamines, to form CH_4.

The archaea capable of this pathway are known as methylotrophic methanogens, and they can proceed via two distinct mechanisms. Some methylotrophs, including members from the genera *Methanomethylovorans* and *Methanosarcina*, can process methylated compounds without an external electron donor (Blaut, 1994). In this self-sufficient process, known as methyl-dismutation methylotrophy, a portion of the methyl group is oxidised to CO_2 to generate the electrons required to reduce the remaining portion to CH_4. In contrast, obligatory H_2-dependent methylotrophs, including members from the genera *Methanomassiliicoccus* and *Methanosarcina*, cannot perform this step. Instead, they must utilise H_2 as an external electron donor to reduce the methyl groups to CH_4, a process known as methyl-reduction methylotrophy (Feldewert et al., 2021).

In well-operating AD reactors, methylotrophic methanogenesis is a minor pathway, contributing to less than 1% of CH_4 production (Ferry, 1993). However, under conditions of ammonia accumulation, this pathway can become a significant contributor to CH_4 production (Beraud-Martínez et al., 2024).

It is important to note that archaea from the genus *Methanosarcina* are versatile methanogens, capable of using multiple metabolic pathways and switching between them in response to environmental stress (De Vrieze et al., 2012). This flexibility makes *Methanosarcina* spp. exceptionally resilient, allowing them to tolerate high concentrations of ammonia, salt, and acetate, as well as withstand significant pH shocks that would inhibit other methanogens.

1.4.1.5. Homo-acetogenesis and syntrophic acetate oxidation

The interconversion between H_2/CO_2 and acetate is a key process in AD reactors, significantly influencing the CH_4 formation pathway. This balance is driven by two opposing metabolic processes: *homo-acetogenesis* and *syntrophic acetate oxidation* (SAO).

During homo-acetogenesis, also known as autotrophic acetogenesis, homo-acetogenic bacteria convert CO_2 to acetate using H_2 as an electron donor through the Wood-Ljungdhal pathway (Karekar et al., 2022). Unlike heterotrophic acetogenesis, homo-acetogenesis is thermodynamically favourable under standard biochemical conditions ($\Delta G^{\circ\prime}$ = -104.6 kJ/mol, **Table 1.3**) and does not require syntrophic relationships. Consequently, homo-acetogenic bacteria often compete with hydrogenotrophic methanogens, as both microbial groups share H_2 and CO_2 as common substrates.

Conversely, syntrophic acetate-oxidising bacteria (SAOB) oxidise acetate to produce H_2 and CO_2. Acetate oxidation is thermodynamically unfavourable under biochemical standard conditions ($\Delta G^{\circ\prime}$ = +104.6 kJ/mol). For the reaction to proceed, SAOB must form an obligatory syntrophic association with hydrogenotrophic methanogens. The consumption of H_2 by the methanogens ($\Delta G^{\circ\prime}$ = -135.6 kJ/mol) makes the overall coupled process spontaneous ($\Delta G^{\circ\prime}$ = -31 kJ/mol). This interspecies hydrogen transfer (Stams et al., 2006) is crucial for the pathway's viability.

SAOB can survive under high temperature and ammonia/VFAs concentrations (Pan et al., 2021). Notably, increased ammonia concentrations in AD reactors can inhibit acetoclastic methanogens, prompting a metabolic shift where the combination of SAO and hydrogenotrophic methanogenesis becomes the dominant route for converting acetate to CH_4 (Hao et al., 2017).

1.4.2. FVFA intoxication

Free VFA (FVFA) intoxication, or acidosis, typically arises from *organic overload*, i.e. when the amount of biodegradable organic material fed into an AD reactor exceeds the degradation capacity of its microbiome. This process disturbance can also occur when AD reactors are supplemented with feedstocks containing a high fraction of quickly hydrolysable and fermentable substrates, such as simple sugars or glycerine. Common causes of FVFA intoxication include changes in feedstock

composition, incorrect input measurements, or increased mixing that suddenly incorporates undigested organic matter (e.g. floating layers) into the slurry (Drosg, 2013).

Biologically, FVFA intoxication is linked to the differing resilience between fermentative bacteria, which can produce acids and H_2 under a wide range of conditions, and the more fragile methanogenic archaea that consume acetate and H_2. Hydrogen plays a critical role in FVFA intoxication because it regulates interspecies electron transfer. When a reactor is fed with quickly hydrolysable and fermentable organic matter, it causes a sudden release of VFAs and H_2 into the slurry. If H_2 production exceeds the consumption capacity of hydrogenotrophic methanogens, the H_2 concentration in the slurry may increase to a level that inhibits acetogenesis. As a result, VFAs longer than acetate (C3-to-C6 VFAs: propionate, butyrate, etc.) remain undegraded. If this feeding regime continues, these VFAs accumulate in the slurry, causing the pH to drop into an acidic range. This acidification is a primary cause of inhibition for methanogenic archaea in cases of FVFA intoxication.

As weak acids, VFAs (RCOOH) partially dissociate in aqueous solution into their anion ($RCOO^-$) and a proton (H^+). The undissociated, neutral form of VFAs (RCOOH), referred to as *free VFA* (FVFA), is considered the primary cause of microbial inhibition, as it can passively diffuse across cell membranes (D. Li et al., 2017). Inside the cytoplasm, FVFA dissociation causes toxicity by disrupting the proton gradient required for ATP synthesis (Ji et al., 2013). In well-functioning AD reactors, where the pH is well above the typical pKa of VFAs (pKa = 4.75 ; Nativ et al., 2021), VFA dissociation is favoured, and FVFAs remain at low concentrations. However, during FVFA intoxication, the reactor pH drops closer to the pKa, shifting the equilibrium towards the undissociated form, and increasing FVFA levels. Although acetate (C2 VFA) is a direct precursor for methane in AD reactors, it is also toxic to microbes. FVFAs primarily inhibit acetoclastic methanogens, though they have less impact on hydrogenotrophic methanogens or acidogens (Kroeker et al., 1979). Consequently, free acetate accumulates in the slurry of reactors experiencing FVFA intoxication, further exacerbating the negative effects of this process disturbance on the archaeal community.

FVFA intoxication can occur suddenly, particularly in the primary digester of multi-stage AD plants. In most biogas facilities, the primary digester is the reactor

the most at risk, as it directly receives incoming organic material. In contrast, downstream post-digesters, which process partially digested matter, typically maintain greater stability.

The concentration of total or individual VFAs is not a reliable indicator of FVFA intoxication in anaerobic digesters since a significant VFA accumulation can occur without being toxic in well-buffered systems. In contrast, a sudden increase in dissolved H_2 concentrations in the slurry or gaseous H_2 in the biogas is widely recognised as an early indicator of FVFA intoxication. Interestingly, formate (C1 VFA) concentrations could also play such role, since formate, like H_2, is involved in interspecies electron transfer. Unfortunately, there are few reports on the use of formate for monitoring the AD process (Schink et al., 2017), as detecting formate in liquid media at micromolar concentrations is challenging, especially in the complex matrix of AD slurries.

1.4.3. FAN intoxication

In agricultural AD plants, animal manure and bio-wastes produced by municipalities, slaughterhouse and dairy industries are commonly used as feedstocks. These feedstocks have a high nitrogen content, leading to the formation of ammonia as a final product. Therefore, AD reactors treating such nitrogen-rich feedstocks and managed with high hydraulic retention time may be exposed to excessive ammonia accumulation in the reactor slurry, a major microbial toxicant.

In aqueous solution, the *total ammonia nitrogen* (TAN) exists in two forms: ionised ammonium nitrogen ($N\text{-}NH_4^+$) and *free ammonia nitrogen* ($N\text{-}NH_3$ or FAN). The dissociation equilibrium of ammonia in aqueous solution (pKa= 9.3) depends on pH and temperature: higher pH and/or temperature increases FAN content at the expense of $N\text{-}NH_4^+$ content. FAN is considered the main compound causing microbial inhibition due to its passive diffusion through cell membranes (Jiang et al., 2019). In AD microbiomes, methanogenic archaea are reported to be most affected by high FAN concentration and are the first to be inhibited. Inside the cytoplasm, FAN protonation causes toxicity by disrupting the proton gradient required for ATP synthesis, directly inhibiting key enzymes in the CH_4 formation pathway(s), and depleting cellular energy reserves. When methanogenesis slows down, VFAs accumulate in the slurry, causing the pH to drop and the FAN concentration to

decrease. This phenomenon results in an "inhibited steady-state" that seriously affects CH_4 production yield (Angelidaki & Ahring, 1993) in anaerobic digesters. If the nitrogen supply to such digesters in inhibited steady-state is further increased, the TAN and FAN content in the slurry can reach extreme levels, interrupting feedstock conversion to biogas.

The inhibitory threshold of FAN in AD reactors varies widely due to multiple factors, including the type of feedstock, inoculum source, FAN acclimation period, and environmental conditions such as temperature and pH.(Rajagopal et al., 2013) As a result, reported inhibition ranges for FAN span from as low as 45 mg L^{-1} to as high as 2600 mg L^{-1}.

1.5. Current limitations of process monitoring techniques in agricultural biogas plants and potential for biogas composition monitoring

To avoid FVFA or FAN intoxication from reaching their critical stage (i.e. interrupted CH_4 production from feedstocks), biogas plant managers should be warned as early as possible if the risk of process disturbance is increasing in a digester. However, such early warnings are currently unavailable due to the poor deployment of adequate instrumentation and measurement methods needed for fast-response monitoring of the AD process.

1.5.1. Lack of online monitoring methods

In *(bio)process monitoring*, sensors and analytical methods are used to diagnose the process status and evaluate the risk of disturbance. These techniques range from manual sampling with *offline* analysis to the fully automated integration of *online* analysers (**Figure 1.3**). The more frequent the measurements (and the interpretation of their results), the higher the chance of detecting process disturbances early enough to mitigate their negative impact. Therefore, online methods should be preferred to offline methods for bioprocess monitoring.

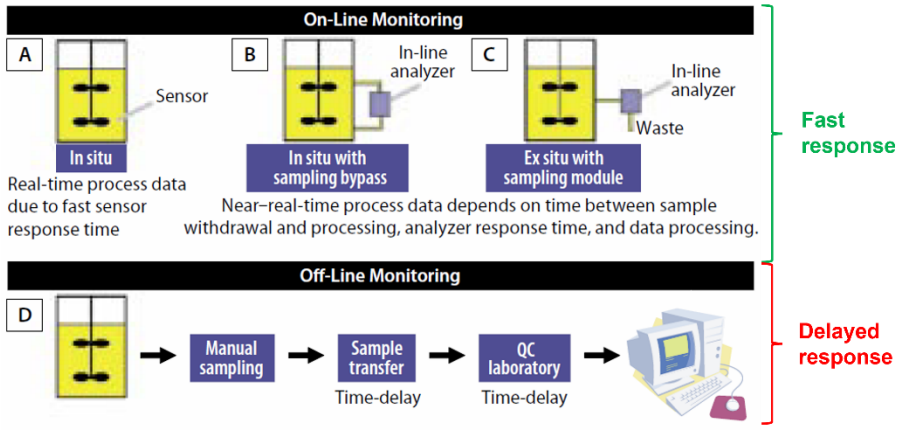

Figure 1.3. Classification of bioprocess monitoring techniques regarding their degree of invasiveness and their response delay. Adapted from Whitford & Julien (2007). QC: quality control.

Based on my personal experience with agricultural biogas plants in Luxembourg and the Greater Region, online monitoring of the AD process remains rudimentary. Common practice is to use a supervisory control and data acquisition (SCADA) system for basic plant operating procedures only. This usually includes only temperature and level control, and logging the biogas flow rate. Typically, when an unusual decrease in biogas production is observed, the plant manager collects slurry samples and sends them to a laboratory. The laboratory performs offline analysis of parameters commonly accepted as good indicators of the AD process status, then delivers a diagnosis. Unfortunately, this procedure is often lengthy, delaying the possible application of corrective actions once the type of process disturbance is identified. Therefore, the near absence of online process monitoring exposes biogas plants to critical disturbances of the AD process, with corresponding risks of heavy economic losses. Only recently, following our advice and demonstration, the members of the Luxembourg Biogas Association (Biogasvereenegung a.s.b.l.) collectively acquired a portable biogas analyser, primarily used to detect emerging process disturbances.

1.5.2. Limitations of slurry analysis for online AD process monitoring

Several physicochemical characteristics of the slurry are widely recognised as valuable indicators for the early detection of both FVFA and FAN intoxication in AD reactors, especially the concentration of individual VFAs. Various techniques

based on spectroscopy (Krapf et al., 2013), chromatography (Boe et al., 2007), electrochemical sensors (Buczkowska et al., 2010), and biosensors (Jin et al., 2017; Zhao et al., 2018) have been investigated at laboratory and full scale to enable the online analysis of AD slurry characteristics, often with satisfactory results. However, none of these online monitoring techniques meet the requirements of robustness, applicability, and low cost necessary for realistic application to full-scale biogas production digesters (Wu et al., 2019). Simple and low-cost analytical methods are indeed unusable in the long-term with matrices as complex, harsh, and variable as agricultural AD slurries. These media are heterogeneous, contain bubbles, and have a high content of particles and total solids resulting in strong opacity and fouling potential. Therefore, to my knowledge, there has been no report of effective adoption of online process monitoring techniques based on slurry indicators in full-scale biogas plants. In practice, biogas plant managers continue to delegate the analysis of these parameters to specialised laboratories for offline measurement.

Consequently, measuring physicochemical characteristics of the slurry presents limited interest for fast-response monitoring of the AD process, at least from today's perspective.

1.5.3. Potential of biogas analysis for online AD process monitoring

Compared to AD slurries, the biogas produced by agricultural digesters is a more homogeneous and "clean" medium. Consequently, the biogas composition can be analysed using sensors that are both robust and low-cost, with a high measurement frequency and good repeatability of results (Drosg, 2013). Moreover, sampling biogas is easy, and gas analysers do not require complex and expensive maintenance and sensor replacement. Surprisingly, research efforts aimed at valorising biogas composition for online monitoring of the AD process are scarce. To my knowledge, only *electronic noses* (e-noses) have been investigated for this purpose. E-noses are arrays of non-specific individual gas sensors. When the responses of these sensors are combined, they form a pattern typical of the gas mixture presented to the array, like a signature. Adam et al. (2013, 2015) investigated the use of an e-nose for online monitoring of the AD process at the pilot-scale level and then upscaled this approach to an agricultural digester. The e-nose derived indicator was in good agreement with the reactor process status at pilot scale but less consistent when tested at the full-scale

level. This highlights two important limitations of e-nose technology that hamper its adoption by biogas plants for AD process monitoring: e-noses are highly sensitive to sensor drift and poisoning by harsh environmental conditions (Wu et al., 2019). Interestingly, the technology of the specific sensors used to analyse the biogas composition in its major compounds (CH_4, CO_2 detected by infrared technology and H_2S, H_2 detected by electro-chemical sensors) is much more robust than the metal oxide semiconductor technology of the non-specific sensors used in e-noses. Nevertheless, CH_4, CO_2, H_2S, and H_2 are potential indicators of the reactor process status, as their concentration in the biogas is directly related to the metabolism of the reactor microbial community (Mizuno et al., 1998; Nordberg et al., 2000). Nowadays, the CH_4 content of the biogas is already measured online in many agricultural biogas plants. Upgrading a gas analyser with CO_2, H_2, and H_2S sensors appears thus both technically feasible and financially affordable.

Consequently, exploiting the dynamics of the biogas composition in CH_4, CO_2, H_2S, and H_2 for online monitoring of the AD process deserves consideration.

1.6. Introduction to multivariate statistical process control

An important part of this work aims to detect both FVFA and FAN intoxication in AD reactors by utilising the concentrations of the major compounds in biogas through statistical tools traditionally used for process monitoring with e-noses. These tools are referred to as *multivariate statistical process control* (MSPC).

1.6.1. Common-cause vs special-cause process variation

Process variability can be decomposed into *common-cause* (or random-cause) and *special-cause* variation. Common-cause variation refers to the many small and unavoidable sources of variability inherent to the process itself. A process exhibiting only common-cause variation is said to be *in (statistical) control*. On the other hand, special-cause variation refers to other sources of variation that may occasionally occur and force an otherwise in-control process to become unstable and unpredictable (Aven & Krohn, 2014). In process monitoring, *out-of-control (process)* observations refer to occurrences of special-cause variation. In this work, we assess whether out-of-control observations can be interpreted as valuable warning signals announcing imminent AD process disturbances.

1.6.2. Statistical process control (SPC)

SPC refers to a set of methods that allow monitoring and ideally improving the performance of a process through statistical analysis of process data. Unlike "time-static" statistical tests (e.g. Student's t-test), SPC methods include the time factor in the statistical analysis: for each sample, a statistic characterising the process is calculated and plotted over time in a visual tool called a *control chart*. Control charts are built based on *individual process variables* (IPVs), i.e. process characteristics that can be expressed by a numerical measurement (e.g. CH_4 concentration in biogas). The control chart includes statistically defined *control limits* that delimit the in-control process region. On a control chart, the hypothesis-testing procedure involved in traditional statistical tests is performed constantly, i.e. for each new sample. A sample statistic falling within the control limits means it does not reject the null hypothesis H_0 that the process is statistically in control, while a point falling outside the control limits means it rejects the null hypothesis H_0 that the process is statistically in control. Control charts help quickly detect occurrences of special-cause variation so corrective action may be undertaken and the special causes removed.

There are two successive phases in constructing control charts. During *Phase I*, a *historical data set* (HDS) is collected to define an in-control process baseline, on which the control limits and model parameters are estimated. During *Phase II*, actual statistical process control is performed: for each new observation, the statistic characterising the process is calculated using the model parameters derived from the HDS and plotted in a control chart to identify out-of-control process observations.

1.6.3. Univariate statistical process control

Even when several IPVs are measured for a particular process, a common practice called *univariate SPC* involves monitoring them on independent control charts. The most common type of univariate control chart, shown in **Figure 1.4**, is often called a *Shewhart control chart* (Shewhart, 1926). These control charts successively display values of individual observations (x-charts) or averages of subgroups of observations ($\bar{x}$-charts). Shewhart control charts include two control limits: a lower control limit (LCL) and an upper control limit (UCL). These control limits are defined assuming that the monitored IPV follows a normal distribution when the process is in control. Control limits are typically set at ±3 standard deviations

(±3σ) from the in-control process mean. This range covers 99.73% of the expected variability under in-control process conditions. Observations falling outside this range are considered statistically out-of-control and are therefore flagged as potential indications of a process disturbance.

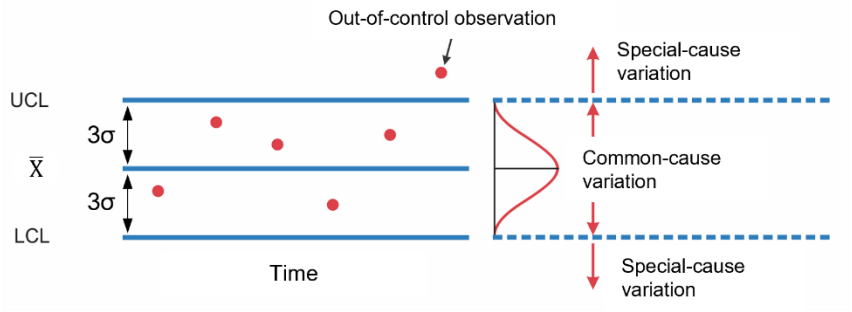

Figure 1.4. Example of a univariate x control chart according to Shewhart for the i^{th} individual process variable (IPV_i) of a fictive process. $\bar{X}$ and σ are respectively the mean and the standard deviation of the IPV_i (assuming in-control process conditions). LCL: lower control limit, UCL: upper control limit.

1.6.4. Multivariate statistical process control (MSPC)

1.6.4.1. MSPC considers the correlation between the individual process variables

Very often, the IPVs of bioprocesses are interrelated and form a correlated data set. This observation applies to the AD process: for example, the toxicity of ammonia and VFAs to the microbiome is highly dependent on the pH of the slurry. MSPC extends univariate SPC by examining the measured IPVs as a group and considering the correlation between them. In MSPC, an out-of-control observation can be caused by: (1) an extraordinary value of an IPV or a set of IPVs, (2) a change in the relationship between two or more IPVs that contradicts the pattern established by the historical data set, or (3) a combination of the former two causes.

Figure 1.5 demonstrates how misleading information could be generated from univariate control charts in the case of processes characterised by IPVs expressing correlation. Suppose a fictive manufacturing process for anaerobic digester mixers is characterised by two key variables: the propeller Diameter (D) and the shaft Length (L). For each mixer produced, the ratio between L and D is expected to remain positive and quite constant to ensure mechanical integrity and performance. On the right side of the figure, two Shewhart control charts are superimposed on the bivariate

plot, corresponding to the vertical (L) and horizontal (D) axes. Due to the positive correlation between L and D, it is expected that the measurement plots will locate within the elliptical region. Following univariate SPC methods, observations corresponding to mixers 1 and 2 are considered in-control because they fall within the control limits of both Shewhart control charts. This information is correct since mixers 1 and 2 correspond to the product specification (the elliptical region). Univariate SPC methods also provide correct information for mixer 4 by identifying it as an out-of-control observation (L > UCL). Indeed, mixer 4 does not meet the product specification as its measurement plot is outside the ellipse. In contrast, univariate control charts lead to misleading information concerning mixer 3. Indeed, the corresponding measurement is located in the in-control region for both Shewhart control charts, whereas the mixer does not meet the product specifications because the shaft is too long for its propeller diameter, causing its measurement plot to fall outside the ellipse.

NB: positive correlation between D and L

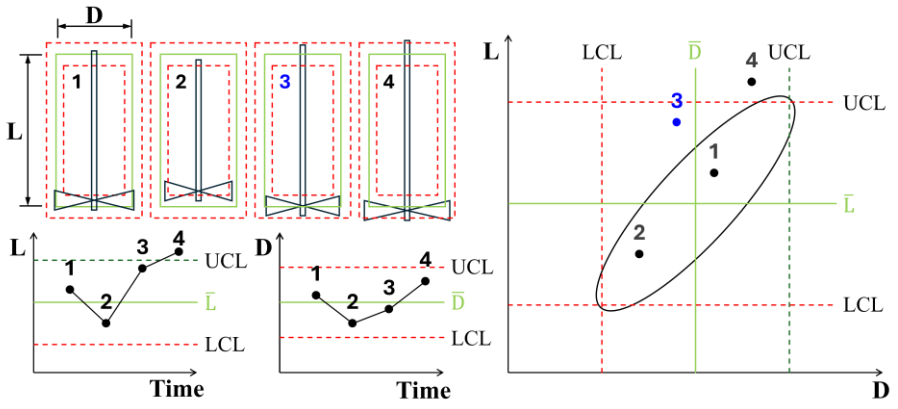

Figure 1.5. Example of misleading information from univariate control charts in a fictive quality control process for an anaerobic digester mixer. The process monitors two positively correlated individual process variables (IPVs): the propeller Diameter (D) and the shaft Length (L). The rectangle is defined by the upper (UCL) and lower (LCL) control limits of the Shewhart control charts, while the ellipse represents the product specification region, which accounts for the positive correlation between the two IPVs.

1.6.4.2. The Hotelling's T^2 statistical index

MSPC involves the measurement of distances between objects in a multidimensional space. The Mahalanobis distance, also called *(Hotelling's) T^2*

statistical index, is the basic tool to monitor the divergences of a multivariate process from an in-control situation. Unlike univariate statistics, the T^2 index considers the (linear) correlation in the data using the variance-covariance matrix of the multidimensional data set in its calculation.

The variance-covariance matrix S of the mean-centred and normalised data set is computed using:

$$S = \frac{1}{m-1} X^T X \tag{1.1}$$

where X is the mean centred and normalised data matrix and m the number of observations.

The Hotelling's T^2 is calculated for the i^{th} observation using:

$$Hotelling's\ T^2 = (X_i - \bar{X}) S^{-1} (X_i - \bar{X})^T \tag{1.2}$$

where X_i is the data vector corresponding to the i^{th} observation and $\bar{X}$ is the mean vector calculated for the m observations.

Since the T^2 statistics describes a geometrical distance, it cannot take negative values. Therefore, T^2 control charts have only one upper control limit (UCL). One common approach for computing the UCL, relies on parametric approximations based on the Beta and Fisher distributions (Mason & Young, 2002). In Phase I, the UCL can be calculated using:

$$UCL_{Phase\ I} = \left[\frac{(m-1)^2}{m}\right] B\left(\alpha; \frac{p}{2}, \frac{m-p-1}{2}\right) \tag{1.3}$$

; while in Phase II, the UCL is typically estimated using:

$$UCL_{Phase\ II} = \left[\frac{p(m+1)(m-1)}{m(m-p)}\right] F(\alpha; p, m-p) \tag{1.4}$$

where α is the significance level, m is the number of in-control observations, p is the number of IPVs, B and F are the upper $1-\alpha$ quantiles of the Beta and Fisher distribution, respectively. The control limit distributions differ between Phase I and II because Phase I accounts for parameter estimation uncertainty, while Phase II assumes fixed parameters. The UCL calculation assumes that the T^2 statistic follows these distributions, which holds true only when the underlying data follow a multivariate normal distribution.

The Hotelling's T^2 index is easy to interpret for a process characterised by only two IPVs. Let's reuse the example of the fictive manufacturing process previously described in **Figure 1.5**. For such a process generating correlated bivariate observations when in statistical control, the geometrical representation of points having an equal T^2 index is an ellipse plotted in the direction of the major variance and centred on the process average $(\bar{L}, \bar{D})$. This elliptic shape corresponds to the in-control region intuitively defined for stirrers fulfilling process expectations. This illustrates the effect of considering the variance–covariance matrix of the data set. Indeed, a new measurement is more likely to be located in the direction of the highest correlation than in the direction of the smallest correlation.

The computation of the Hotelling's T^2 index implicitly relies on the assumption that linear relationships exist among the IPVs, but that they are not so strong as to induce numerical instability (Ferrer, 2007). As shown in relation (1.1), computing the Hotelling's T^2 statistics in the original data space needs the inversion of the estimated variance-covariance matrix S, involving that S has to be well-conditioned (slightly correlated IPVs). When *multicollinearity* is present (i.e. when two or more IPVs are highly linearly correlated), the covariance matrix can become nearly singular (ill-conditioned), rendering its inversion unreliable and potentially distorting the T^2 statistic.

1.6.4.3. MSPC based on principal component analysis (PCA-MSPC)

Principal component analysis (PCA) is commonly employed for MSPC as it reduces the dimensionality of the problem. Indeed, MSPC based on PCA (PCA-MSPC) allows for separating the main signal space from the stochastic variation (i.e. the "noise") by selecting the appropriate number of principal components (PCs) representative of the process.

Assuming a process characterised by n IPVs, two statistical indices can be derived from a PCA model:

- The *Hotelling's T^2 index computed with the scores obtained for the A dominant principal components* (i.e. T_A^2 with $A < n$) that represent the main process space;
- The *squared prediction error (SPE)*, representative of the residuals (n-A dimensions) that characterise the "noise" signal.

A geometrical representation of the T_A^2 and SPE relation is presented in **Figure 1.6**. The T_A^2 control chart will detect the process variation in the "plane" of the *A* dominant PCs. If a totally new type of event occurs, which was not present in the reference data set used to build the PCA model and changes the relation between IPVs, this new observation X_{new} will move off the "plane." However, such a new event will still be detected using the SPE control chart.

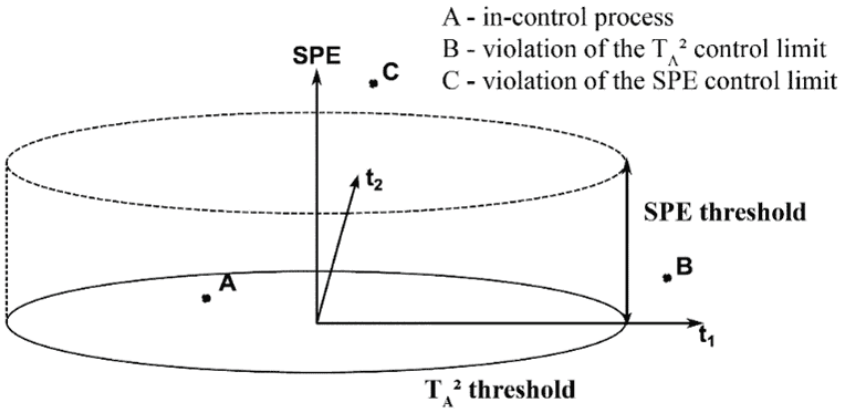

Figure 1.6. Geometrical interpretation of the T_A^2 and the squared prediction error (SPE) for a tri-variate process summarized by a principal component analysis model retaining *A*=2 principal components.

After applying PCA to the historical data set, the number *A* of dominant PCs is determined using criteria such the eigenvalue-one rule (Kaiser, 1960). Then, the T_A^2 statistic is calculated for each observation using:

$$T_A^2 = \sum_{i=1}^{A} \frac{t_i^2}{\lambda_i} \tag{1.5}$$

where λ_i is the eigenvalue of the i[th] PC, corresponding to $s_{t_i}^2$, i.e., the estimated variance of score t_i. The corresponding value of the SPE index is calculated using:

$$SPE = \sum_{i=1}^{p} (\hat{x}_i - x_i)^2 \tag{1.6}$$

where *p* is the number of IPVs, x_i is the observed value for the i[th] IPV and $\hat{x}_i$ is the corresponding value computed using the PCA model. The UCL of the T_A^2 control chart can be calculated using the relations (1.3) and (1.4) for Phase I and Phase II, respectively, by replacing the number *p* of IPVs by the number *A* of dominant PCs. The upper control limit SPE_{lim} of the corresponding SPE control chart can be

calculated according to (Kourti & MacGregor, 1995). An example of a T_A^2 control chart with its corresponding SPE control chart is presented in **Figure 1.7** for a fictive process.

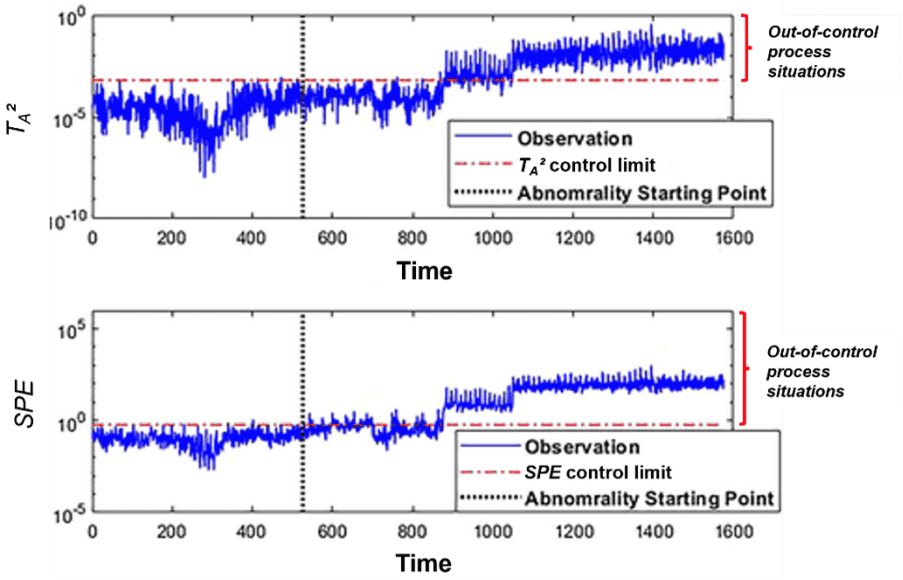

Figure 1.7. Combination of a T_A^2 control chart and its corresponding SPE control charts plotted for a hypothetical process. Beginning on day 550, the SPE control chart statistically detected repeated occurrences of out-of-control process situations. Unfortunately, these early warning signals were disregarded by the process manager, who failed to implement appropriate corrective measures. As a result, the abnormality escalated starting on day 900, leading to significant economic losses.

PCA-MSPC is a powerful tool to monitor multivariate processes (Kourti, 2005; Kourti & MacGregor, 1995) that was successfully applied by Adam et al. (2015) for biogas-based AD process monitoring using e-nose data. Compared to standard MSPC, PCA-MSPC is inherently robust to non-normal data. Indeed, from the central limit theorem, the score variables are asymptotically normal even if the process variables themselves are not normally distributed (Wang et al., 2008). Additionally, PCA is particularly advantageous in the presence of multicollinearity (Ferrer, 2007), as it transforms correlated IPVs into uncorrelated PCs that concentrate the variance into a reduced number of dimensions. This transformation stabilises the statistical model and enhances the sensitivity and interpretability of the derived control indices.

1.6.4.4. Static PCA-MSPC and contribution plots

Static PCA-MSPC is the basic way to implement PCA-MSPC (Mason & Young, 2002). In static PCA-MSPC, the model parameters calculated during Phase I are left unchanged during Phase II.

Static PCA-MSPC allows the easy computation of *contribution plots* (Kourti, 2005). When an out-of-control process observation is detected by the T_A^2 or SPE control chart, a physical interpretation can be found by transforming the model output back into the original variable space (IPVs). Contribution plots indicate the IPVs that have mostly contributed to the deviation of the T_A^2 or SPE index. Although these plots will not unequivocally diagnose the cause of the out-of-control observations, they will greatly facilitate their interpretation.

1.6.4.5. Recursively updated PCA-MSPC

A major limitation of static PCA-MSPC is that the PCA model, once built from the HDS, is time-invariant, while most real industrial processes are time-varying. False alarms are observed rapidly when such time-variant processes are monitored using static models, which significantly compromises their reliability. Agricultural AD reactors commonly demonstrate time-varying behaviour due to changes in feeding quality and quantity over time. For the same reasons, their microbiome also changes over time.

Recursively updated PCA-MSPC (RU-PCA-MSPC) is a way to reduce the problem of time-varying conditions by making the model adaptive. Unlike static PCA-MSPC, the model parameters are updated during Phase II on an appropriate timescale, giving a higher weight to more recent observations. To avoid biasing the updated process baseline with new out-of-control process observations, the recursive update of the PCA model is only performed for new observations corresponding to in-control values of both the T_A^2 and SPE indexes. A potential limitation of RU-PCA-MSPC lies in the critical selection of the effective memory length, which governs how quickly the model adapts to new data. If set too short, the model may become overly sensitive to transient variations; if too long, it may fail to track gradual process changes effectively. More exhaustive information about RU-PCA-MSPC can be found in specialised literature (W. Li et al., 2000).

1.7. Restoring a functional AD process in critically intoxicated digesters is challenging

Due to the current limitations of methods allowing online monitoring of the AD process in agricultural digesters, process disturbances are often not detected early enough to prevent significant damage to microbial communities. In their most critical form, both VFA and FAN intoxication lead to the complete interruption of feedstock conversion to CH_4. Besides the economic losses due to disrupted energy production, this event forces the shutdown of the CHP units that heat the digesters, amplifying microbial stress. Additionally, eliminating the digestate content of critically intoxicated digesters (often representing several thousand cubic meters) is a major issue since this digestate cannot be used for crop fertilisation due to agronomic concerns, generation of olfactive nuisances, and emissions of environmentally damaging aerosols.

Most methods proposed to recover the AD process in reactors exposed to critical FVFA intoxication involve bioaugmentation (Basak et al., 2021; Y. Li et al., 2018), which implies adding specialised microorganisms to the slurry as a corrective treatment. Recent research also focuses mainly on bioaugmentation techniques to solve ammonia issues in AD reactors (Z. Y. Li et al., 2023). However, these efforts aim at preventing FAN inhibition (Y. Li et al., 2017) or optimising biogas production after a moderate FAN intoxication (Yang et al., 2019) rather than restoring CH_4 production in critically intoxicated reactors. Although these methods show encouraging results for laboratory-scale reactors, no successful process recovery cases using bioaugmentation have been reported for full-scale biogas plants. The main reason is probably the difficulty of preparing and storing on-site large volumes of inoculum acclimatised to specific toxicants, which would require the costly and delicate operation of an additional large-scale bioreactor.

Consequently, there is a significant challenge in identifying realistically scalable process recovery methods. Interestingly, the equilibrium between the free and ionised forms of VFA and ammonia is highly dependent on pH. Process recovery strategies involving pH correction with specific chemicals should therefore be evaluated to counteract FVFA and FAN intoxication.

Chapter 2

Objectives, research questions and approaches

2.1. General objectives

This PhD thesis addresses the challenge of sustainable agricultural biogas production by investigating innovative strategies to enhance the resilience and efficiency of AD systems. The research focuses on preventing and mitigating common process disturbances.

To this end, the thesis has **two primary objectives**:

1. To determine whether online monitoring of biogas composition, using low-cost and robust sensors combined with multivariate statistical process control (MSPC), can enable the early detection of process disturbances caused by organic and nitrogen overload.
2. To develop and validate, at a pilot scale, practical and scalable process recovery strategies to restore AD process functionality in reactors that have ceased producing methane due to critical forms of these same disturbances.

2.2. Research questions

To achieve the stated objectives, this work addresses **three research questions**:

- **Q1 Disturbance detection:** ***Is a MSPC approach based on biogas composition useful for detecting the two main disturbances of the AD process (FVFA and FAN intoxication)?***
- **Q2 Recovery from FVFA intoxication:** ***Can the AD process be recovered after a critical FVFA intoxication without supplementing the intoxicated reactors with inocula acclimatised to VFAs?***
- **Q3 Recovery from FAN intoxication:** ***Can the AD process be recovered after a critical FAN intoxication without supplementing the intoxicated reactors with inocula acclimatised to ammonia?***

2.3. Thesis plan

The plan outlined in **Figure 2.1** was adopted for this work.

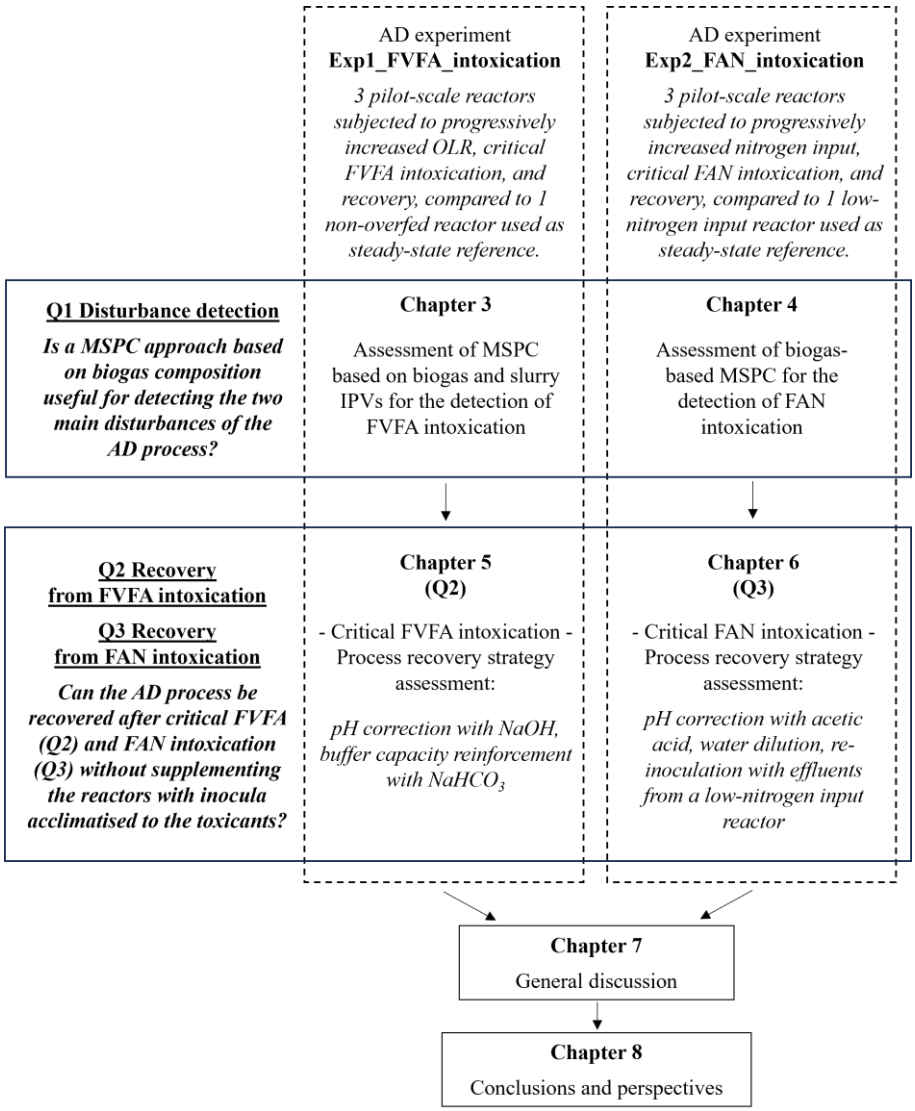

Figure 2.1. Thesis plan. AD: anaerobic digestion, FAN: free ammonia nitrogen, FVFA: free volatile fatty acids, IPV: individual process variable, MSPC: multivariate statistical process control.

2.4. Approaches

The approaches adopted to address the research questions are graphically summarised in **Figure 2.2**. and described hereafter.

Two AD experiments were conducted in continuously stirred tank pilot-scale reactors with a working volume of 100 litres, aiming to closely replicate the behaviour of agricultural digesters; lab-made biogas monitoring tools were developed for this specific purpose:

- **Exp1_FVFA_intoxication:** AD reactors progressively overfed until critical FVFA intoxication + Assessment of a process recovery strategy.
- **Exp2_FAN_intoxication**: AD reactors exposed to progressive increase of their nitrogen input until critical FAN intoxication + Assessment of a process recovery strategy.

Chapter 3 and **Chapter 4** aim to answer question **Q1 Disturbance detection**.

Chapter 3: ***Transfer of a static PCA-MSPC model from a steady-state anaerobic reactor to an independent anaerobic reactor exposed to organic overload***
This chapter utilises the results of AD experiment **Exp1_FVFA_intoxication** and aims to answer the following sub-questions:

- *Can we detect a FVFA intoxication in an AD reactor with MSPC models combining biogas composition with individual process variables (IPVs) measured in the slurry?*
- *Can we use the dataset of an independent reactor maintained in steady-state to define the in-control process baseline of an MSPC model, and use it to detect a FVFA intoxication in another reactor?*
- *Are all the IPVs measured in the slurry relevant to be included in such MSPC models?*
- *Could MSPC models based solely on biogas composition be considered for detecting process disturbances in AD reactors?*

Approach: Two static MSPC models based on principal component analysis (PCA-MSPC) combining biogas composition (CH_4, CO_2, and H_2) with two distinct sets of slurry properties were built using the dataset of a reactor maintained in steady-state as

the in-control process baseline. The two models were then applied to monitor the process of a second pilot-scale reactor that was progressively overfed until it stopped producing CH_4 from fed feedstock due to critical FVFA intoxication. By comparing the dynamics of metabolic process stability indicators between the two reactors, the models were assessed for their ability to provide early warning signals of the upcoming process collapse in the overfed reactor. For each model, the contribution of the IPVs measured in the slurry and the biogas was compared and discussed.

Chapter 4: ***Potential of multivariate statistical process control based on biogas composition to detect free ammonia intoxication in anaerobic reactors***

This chapter utilises the results of AD experiment **Exp2_FAN_intoxication** and aims to answer the following sub-questions:

- *Can we detect FAN intoxication in AD reactors in using MSPC models based exclusively on biogas composition?*
- *Can we use the composition of the biogas produced by these reactors when in steady state to define the in-control process baseline?*

Approach: Static and recursively updated PCA-MSPC models, using only biogas composition (CH_4, CO_2, H_2, and H_2S), were compared to monitor the process of three pilot-scale AD reactors exposed to increasing nitrogen input until they stopped producing CH_4 from fed feedstock due to critical FAN intoxication. A fourth reactor, maintained at low nitrogen input served as reference for steady-state operation. However, its dataset was not used to establish the in-control process baseline of the PCA-MPSC models. Instead, for each reactor, data from an initial steady-state process period were used to define the in-control process baseline, which was further updated in the case of the recursively updated models. Metabolic process stability indicators and microbial community dynamics were monitored in all four reactors to assess the relevance of the warning signals generated by the models.

Chapter 5 aims to answer question **Q2 Recovery from FVFA intoxication**.

Chapter 5: ***Microbial community dynamics in replicate anaerobic reactors exposed sequentially to increasing organic loading rate, free volatile fatty acids intoxication, and process recovery***

This chapter utilises the results of AD experiment **Exp1_FVFA_intoxication** and aims to answer the following sub-questions:

- *After a critical FVFA intoxication, is restoring more favourable environmental conditions for microbial growth sufficient to ensure process recovery?*
- *In AD reactors facing critical FVFA intoxication, are there persistent microbes that could play a key role in process recovery? If so, which ones?*
- *Is it useful to supply reactors exposed to critical FVFA intoxication with exogenous microbes to restore the process? If so, why and from which type of source?*

Approach: A process recovery strategy was applied to the overfed reactor described in **Chapter 3** and two other reactors that were exposed to an identical treatment since their inoculation. The recovery strategy did not involve any re-inoculation. Instead, after an 11-day starvation period, sodium hydroxide (NaOH) and sodium hydrogen carbonate ($NaHCO_3$) were introduced into the three intoxicated reactors to correct the pH back to neutrality and restore the buffer capacity of the slurry. The effect of the process recovery strategy was assessed using both metabolic and microbial monitoring.

Chapter 6 aims to answer question **Q3 Recovery from FAN intoxication**.

Chapter 6: ***Potential of acetic acid to restore methane production in anaerobic reactors critically intoxicated by ammonia, as evidenced by metabolic and microbial monitoring***

This chapter utilises the results of AD experiment **Exp2_FAN_intoxication** and aims to answer the following sub-questions:

- *After a critical FAN intoxication, is restoring more favourable environmental conditions for microbial growth sufficient to ensure process recovery?*
- *In AD reactors facing critical FAN intoxication, are there persistent microbes that could play a key role in process recovery? If so, are they the same as in reactors exposed to critical FVFA intoxication?*
- *Is it useful to supply reactors exposed to critical FAN intoxication with exogenous microbes to restore the process? If so, why and from which type of source?*

Approach: A process recovery strategy was applied to three FAN-intoxicated reactors resulting from the treatment described in **Chapter 4**. This strategy included, successively, a pH correction back to neutrality using acetic acid, washing out total ammonia with water, and re-inoculation with the effluents of the fourth (low-nitrogen input) reactor that was not exposed to FAN. The effect of the process recovery strategy was assessed using both metabolic and microbial monitoring.

Graphical presentation of the thesis

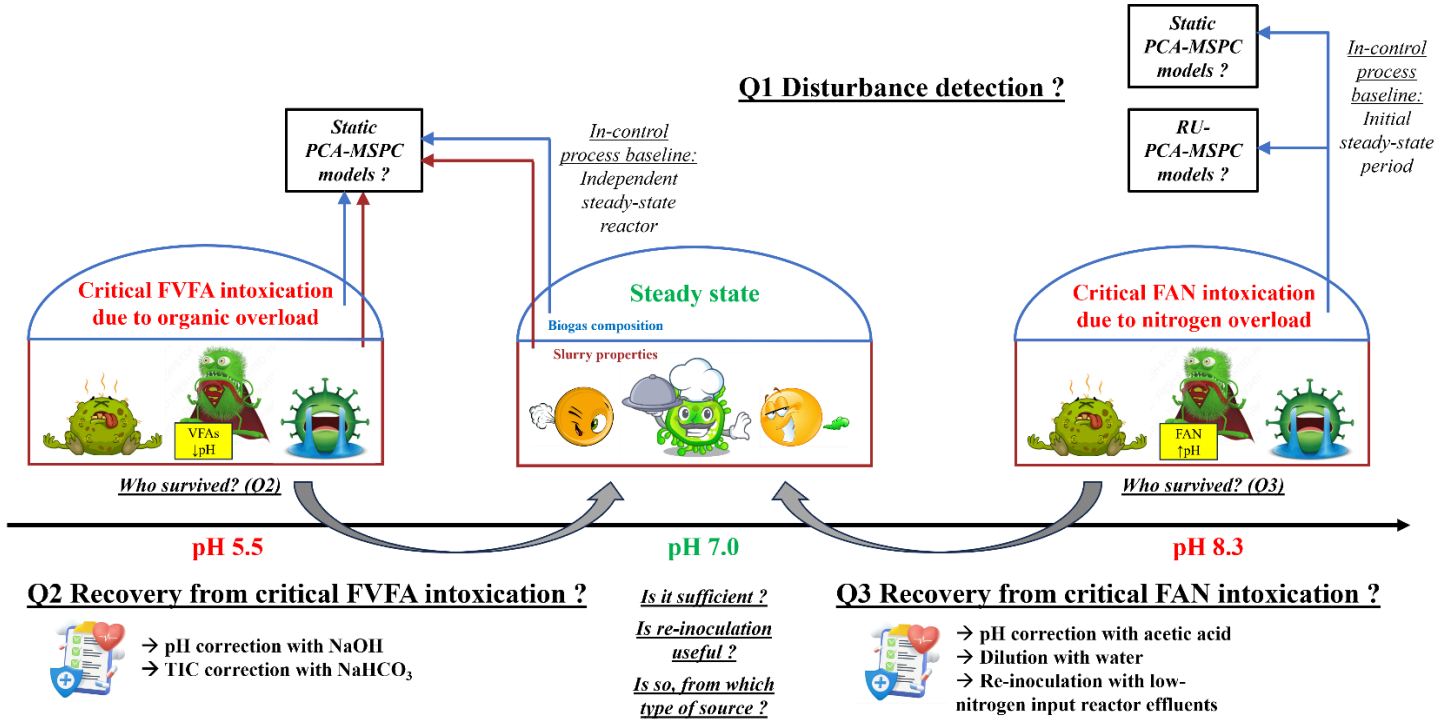

Figure 2.2. Approaches adopted to answer the research questions. LNR: low-nitrogen input reactor, PCA-MSPC: multivariate statistical process control based on principal component analysis, RU-PCA-MSPC: recursively updated PCA-MSPC, FAN: free ammonia nitrogen, FVFA: free volatile fatty acids, TIC: total inorganic carbon.

Chapter 3

Transfer of a static PCA-MSPC model from a steady-state anaerobic reactor to an independent anaerobic reactor exposed to organic overload

Adapted[4] from:

Lemaigre, S., Adam, G., Goux, X., Noo, A., De Vos, B., Gerin, P. A., & Delfosse, P. (2016). Transfer of a static PCA-MSPC model from a steady-state anaerobic reactor to an independent anaerobic reactor exposed to organic overload. *Chemometrics and Intelligent Laboratory Systems*, 159, 20–30. doi:10.1016/j.chemolab.2016.09.010

[4] Minor changes were made to some units and vocabulary terms to enhance consistency between the chapters of this thesis, particularly between **Chapters 3** and **5**, which both utilise results from the same experiment. Specifically, the term "free VFA intoxication" is now more frequently used to refer to the assessed AD process disturbance. Additionally, the comparison of the two PCA-MSPC models was more clearly emphasised in some section titles and figure captions. Finally, the original highlights were replaced by those provided at the beginning of this chapter, which are more relevant in the context of the thesis.

Context and contribution to the thesis

Free VFA intoxication resulting from organic overload frequently occurs in anaerobic digesters, leading to severe economic consequences for biogas plant managers. The primary challenge is the absence of low-cost, robust, and applicable online process monitoring methods to detect these disturbances early, before they reach a critical stage. Unlike the slurry in digesters, biogas has a simpler composition that can be easily analysed online using relatively low-cost and robust gas analysers. Multivariate statistical process control (MSPC) techniques could potentially leverage the dynamics of biogas composition for AD process monitoring.

In this context, **Chapter 3** of this thesis utilises results from AD experiment **Exp1_FVFA_intoxication**[5] to address the research question **Q1 Disturbance detection** (*Is a MSPC approach based on biogas composition useful for detecting the two main disturbances of the AD process?*).

Personal contribution:

- Equipped four 100-L reactors with components for heating, temperature regulation, and stirring (**Chapter 10**; Annex 1).
- Developed and assembled equipment for the automatic sampling and analysis of biogas produced by the reactors (**Chapter 10**; Annex 1).
- Defined the treatment and analytical protocol applied to the reactors.
- Conducted the experiment in the laboratory.
- Developed the software for biogas data acquisition and MSPC.
- Critically analysed and interpreted the models and results to lead the publication as first author.

[5] AD reactors progressively overfed until critical FVFA intoxication + Assessment of a process recovery strategy

Highlights

- Two static PCA-MSPC models were developed post-experimentally using data from a steady-state reactor as the in-control baseline, aiming to detect early signs of FVFA intoxication in an independent, progressively overfed reactor.
- Combining biogas composition with slurry-measured parameters in a single model proved challenging due to limited correlation.
- The first model, primarily based on slurry parameters, generated continuous false alarms.
- The second model, essentially based on biogas composition, identified out-of-control observations that aligned with early symptoms of FVFA intoxication.
- For the second model, biogas composition was more informative than slurry parameters for process disturbance detection.
- PCA-MSPC can effectively monitor AD performance using data from a separate, steady-state reactor.
- Biogas-based MSPC should be considered for AD process monitoring.

Abstract

A static multivariate statistical process control model based on principal component analysis (PCA-MSPC) was developed for an anaerobic reactor maintained in steady-state, joining the biogas composition (CH_4, CO_2, H_2) to the total solids (TS), volatile solids (VS), total inorganic carbon (TIC) and total ammonia nitrogen (TAN) contents of the slurry. The principal component analysis (PCA) highlighted a lack of correlation between the individual process variables (IPVs) measured in the slurry and the gas phase. The application of this model to the data set collected for an independent anaerobic reactor progressively overfed (with the same feedstock) from steady state to critical free volatile fatty acids (FVFA) intoxication did not allow evaluating its process status. A second static PCA-MSPC model was built for the steady-state reactor in excluding the TS and VS content of the slurry and was successfully transferred to the overfed reactor. The T_A^2 and SPE control charts built for the overfed reactor using this second model closely reflected its process status and delivered valuable warning signals approaching the FVFA intoxication. The gas phase composition (CH_4, CO_2, H_2) brought the main contribution to these warnings.

3.1. Introduction

In recent decades, anaerobic digestion (AD) of organic feedstocks for biogas production has become one of the most mature technologies to produce renewable energy from wet biomass (Ward et al., 2008). The life cycle assessment of the process shows an interesting environmental performance (Adelt et al., 2011) and allows the valorisation of organic co-products that would otherwise undergo elimination processes, leading to nutrient losses in the agricultural systems.

One of the main obstacles for further development of the AD sector is the difficulty in keeping the biological process in optimal and stable conditions of activity, especially in a context of organic waste that varies in price, composition, and availability. So far, various methods have been evaluated to monitor the AD process but none seem to be ideal (Madsen et al., 2011). These methods usually consist in measuring a set of variables expected to be characteristic of the process status (i.e., pH of the slurry, CH_4/CO_2 ratio of the biogas…) and interpreting the collected data for each parameter individually (Boe et al., 2010; Lay et al., 1998). However, since these variables reflect the behaviour of the microbial community of the reactor, they probably present a certain degree of correlation. An efficient tool for AD process monitoring should therefore benefit from the integration of information on how the measured parameters interact when the process is in control. A method to satisfy this condition is to monitor the reactors using multivariate statistical process control (MSPC) as an alternative to usual univariate approaches. MSPC techniques reduce the information contained within a potentially high number of individual process variables (IPVs) down to a low number of composite indexes through the application of statistical modelling.

Several studies assessed MSPC for monitoring of anaerobic biological processes such as biological anaerobic filters exploited for wastewater treatment (D. S. Lee et al., 2006) or batch AD reactors (Gunther et al., 2007; D. S. Lee et al., 2005). Nevertheless, very few studies focussed on (semi-)continuously fed AD reactors targeting biogas production. Attempts to exploit multivariate statistics for process monitoring of semi-continuous AD reactors mainly use near infrared spectroscopy (NIR) and aim to correlate the NIR response with common AD process indicators measured in the slurry (Jacobi et al., 2009; Krapf et al., 2013; Lomborg et al., 2009).

However, the main purpose of these studies was not to assess the potential of these parameters as IPVs exploited for MSPC but to find an alternative to their expensive and time-consuming traditional measurement methods (and to allow their online measurement). Reed et al. (2013) applied MSPC to evaluate the process status of a semi-continuous AD reactor on the basis of IPVs measured in the slurry, the feeding feedstock, and the effluents of the reactors but neglected to exploit the composition of the biogas produced. However, analysing the composition of the biogas offers multiple advantages compared to slurry analysis in terms of AD process monitoring, such as a potentially higher measurement frequency, the immediate availability of the results or the lower clogging risk inside the tubing. In recent years, electronic nose (e-nose) was the main method studied exploiting the gas phase for AD process monitoring through MSPC (Adam et al., 2015; Nordberg et al., 2000). In process monitoring using e-nose, the responses of low-selectivity gas sensors are used as IPVs to perform MSPC. If the technology is promising, the metal oxide semiconductor sensors (MOS) exploited in e-noses are subject to drift and need frequent replacement (Arshak et al., 2004). Nevertheless, specific sensors that are more robust and less subject to drift (if regularly calibrated) can be used to measure the concentration of the biogas in its major compounds (CH_4, CO_2, H_2 and H_2S). To our knowledge, exploiting these parameters for AD process monitoring through MSPC was never attempted. However, a MSPC model joining parameters commonly measured in the slurry to the biogas composition in its major compounds could present interesting potential for AD process monitoring and deserves investigation.

MSPC involves the construction of control charts that represent the progress over time of the process status. In these control charts, the value of an index is compared to a control limit that defines the index value above which the process is considered as out-of-control. Control charts based on the Hotelling's T^2 index are nowadays the basic tools exploited for MSPC and numerous descriptions of the technique can be found in the literature (MacGregor, 1995; Mason & Young, 2002). For processes characterized by two or more highly correlated IPVs and/or by a large set of IPVs, a common procedure to reduce the dimensionality of the problem is to perform a principal components analysis (PCA). In PCA-MSPC, a limited number A of principal components is used to compute the T^2 index. The T^2 index calculated on this basis (T_A^2) can express the deviation in the IPVs that are the most meaningful in

describing a process (Kourti & MacGregor, 1995). Since the T_A^2 index only describes the variation amplitude of the IPVs in the "plane" defined by the *A* PCs retained in the model, a complementary index, squared prediction error (SPE), is combined to the T_A^2 to quantify the residuals. The pair of control charts based on the T_A^2 and SPE indexes is an effective tool to monitor multivariate processes. The basic way to implement PCA-MSPC, called *static* PCA-MSPC, consists in calculating the model parameters on the basis of data collected for a period during which the process is judged stable. PCA-MSPC is easy to implement and requires only a few computations once the model is defined (the model is not updated after it has been built). In addition, static PCA-MSPC allows the easy computation of contribution plots that provide valuable information about the relationship between each out-of-control process observation detected by the T_A^2 and SPE control charts and the IPVs (Kourti, 2005; J. M. Lee et al., 2004; Westerhuis et al., 2000). Nevertheless, static PCA-MSPC is limited in the case of processes that demonstrate a drift of their stable behaviour such as AD, which is affected by the permanent evolution of the microbiome or accumulation of chemical compounds in the slurry. However, a reactor maintained in a steady-state over a long period could allow measuring of the relationship existing between the IPVs for a large diversity of in-control process situations. On this basis, a static PCA-MSPC model integrating exhaustive information on the in-control process could be built and transferred to independent reactors to evaluate their process status.

The main objective of the present paper was to assess whether a static PCA-MSPC model joining the biogas composition to parameters measured in the slurry and built using an AD reactor maintained in a steady-state could be transferred to an independent AD reactor progressively overfed until free volatile fatty acids (FVFA) intoxication and reflect its process status. The experiment described in this study focussed on large scale semi-continuous lab reactors expected to be comparable to real-scale co-digestion digesters regarding the complexity of the feedstock and the hydraulic retention time (HRT).

3.2. Materials and methods

3.2.1. Anaerobic digestion

The experiment was performed using two stainless steel tank reactors of 100L working volume (**Figure 3.1**), continuously stirred at 1rpm, with 25L headspace volume connected to a 10L gas bag (Tecobag, Tesseraux, Germany) to equilibrate the pressure (feeding, gas sampling). Tygon tubing (VWR International, USA) was used for all the gas connections.

Each reactor was inoculated with 100 kg of anaerobic sludge [total solids (TS): 0.013 ± 0.0027 gTS gFM^{-1}, volatile solids (VS): 0.542 ± 0.042 gVS gTS^{-1}] collected in the mesophilic anaerobic reactor of a wastewater treatment plant (Schifflange, Luxembourg). The reactors were first acclimated to sugar beet pulp as mono-feedstock for 16 months (**Chapter 5**; Goux et al., 2015). The experimental period described in the present paper starts with the last 14 days of the acclimation period and spread over 63 days. The dry sugar beet pulp described by Adam et al. (2013) was selected for its complex composition (**Table 3.1**), as compared to pure substrates (i.e., glucose), in order to offer to the microbial community a growth environment comparable to a real scale co-digestion reactor. The balanced composition of the feedstock was also expected to avoid deficiencies of the microbial consortium concerning essential elements and to promote adequate microbial turn-over. The pulps were manually introduced in the reactors 5 consecutive days a week, following a semi-continuous feeding scheme. The pulps were suspended in with tap water at 37°C to adjust the HRT. The digestion was performed in the mesophilic temperature range at 37°C.

During the last 14 days of the acclimation period, both reactors were first submitted to monitoring under cautious steady-state organic loading rate (OLR) of 1.6 grams of VS per litre of slurry and per working day (gVS L_{slurry}^{-1} day^{-1}), i.e., 1.14 g of VS per litre of slurry and per day on a weekly average, with HRT maintained at 28 days. After this period, while the feeding regime of the reference reactor was left unchanged (steady-state reactor SSR), the OLR of the second, overfed reactor (OR), was increased weekly by increments of 0.4 $gVS.L_{slurry}^{-1}.day^{-1}$, with HRT kept at 28 days. A 28-day HRT was expected to ensure efficient digestion of sugar beet pulp, while avoiding washout of methanogenic microbial populations.

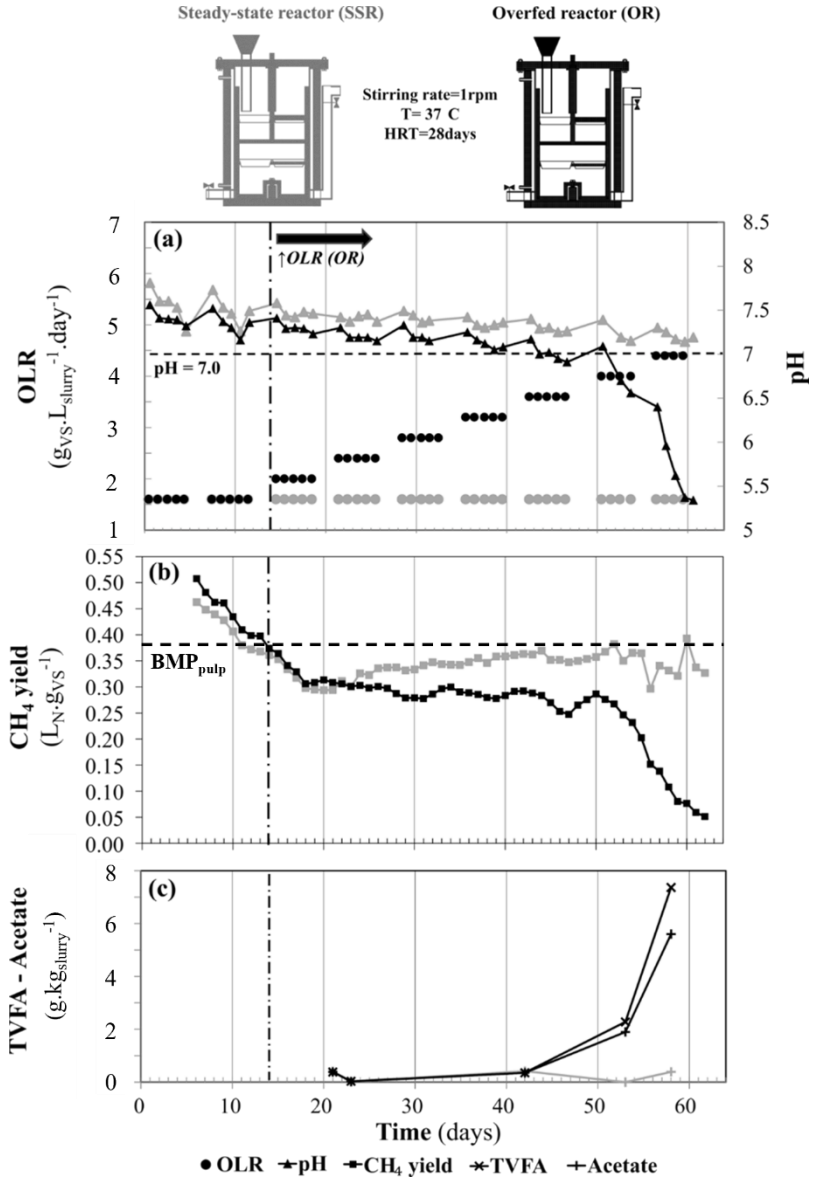

Figure 3.1. Progress over time of the 3 selected process stability indicators (pH, CH_4 yield, volatile fatty acids content in the slurry) for the steady-state reactor (SSR, grey) and the overfed reactor (OR, black): (a) organic loading rate (OLR) and pH; (b) methane yield; (c) total volatile fatty acids (TVFA) and acetate concentrations in the slurry.

Table 3.1. Composition of the sugar beet pulp pellets used to feed the 2 anaerobic reactors.

	Dry basis (%)	As fed (%)
Total solids		86.86
Moisture		13.14
Volatile solids	92.1	79.96
Ash	7.94	6.90
Protein	8.29	7.20
Crude fibre	16.97	14.74
Acid detergent fibre (ADF)	26.68	23.17
Total digestible nutrients (TDN)	69.40	60.28
Fat	1.09	0.95
Nitrogen free extract (NFE)	66.09	57.41
Calcium	1.00	0.87
Phosphorus	0.07	0.06
Potassium	0.56	0.49
Reducing sugars	2.60	2.26
Sucrose	8.96	7.78
Total sugars as invert (TSI)	8.23	7.15

Adapted from Adam et al. (2013).

3.2.2. Analytical monitoring

The anaerobic digestion process was monitored through hourly biogas analyses, daily pH analyses and weekly analyses for other properties of the slurry.

3.2.2.1. Biogas monitoring

The biogas passed through a cooling unit at ~8°C at the outlet of the reactor to remove excess water vapour. The biogas production of each reactor was measured by a drum-type wet gas meter (TG-0.5, Ritter, Germany) and was normalized to normal temperature and pressure conditions (0°C ; 1025hPa). For gas composition analysis, the headspace gas was recirculated every hour for 3 minutes through CH_4 and CO_2 non-dispersive infrared sensors (Dynament, UK). The H_2 content was also measured for each measurement cycle. A biogas volume of 600mL was pumped and mixed with 300mL of air measured by a mass flow meter (AWM series, Honeywell, USA). The gas mix was pumped to an H_2 MOS sensor (RKI Instruments Inc., USA) including a molecular sieve to warrant selectivity to hydrogen molecules. The feedstock to CH_4 conversion yield [$L_N.gVS^{-1}$] was calculated for each day using the total CH_4 production measured for the seven preceding days divided by the total mass of feedstock introduced over the same period. The seven-day window was selected in accordance with the frequency of the OLR increase applied to the OR.

3.2.2.2. Slurry monitoring

The total inorganic carbon (TIC), total ammonia nitrogen (TAN), total solids (TS), volatile solids (VS) and volatile fatty acids (VFA) contents in the slurry and its pH were measured using the analytical methods described in **Chapter 5** (Goux et al., 2015). The pH was measured on a daily basis while the TIC, TAN, TS and VS contents were measured weekly (on Mondays).

3.2.2.3. Individual process variables and process stability indicators

Seven of the measured variables (**Table 3.2**) related to gas and slurry compositions were used as *IPVs* to build the PCA-MSPC models. The pH, the VFA individual concentrations in the slurry and the CH_4 yield were not included as IPVs to build the models, but used as *process stability indicators* to assess the adequacy of

the models, i.e., comparing the alarm signals provided by the models with the ability of the microbiome to convert the introduced feedstock into CH_4.

Table 3.2. Individual process variables measured in the biogas and the slurry, used for multivariate statistical process control.

	Individual process variable	Units	Frequency of measurement
Gas phase	CH_4	%vol	h^{-1}
	CO_2	%vol	h^{-1}
	H_2	ppmv	h^{-1}
Slurry	TS	$gTS.gFM^{-1}$	$week^{-1}$
	VS	$gVS.gTS^{-1}$	$week^{-1}$
	TIC	$L_{CO2}.L_{slurry}^{-1}$	$week^{-1}$
	TAN	$g_{N\text{-}NH4}.L_{slurry}^{-1}$	$week^{-1}$

3.2.3. Transfer of static PCA-MSPC models from the SSR to the OR

For each model built, the data set collected for the SSR, maintained at a cautious OLR, was used to define the in-control process baseline and to calculate the static PCA-MSPC model parameters. The model was then transferred to the OR in applying the model parameters to its data set. In this aim, a T_A^2 control chart and its corresponding SPE control chart were built as well as their corresponding contribution plots.

3.2.3.1. Data pre-processing

Since the IPVs were not measured at the same frequency in the gas phase and the slurry and that each sample must contain information for the full set of IPVs, values had to be attributed for the missing data. An overview of modern methods for gap filling in incomplete data sets can be found in Baraldi & Enders (2010). Given the continuous nature of the studied process and expected continuous evolution of the IPVs, linear interpolation between adjacent available measurements was selected as a reasonable compromise to attribute a value to each missing data. This method was applied to the data corresponding to TS, VS, TIC and TAN contents in the slurry, which were measured on a weekly basis.

3.2.3.2. Definition of the in-control process baseline based on the SSR data set

For each model built, the outliers were first purged using the iterative method described by Mason & Young (2002) in which several changes required by the PCA were included:

(a) Each IPV was centred and scaled to unit variance.

(b) PCA was performed and the loading vectors and eigenvalues were computed.

(c) The number A of principal components (PCs) retained in the model was calculated using the eigenvalue-one rule (Valle et al., 1999).

(d) For each sample, the T_A^2 index was calculated on the basis of the scores obtained for the A first PCs using:

$$T_A^2 = \sum_{i=1}^{A} \frac{t_i^2}{s_{t_i}^2} \tag{3.1}$$

where t_i and s_{t_i} are, respectively, the score calculated on the i[th] PC and the standard deviation related to this PC. The T_A^2 upper control limit (UCL) was calculated according to Tracy et al. (1992):

$$UCL = \left[\frac{(m-1)^2}{m}\right] B\left(\alpha; \frac{A}{2}, \frac{m-A-1}{2}\right) \tag{3.2}$$

where α is the significance level (set to 0.01), A is the number of PCs retained in the model, m is the number of samples included in the data set and $B\left(\alpha; \frac{A}{2}, \frac{m-A-1}{2}\right)$ is the upper $(1-\alpha)$ quantile of the beta distribution with $\left(\frac{A}{2}, \frac{m-A-1}{2}\right)$ degrees of freedom.

(e) The value of the SPE index was calculated for each sample using:

$$SPE = \sum_{i=1}^{p} (\hat{x}_i - x_i)^2 \tag{3.3}$$

where p is the number of IPVs, x_i is the observed value for the i[th] IPV and $\hat{x}_i$ is the corresponding value computed using the PCA model. The corresponding control limit SPE_{lim} was calculated according to Kourti & MacGregor (1995) with a significance level set to 0.01

(f) The samples corresponding to out-of-control values for one of the two indices were considered as outliers and eliminated of the SSR data set.

The iterative operation was then repeated from step (a) until no outlier was detected anymore for the SSR. The parameters characterizing the stable process were finally calculated on the basis of this purged data set: average value/standard deviation of each IPV and loading vectors/eigenvalues associated with each PC.

3.2.3.3. Application of the models to the OR data set

For each model built, each IPV was first centred and scaled using the average value and standard deviation calculated for the in-control process on the basis of the SSR data set. For each sample of the OR data set, the scores corresponding to the *A* retained PCs were calculated using the loading vectors computed on the basis of the SSR data set and the T_A^2 index was computed using relation (3.1). On this basis, the T_A^2 control chart was built with its UCL calculated according to Tracy et al. (1992):

$$UCL = \left[\frac{A(m+1)(m-1)}{m(m-A)}\right] F(\alpha; A, m-A) \tag{3.4}$$

where α is the significance level and $F(\alpha; A, m-A)$ is the upper $(1-\alpha)$ quantile of the Fisher distribution with $(A, m-A)$ degrees of freedom.

For each out-of-control observation for the OR by the T_A^2 control chart during the experiment, the contribution of each IPV was computed using the method described by Kourti (2005). Briefly, the scores obtained for the *A* PCs were first compared to an individual control limit expressed by:

$$conf_i = \pm\sqrt{\lambda_i}.t(m-1, \alpha) \tag{3.5}$$

where α is the significance level, λ_i is the eigenvalue associated to the PC *i* and $t(m-1, \alpha)$ is the probability point on the single sided t-distribution with $m-1$ degrees of freedom and area $\frac{\alpha}{2}$. For the $K \leq A$ scores excessing this control limit, individual contributions were computed using:

$$cont_{i,j}^{T2} = \frac{t_i}{s_{t_i}^2} l_{i,j} x_j \tag{3.6}$$

where $l_{i,j}$ is the loading of the IPV *j* for the PC *i*. The individual contributions were set equal to zero if negative. Finally, the "overall average contribution" was computed for each IPV using:

$$CONT_j^{T2} = \sum_{i=1}^{K} \left(cont_{i,j}^{T2}\right) \tag{3.7}$$

For each sample of the OR data set, the SPE index was computed using relation (3.3) and the SPE control chart was built. Finally, the corresponding contribution plot has been computed for each IPV. The contribution of a given IPV is expressed by the squared value of the residual measured for this variable:

$$CONT_{x_i}^{SPE} = (\hat{x}_i - x_i)^2 \quad (3.8)$$

All control limits were calculated using a significance level $\alpha = 0.01$, corresponding to a 99% confidence level. All calculations were performed using R software (R Core Team, 2013) and the package MSQC v1.0.1 (Santos-Fernández, 2012).

3.3. Results and discussion

3.3.1. Anaerobic digestion

Figure 3.1 shows the progress over time of the three process stability indicators (pH, CH_4 yield and VFA individual concentrations) for both reactors during the 64-day experiment.

The SSR, fed with fixed and low OLR (1.6 $gVS.L_{slurry}^{-1}.day^{-1}$; HRT of 28 days), showed no signs of process disturbance. The pH remained permanently above 7.0 (**Figure 3.1**a) and the highest value measured in its slurry for the TVFA content was 0.42 $g.kg_{slurry}^{-1}$ at day 42 (**Figure 3.1**c). Only acetate was detected during the whole experiment. The CH_4 yield of the SSR remained permanently higher than that of the OR (**Figure 3.1**b). For the OR, the three process stability indicators showed an initial period of process stability (from day 14 to day 41) during which their values remained close to those observed for the SSR. From day 42 to 48 (OLR = 3.6 $gVS.L_{slurry}^{-1}.day^{-1}$), the pH dropped for the first time in the acidic range (**Figure 3.1**a), reached a minimal value of 6.9 at day 46 and re-increased above neutrality during the end-of-week interruption of the feeding. This transient pH drop was concomitant with a transient decrease of the CH_4 yield (**Figure 3.1**b). From day 49 to 55 (OLR = 4.0 $gVS.L_{slurry}^{-1}.day^{-1}$), the pH value dropped again in the acidic range but the end-of-week interruption of the feeding was not enough to allow the pH value to increase above neutrality (**Figure 3.1**a). A significant increase of the TVFA concentration was also detected at day 53 (2.3 $g.kg_{slurry}^{-1}$ including 87% of acetate), indicating that the microbiome was not able to efficiently convert the feedstock into methane at such a

high OLR value (**Figure 3.1**c). A continuous decrease of the CH_4 yield was observed along the week, which confirmed the irreversible process disturbance. From day 56 (OLR = 4.4 $gVS.L_{slurry}^{-1}.day^{-1}$), the process stability indicators showed evidence of a complete collapse of the process, presenting the symptoms of a critical FVFA intoxication. Indeed, the pH value dropped below 5.5 at day 60 (**Figure 3.1**a) and the methane production almost stopped (**Figure 3.1**b). VFA accumulated in the slurry (**Figure 3.1**c) up to 7.4 $g.kg_{slurry}^{-1}$, essentially as acetate (5.6 $g.kg_{slurry}^{-1}$). Concentrations for the longer chain VFA were respectively, 1.1, 0.12, 0.36, 0.16, 0.012 and 0.016 $g.kg_{slurry}^{-1}$ for propionate, isobutyrate, butyrate, isovalerate, valerate and caproate. From day 64, the biogas production of the OR was not sufficient to allow analyses. Five days without feeding did not allow the process to recover. No biogas was produced despite the high amount of accumulated organic matter available in the slurry, confirming the critical FVFA intoxication.

3.3.2. Validation of the SSR data set as in-control process baseline

After data pre-processing, the raw SSR data set included 2483 time points, each of them including one value for each of the seven IPVs. Results of the PCA are summarized in **Table 3.3** and **Figure 3.2**. Two PCs were retained in the model according to the eigenvalue-one rule (**Figure 3.2**a,b). The variance explained by these two PCs equalled 74.9% and 81.6% before and after outliers purge, respectively (**Table 3.3**). Four purge cycles were necessary to purge 121 outliers from the 2483 time points (**Table 3.4**). Outliers purge was essentially based on SPE values exceeding control limit whereas T_A^2 value had minor impact on the purge operation. Regarding the loadings of the two first PCs, the IPVs measured in the slurry contributed principally to the first PC (explaining 53.3% and 54.9% of the variance before and after outliers purge, respectively) (**Figure 3.2**c,d). Positive correlation was clearly detected between the TS, TIC and TAN contents of the slurry while its VS content appeared negatively correlated with these IPVs. The CH_4 and CO_2 contents in the gas phase showed only minor impact on the scores computed for the first PC but major impact on the scores computed for the second one. The negative correlation between these two IPVs was clearly detected by the PCA and the outliers purge appeared to amplify it. The variation related to the H_2 content of the gas phase was poorly captured by the two PCs retained in the model. The H_2 concentration in the gas phase mainly

contributed to the second PC before the outliers purge but the largest part of its contribution was transferred on the first PC after the outliers purge.

Table 3.3. Importance of each principal component calculated on the basis of the in-control data set (steady-state reactor) before and after the outliers purge (full set of individual process variables included in the model).

		PC1	PC2	PC3	PC4	PC5	PC6	PC7
Raw SSR data set	Eigenvalues	3.728	1.512	0.934	0.475	0.225	0.101	0.025
	Proportion of Variance	0.533	0.216	0.133	0.068	0.032	0.015	0.004
	Cumulative Proportion	0.533	0.749	0.882	0.950	0.982	0.996	1.000
Purged SSR data set	Eigenvalues	3.844	1.868	0.640	0.375	0.195	0.052	0.028
	Proportion of Variance	0.549	0.267	0.091	0.054	0.028	0.007	0.004
	Cumulative Proportion	0.549	0.816	0.907	0.961	0.989	0.996	1.000

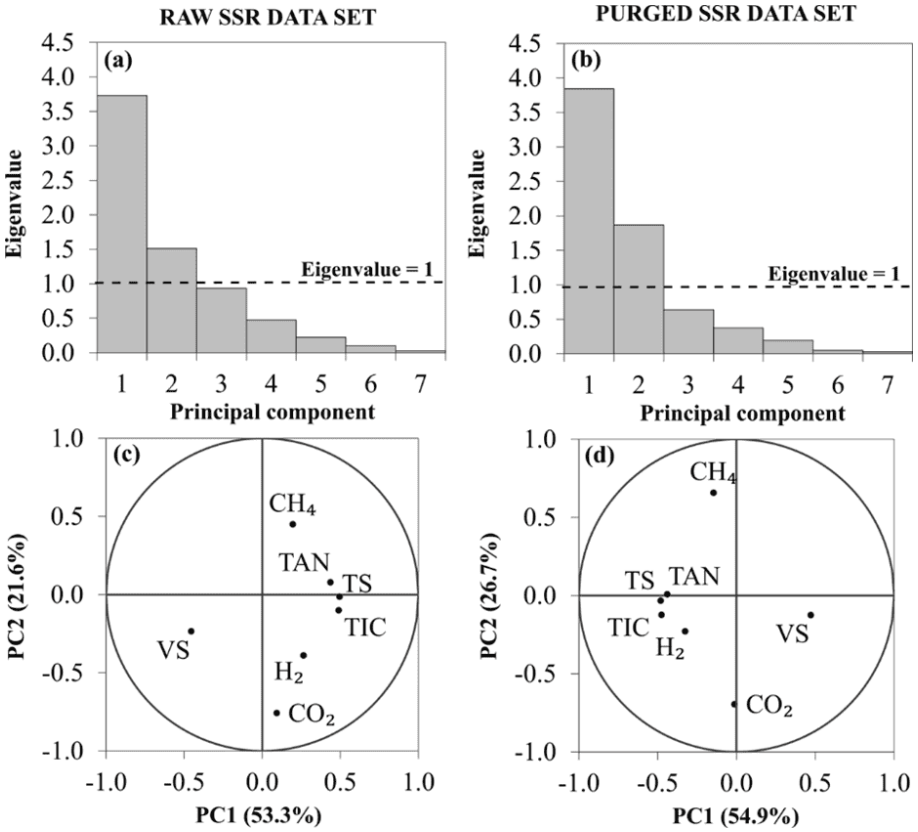

Figure 3.2. Scree plots of the eigenvalues resulting from the principal component analysis performed on the steady-state reactor data set exploited to define the in-control process baseline (full set of individual process variables included in the model): (a) raw data set; (b) data set purged of outliers. Loading plots for the 2 principal components retained in the model: (c) raw data set; (d) data set after outliers purge.

Table 3.4. Number of outliers eliminated from the in-control data set (steady-state reactor) during its iterative outliers purge and reason for their removal (full set of individual process variables included in the model).

Cycle	Number of outliers purged	T_A^2 > UCL	SPE > SPE_{lim}
1	30	2	28
2	73	0	73
3	14	0	14
4	4	0	4

T_A^2: Hotelling's T^2 index (A=2 principal components)
UCL: upper control limit of the T_A^2 control chart
SPE: squared prediction error index
SPE_{lim}: control limit of the SPE control chart

Figure 3.3 illustrates the effect of the outliers purge on the scores obtained for the two retained PCs and the centred and scaled IPVs. The largest part of the 121 outliers purged, concerns samples collected towards the end of the experiment, between day 60 and day 64. It must be highlighted that the main IPV causing the outlier removal was the H_2 concentration in the gas phase (**Figure 3.3**g,h). Indeed, during this period, a sensor-memory effect may have caused unrealistically high H_2 measurements for the SSR due to saturation of the sensor cell, also exposed to the high H_2 content present in the biogas of the OR during a measurement cycle. It therefore justifies the intense iterative purge method exploited in this study. **Figure 3.3**g,h also highlights a linear progress of the IPVs measured in the slurry that was mainly captured by the PC1 (**Figure 3.3**e,f). Oppositely, the IPVs measured in the gas phase appear clearly related to the daily feeding scheme applied to the reactor, and mainly affected the progress of the scores computed for the PC2 (**Figure 3.3**e,f).

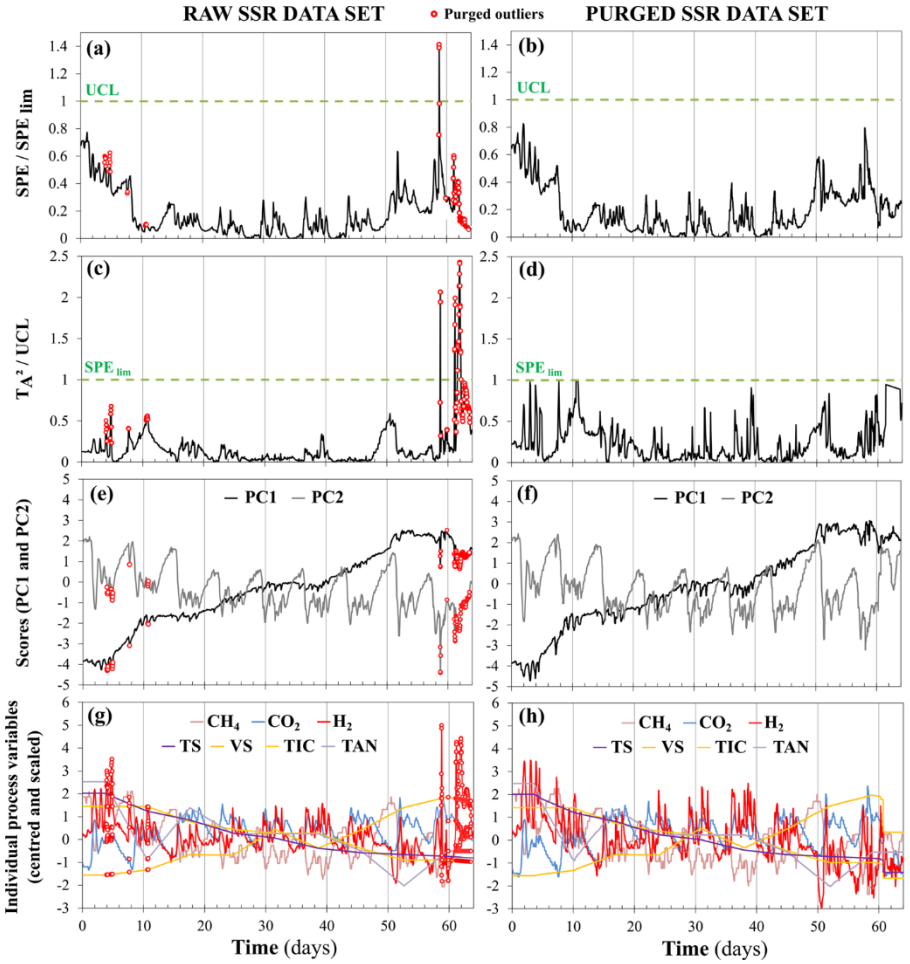

Figure 3.3. Impact of the outliers purge on the steady-date reactor data set exploited to define the in-control process baseline (full set of individual process variables included in the model): (a, b) T_A^2 index; (c, d) squared prediction error (SPE) index; (e, f) scores on the 2 retained principal components; (g, h) centred and scaled individual process variables. The T_A^2 and the SPE are expressed as a ratio between the index value and its upper control limit (UCL and SPE_{lim}, respectively).

These results express a weak correlation between the IPVs measured in the slurry and in the gas phase. In addition, the PCA model appears to give high weight to the IPVs measured in the slurry compared to those measured in the gas phase. Nevertheless, the static PCA model built on the basis of this combination of IPVs detected only few outliers (4.9%) indicating that the SSR data set only included a minor amount of time points presenting unusual characteristics. These results are in accordance with the good process stability showed by the three process stability

indicators. Consequently, the data set measured for the SSR was judged as a proper baseline to define the in-control process status.

3.3.3. Transfer of a first static PCA-MSPC model from the SSR to the OR (full set of IPVs)

The control chart of the SPE index computed for the OR is illustrated in **Figure 3.4**a, together with the pH value as process stability indicator. The control limit SPE_{lim} equalled 5.45 (α=0.01).

The chart shows that the largest part of the samples presented a SPE value greater than the control limit (**Figure 3.4**a), even in the periods during which the process remained stable (until day 42). It demonstrates that the static PCA model built for the SSR using the complete set of IPVs could not be transferred to the OR data set. Therefore, the T_A^2 index based on the two PCs retained in the model could not be used to monitor the process status of the OR and its control chart was not presented.

The contribution of each IPV to the out-of-control values of the SPE index is illustrated in **Figure 3.4**b. It can be noted that the TS and VS content in the slurry brought the main contribution to the out-of-control SPE values observed in the period during which the process remained stable for the OR, i.e., before the start of its overfeeding and during its stable process period. The progress over time of the seven (centred and scaled) IPVs is illustrated in **Figure 3.5** for the two reactors. For the initial acclimation period and for the period during which the process remained stable for the OR, only minor difference was observed between the two reactors regarding the CH_4 and CO_2 concentration in their gas phase (**Figure 3.4**a,b). Oppositely, an important difference between the TS and VS content measured for the OR and the average value measured for the SSR data set could be highlighted during the same period (**Figure 3.4**d,e). Since the model attributed high weight to the IPVs measured in the slurry compared to these measured in the gas phase, this difference caused the failure of the model transfer from the SSR to the OR, illustrated by the permanently out-of-control SPE values detected for the OR. It can be noted that the TIC and TAN content measured in the slurry for the OR during its acclimation period and its stable process period remained very close of the average measured for the SSR data set (**Figure 3.5**f,g), explaining their minor contribution in the out-of-control SPE values detected for the OR during these periods (**Figure 3.4**b).

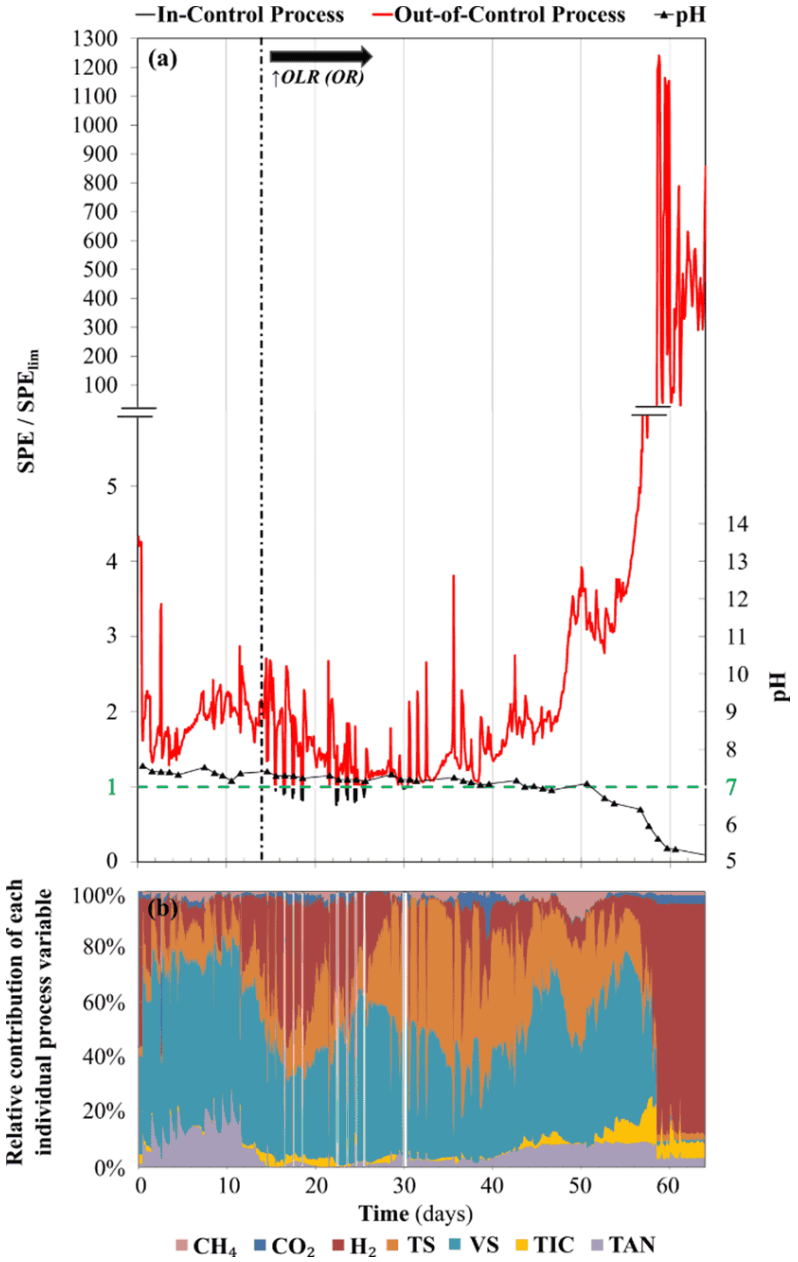

Figure 3.4. Transfer of a first static PCA-MSPC model (full set of individual process variables included) to the overfed reactor (OR) after having built the model using the steady-state reactor data set to define the in-control process baseline: a) Squared prediction error (SPE) control chart. The SPE is expressed as a ratio between the index value and its control limit (SPE_{lim}). The levels corresponding to $SPE/SPE_{lim}=1$ and pH=7.0 are represented as a common horizontal line on the chart. b) Relative contribution of each individual process variable to the out-of-control process observations detected by the SPE control chart. OLR: organic loading rate.

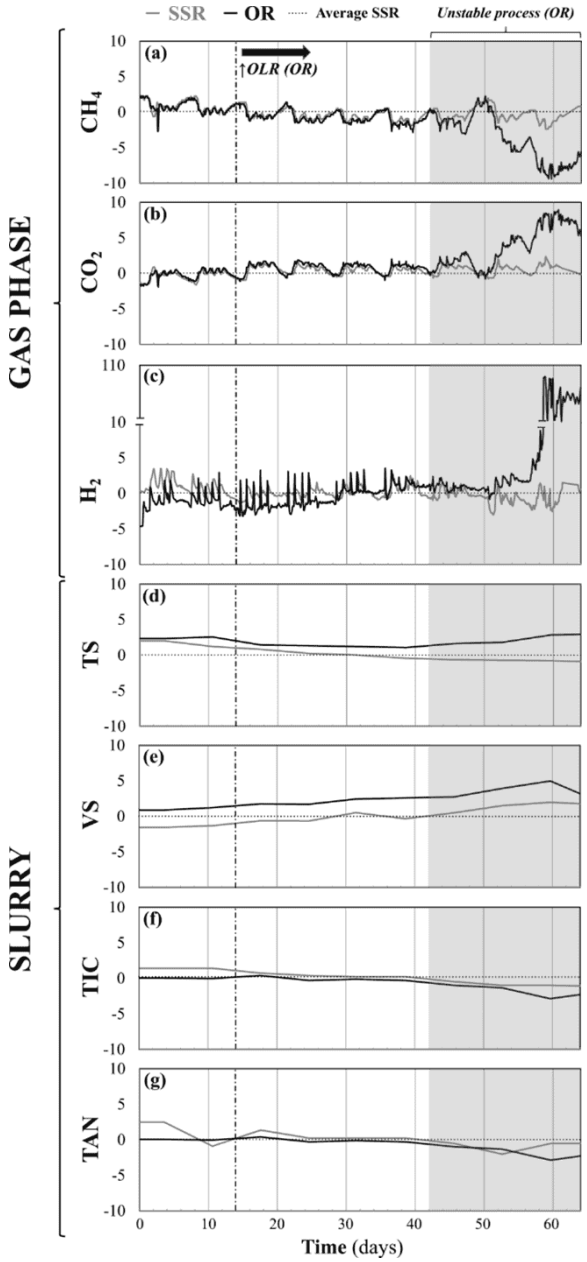

Figure 3.5. Progress over time of the observed (centred and scaled) values of each individual process variable (IPV) for the steady-state reactor (SSR, grey) and the overfed reactor (OR, black): (a) CH_4 concentration in the gas phase; (b) CO_2 concentration in the gas phase; (c) H_2 concentration in the gas phase; (d) total solids content in the slurry (TS); (e) volatile solids content in the slurry (VS); (f) total inorganic carbon content in the slurry (TIC); (g) total ammonia nitrogen content in the slurry (TAN). The zero value expressing the average measured for the steady-state reactor is represented as a dotted line for each IPV. OLR: organic loading rate.

3.3.4. Transfer of a second static PCA-MSPC model from the SSR to the OR (TS and VS content of the slurry excluded)

A second static PCA-MSPC model was built on the basis of the SSR data set without including the TS and VS content of the slurry among the IPVs. Only CH_4, CO_2 and H_2 content of the gas phase and TIC and TAN content of the slurry were therefore exploited.

Results of the PCA performed on the purged SSR data set are summarized in **Figure 3.6**a,b. As for the first model, two PCs were retained according to the eigenvalue-one rule (**Figure 3.6**a). The variance explained by the model is similar compared to the first model (81.6% vs 82.2%) but is more balanced between the two PCs retained in the model (**Figure 3.2**a vs **Figure 3.6**a) while the low significance of the un-retained PCs is clearer. The low correlation between the IPVs measured in the slurry and in the gas phase remains highlighted by the PCA. Nevertheless, the variance of the H_2 content in the gas phase appears more clearly captured by the model (PC1).

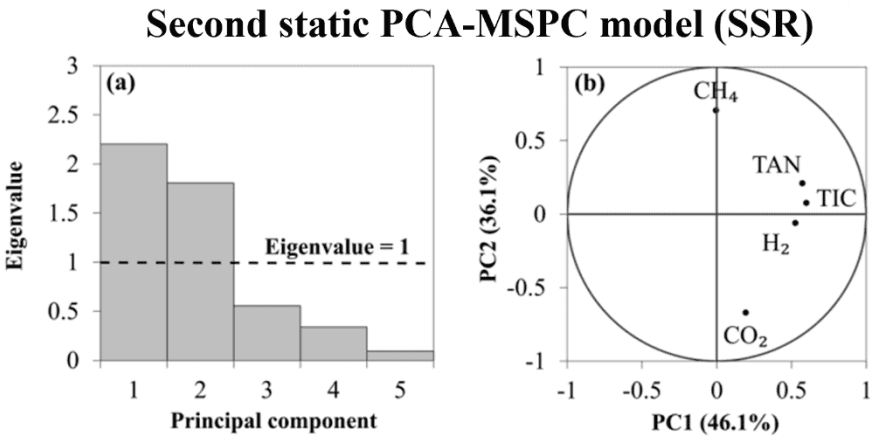

Figure 3.6. Second static PCA-MSPC model built for the steady-state reactor data set using only the biogas composition (CH_4, CO_2, H_2), the total inorganic carbon (TIC) content of the slurry and its total ammonia nitrogen (TAN) content as individual process variables (data set purged of outliers): (a) scree plots of the eigenvalues; (b) loading plot for the 2 principal components retained in the model.

This second static PCA-MSPC model was applied to the OR data set. The control chart of the SPE index is illustrated in **Figure 3.7**a, together with the pH value as process stability indicator. The contribution of each IPV to the out-of-control values

of the SPE index is illustrated in **Figure 3.7**c. The control limit SPE_{lim} equalled 4.53 (α=0.01).

For the acclimation period and the period during which the process remained stable (until day 42), the SPE index remained essentially in its in-control range (SPE > SPE_{lim} for 10.8% of the time points). The out-of-control values detected by the SPE control chart were essentially transient and mainly due to the H_2 content of the gas phase (**Figure 3.7**c). These transient out-of-control SPE values are attributable to the H_2 concentration peaks observed in the gas phase of the OR after each new feedstock introduction (**Figure 3.5**c).

These results confirm that the difference between the two reactors regarding the TS and VS content of their slurry caused the failure of the model transfer when exploiting the full set of IPVs.

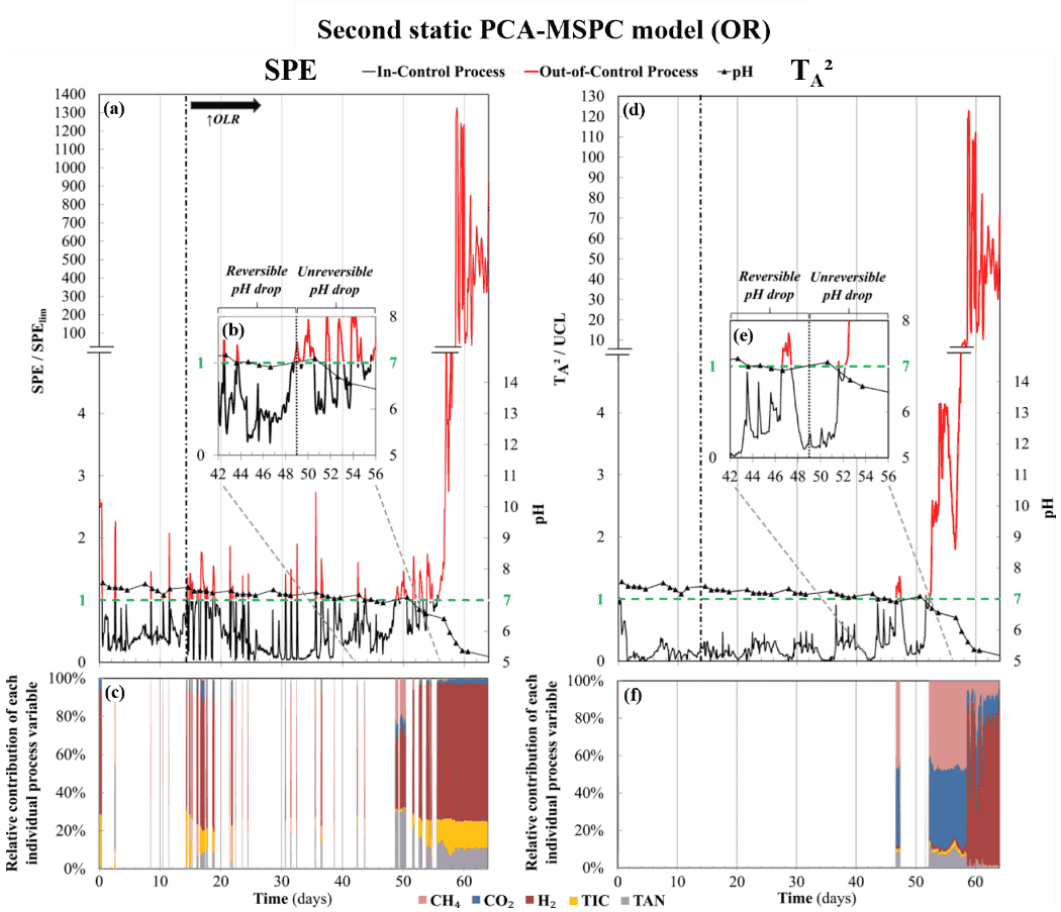
Second static PCA-MSPC model (OR)
SPE
In-Control Process
Out-of-Control Process
pH
T_A^2
(a)
↑OLR
(b)
Reversible pH drop
Unreversible pH drop
(c)
(d)
(e)
(f)
SPE / SPE$_{lim}$
T_A^2 / UCL
pH
Relative contribution of each individual process variable
Time (days)
CH$_4$ CO$_2$ H$_2$ TIC TAN

Figure 3.7. Transfer of a second static PCA-MSPC model (TS and VS content of the slurry excluded) from the steady-state reactor (SSR) to the overfed reactor (OR): (a) squared prediction error (SPE) control chart; (b) detail of the period corresponding to the first occurrence of acidic pH values for the SPE control chart; (c) relative contribution of each individual process variable to the out-of-control observations detected by the SPE control chart; (d) T_A^2 control chart; (e) detail of the period corresponding to the first occurrence of acidic pH values for the T_A^2 control chart; (f) relative contribution of each individual process variable to the out-of-control observations detected by the T_A^2 control chart. The SPE and T_A^2 are expressed as a ratio between the index value and their control limit (UCL and SPE_{lim}, respectively). The levels corresponding to $T_A^2/UCL=1$, $SPE/SPE_{lim}=1$ and pH=7.0 are represented as a common green dotted line on the charts. OLR: organic loading rate.

3.3.5. Performance of the second PCA-MSPC model for the evaluation of the OR process stability

The control chart of the T_A^2 index computed for the OR using the second model (TS and VS not included among the IPV) built on the basis of the purged SSR data set is presented in **Figure 3.7**d, together with the pH value as process stability indicator. The value of the UCL equalled 9.23 (α=0.01).

From day 14 to day 41, the progression of the T_A^2 index (**Figure 3.7**d) mainly reflected the feeding pattern applied to the reactors (feeding for 5 consecutive days + rest for 2 days): for each feeding day, a peak of the T_A^2 index was observed while during each end-of-week interruption of the feeding, the value of the index dropped. Nevertheless, the T_A^2 index remained permanently under its control limit, which is in good accordance with the process stability detected during this period for the OR on the basis of the three process stability indicators. From days 42 to 48 (OLR = 3.6 $gVS.L_{slurry}^{-1}.day^{-1}$), the T_A^2 control chart detected marked out-of-control process observations at day 46, following the last feeding of the week (**Figure 3.7**e). Nevertheless, the consecutive interruption of the feeding allowed the T_A^2 to drop back in its in-control range at day 48. This transient out-of-control T_A^2 value, validated by the in-control value simultaneously observed for the SPE index (**Figure 3.7**b), was in good accordance with the reversible process disturbance observed for the OR during this week. Especially, the out-of-control T_A^2 value was concomitant to the transient pH value observed for the OR under the neutrality limit at day 46. From days 49 to 55 (OLR = 4.0 $gVS.L_{slurry}^{-1}.day^{-1}$), the T_A^2 value definitely increased in its out-of-control range (day 52), reached a maximal value at day 54 (T_A^2/UCL = 4.0), then decreased during the end-of-week interruption of the feeding. This behaviour is in agreement

with the irreversible process disturbance observed during this week (no process recovery during the end-of-week interruption of the feeding). Concomitantly, the SPE index showed marked peaks in its out-of-control range, indicating a progressive change in the relationship between the IPVs compared to that detected by the PCA for the SSR. At day 56 (OLR = 4.4 $gVS.L_{slurry}^{-1}.day^{-1}$), the SPE index abruptly increased (SPE/SPE_{lim} max ~ 1300) and maintained extremely high out-of-control values until the end of the measurements, invalidating the static PCA model built for the SSR regarding its ability to reflect the process status of the OR. This event only occurred during the critical process disturbance observed for the OR (interruption of the CH_4 production). It must be highlighted that the PCA model remained valid during the period during which process monitoring could still allow to avoid the process failure.

These results show that the second static PCA-MSPC model built on the basis of the SSR data set could be transferred to the OR data set and closely reflected its process status. Approaching FVFA intoxication, occurrences of out-of-control values of the T_A^2 index were in close relation with the first acidic pH values observed in the slurry, although pH was not included among the individual process variables. In addition, the first peak of the T_A^2 in its out-of-control range that occurred during the reversible process disturbance period can be interpreted as a valuable early warning announcing the approaching collapse of the process.

3.3.6. Gas phase vs slurry monitoring

The contribution plot corresponding to the out-of-control process observations detected by the T_A^2 control chart derived from second PCA-MSPC model is illustrated in **Figure 3.7**f. It shows that the CH_4 and CO_2 content of the gas phase brought the highest contribution to the valuable warning detected by the T_A^2 control chart at day 48 and can thus be identified as the most valuable IPVs regarding the earliness of detection of the targeted FVFA intoxication. H_2 concentration in the gas phase contributed the most to the SPE out-of-control values detected between day 49 and day 56 (**Figure 3.7**c), indicating that the PCA model detected a progressive change in its relationship with the other IPVs. These SPE peaks in the out-of-control range started 7 days before the abrupt increase of the H_2 content (easily detectable visually, **Figure 3.5**c) concomitant to the critical process disturbance, showing that this parameter was better exploited as an IPV in the PCA-MSPC model than

monitored individually. Currently, only CH_4 concentration in the biogas is measured in most agricultural AD plants (Weiland, 2010). These results suggest that two additional gas sensors, for CO_2 and H_2, could substantially improve the process control, possibly at minor cost.

The fact that the IPVs measured in the gas phase delivered the most valuable information for the early prediction of the FVFA intoxication deserves further discussion. Indeed, Boe et al. (2010) observed that the parameters measured in the gas phase provided delayed information on the AD process status in comparison to those measured in the slurry. In this study, the IPVs measured in the slurry were selected regarding their ability to be measured on-site, at low cost and with only basic requirements in analytical skills and materials. Nevertheless, key metabolites such as individual VFA concentrations in the slurry could potentially express a relationship with the biogas composition and be joined to it in a powerful PCA-MSPC model. Unfortunately, VFA analysis (by gas chromatography after extraction) remains expensive, is rarely performed on-site, and delivers delayed results incompatible with fast-response process monitoring. For these reasons, the VFA concentrations were not included among the IPVs exploited for MSPC, but only as an independent process stability indicator.

The parameters measured in the slurry are generally monitored at a much lower frequency than the biogas composition due to their time-consuming and often expensive (VFA) measurement methods. Consequently, their in-control variability cannot be evaluated as accurately as the parameters measured in the gas phase. The actual relationship existing between parameters measured in the slurry and in the gas phase is therefore difficult to evaluate, which may cause unrealistic modelling when applying PCA on data sets mixing these parameters. Currently, attempts are done to allow higher frequency online measurements for parameters measured in the slurry, essentially exploiting NIR spectroscopy (Jacobi et al., 2009; Lomborg et al., 2009). Nevertheless, NIR analyses remain highly influenced by the variability of the slurry matrix and thus, by the feedstocks. In addition, taking *representative* samples of the slurry present in a digester is a challenge, especially for digesters with a capacity of several thousands of cubic meters. In contrast, the sampling conditions affect less the measurements performed in the gas phase since the headspace of a reactor can be easily homogenized, as compared to its slurry content.

The fact that the model including the TS and VS content of the slurry could not be transferred from the SSR to the OR can be explained by the very slow progression of these parameters, as compared to the biological and chemical processes that are related to the biogas production. Indeed, the gas contained in the reactor headspace is renewed at a high frequency (the gas retention time in the headspace of the OR varied between ~3h and ~1day before day 50) compared to the slurry content (HRT of 28 days) which implies that the chemical composition of the biogas changes much faster than the TS and VS content of the slurry. Joining them to IPVs measured in the gas phase through a static PCA model is therefore not relevant.

The pH of the slurry was not included among the IPVs exploited for PCA-MSPC due to its limited reliability as an indicator of VFA accumulation in real scale agricultural digesters. Indeed, the alkalinity of these digesters regularly reaches values close to 300 $mM_{H+\text{-equivalents}}$ (unpublished internal data from the 1-year survey of 5 Luxembourgish agricultural digesters). Therefore, the resulting buffer capacity allows VFA to accumulate up to a few mg/g_{slurry} without significant influence on pH that can be easily detected. In comparison, the alkalinity of the laboratory reactors described in the present study was low (90 $mM_{H+\text{-equivalents}}$), due to the necessity to maintain a low dry matter content in the slurry for proper mixing. Secondly, online pH measurement is often affected by the rapid fouling of the electrode membranes that result in biased pH measurement and would require frequent cleaning and replacement (Drosg, 2013).

While the feedstock to CH_4 conversion yield (**Figure 3.1**b) was not included in the PCA model, this yield could be a powerful indicator for AD process disturbances. In the present study, the CH_4 yield was easy to assess as the reactors were fed with known amounts of a single feedstock. However, the CH_4 yield is often difficult to evaluate accurately in a real-scale co-digestion plant because of the practical uncertainty on the amount of the various feedstocks introduced in the digesters.

3.3.7. Potential of *dynamic* PCA-MSPC for AD process monitoring

In this study, *static* PCA-MSPC was used to capture the overall in-control variability expressed by the AD process for a reactor maintained in steady-state during the experiment. Nevertheless, *dynamic* MSPC approaches could have been assessed to evaluate the OR process status. These methods expend the static method in taking into account the normal dynamics exhibited by a process. Dynamic PCA (DPCA) exploits time-shifted versions of the IPVs, in order to model their dynamic behaviour within the PCA model (Ku et al., 1995). An extension of this method (DPCA-DR) combines decorrelated residuals based on missing data imputation techniques to better handle auto-correlation problems (Rato & Reis, 2013a, 2013b). Another approach proposed by Li et al. (2000) consists in recursively updating the PCA model parameters by including a forgetting factor in the recursive calculation, making old data exponentially ignored and giving more weight to new data. This approach was already assessed for process monitoring of a full-scale AD reactor using e-nose data (Adam et al., 2015).

3.4. Conclusions

This study demonstrated that a data set collected for an AD reactor maintained in steady-state can be exploited as in-control process baseline to monitor the process status of an independent reactor progressively overfed from steady-state to critical FVFA intoxication using static PCA-MSPC. The results highlight that coupling parameters measured in the biogas and the slurry in a PCA-MSPC model is challenging since the lack of correlation existing between these two types of IPVs. Properties of the slurry that are closely connected to the biological and chemical processes that influence the biogas composition should be preferred for MSPC, such as its VFA content. Nevertheless, their current measurement methods are not compatible with fast response process monitoring and innovative measurement techniques should still progress to allow their online measurement at high frequency. CH_4, CO_2 and H_2 content of the gas phase were the most valuable IPVs regarding the detection earliness of FVFA intoxication. This result is very interesting since these parameters are nowadays poorly exploited for AD process monitoring and their online sensing can be easily implemented at the real-scale level.

Acknowledgements

The research was partly realized in the framework of the Interreg IVA OPTIBIOGAZ project (001/GR/2/3/003), which was co-financed by the European Union through the FEDER for the INTERREG IVa program.

Chapter 4

Potential of multivariate statistical process control based on biogas composition to detect free ammonia intoxication in anaerobic reactors

Adapted[6] from:

Lemaigre, S., Adam, G., Gerin, P. A., Noo, A., De Vos, B., Klimek, D., Goux, X., Calusinska, M., & Delfosse, P. (2018). Potential of multivariate statistical process monitoring based on the biogas composition to detect free ammonia intoxication in anaerobic reactors. *Biochemical Engineering Journal*, *140*, 17–28. doi:10.1016/j.bej.2018.08.018

[6] The term "multivariate process monitoring" was replaced by "multivariate statistical process control (MSPC)." Additionally, the original highlights were replaced by those provided at the beginning of this chapter, which are more relevant in the context of the thesis.

Context and contribution to the thesis

Similarly to free VFA intoxication, free ammonia nitrogen (FAN) intoxication frequently occurs in agricultural anaerobic digesters. FAN intoxication develops in digesters exposed to excessive nitrogen input and can interrupt methane production if detected too late. In **Chapter 3**, we showed that PCA-MSPC models based solely on biogas composition should be considered to detect AD process disturbances. In **Chapter 4**, we will explore the potential of such models to detect AD process disturbance due to FAN intoxication.

In this context, **Chapter 4** utilises results from AD experiment **Exp2_FAN_intoxication**[7] to address the research question **Q1 Disturbance detection** (*Is a MSPC approach based on biogas composition useful for detecting the two main disturbances of the AD process?*).

Personal Contribution:

- Equipped four 100-L reactors with components for heating, temperature regulation, and stirring (**Chapter 10**; Annex 1).
- Developed and assembled equipment for automatic sampling and analysis of the biogas produced by the reactors (**Chapter 10**; Annex 1).
- Defined the treatment and analytical protocol applied to the reactors.
- Conducted the experiment in the laboratory.
- Developed the software for acquiring biogas datasets and building MSPC models.
- Critically analysed the data and wrote the study as the first author

[7] AD reactors exposed to increased nitrogen input until critical FAN intoxication + Assessment of a process recovery strategy.

Highlights

- PCA-MSPC models based solely on biogas composition were developed and assessed post-experimentally to monitor the process status of three pilot-scale AD reactors progressively overloaded with nitrogen, ultimately leading to CH_4 production failure due to critical FAN intoxication (max. FAN content ~ 5.0 g_N L^{-1}) .
- Static models built from an initial steady-state period failed to distinguish actual process deterioration from baseline drift.
- Recursively updated models identified out-of-control observations concurrent with early signs of FAN intoxication.
- RU-PCA-MSPC model performance declined following abrupt microbiome shifts, which rendered previously learned patterns obsolete despite recursive updates.
- An independent steady-state reactor remained essential for tuning the effective memory length in RU-PCA-MSPC.

Abstract

Three anaerobic digestion reactors were initially maintained at steady state with low nitrogen input, then progressively exposed to increasing nitrogen input until extreme ammonia intoxication, leading to interruption of biogas production. Such interruption occurred for a free ammonia nitrogen (FAN) concentration of about 5 g_FAN L_{slurry}^{-1}. A fourth reactor used as a control was maintained at low-nitrogen steady state. The biogas composition (CH_4, CO_2, H_2 and H_2S) was recorded over time and data were fed into a multivariate statistical process control model based on principal components analysis (PCA-MSPC). Static PCA-MSPC failed to distinguish between the actual reactor performance decrease and the drift of the in-control process baseline. However, recursively updated PCA-MSPC (effective memory length of 14 days, i.e., 0.25 hydraulic retention time) allowed detection of the early signs of FAN-induced process disturbance, which were simultaneous with drastic changes in the microbiome of the replicate reactors. However, the process control model could not adapt to a drastic modification of the microbiome. Propionate continuously accumulated after the detection of the first signs of process disturbance.

4.1. Introduction

In 2014, the European Union leaders agreed on a new climate and energy framework, establishing challenging objectives for the member states for the year 2030. These objectives include a 40% reduction of the greenhouse gas emissions and an increase of the renewable energy contribution to 27% of the global energy mix (Helm, 2014). To meet these objectives, agricultural anaerobic digestion (AD) can bring a valuable contribution since it is an efficient technology for renewable energy production from wet fermentable feedstocks and for recovery of the essential nutrients, especially nitrogen and phosphorus (Batstone & Virdis, 2016).

Animal manure should be digested in AD reactors to take advantage of its carbon content for energy production, while avoiding the emission of methane during its storage (Rajagopal et al., 2013). However, the high nitrogen load present in manure in the form of urea and proteins leads to the accumulation of ammonia as a final product of AD (González-Fernández & García-Encina, 2009). In addition, the carbon present in manure is mostly recalcitrant to AD because the animal has already assimilated the most available part of the organic matter present in its feed. Consequently, AD plants exploiting manure as the principal feedstock must adopt long hydraulic retention times (HRT) to efficiently convert recalcitrant carbon into methane. This exacerbates ammonia accumulation in the reactor slurry.

Excessive concentration of ammonia is a major cause of AD reactor process inhibition (Yenigün & Demirel, 2013). Indeed, the free ammonia nitrogen (FAN: NH_3) is toxic for the methanogenic archaea due to its high diffusion rate through cell membranes (Rajagopal et al., 2013). The FAN proportion in the total ammonia nitrogen (TAN) content of the slurry (TAN = FAN + $N\text{-}NH_4^+$) is driven by the pH value and the operating temperature (Calli et al., 2005). FAN inhibition can strongly affect the performance of AD reactors by reducing the organic carbon to CH_4 conversion ratio, causing important economic losses for the plant manager. In this context, process monitoring that allows early detection of FAN inhibition is a major challenge for further development of the AD sector, especially in agriculture.

Classical AD process monitoring involves measuring indicators in the slurry and comparing these measurements to threshold values. However, literature on the FAN inhibition in AD reactors shows a wide range of threshold values (L. Li et al.,

2014; Resch et al., 2011). The main cause is that the FAN toxicity for a given AD reactor depends on the degree of microbial acclimation to nitrogen-rich feedstocks (Rajagopal et al., 2013)

Compared to classical methods used for AD process monitoring, multivariate statistical process control (MSPC) methods exploit statistically defined control limits and are thus independent of uncertain toxicity thresholds. MSPC based on principal component analysis (PCA-MSPC) is nowadays the basic tool to monitor multivariate processes (Kourti, 2005; Kourti & MacGregor, 1995; MacGregor, 1995). In PCA-MSPC, the information contained within the measured individual process variables (IPVs) is reduced to two monitoring indexes through statistical modelling (MacGregor, 1995): (1) the T_A^2 index describes the variation amplitude of the IPVs in the "plane" defined by a limited number *A* of principal components (PCs) retained in the model; (2) the squared prediction error (SPE) index quantifies the residuals, i.e., the part of variability unexplained by the model. For each time point, the value of each monitoring index is plotted in a control chart and compared to a control limit above which the process is considered as out-of-control. The *static* PCA-MSPC is the basic way to implement PCA-MSPC. This method consists of calculating the model parameters on the basis of data collected for an initial period during which the process stability is verified. Static PCA-MSPC is easy to implement and requires only a few computations once the model is defined, but is limited in the case of processes that demonstrate a drift of their in-control baseline. To handle such situations, *recursively updated* PCA-MSPC methods (RU-PCA-MSPC) were proposed (W. Li et al., 2000). RU-PCA-MSPC methods take into account the normal dynamics exhibited by a process through continuous updating of the model parameters.

In AD process monitoring, analysing the biogas composition offers multiple advantages as compared to slurry analysis. Biogas analyses allow a high measurement frequency and deliver immediate results (Lemaigre et al., 2016). In recent years, the electronic nose (e-nose) technology was the main technology using the biogas composition investigated for AD process monitoring by Adam et al. (2013, 2015). In process monitoring using e-noses, PCA-MSPC techniques are used to interpret the response of an array of low-selectivity gas sensors. Although the e-nose technology is promising, it presents two major limitations. On the one hand, the metal oxide semiconductor sensors (MOS) used in e-noses are subject to drift when exposed to

harsh environmental conditions (Romain & Nicolas, 2010; L. Zhang & Zhang, 2015). On the other hand, MOS sensors need frequent replacement due to their high sensitivity to poisoning (Romain & Nicolas, 2010). As an alternative, the major components of the biogas (CH_4, CO_2, H_2 and H_2S) can be analysed using specific sensors that are less subject to drift (if regularly calibrated) and more robust.

Lemaigre et al. (2016) recently assessed a *static* PCA-MSPC model for process monitoring of an AD reactor progressively exposed to intoxication by volatile fatty acids (VFAs) using the CH_4, CO_2 and H_2 concentrations in the biogas as IPVs, as well as parameters measured in the slurry (**Chapter 3**). The model delivered valuable warning signals announcing the process disturbance in the reactor, which were mostly derived from the dynamics of the biogas composition. On the other hand, the dynamics of the parameters measured in the slurry contributed poorly to the warning.

The main objective of the study presented below was thus to assess the potential of PCA-MSPC using the CH_4, CO_2, H_2 and H_2S concentrations in the biogas as exclusive IPVs to allow early detection of FAN inhibition in AD reactors. In particular, static and recursively updated PCA-MSPC methods were compared regarding their ability to discriminate the periods that demonstrate stable and altered reactor performance. The experiment described in this study focussed on 100-L semi-continuous laboratory reactors that were successively submitted to feedstock acclimation and progressive FAN intoxication until complete process failure. To assess the reliability of the PCA-MSPC model as a process status monitoring tool, a chemical and microbial monitoring of the reactor slurry was conducted.

4.2. Materials and methods

4.2.1. Anaerobic digestion

The experiment was performed using four stainless steel tank reactors of 100-L working volume with an additional 25-L headspace volume. The reactor working volume was completely and continuously stirred at 60 rpm with a central anchor-type stirrer.

Each reactor was inoculated with 100 kg of anaerobic sludge [total solids (TS): 0.04 gTS gFM^{-1}; volatile solids (VS): 0.56 gVS gTS^{-1}] collected on April 21, 2015 in the mesophilic anaerobic reactor of an urban wastewater treatment plant (Schifflange, Luxembourg). The digestion was performed in the mesophilic

temperature range with the operating temperature set at 37 ± 0.5 °C. The reactors were fed as real digesters with unsterilized feedstocks. The main feedstock was dry sugar beet pulp pellets. This feedstock was selected for its low nitrogen content (0.012 g_N gVS^{-1}; C/N = 39.6) and its complex composition (**Table 3.1**), offering a growth environment similar to a real-scale co-digestion reactor to the microbial community (**Chapter 5**; Goux et al., 2015). The biochemical methane potential (BMP) of the sugar beet pulp pellets was evaluated as 0.38 L_N CH_4 gVS^{-1} according to the methods described by Mayer et al. (2014). The reactors were manually fed every legal working day, usually five consecutive days per week, following a semi-continuous scheme (**Chapter 5**; Goux et al., 2015). The HRT was adjusted at 56 days during the whole experiment by completing the feed with tap water at 37°C. Such high HRT value was selected to promote TAN accumulation.

The experimental design stretched over 23 weeks (**Figure 4.1**). The progress over time of the feeding regime of the reactors, expressed in terms of sugar beet pulp, urea and nitrogen input, is presented in **Figure 4.2**a and **Figure 4.2**b. The four reactors were initially acclimatized for 8 weeks (1 HRT), during which their organic loading rate (OLR) was progressively increased to reach a value of 2 gVS L^{-1} per feeding day (10 gVS L^{-1} $week^{-1}$), using sugar beet pulp as the sole feedstock and equivalent to a nitrogen supply of 0.024 g_N L^{-1} per feeding day (0.12 g_N L^{-1} $week^{-1}$).

From week 8, urea powder (Sigma-Aldrich, USA) was progressively added to the feed of three reactors (high nitrogen input reactors 1, 2 and 3; HNRs) while the feed of the remaining reactor (low nitrogen input reactor; LNR) was left unchanged (**Figure 4.2**a,b). Urea was selected as an additional nitrogen source for the high nitrogen input reactors due to its ease of degradation to ammonia by a large diversity of micro-organisms (Sterling et al., 2001) and because it is a major form of nitrogen in farm manure. For each feeding day, the high nitrogen input reactors were fed with the same mass of sugar beet pulp as the low nitrogen input reactor (**Figure 4.2**a). From week 20 onwards, large amounts of urea (maximal nitrogen supply of 0.95 g_N L_{slurry}^{-1} per feeding day) were added to the feed of the high nitrogen input reactors until almost complete interruption of their biogas production was observed (end of week 22).

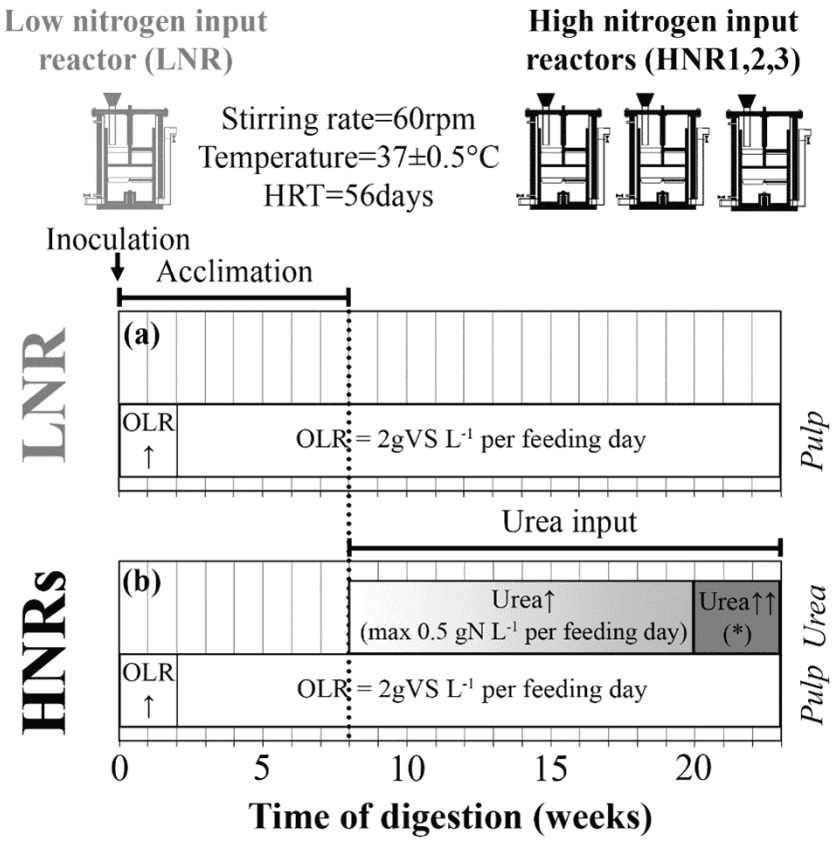

(*) max 0.95 gN L^{-1} per feeding day

Figure 4.1. Schematics of the experimental design. Organic loading rate (OLR) as sugar beet pulp and nitrogen load as urea for the low nitrogen input reactor LNR (a), and for the high nitrogen input reactors HNRs (b). The hydraulic retention time (HRT) was adjusted at 56 days with tap water at 37°C in the feed.

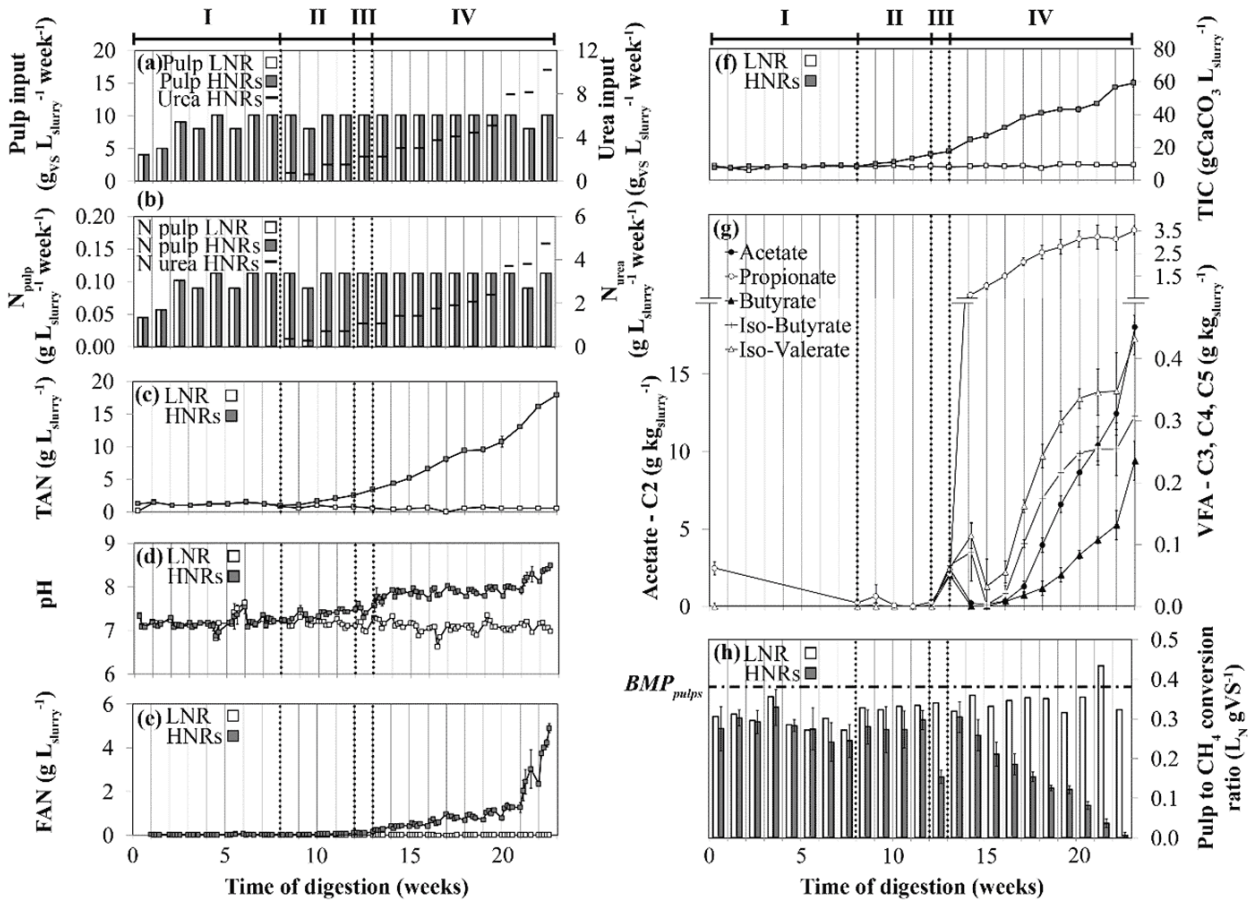
I
II
III
IV
(a) Pulp LNR
Pulp HNRs
Urea HNRs
Pulp input (g_{VS} L_{slurry}^{-1} week^{-1})
Urea input (g_{VS} L_{slurry}^{-1} week^{-1})
(b)
N pulp LNR
N pulp HNRs
N urea HNRs
N_{pulp} (g L_{slurry}^{-1} week^{-1})
N_{urea} (g L_{slurry}^{-1} week^{-1})
(c) LNR
HNRs
TAN (g L_{slurry}^{-1})
(d) LNR
HNRs
pH
(e) LNR
HNRs
FAN (g L_{slurry}^{-1})
Time of digestion (weeks)
(f) LNR
HNRs
TIC (g$CaCO_3$ L_{slurry}^{-1})
(g)
Acetate
Propionate
Butyrate
Iso-Butyrate
Iso-Valerate
Acetate - C2 (g kg_{slurry}^{-1})
VFA - C3, C4, C5 (g kg_{slurry}^{-1})
(h) LNR
HNRs
BMP_{pulps}
Pulp to CH_4 conversion ratio (L_N gVS^{-1})
Time of digestion (weeks)

Figure 4.2. Progress over time of: the loading rate in term of sugar beet pulp and urea (a), load of nitrogen introduced weekly in the reactors (nitrogen from both sugar beet pulp and urea) (b); total ammonia nitrogen (TAN) (c); pH (d); calculated free ammonia nitrogen (FAN) (e); total inorganic carbon (TIC) (f); volatile fatty acids (VFAs) individual concentrations in the slurry (g); pulp to CH_4 conversion ratio (g). For the reactors with high nitrogen input (HNRs), the data are expressed as the average of the 3 reactors ± the standard error (error bars). LNR: reactor with low nitrogen input.

4.2.2. Analytical monitoring

4.2.2.1. Biogas monitoring

The biogas produced by each reactor passed through a cooling unit at ~8°C to remove excess water vapour and was collected in an 80-L gas bag (Tecobag, Tesseraux, Germany).

Every 2 h, the content of the bag was automatically pumped through a recirculation loop for 4 min to allow proper mixing in the sampling tubing (Tygon, VWR International, USA). About 50 mL of gas was then pumped from the recirculation loop to a three-channel gas chromatograph (CompactGC, global analyser solutions™, Interscience, Belgium) for analysis of the CH_4, CO_2, H_2, H_2S, O_2 and N_2 concentrations. The gas chromatograph was equipped with a thermal conductivity detector on each channel. The detectors were heated at 80 °C and the filaments at 110 °C. The first channel was equipped with a RI-QBond column (10 m × 0.32 mm) and allowed separation and analysis of CO_2. The second channel was equipped with a Rtx-1 column (30 m × 0.32 mm) and allowed separation and analysis of H_2S. The third channel was equipped with a RI-QBond pre-column (3 m × 0.32 mm) followed by a Molsieve 5A column (7 m × 0.32 mm), the latter allowing separation of the H_2, O_2, N_2 and CH_4 gases. The RI-QBond pre-column allowed separation of CO_2 from the other gases to protect the Molsieve column from CO_2 poisoning; then the H_2, O_2, N_2 and CH_4 gases were separated in the Molsieve column while the CO_2 was back-flushed through the RI-QBond pre-column and eliminated through the GC exhaust. Helium was used as the carrier gas for the first two channels. Argon was used as the carrier gas for the third channel. For the three channels, the elution was performed under isothermal conditions at 50 °C and with a flow of 10 mL min^{-1}.

The remaining content of the gas bag was pumped through a drum-type wet gas meter (TG-5, Ritter, Germany) for volume measurement, which was normalized

to normal conditions of temperature and pressure (0°C; 1013 hPa). Between each analysis, the recirculation loop was flushed with ambient air for 2 min. After each measurement cycle, ambient air was pumped through the GC to prevent potential corrosion due to H_2S.

During weeks 3, 8 and 17, the CH_4 and CO_2 contents of the biogas were measured using specific non-dispersive infrared sensors (Dynament, UK) as an alternative during compact GC maintenance.

4.2.2.2. Slurry monitoring

The total ammonia nitrogen (TAN, g L_{slurry}^{-1}), total inorganic carbon (TIC, g$CaCO_3$ L_{slurry}^{-1}), individual VFA concentrations (C2 to C6, g kg_{slurry}^{-1}) and pH were measured in the slurry using the analytical methods described by Goux et al. (2015) in **Chapter 5**. The pH was measured on a daily basis (feeding days) while the individual VFA, TIC and TAN contents were measured weekly (every Monday). The FAN content in the slurry (g L_{slurry}^{-1}) was calculated on the basis of the TAN content and the pH using the formulae provided by Calli et al. (2005), with an operating temperature fixed at 37°C (pKa = 8.89). The FAN content was only calculated when the pH was measured (feeding days), with interpolated TAN values being used if TAN was not measured on the same day.

Over the experiment, aliquots of around 200 µL of slurry were sampled weekly (every Wednesday), directly frozen in liquid nitrogen and stored at -80 °C prior to a 16s rRNA gene amplicon high throughput sequencing targeting a monitoring of both bacteria and archaea. Based on the reactor performances toward progressive FAN intoxication and PCA-MSPC results, samples for weeks 0, 6, 7, 8, 10, 11, 12, 14, 18, 20, 21 and 22 were selected for the microbial community analysis. For that purpose, DNA from the selected slurry samples was extracted using the DNeasy PowerSoil Kit (Qiagen) according to the manufacturer's protocol. The 16S rRNA amplicon libraries were then prepared, sequenced, de-multiplexed and quality trimmed as detailed by Goux et al. (2016) and Calusinska et al. (2018).

4.2.2.3. Individual process variables and process stability indicators

The CH_4, CO_2, H_2S and H_2 concentrations in the biogas were used as IPVs to build the PCA-MSPC models (Lemaigre et al., 2016). The pulp to CH_4 conversion

ratio as well as the TAN, TIC, FAN and VFA individual contents of the slurry were used as process stability indicators, but were not used for building the PCA-MSPC models. The sugar beet pulp to CH_4 conversion ratio (L_N CH_4 gVS^{-1}) was chosen as the principal process stability indicator. This ratio was calculated for each week using the normalized total volume of CH_4 produced divided by the total mass of sugar beet pulp (expressed in VS) introduced during the week.

4.2.3. PCA-MSPC using exclusively the biogas composition

For each reactor, the biogas composition measurements collected from week 2 to the end of week 6 were used as a historical data set (HDS). The model parameters were calculated from this initial stable process period. PCA-MSPC was then performed for the next biogas composition measurements (12 measurements per day) using: (1) static PCA-MSPC and (2) RU-PCA-MSPC. The calculations were performed using the Scilab open-source software (Scilab Enterprises, 2012).

4.2.3.1. Initial model building on the basis of the HDS

The outliers were first removed from the HDS using the iterative method described by Lemaigre et al. (2016) and exposed in **Chapter 3** (significance level α set to 0.01). The parameters characterizing the initial stable process baseline were calculated on the basis of the cleaned HDS: average value and standard deviation of each IPV; loading vectors and eigenvalues associated with a limited number *A* of PCs retained in the model on the basis of the eigenvalue > 1 criterion.

4.2.3.2. Static PCA-MSPC

For each new biogas composition measurement, static PCA-MSPC was performed using the parameters calculated based on the outlier-cleaned HDS, without any update of the model parameters. For that purpose, the T_A^2 index and its corresponding SPE index were calculated and plotted in a control chart in which they were compared to their respective upper control limits.

The upper control limit of the T_A^2 control chart (UCL) was calculated using:

$$UCL = \left[\frac{A(m+1)(m-1)}{m(m-A)}\right] F(\alpha; A; m-A) \qquad (4.1)$$

where α is the significance level, *A* is the number of PCs retained in the model, *m* is the number of biogas composition measurements included in the outlier-cleaned HDS

and $F(\alpha; A, m-A)$ is the upper $(1-\alpha)$ quantile of the Fisher distribution with $(A, m-A)$ degrees of freedom.

The upper control limit of the SPE control chart (SPE_{lim}) was calculated according to Kourti & MacGregor (1995).

The upper control limits of the T_A^2 and the SPE indices were calculated using a significance level α set to 0.01 (i.e., 99% confidence level).

The values of the T_A^2 and SPE indices corresponding to each new biogas composition measurement were calculated using the following method:

(a) Each IPV was centred and scaled using the average value and the standard deviation calculated on the basis of the outlier-cleaned HDS.

(b) The T_A^2 index was calculated on the basis of the scores obtained for the A PCs retained in the model using:

$$T_A^2 = \sum_{i=1}^{A} \frac{t_i^2}{s_{t_i}^2} \tag{4.2}$$

where t_i and s_{t_i} are, respectively, the score calculated on the ith PC and the standard deviation related to this PC.

(c) The SPE index was calculated for each sample using:

$$SPE = \sum_{i=1}^{p} (\hat{x}_i - x_i)^2 \tag{4.3}$$

where p is the number of IPVs, x_i is the observed value for the ith IPV and $\hat{x}_i$ is the corresponding value computed using the PCA model.

For each out-of-control observation detected by the T_A^2 and the SPE control charts, the contribution of each IPV was computed and plotted in a contribution plot. We refer to Lemaigre et al. (2016) or **Chapter 3** for an exhaustive description of the methods and formulae used to build the T_A^2 and the SPE contribution plots.

4.2.3.3. Recursively updated PCA-MSPC (RU-PCA-MSPC)

For each new biogas composition measurement, the model parameters defined on the basis of the outlier-cleaned HDS were recursively updated using the method proposed by W. Li et al. (2000):

(a) Recursive update of the mean and the standard deviation.

(b) Recursive update of the correlation matrix.

(c) PCA on the basis of the updated correlation matrix.

(d) Selection of PCs using the eigenvalue > 1 criterion.

(e) T_A^2 and SPE calculation using the updated loading vectors and eigenvalues.

(f) Update of the control limits of the T_A^2 and SPE indexes (99% confidence level).

The previous biogas composition measurements were exponentially ignored, giving more weight to the new ones. For that purpose, a forgetting factor β ($0 \leq \beta \leq 1$) was introduced into the recursive calculation of the PCA model. The effective memory length N_{eff}, giving an idea of the number of data that are accounted for in the model, is given by $N_{eff} = \frac{1}{1-\beta}$

To avoid biasing the updated process baseline with new biogas composition measurements corresponding to out-of-control process observations, the recursive update of the PCA model was only performed for new biogas composition measurements corresponding to in-control values of the T_A^2 and SPE indexes ($T_A^2 \leq$ UCL and SPE $\leq SPE_{lim}$). For new biogas composition measurements corresponding to out-of-control values of the T_A^2 or the SPE index, the values of the T_A^2 and the SPE indexes were therefore calculated using the model parameters resulting from the previous model update.

We refer to W. Li et al. (2000) for an exhaustive description of the methods and formulae exploited for the recursive update of PCA-MSPC models using a forgetting factor.

4.3. Results and discussion

4.3.1. Anaerobic digestion process efficiency and evolution of the microbial community composition

The evolution over time of the CH_4, CO_2, H_2 and H_2S concentrations in the biogas, exploited as IPVs to build the statistical process control models, is presented in **Figure 4.3** for the four reactors. In relation to these parameters, the changes over

the whole experiment of the bacterial[8] and archaeal communities highlighted by high-throughput 16S rRNA amplicon sequencing are also presented in **Figure 4.3**.

[8] The bacterial taxonomy reflects the nomenclature in use at the time the study was conducted. The correspondence with the most recent taxonomic classification is provided in **Table 1.1** of the general introduction.

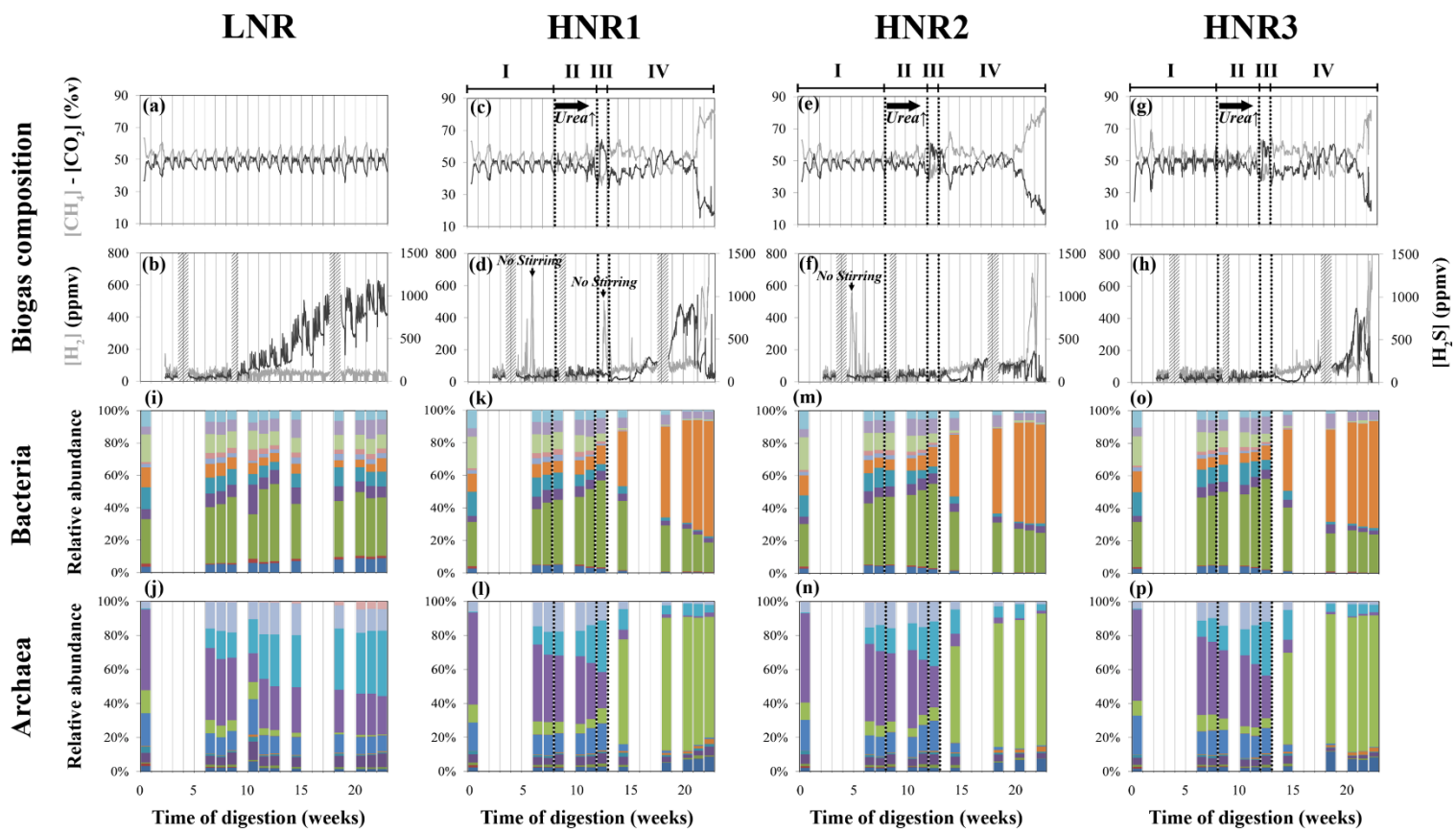
LNR
HNR1
HNR2
HNR3
I
II
III
IV
Urea
No Stirring
Biogas composition
Bacteria
Archaea
[CH4] - [CO2] (%v)
[H2] (ppmv)
[H2S] (ppmv)
Relative abundance
Time of digestion (weeks)
(a)
(b)
(c)
(d)
(e)
(f)
(g)
(h)
(i)
(j)
(k)
(l)
(m)
(n)
(o)
(p)

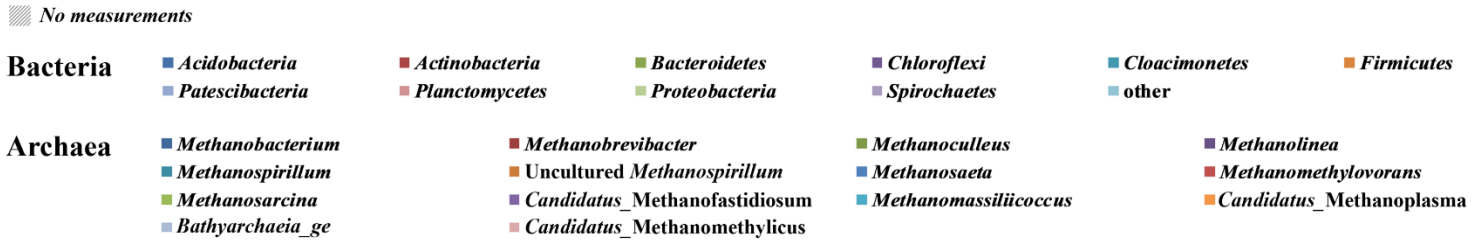

Figure 4.3. Progress over time of the biogas concentrations in CH_4, CO_2, H_2 and H_2S for: the low nitrogen input reactor LNR (a, b), the high nitrogen input reactor HNR1 (c, d), the HNR2 (e, f) and the HNR3 (g, h). Biogas composition measurements could not be performed during three short periods for H_2 and H_2S due to gas chromatograph maintenance (hatched grey area). Short stirrer blockings events occurred for HNR1 and HNR2, leading to transient increase of the H_2 production. Bacterial (phylum level) and archaeal (genus level) diversity dynamics over time as assessed by high-throughput 16S rRNA amplicon sequencing for the LNR (i, j), the HNR1 (k, l), the HNR2 (m, n) and the HNR3 (o, p). The presented data correspond to slurry samples collected on Wednesdays. I, II, III and IV correspond to the phases described in **Table 4.1**.

For the low nitrogen input reactor, the H_2 concentration remained very low during the whole experiment (**Figure 4.3**b) and the $[CH_4]/[CO_2]$ ratio showed a weekly pattern related to the feeding mode but CH_4 remained the dominating gas component (**Figure 4.3**a). The reactor efficiency remained above 0.3 $L_N\ CH_4\ gVS^{-1}$ (**Figure 4.2**h). The H_2S concentration in the biogas increased during the experiment (**Figure 4.3**b) probably due to sulfur accumulation in the slurry associated with the feeding of pulp over a 56-day HRT (the sulfur content of the sugar beet pulp is 0.4 $mg\_S\ gVS^{-1}$).

The three high nitrogen input reactors showed well synchronized behavior regarding the efficiency of conversion of pulp into CH_4 (**Figure 4.3**c,e,g). The pulp to CH_4 conversion ratio was used as the main process efficiency indicator since it reflects well the main purpose of the AD process, which is to convert organic matter into CH_4.

The evolution over time of the pulp to CH_4 conversion ratio (**Figure 4.2**h), the biogas composition and the process stability indicators measured in the slurry allowed the definition of 4 successive distinct phases characterizing the reactor process status (**Table 4.1**).

Table 4.1. Process status of the high nitrogen input reactors.

Phase	Time period	Process status of the high nitrogen input reactors
I	Week 0 to week 7	Stable process (no urea provided)
II	Week 8 to week 11	Process status unaffected by urea
III	Week 12	Acute process disturbance
IV	Week 13 to week 22	Apparent process status improvement followed by progressive establishment of complete process failure

During phase I (weeks 0 to 7), no urea was fed and the pulp was efficiently converted into CH_4 (**Figure 4.2**h). Short stirrer blocking events occurred for the high nitrogen input reactors 1 and 2 and led to clear increase of the H_2 concentration in the biogas (**Figure 4.3**d,f). During phase I, no drastic change in the bacterial and archaeal communities of the four studied reactors could be identified, with respectively *Bacteroidetes*, *Cloacimonetes*, *Firmicutes* and *Proteobacteria* being the dominant bacterial phyla and *Methanosaeta* and *Candidatus* Methanofastidiosum being the dominant archaeal genera (**Figure 4.3**). These different groups of organisms are

commonly found in anaerobic mesophilic reactors (Calusinska et al., 2018; Goux et al., 2015).

During phase II (weeks 8 to 11, start of urea supply), the three high nitrogen input reactors maintained stable performance while urea was introduced in the feed. The pulp to CH_4 conversion ratio was not affected (**Figure 4.2**h) and FAN remained at low concentration in the slurry (**Figure 4.2**e). No important change occurred in the microbial community, except that the relative abundance of *Bacteroidetes* (for bacteria) and *Methanomassiliicoccus* (for archaea) increased over time while at the same time the relative abundance of the archaeal "*Candidatus* Methanofastidiosum" decreased from around 40% to 20% in all studied reactors (**Figure 4.3**). The supply of urea contributed to increase the TIC content in the slurry (**Chapter 10**: Annex 2 - **Figure Ch4_S1**), but did not affect the CH_4 production (**Figure 4.3**). This is consistent with a previous report (Moestedt et al., 2016) and with urea hydrolysis that releases CO_2 ($H_2N\text{-}CO\text{-}NH_2 + H_2O \rightarrow CO_2 + 2\ NH_3$; Huang & Chen, 2007). CO_2 accumulates in the slurry due to the increasing pH, as a consequence of ammonia accumulation. Urea does not generate H_2 or reducing equivalents and does not contribute stoichiometrically to hydrogenotrophic methane production.

During phase III (week 12), an acute process disturbance was observed for the three high nitrogen input reactors, marked by a sudden drop of the pulp to CH_4 conversion ratio (**Figure 4.2**h). Simultaneously, the $[CH_4]/[CO_2]$ ratio showed values < 1 (**Figure 4.3**c,e,g) and all the measured VFAs accumulated in the slurry, especially acetate (**Figure 4.2**g). A short stirrer blocking event occurred for the high nitrogen input reactor 1 and led to clear increase of the H_2 concentration in the biogas (**Figure 4.3**d).

During phase IV (weeks 13 to 22), FAN accumulation in the slurry became clearly detectable (**Figure 4.2**e). After week 13, a drastic change appeared in the microbial community profile for the three HNRs while the microbial community remained stable for the LNR (**Figure 4.3**). In the three HNRs, *Firmicutes* replaced *Bacteroidetes* in the bacterial community while *Methanosarcina* replaced the two previously dominant archaeal genera *Methanomassiliicoccus* and "*Candidatus* Methanofastidiosum". This total reshaping of the microbial community clearly indicates that the anaerobic digestion process suffered from an acute disturbance between week 12 and 13. From week 13 onwards, the AD process was no longer run

by the microbes that prevailed during weeks 0 to 12. In consequence, even if the three high nitrogen input reactors showed first transient signs of process recovery, a progressive process performance decline followed thereafter (from week 14 onwards). Indeed, the pulp to CH_4 conversion ratio of the three high nitrogen input reactors initially increased (week 13), but then continuously decreased until the end of the experiment (**Figure 4.2**h). During week 13, the concentrations of acetate and butyrate in the slurry initially decreased, while iso-butyrate, iso-valerate and, especially, propionate continued to accumulate (**Figure 4.2**g). During week 14, the iso-valerate and iso-butyrate concentrations in the slurry temporarily decreased. From week 15 onwards, all the measured individual VFAs accumulated in the slurry until the end of the experiment (**Figure 4.2**g). The consumption of most VFAs and their likely conversion into CH_4 during weeks 13 and 14 might be correlated with the transient improvement of the process efficiency as evaluated by the pulp to CH_4 conversion ratio observed in the three high nitrogen input reactors. Indeed, the microbial conversion of the acetate that accumulated in the slurry during week 12 could explain ~27% of the CH_4 production observed during week 13. This suggests that the ability of the high nitrogen input reactors to convert the fed sugar beet pulp into CH_4 remained altered during week 13, and that the process status improvement observed during that period was only transient. This assumption is supported by the fact that volatile solids accumulated in the slurry of the high nitrogen input reactors from week 12 onwards (**Chapter 10**: Annex 2 - **Figure Ch4_S2**). This also indicates a limitation of the pulp to CH_4 conversion ratio as a direct indicator of the process status since accumulation of methanogenic substrates in the reactor, in this case acetate, can allow continued release of CH_4 when the microbial community adapts to or recovers from harsh environmental conditions.

For the three high nitrogen input reactors, propionate abruptly accumulated in the slurry during week 12 (phase III) and its concentration continued to increase until the end of the experiment, while the concentrations of the other VFAs decreased during weeks 13 and 14 (**Figure 4.2**g). Zhou & Qiu (2006) and Calli et al. (2005) have already observed that the acetogenic bacteria that use propionate as a substrate particularly suffer from inhibition caused by FAN. Thus, the accumulation of propionate could be a useful factor for FAN intoxication diagnosis as the acetotrophic

methane production is the first methane production pathway hampered by high FAN content (Fotidis et al., 2013).

During early phase IV, the alkaline pH values due to FAN accumulation may have contributed to a significant sulphide sequestration in the slurry of the high nitrogen input reactors while lower pH in the low nitrogen input reactor allowed the process to eliminate this toxic compound via the biogas extracted from the system. The large release of gaseous H_2S observed during the last weeks of phase IV for the high nitrogen input reactors 1 and 3 (**Figure 4.3**d,h) was not associated with a pH drop (**Figure 4.2**d) and therefore can only be explained by a large increase of the total sulphide content in the slurry. Extreme FAN intoxication may have caused a high microbial death rate, causing cellular lysis and release of sulphur-containing microbial proteins in the slurry. Indeed, several operational taxonomic units (OTUs) were no longer detected during the microbial monitoring (data not presented). At the alkaline pH observed in phase IV, sulphide is mostly in the form of HS^- (~90%) while the main toxic form H_2S is not dominant (~10%) (J. L. Chen et al., 2014). Nevertheless, the presence of the H_2S toxic form in the slurry might have added to the FAN toxicity encountered by the microbiome, causing cumulated inhibition by NH_3 and H_2S.

After the urea addition was started (week 8), the TIC content in the slurry continuously increased for the three high nitrogen input reactors (**Figure 4.2**f), indicating that a major part of the CO_2 released by the degradation of the pulp and the urea remained trapped in the slurry as bicarbonate due to the pH increase (**Figure 4.2**d).

4.3.2. Static PCA-MSPC based on the biogas composition

The potential of static PCA-MSPC to deliver valuable warning signals of process dist was assessed by analysing the dynamics of the biogas composition. The concentrations of CH_4, CO_2, H_2 and H_2S in the biogas were used as IPVs.

Table 4.2 shows the results of the outlier cleaning performed on the raw historical data sets (HDSs) collected for the four reactors from week 2 to week 6 (during the acclimation period). The outlier-cleaned HDSs were used to build the static PCA-MSPC models of the four reactors. The results of the PCA are presented in **Table 4.3** and **Figure 4.4**.

Table 4.2. Outliers cleaned from the raw historical data sets (HDS) collected for the four reactors from week 2 to week 6 (concentrations of CH_4, CO_2, H_2 and H_2S in the biogas used as individual process variables).

		Outliers cleaned from the raw HDS	
Reactor	Biogas composition measurements (raw HDS)	Number of outliers	Percentage of outliers in raw HDS (%)
LNR	311	9	3
HNR1	309	58	19
HNR2	308	50	16
HNR3	297	27	9

LNR: Low nitrogen input reactor; HNR: High nitrogen input reactor.

Table 4.3. Contribution of each principal component (PC) in the PCA performed for each reactor on the basis of the historical data sets cleaned from outliers (concentrations of CH_4, CO_2, H_2 and H_2S in the biogas used as individual process variables).

		PC1	PC2	PC3	PC4
LNR	Eigenvalues	2.732*	0.857	0.411	0.000
	Proportion of Variance	0.683	0.214	0.103	0.000
	Cumulative Proportion	0.683	0.897	1.000	1.000
HNR1	Eigenvalues	2.477*	1.016*	0.506	0.000
	Proportion of Variance	0.619	0.254	0.127	0.000
	Cumulative Proportion	0.619	0.873	1.000	1.000
HNR2	Eigenvalues	2.522*	0.972	0.506	0.000
	Proportion of Variance	0.631	0.243	0.126	0.000
	Cumulative Proportion	0.631	0.874	1.000	1.000
HNR3	Eigenvalues	2.513*	1.008*	0.479	0.000
	Proportion of Variance	0.628	0.252	0.120	0.000
	Cumulative Proportion	0.628	0.880	1.000	1.000

LNR: Low nitrogen input reactor; HNR: High nitrogen input reactor. * PCs retained to build the static PCA models on the basis of the eigenvalue > 1 criterion.

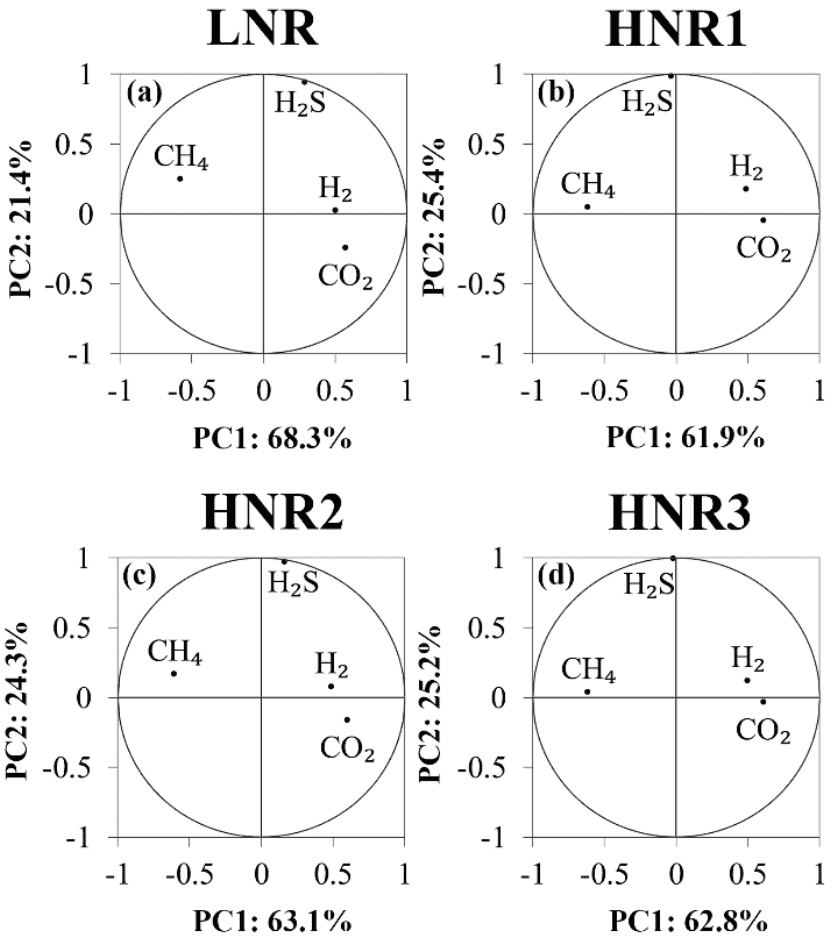

Figure 4.4. Principal component analysis (PCA) performed for the four reactors using the biogas concentrations in CH_4, CO_2, H_2 and H_2S measured during their acclimation period (week 2 to week 6) as individual process variables (purged historical data set). Loading plots of the 2 first principal components (PCs) for: the low nitrogen input reactor LNR (a), the high nitrogen input reactor HNR1 (b), the HNR2 (c) and the HNR3 (d).

The loadings of the IPVs regarding the two first PCs were similar for the four PCA models (**Figure 4.4**). The CH_4, CO_2 and H_2 concentrations in the biogas mainly contributed to PC1 while the H_2S concentration in the biogas mainly contributed to PC2. One PC was retained in the model built for the low nitrogen input reactor and the high nitrogen input reactor 2. These PCs explained, respectively, 68.3% and 63.1% of the variance exhibited by the process during the initial model building period (**Table 4.3**). Two PCs were retained in the models built for the high nitrogen input

reactors 1 and 3. These PCs explained, respectively, 87.3% and 88.0% of the variance exhibited by the process during the initial model building period. For all the reactors, PC1 was highly significant (eigenvalue > 2) but PC2 was close to the significance limit (eigenvalue ~ 1). This explains why PC2 was integrated in the model for the high nitrogen input reactors 1 and 3, while it was not for the low nitrogen input reactor and the high nitrogen input reactor 2 (PC2 eigenvalue < 1, **Table 4.3**).

The resulting T_A^2 and SPE control charts are presented in **Figure 4.5** for the four reactors, together with the pulp to CH_4 conversion ratio as an indicator of process efficiency.

The increases of the H_2 concentration related to the short stirrer blocking events that occurred for the high nitrogen input reactors 1 (**Figure 4.3**d) and 2 (**Figure 4.3**f) were detected by the T_A^2 control chart for the high nitrogen input reactor 1 (**Figure 4.5**c) and by the SPE control chart for the high nitrogen input 2 (**Figure 4.5**f). This shows that the number of PCs that are retained in the model (2 and 1 PCs for the high nitrogen input reactors 1 and 2, respectively) is not crucial for the detection of the out-of-control process observations. Indeed, the SPE control chart complements the T_A^2 control chart by controlling the amplitude of the model residuals.

For the low nitrogen input reactor, both the T_A^2 and the SPE indexes showed a drift in their out-of-control range, starting at week 9 (**Figure 4.5**a,b). According to the individual contributions, the H_2S concentration in the biogas was the main IPV responsible for these alarms. The cause was probably the increase of the H_2S concentration observed for the low nitrogen input reactor from week 9 till the end of the experiment (**Figure 4.3**b). However, no reduction of the reactor performance was observed while the H_2S concentration increased. The T_A^2 and SPE out-of-control status is therefore interpreted as a drift of the in-control process baseline that causes false alarms.

These results show the limitations of static PCA-MSPC in distinguishing between an actual performance decrease and a drift of the reactor in-control process baseline. Adequate update of the model parameters should therefore be performed to take into account the evolution over time of the in-control process baseline. Such an approach is evaluated below using recursively updated PCA-MSPC.

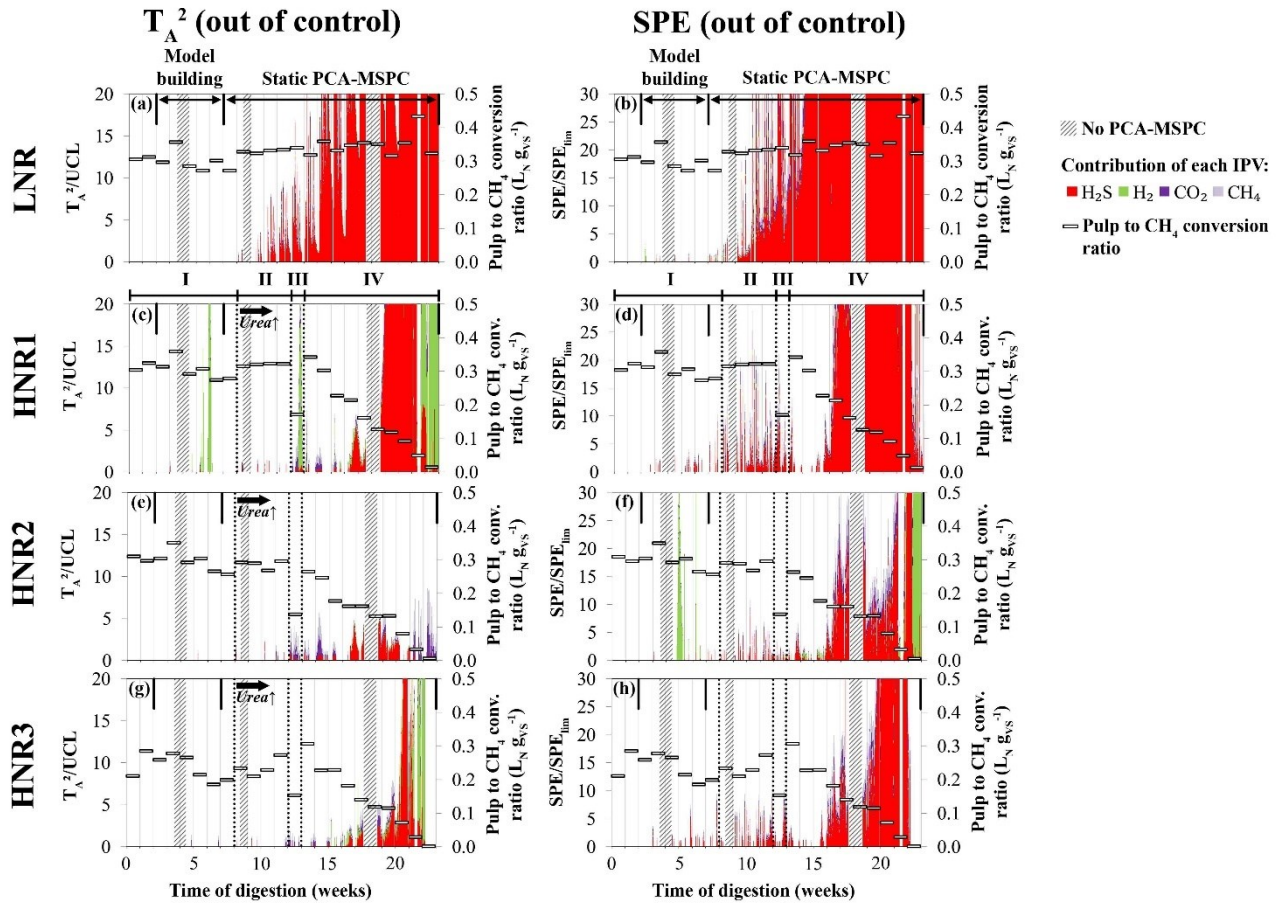
T_A^2 (out of control)
SPE (out of control)
Model building
Static PCA-MSPC
LNR
HNR1
HNR2
HNR3
(a)
(b)
(c)
(d)
(e)
(f)
(g)
(h)
I
II
III
IV
Urea↑
T_A^2/UCL
SPE/SPE_lim
Pulp to CH4 conversion ratio (L_N g_VS^-1)
Pulp to CH4 conv. ratio (L_N g_VS^-1)
Time of digestion (weeks)
No PCA-MSPC
Contribution of each IPV:
H2S H2 CO2 CH4
Pulp to CH4 conversion ratio

Figure 4.5. Static PCA-MSPC performed for the four reactors on the basis of the biogas concentrations in CH_4, CO_2, H_2 and H_2S collected during their acclimation period (week 2 to week 6) as individual process variables (IPVs). According to the constraint set to eigenvalue > 1, one PC was retained in the process control models built for the LNR and the HNR2 while two PCs were retained in the model built for the HNRs 1 and 3 (**Table 4.3**). T_A^2 and squared prediction error (SPE) control charts built for the LNR (a, b), the HNR1 (c, d), the HNR2 (e, f) and the HNR3 (g, h). The T_A^2 and the SPE are expressed as a ratio between the index value and its control limit (UCL and SPE, respectively). Only T_A^2/UCL and SPE/SPE_{lim} > 1 are plotted, indicating out-of-control process (coloured columns). The relative contribution of each IPV for each out-of-control process value is identified by a different colour. When the T_A^2/UCL or SPE/SPE_{lim} are out of the graphic scale, the colour indicates the main IPV contributor while the others have negligible contribution. The pulp to CH_4 conversion ratio is presented for each control chart as the process efficiency indicator. PCA-MSPC was not performed during three periods due to gas chromatograph maintenance (hatched grey area). I, II, III and IV correspond to the phases described in **Table 4.1**.

4.3.3. Recursively updated PCA-MSPC based on the biogas composition

PCA-MSPC with recursive update of the model parameters (RU-PCA-MSPC) was assessed for its ability to distinguish between drift of the in-control process baseline and real signs of decreasing reactor performance.

First, the effective memory length N_{eff}, describing the rate of update, was selected on the basis of the data set from the low nitrogen input reactor. The aim was to maintain the false alarm rate as low as possible, given the stable pulp to CH_4 conversion ratio exhibited by this control reactor during the experiment (**Figure 4.2**h). Three N_{eff} values were compared, corresponding to: *fast* model update (1 day: 12 biogas composition measurements), *moderately fast* model update (14 days: 168 biogas composition measurements corresponding to 0.25 HRT) and *slow* model update (28 days: 336 biogas composition measurements corresponding to 0.5 HRT). The T_A^2 and SPE control charts obtained for each new biogas composition measurement collected following the initial model building period (week 2 to week 6), as well as the rate of the model update and the number of PCs retained in the model, are presented in **Figure 4.6** for the three N_{eff} values.

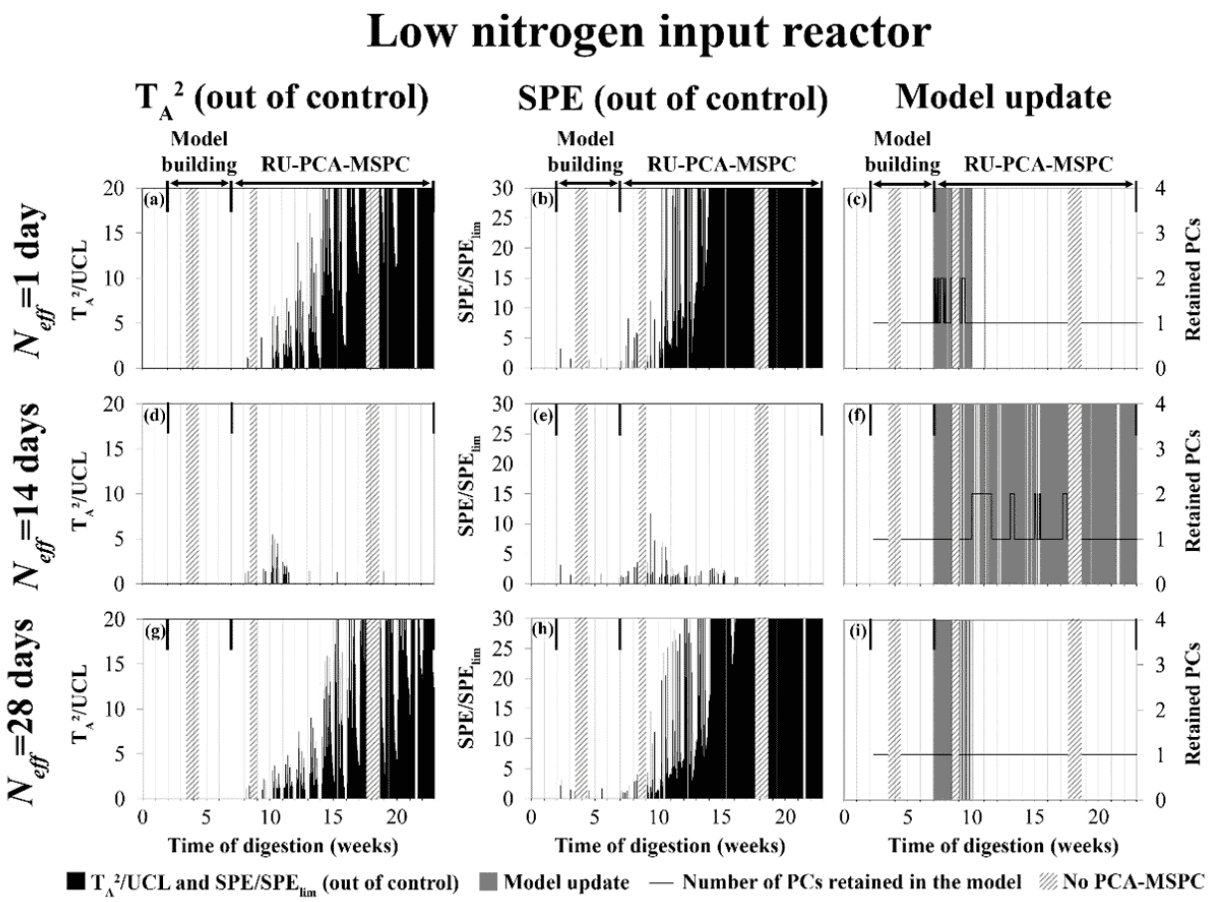
Low nitrogen input reactor
T_A^2 (out of control)
SPE (out of control)
Model update
Model building
RU-PCA-MSPC
N_eff=1 day
N_eff=14 days
N_eff=28 days
T_A^2/UCL
SPE/SPE_lim
Retained PCs
(a)
(b)
(c)
(d)
(e)
(f)
(g)
(h)
(i)
Time of digestion (weeks)
T_A^2/UCL and SPE/SPE_lim (out of control)
Model update
Number of PCs retained in the model
No PCA-MSPC

Figure 4.6. Influence of the model effective memory length N_{eff} on the T_A^2 and SPE of recursively updated PCA-MSPC (RU-PCA-MSPC) for the low nitrogen input reactor (LNR). The PCA-MSPC model was initially built using the biogas concentrations in CH_4, CO_2, H_2 and H_2S collected from week 2 to week 6 (during the acclimation period) as individual process variables (IPVs). Then the model was recursively updated with the new biogas composition measurements using 3 different values: N_{eff} =1 day (fast model update, a,b,c); N_{eff} =14 days (moderately fast model update, d,e,f) and N_{eff} =28 days (fast model update, g,h,i). The resulting T_A^2 and SPE control charts as well as the rate of model update and the impact of the model update on the number of principal components (PCs) retained in the model are presented. The T_A^2 and the SPE are expressed as a ratio between the index value and its control limit (UCL and SPE_{lim}, respectively). Only T_A^2/UCL and SPE/SPE_{lim} > 1 are plotted (i.e., out-of-control process). PCA-MSPC was not performed during three periods due to gas chromatograph maintenance (hatched grey area).

Figure 4.6c and **Figure 4.6**f show that each model update can induce the modification of the number of PCs retained in the model. However, the control limit (SPE_{lim}) of the SPE control chart is recalculated for each model update. As for the static models, the out-of-control process observations detected by the SPE control chart are thus complementary to those detected by the T_A^2 control chart. It can therefore be assumed that the change in the number of PCs retained in the model has only a minor impact on the detection of the out-of-control process observations detected by the recursively updated PCA-MSPC models.

The T_A^2 and SPE control charts built using the *fast* model update (**Figure 4.6**a,b) and the *slow* model update (**Figure 4.6**g,h) are similar to those obtained using static PCA-MSPC. Indeed, the model was updated only for new biogas composition measurements corresponding to in-control values of the T_A^2 and SPE indexes. For the *fast* model update, much more weight was attributed to the most recent individual measurements than the oldest ones. Therefore, the model parameters were updated on the basis of too few data to capture the variability associated with the daily and weekly dynamics of the biogas composition. The amplitude of these dynamics clearly increased from week 10 in the case of the H_2S concentration (**Figure 4.3**b). As we imposed the condition of not updating the model parameters for biogas composition measurements corresponding to out-of-control process obseravations, the model parameters were not updated from week 10 onwards (**Figure 4.6**c). For *slow* model update, more weight was attributed to the oldest individual measurements than to the most recent ones. Therefore, new data brought only a minor contribution to each re-estimation of the model parameters. In consequence, the model did not adapt fast

enough to the progressive increase of the H_2S concentration observed for the low nitrogen input reactor. This caused a progressive drift of the T_A^2 and SPE indexes in the out-of-control range, which also stopped the model update (**Figure 4.6**i).

More interestingly, the *moderately fast* model update (N_{eff} = 14 days; 0.25 HRT) allowed continuous model adaptation until the end of the experiment. The T_A^2 and SPE control charts only delivered a few short alarm signals (**Figure 4.6**d,e), which is in accordance with the stable pulp to CH_4 conversion ratio measured for the low nitrogen input reactor.

4.3.4. RU-PCA-MSPC: Prediction quality assessment for process disturbance detection

RU-PCA-MSPC using an effective memory length of 14 days was applied to the biogas samples collected after the initial model building period for the three high nitrogen input reactors. The resulting T_A^2 and SPE control charts are presented in **Figure 4.7** for the four reactors, together with the pulp to CH_4 conversion ratio as the process efficiency indicator.

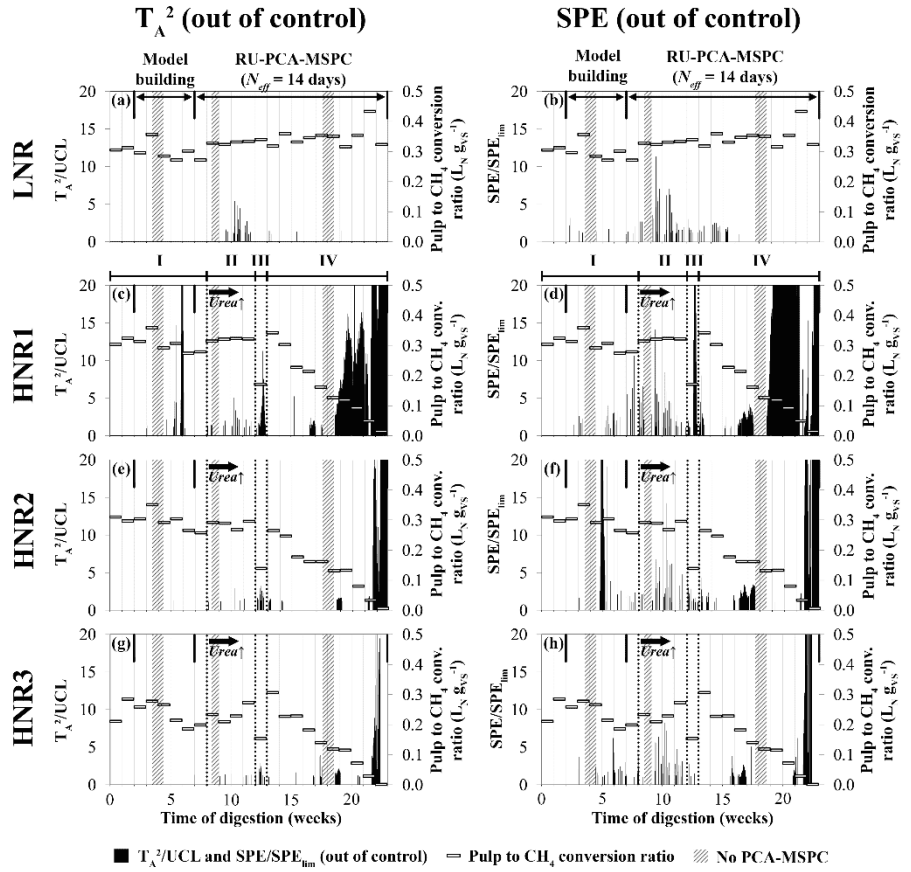

Figure 4.7. Recursively updated PCA-MSPC (RU-PCA-MSPC) performed for the four reactors using the biogas concentrations in CH_4, CO_2, H_2 and H_2S as individual process variables (IPVs) and an effective memory length N_{eff} of 14 days for the model update. The initial model building considered the biogas composition measurements collected from week 2 to week 6. T_A^2 and squared prediction error (SPE) control charts built for: the low nitrogen input reactor LNR (a, b), the high nitrogen input reactor HNR1 (c, d), the HNR2 (e, f) and the HNR3 (g, h). The T_A^2 and the SPE are expressed as a ratio between the index value and its control limit (UCL and SPE_{lim}, respectively). Only T_A^2/UCL and $SPE/SPE_{lim} > 1$ are plotted (i.e., out-of-control process). The pulp to CH_4 conversion ratio is presented for each control chart as the process efficiency indicator. PCA-MSPC was not performed during three short periods due to gas chromatograph maintenance operations (hatched grey area). I, II, III and IV correspond to the phases described in **Table 4.1**.

For the low nitrogen input reactor, only minor and transient out-of-control values were observed for both the T_A^2 and SPE indexes (**Figure 4.7**a,b), while the reactor exhibited a stable pulp to CH_4 conversion ratio throughout the experiment. Therefore, these transient alarm signals, probably due to the daily feedstock supply,

did not announce a risk of process disturbance that would require adaptation of the reactor's feeding regime.

For the high nitrogen input reactors, the process control models initially delivered only minor and transient alarm signals during phase II, similar to those observed for the low nitrogen input reactor. The process status was not affected by urea.

Interestingly, during phase III, the process control model delivered a clear and persistent alarm signal (T_A^2 > UCL) for the three high nitrogen input reactors (**Figure 4.7**c,e,g) during which an acute process disturbance occurred (a sudden drop of the pulp to CH_4 conversion ratio and VFA accumulation in the slurry). At that time, the microbial community was completely reshaped (**Figure 4.3**). A skilled reactor manager would have taken into account these early and persistent alarm signals seriously and would have verified the value of slurry indicators to identify the cause of these alarms, in this case a probable FAN intoxication characterized by an increase in VFA concentration (**Figure 4.2**g) which was contradictory to a pH above neutrality (**Figure 4.2**d) and increasing TIC and TAN contents in the slurry (**Figure 4.2**c,f). In consequence, the reactor manager would probably have lowered the nitrogen supply to the reactors to reduce the risk of further deterioration of the process.

For the experimental purpose of assessing the robustness of RU-PCA-MSPC model to predict the AD process performance status under a severe FAN intoxication, the nitrogen input was further increased in the high nitrogen input reactors during phase IV. During this phase, characterized by an initial transient improvement of the process status followed by a clear drop of the pulp to CH_4 conversion ratio and a drastic change in the microbiome composition, the three high nitrogen input reactors behaved differently. As the decline of process performance in early phase IV was progressive, the RU-PCA-MSPC model did not detect major out-of-control process values (**Figure 4.7**). Later in phase IV, the process progressively declined further in efficiency while the model provided inconsistent alarms between the replicate HNRs until the final process collapse characterized by extreme and frequent alarms (weeks 19-22). During this period, the alarm rate was clearly higher for the high nitrogen input reactor 1 than for the other high nitrogen input reactors. Differences between the reactors regarding the dynamics of the biogas composition explain this different alarm rate. As reported elsewhere (**Chapter 5**; Goux et al., 2015), these differences

in the behaviour of replicated AD reactors can be explained by a distinctive change in the reactor microbiome composition. Indeed, under sub-optimal conditions (i.e., severe stress) the microbial populations driving the AD process for each reactor progressed differently at the OTU level (data not presented). For the high nitrogen input reactor 1, the H_2S concentration abruptly increased during week 19 (**Figure 4.3**d), thus preventing adaptation of the model parameters using the selected N_{eff} value (14 days). This caused permanent out-of-control values of the T_A^2 and SPE indexes (**Figure 4.7**c,d) for the following biogas composition measurements. As compared to the high nitrogen input reactor 1, the biogas composition was more stable for the high nitrogen input reactors 2 and 3 during that period, which allowed adaptation of the model and explains the lower alarm rate observed for these reactors. This suggests that there is room for further optimisation of the N_{eff} value to be selected. Data generated during this critical process performance decline under severe FAN intoxication showed clearly the limitation of the RU-PCA-MSPC to adapt to a new process driven by a drastically modified microbiome.

Nevertheless, the RU-PCA-MSPC models also delivered marked alarm signals during all three stirrer blocking events, demonstrating a good sensitivity of disturbance detection both during low and high nitrogen input in the feed (**Figure 4.7**d,e,f).

4.3.5. Perspectives for process monitoring in full-scale AD reactors

The use of the concentrations of the major components in the biogas through PCA-MSPC models has already been assessed for early detection of FVFA intoxication in AD reactors under organic overload condition (**Chapter 3**; Lemaigre et al., 2016). However, this MSPC model used IPVs measured in the slurry in addition to the biogas composition. In the present study, RU-PCA-MSPC models using exclusively the biogas composition showed potential to predict the first signs of performance decrease of reactors exposed to FAN accumulation in the slurry (a sudden decrease of the pulp to CH_4 conversion ratio and VFA accumulation in the slurry). The RU-PCA-MSPC models correctly detected these first symptoms of process disturbance for three independent high nitrogen input reactors. These symptoms were also correlated with a drastic change in the bacterial and archaeal anaerobic communities. The model capacity to detect early signs of process

disturbance suggests a potential applicability for a large diversity of AD reactors. These results are interesting since the concentrations of the major components of the biogas are parameters that are often neglected for AD process monitoring due to lagged response (CH_4 and CO_2) or oversensitivity (H_2) to process perturbations (Björnsson et al., 2000; Boe et al., 2010). In comparison with univariate statistical process control techniques, the multivariate approach presented here considers the correlation structure of the IPVs, which could potentially compensate the lagged warning of IPVs such as CH_4 and CO_2. In addition, the PCA-MSPC models were trained on an initial period during which the process and its associate microbiome were stable. This could potentially resolve the oversensitivity to H_2 by taking into account its in-control variation in the model. These results are also promising because analysing the biogas composition allows high frequency online measurements involving low workload and reduced sampling issues, as compared to slurry analysis. Indeed, biogas analysers are often present in biogas production plants.

The RU-PCA-MSPC models showed nevertheless limitation to adapt to a process driven by a drastically modified microbiome. The models were trained on stable reactors characterized by similar microbial communities but when applied to the same reactors after they encountered a major shift in their bacterial and archaeal communities, the models provided inconsistent alarms that could not be directly related to the process performance. Thus, even if recursively updated, PCA-MSPC models show limitations when applied to a microbiome they were not trained on.

The results obtained here for the detection of a FAN intoxication suggest good versatility of the PCA-MSPC approach for the monitoring of the process in real-scale AD reactors, which are exposed to a large diversity of process disturbances. In addition, the control limits used in MSPC are independent of toxicity thresholds (L. Li et al., 2014), which are especially uncertain for FAN due to potential reactor acclimation to nitrogen-rich feedstocks (Rajagopal et al., 2013).

In the study presented in **Chapter 3** (Lemaigre et al., 2016), data collected from an independent reactor maintained in a steady state were required to build the (static) PCA-MSPC model used to monitor the process of a reactor exposed to organic overload. In the present study, we attempted to build the MSPC models by using only data collected from the monitored reactors themselves. Recursively updated PCA-MSPC showed good results in distinguishing between the actual process disturbances

and drift of the reactor in-control process baseline. However, it was demonstrated that the value of the effective memory length should be carefully selected in such recursively updated models. An optimal effective memory length value representing one quarter of the actual HRT (N_{eff} = 14 days) was selected among the tested values on the basis of the lowest alarm rate detected for a reactor known to show permanent and optimal process performance (pulp to CH_4 conversion ratio close to the BMP). An independent steady-state reactor remains therefore necessary to optimize the prediction quality of the recursively updated MSPC model. In a practical situation, the effective memory length of the model could be selected on the basis of the behaviour of post-reactors, which are known to be rarely exposed to process failure.

In the present study, MSPC techniques were demonstrated as an interesting tool to assess the process status of AD reactors by measuring the concentrations of the major components in the biogas. Currently, many biogas plant operators install biogas analysers, allowing the online measurement of the CH_4 and CO_2 concentrations in the biogas, as well as, in most cases, of its H_2S concentration (Drosg, 2013). The measurement of the H_2 concentration is also proposed as an option by many manufacturers of biogas analysers. The process monitoring method proposed here can be applied to those biogas plants that have installed such a biogas analyser, having the advantage of not requiring the installation of additional measuring equipment. This is a clear advantage as compared to the e-nose (Adam et al., 2013, 2015) or NIR-based monitoring technologies (Jacobi et al., 2009; Lomborg et al., 2009) that require additional investment for operational use.

4.4. Conclusions

Using the biogas composition through recursively updated PCA-MSPC showed potential for early warning of FAN intoxication in AD reactors, which is useful given the uncertainty related to FAN toxicity thresholds in individual reactors. The models also repeatedly detected mixing failures in the studied reactors both during low and high nitrogen input in the feed. An effective memory length of 14 days (0.25 HRT) allowed model adaptation to limit the false alarm rate. Early signs of FAN intoxication, coinciding to drastic changes in the reactor microbiomes were detected by the models for three high nitrogen input reactors, confirming their potential for general application. However, the models presented here lost their prediction

capability for process performance after a major shift in the microbiome composition of the reactor. Using only the biogas composition to detect the two main AD process disturbances (FVFA and FAN intoxication) is promising, given the general use of biogas analysers in most biogas production plants and the limitations related to slurry analysis.

Acknowledgements

This work was supported by the Fond National de la Recherche, Luxembourg (FNR CORE 2011 project GASPOP, CO11/SR/1280949: Influence of the Reactor Design and the Operational Parameters on the Dynamics of the Microbial Consortia Involved in the Biomethanation Process) and the LIST core funding. The authors are most grateful to Jillian M. Lenné and Pau Ferrer Alegre for proofreading the manuscript and their useful comments.

Chapter 5

Microbial community dynamics in replicate anaerobic reactors exposed sequentially to increasing organic loading rate, free volatile fatty acids intoxication, and process recovery

Adapted[9] from:

Goux, X., Calusinska, M., Lemaigre, S., Marynowska, M., Klocke, M., Udelhoven, T., Benizri, E., & Delfosse, P. (2015). Microbial community dynamics in replicate anaerobic digesters exposed sequentially to increasing organic loading rate, acidosis, and process recovery. *Biotechnology for Biofuels*, *8*(1), 122. doi:10.1186/s13068-015-0309-9

[9] Changes were made to some units and vocabulary terms to enhance consistency between the chapters of this thesis, particularly between **Chapters 3** and **5**, which both utilise results from the same experiment. Specifically, the term "free VFA intoxication" is now more frequently used to refer to the assessed AD process disturbance. Reactor acronyms CR and R1-R3 were replaced with SSR and OR1-OR3, respectively. In § 5.2.1, the biogas monitoring methods described in **Chapter 3** were not repeated. **Figure 5.2** was divided into four separate figures (one for each reactor) for improved readability in the thesis format. A brief statement was added at the beginning of § 5.3.7 to emphasise that the intoxicated reactors had nearly stopped producing methane before our process recovery strategy was implemented. Finally, the original highlights were replaced with those provided at the beginning of this chapter, which are more relevant to the context of the thesis.

Context and contribution to the thesis

Bioaugmentation has proven effective in restoring AD performance following free VFA intoxication at laboratory scale, but its application to full-scale digesters remains limited, mainly due to the logistical challenges of cultivating, storing, and delivering specialised inoculum on-site. As a more practical alternative, chemical recovery strategies warrant investigation. In this chapter, reactors were sequentially subjected to increasing organic loading, critical intoxication by free VFAs, and finally a chemical recovery approach aimed at restoring neutral pH conditions in the slurry and reinitiating methane production..

In this context, **Chapter 5**[10] of this thesis utilises results from AD experiment **Exp1_FVFA_intoxication**[11] to address the research question **Q2 Recovery from FVFA intoxication** (*Can the AD process be recovered after a critical FVFA intoxication without supplementing the intoxicated reactors with inocula acclimatised to VFAs?*).

[10] This chapter is an adapted version of a publication that examined experiment **Exp1_FVFA_intoxication** from a microbiological perspective. As a co-author of this paper, I developed the reactors, conducted metabolic monitoring, and designed the process recovery strategy. In addition to the overfed reactor OR described in **Chapter 3** (referred to as OR3 in this chapter), this recovery strategy was applied to two additional reactors (referred to as OR1 and OR2) that underwent the same treatment since their inoculation.

[11] AD reactors progressively overfed until critical FVFA intoxication + Assessment of a process recovery strategy

Highlights

- A chemical recovery strategy combining starvation, pH correction (NaOH), and buffering ($NaHCO_3$) restored CH_4 production in three pilot-scale AD reactors affected by critical FVFA intoxication.
- Methane production resumed within 20 days, significantly faster than recovery times previously reported with bioaugmentation.
- Re-inoculation was not required, as methanogenic populations survived despite extremely acidic conditions (pH 5.2 ± 0.4).
- Recovery was associated with shifts in the archaeal community, notably the proliferation of *Methanosarcina* spp. in two reactors.
- Propionate accumulation persisted post-recovery, highlighting the importance of long-term process supervision.

Abstract

Background: Free volatile fatty acids (FVFA) intoxication, a common process disturbance in anaerobic reactors, leads to drastic losses in methane production. Unfortunately, little is known about the microbial mechanisms underlying this disturbance and the potential to recover the process. In this study, three mesophilic anaerobic reactors of 100 L were exposed to FVFA intoxication resulting from an excessive feeding with sugar beet pulp; they were compared to a steady-state reactor.
Results: Stable operational conditions at the beginning of the experiment initially led to similar microbial populations in the four reactors, as revealed by 16S rRNA gene T-RFLP and high-throughput amplicon sequencing. *Bacteroidetes* and *Firmicutes* were the two dominant phyla, and although they were represented by a high number of operational taxonomic units, only a few were dominant. Once the environment became deterministic (selective pressure from an increased organic loading rate), microbial populations started to diverge between the overfed reactors. Interestingly, most of bacteria and archaea showed redundant functional adaptation to the changing environmental conditions. However, the dominant *Bacteroidales* were resistant to high volatile fatty acids content and low pH. The severe FVFA intoxication did not eradicate archaea and a clear shift in archaeal populations from acetotrophic to hydrogenotrophic methanogenesis occurred in the overfed reactors. After 11 days of severe intoxication (pH 5.2 ± 0.4), the process was quickly recovered (restoration of the biogas production with methane content above 50 %) in the overfed reactors, by adjusting the pH to around 7 using NaOH and $NaHCO_3$.
Conclusions: In this study, we show that once replicate reactors are confronted with sub-optimal conditions, their microbial populations can start to evolve differentially. Furthermore, the alterations of commonly used ecological parameters to monitor the process, such as richness, evenness and diversity indices were unsuccessful to detect the process disturbance. At the same time, we tentatively propose the replacement of the dominant *Methanosaeta* sp. in this case by *Methanoculleus* sp., to be a potential warning indicator of FVFA intoxication.

5.1. Background

Anaerobic digestion (AD) of biomass, including wastewater, agro-food residues, municipal solid waste, and energy crops, is not only regarded as a promising source of renewable energy, but also generates environmental benefits. Especially, AD contributes to reduce the emission of greenhouse gases, manure odour and pathogens (Möller & Stinner, 2009; Yiridoe et al., 2009), while allowing the recovery of essential nutrients (N, P, and K). The main products of the AD process are the biogas and the digestion residue (syn. digestate). Biogas is composed of methane (CH_4), carbon dioxide (CO_2) and trace gases such as H_2S, NH_3 and H_2. Due to its high calorific value, biogas can be combusted in combined heat and power units (CHP) to provide electricity and heat. Alternatively, by eliminating CO_2 and trace gases, biogas can be upgraded to biomethane, which is equivalent to natural gas in terms of CH_4 purity and can thus be injected into the gas grid or compressed to be used as transport fuel. On the other hand, digestion residue is rich in nutrients and progressively gains reputation as a fertilizer in agriculture (Wilkie, 2014).

The AD process is conducted by various microbial groups interacting to decompose organic matter into simple molecules. During the first stage called hydrolysis, facultative or obligatory anaerobic fermenting bacteria decompose proteins, fats and polysaccharides into soluble compounds (i.e., amino acids, long-chain fatty acids and sugars). In continuation, during the acidogenic stage, fermentative bacteria convert these by-products into volatile fatty acids (VFAs), CO_2, H_2, and alcohols. Furthermore, VFAs, CO_2 and H_2 are transformed by acetogenic bacteria to produce acetate (acetogenesis stage). Finally, during the methanogenesis stage, acetate on the one hand, and H_2 and CO_2 on the other hand, are converted to methane by the acetotrophic (syn. acetoclastic) and the hydrogenotrophic methanogenic archaea, respectively (Ahring, 2003). Even though the major paths of the AD process are well described, the complexity of the microbial activities, competition, and syntrophies are not well understood (Carballa et al., 2015). Importantly, the performance of an AD reactor is closely linked to the structure and dynamics of its microbiome (Demirel & Scherer, 2008). Therefore, the importance of understanding the AD microbiome and the need of establishing microbial indicators of process performance are currently considered as key research subjects towards the

improvement of the AD process and the understanding of its disturbances (Carballa et al., 2015).

Free VFA (FVFA) intoxication is an AD process disturbance where un-ionised VFAs inhibit methanogens by permeating across their cell membrane, causing intracellular acidification and altering their CH_4 production. It usually results from excessive reactor feeding or the use of rapidly degradable feedstocks (Akuzawa et al., 2011). This disturbance can cause the acidification of the slurry due to accumulation of VFAs. VFAs accumulation directly reflects the kinetic imbalance between their production by fermentative bacteria and their consumption by a combined effort of acetogenic bacteria and methanogenic archaea (Ahring et al., 1995). FVFA intoxication is the most common process disturbance taking place in AD reactors (Akuzawa et al., 2011). As a proof, biogas plant managers regularly seek advice and recommendation on how to quickly and efficiently recover the process after the occurrence of a FVFA intoxication in their digester (personal interactions with several biogas plants managers of the Greater Region including Luxembourg, and part of Belgium, France and Germany). In general, FVFA intoxication is not easy to prevent using conventional AD process indicators (Adam et al., 2015). For instance, VFAs accumulation in the slurry does not result in a quick pH drop in well-buffered reactors (Franke-Whittle et al., 2014). However, due to their high sensitivity to increased VFAs concentrations and pH changes, archaeal communities are quickly inhibited in case of FVFA intoxication, which causes the CH_4 production to decrease in the AD reactors that are exposed to this process disturbance (Weiland, 2010). Consequently, FVFA intoxication represents an important economic loss for the biogas plant managers, which is amplified by the massive production of acidic digestion residue that does not meet the fertilisation requirements anymore (Möller & Müller, 2012). For these reasons, it is important on the one hand, to efficiently predict and prevent FVFA intoxication and on the other hand, to quickly restart the process after it collapses (Lerm et al., 2012). Indeed, the poor biogas quality (low CH_4 content) often prevents from heating the AD reactors exposed to FVFA intoxication (due to forced shutdown of the CHP unit), which amplifies the microbial stress. While recent studies have brought more evidence about changes in the microbiome structure of AD reactors exposed to VFAs accumulation (Akuzawa et al., 2011; Blume et al., 2010; Delbès et al., 2006; Franke-Whittle et al., 2014), little is known about the individual

sensitivity of each reactor regarding FVFA intoxication, and the capability of the process to recover when the pH is brought back to neutrality.

Therefore, this study had two objectives. Firstly, to investigate the assumption that an increasing content of VFAs in the slurry (and the consecutive pH drop) directly influences the microbial communities of AD reactors (what is reflected by a decreased methane production), we gradually increased the organic loading rate (OLR) in three test reactors (OR1, OR2 and OR3), while a steady-state reactor (SSR) was maintained in cautious feeding regime and used as a reference (**Figure 5.1**). Secondly, to establish potential (microbial) warning indicators of AD process failure, we characterized the dynamics of the microbial (bacterial and archaeal) communities for six sampling periods P0-P5 (**Figure 5.1**) in relation to physicochemical parameters in the continuously (completely) stirred tank reactors (CSTRs) sequentially exposed to (1) an increasing OLR of sugar beet pulp, (2) FVFA intoxication, and (3) process recovery. Microbial communities were investigated in the four reactors by means of molecular techniques including, 16S rRNA gene-based terminal restriction fragment length polymorphism (T-RFLP) and 16S rRNA high-throughput amplicon sequencing (HTS). In addition, common process parameters such as pH, total solids (TS), volatile solids (VS), total inorganic carbon (TIC), total ammonia nitrogen (TAN) and biogas production and quality were monitored during the experiment and analyzed with respect to the dominant microbes and the AD process status.

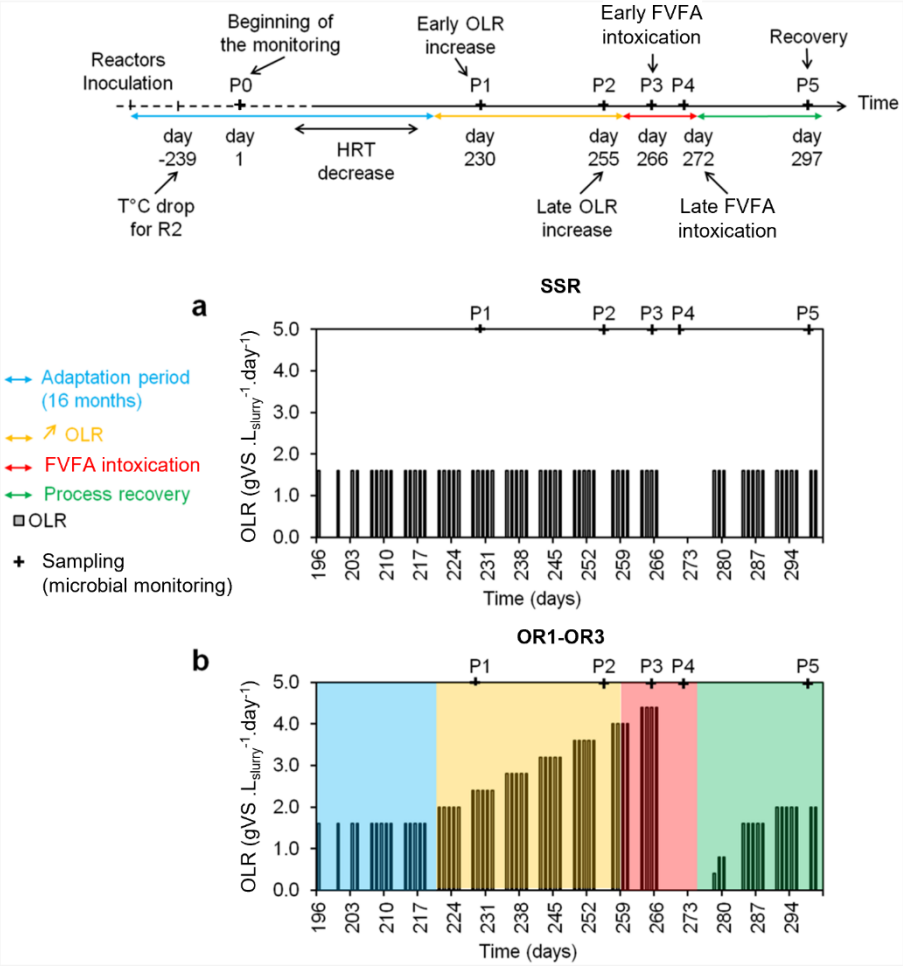

Figure 5.1. Diagram of the anaerobic digestion experiment. Progress over time of the organic loading rate (OLR, vertical bars) for the control reactor maintained in steady-state (SSR, a) and the test reactors (OR1-OR3, b); P0 (beginning of the microbial monitoring), P1 (early OLR increase), P2 (late OLR increase), P3 (early FVFA intoxication), P4 (late FVFA intoxication), and P5 (recovery) are the sampling periods chosen for microbial community analyses. FVFA: free volatile fatty acids. *Note: The reactors referred to as SSR and OR3 correspond to the reactors referred to as SSR and OR in* **Chapter 3***, respectively. Additionally, the day 207 of the assessed period corresponds to the day 0 of the period assessed in* **Chapter 3**.

5.2. Material and methods

5.2.1. Reactors operation, monitoring and sampling

Four anaerobic pilot-scale CSTRs were inoculated with slurry originating from a mesophilic AD reactor of a wastewater treatment plant (WWTP) located in Schifflange, Luxembourg (SIVEC-Schifflange). To mimic as closely as possible the conditions of full-scale anaerobic digesters, the reactor working volume was 100L. Each reactor was equipped with an individual temperature control system to ensure a constant temperature of 37 ± 0.2 °C corresponding to mesophilic digestion conditions.

The pH of the slurry was measured daily with a pH 196 Microprocessor pH meter connected to a SenTix® 21 pH electrode (WTW, Weilheim, Germany). The contents of total solids (TS, expressed in gram per gram of fresh matter, $gTS.gFM^{-1}$) and volatile solids (VS, $gVS.gTS^{-1}$) in the slurry were measured weekly, according to the VDI 4630 norm (Kaltschmitt et al., 2005). The contents of total inorganic carbon (TIC, $gCaCO_3.L_{slurry}^{-1}$) and total ammonia nitrogen (TAN, $gN\text{-}NH_4.L_{slurry}^{-1}$) were measured weekly in the slurry using the BiogasPro system (RIMU, Königsbrunn, Germany), in conformity with the manufacturer's protocol. The concentrations of VFAs in the slurry were measured following an ether extraction and using a gas chromatograph (Agilent technologies, Santa Clara, USA) equipped with a Varian CP-FFAP column and a flame ionization detector (FID). The ellution was done with helium (He) as a carrier gas. The total VFAs concentration ($g.kg_{slurry}^{-1}$) was calculated as the sum of the individual VFAs concentrations, measured for acetate, propionate, isobutyrate, butyrate, isovalerate, valerate and caproate. The biogas production and composition in CH_4, CO_2 and H_2 were monitored hourly using the methods described in **Chapter 3**. In addition, the H_2S content of the biogas was measured hourly in the 0-10000 ppm range with an electro-chemical sensor (I-41, ITG, Wismar, Germany).

The reactors were fed every working day (i.e., Monday to Friday), using dried sugar beet pulp pellets (**Table 3.1**) as a mono-feedstock The pulps were suspended in with tap water at 37°C to adjust the HRT. To mimic the operation of full-scale anaerobic digesters, the feedstock was not sterilised. Following the inoculation, during a 16-month adaptation phase (data not shown), the four reactors were fed with a constant OLR of 1.6 grams of VS per litre of slurry and per working day ($gVS\ L_{slurry}^{-1}\ day^{-1}$), i.e., 1.14 g of VS per litre of slurry and per day on a weekly

average. This led the TS content of the slurry to increase from ~0.01 gTS gFM^{-1} to ~0.07 gTS gFM^{-1}, a value commonly observed in agricultural biogas digesters. Once the TS content stabilized, slurry was sampled (sampling period zero: P0, day 1) and the experimental campaign was initiated (**Figure 5.1**). Following this first sampling, the hydraulic retention time (HRT) was progressively reduced to 28 days, by mixing the sugar beet pulp with increasing volumes of tap water. From day 207 onwards, this 28-days HRT was left unchanged for the four reactors. After two weeks (day 221), the acclimation period terminated. Three reactors (overfed test reactors: OR1, OR2, OR3) were then fed with an increasing OLR, while the remaining reactor was used as a reference (steady-state reactor; SSR), which remained cautiously fed with a constant OLR of 1.6 $gVS.L_{slurry}^{-1}.day^{-1}$. The choice of this experimental design (three replicated test reactors versus only one control reactor) was dictated by the fact that only four reactors of 100L capacity were available. Therefore, we decided to give priority to the test reactors for data generation. For the three test reactors ORs, the OLR was gradually increased every week, by increments of 0.4 $gVS.L_{slurry}^{-1}.day^{-1}$, until a free VFA intoxication was reached (**Figure 5.1**b).

The following strategy was applied to the ORs to promote the recovery of the AD process. The feeding was stopped at day 267. After 6 days of starving under highly acidic pH (5.2 ± 0.4), the pH was artificially increased to reach a value of 7.0. First, for each OR, a sample of slurry was titrated against 1M NaOH until the pH was increased to 7.0. This required the introduction of 0.07, 0.02 and 0.05 L of solution per litre of slurry for the OR1, OR2 and OR3, respectively (i.e 0.07, 0.02 and 0.05 $mol\_NaOH.L_{slurry}^{-1}$, respectively). Then, the corresponding volumes of 1M NaOH were introduced in the slurry the ORs. In continuation, $NaHCO_3$ dry salt was progressively added in the ORs to increase the TIC content of the slurry until a pH of 7.5 was reached. This required the introduction of 9, 6 and 8 g $NaHCO_3$ per litre of slurry for the OR1, OR2 and OR3, respectively (i.e., 0.107, 0.070 and 0.095 $mol\_NaHCO_3.L_{slurry}^{-1}$). The three test reactors were then starved for 5 more days. The total starving period of 11 days was also applied to the SSR. Finally, as the methane content in the biogas reached again at least 50 %v/v for the ORs, the feeding was progressively restarted for all the reactors to reach an OLR of 1.6 $gVS.L_{slurry}^{-1}.day^{-1}$. Slurry aliquots were sampled from the four reactors for six periods P0-P5 (**Figure 5.1**) and stored at -20 °C prior the microbial community analyses.

5.2.2. Microbial monitoring by 16S rRNA gene-based T-RFLP analysis

Genomic DNA was extracted as previously described by Klocke et al. (2007). Bacteria-specific 16S rRNA gene forward primer 27f, labelled with 6-carboxyfluorescein (6-FAM), and the reverse primer 926MRr (**Table 5.1**; Eurogentec, Seraing, Belgium), were used for amplification with the following PCR conditions: initial denaturation at 98 °C for 3 min, followed by 25 cycles of denaturation at 98 °C for 20 s, annealing at 54 °C for 15 s, elongation at 72 °C for 1 min and a final elongation at 72 °C for 7 min. To amplify the archaeal 16S rRNA gene, forward primer Ar109f labelled with 6-FAM and the reverse primer Ar912r (**Table 5.1**; Eurogentec, Seraing, Belgium) were used with the following PCR conditions: initial denaturation at 98 °C for 3 min, followed by 29 cycles of denaturation at 98 °C for 20 s, annealing at 55 °C for 15 s, elongation at 72 °C for 1 min, and a final elongation at 72 °C for 7 min. Amplifications were done using a TProfessional Thermocycler (Biometra GmbH, Goettingen, Germany) and the Phusion® Taq polymerase (New England Biolabs Inc., Ipswich, USA) in a final volume of 25 µL with 0.4 µM of each primer and 0.5 µL of a 1:10 and 1:50 dilution of the DNA extracts, for bacteria and archaea respectively. PCR products were purified with the QIAquick PCR Purification Kit (Qiagen, Hilden, Germany) according to the manufacturer's protocol. In continuation, 100-200 ng of purified bacterial 16S rRNA amplicons were digested at 37 °C for 4 h with the MspI and Hin6I restriction enzymes (Thermo Fisher Scientific, Waltham, USA). For Archaea, between 200 and 500 ng of PCR products were digested at 37 °C for 4 h with the AluI restriction enzyme (Thermo Fisher Scientific, Waltham, USA). Digested products were precipitated with 0.1 v/v of sodium acetate (3 M) and 10 v/v of ethanol (75 %). Samples were incubated for 30 min in the dark and at room temperature, and centrifuged at 14,000 rpm at 4 °C for 30 min. Following the centrifugation, the supernatant was discarded, 10 v/v of ethanol (75 %) was added, and samples were incubated for a second time during 10 min in the dark and at room temperature; and centrifuged at 14,000 rpm and 4 °C for 30 min. Finally, following the centrifugation, the supernatant was discarded, samples were dried at 37 °C, re-suspended in 40 µL of sterile ultrapure water and incubated at 55 °C for 15 min at 300 rpm. In continuation, samples were mixed with 10 µL of Hi-Di formamide (Applied Biosystems, Stafford, USA) containing 1:250 (v/v) carboxy-X-rhodamine (ROX)-labeled MegaBace™ ET900-R size standard (GE Healthcare,

Piscataway, USA). Ultrapure water was added to reach the final volume of 16 µL. Samples were denatured at 95 °C for 3 min and directly placed on ice. The sizes of generated DNA fragments were determined using an Applied Biosystems 3130 Genetic Analyser (Applied Biosystems, Stafford, USA) (POP 7 matrix, capillary size: 50 cm) with the following parameters: injection voltage, 3.0 kV; injection duration, 12 s; run voltage, 8.5 kV; run time at 60 °C, 5500 s. The GeneMapper software (version 4.0; Applied Biosystems, Stafford, USA) was used to analyse the T-RFLP chromatograms. Fragments with fluorescence intensity below 200 relative fluorescence units were discarded from further analysis and, following Dunbar et al. (2001), the total fluorescence of each sample was standardized three times to the smallest quantity. Online T-Rex software was used to align the T-RFs with a clustering threshold of 0.8 (Culman et al., 2009). The length of each T-RF was expressed in base pair (bp). An average of three technical replicates performed for each sample is presented as results.

Table 5.1. PCR primers targeting the 16S rRNA genes of the bacterial and archaeal community.

Primer	Direction	Sequence [5' -> 3']	Targeted domain	Reference
27f	forward	AGA GTT TGA TCM TGG CTC AG	Bacteria	(Lane, 1991)
926MRr	reverse	CCG TCA ATT CMT TTR AGT TT	Bacteria	(Weisburg et al., 1991)
S-D-Bact-0341-a-S-17	forward	CCT ACG GGA GGC AGC AG	Bacteria	(Klindworth et al., 2013)
S-D-Bact-0787-b-A-20	reverse	GGA CTA CHV GGG TAT CTA AT	Bacteria	(Klindworth et al., 2013)
Ar109f	forward	ACK GCT CAG TAA CAC GT	Archaea	(Großkopf et al., 1998)
Ar 912r	reverse	CTC CCC CGC CAA TTC CTT TA	Archaea	(Lueders & Friedrich, 2000)
S-D-Arch-0519-a-S-15	forward	CAG CMG CCG CGG TAA	Archaea	(Klindworth et al., 2013)
S-D-Arch-1041-a-A-18	reverse	GGC CAT GCA CCW CCT CTC	Archaea	(Klindworth et al., 2013)

5.2.3. Microbial monitoring by high-throughput 16S rRNA amplicon sequencing

Genomic DNA extractions from samples of the six sampling periods P0-P5 were performed this time using the PowerSoil DNA Isolation Kit (Mobio Laboratories Inc., Carlsbad, CA, USA) in accordance with the manufacturer's protocol. The 16S rRNA gene libraries were constructed with a modified primer pair S-D-Bact-0341-a-S-17 and S-D-Bact-0787-b-A-20 targeting a fragment of 466 bp of the bacterial V3-4 region and primer pair S-D-Arch-0519-a-S-15 and S-D-Arch-1041-a-A-18 targeting a fragment of 526 bp of the archaeal V4-6 region (**Table 5.1**). The modification included the incorporation in the 5' end of the Nextera XT® transposase sequence (Illumina Inc., San Diego, USA) in the forward and the reverse primer, and additional four N (i.e., four random nucleotides) in the forward primer to increase the nucleotide diversity. Amplicons were generated using the Q5® Hot Start High-Fidelity DNA Polymerase (New England Biolabs Inc., Ipswich, USA), purified with the AMpure magnetic beads (Agencourt, Beckman Coulter Inc., Fullerton, USA) and quantified with the Qubit® dsDNA HS assay kit (Life technologies, Carlsbad, USA). The concentration of the amplicons was adjusted to 1 ng μL^{-1} and 1 µL of each library was used as a template in a second PCR reaction where the Nextera XT® barcodes and the Illumina adapters necessary for hybridization to the flow cell were added with the Nextera XT Index kit. The resulting amplicons were purified with the AMpure magnetic beads (Agencourt) and pooled in equimolar concentrations. The final concentration of the library pool was determined with a KAPA SYBR® FAST Universal qPCR Kit (Kapa Biosystems, Wilmington, USA). Libraries were mixed with Illumina-generated PhiX control libraries (5 %) and sequenced with the MiSeq Reagent Kit V3-600 cycles. The obtained sequence reads were de-multiplexed, quality trimmed and assigned to OTUs at 97 % similarity with Usearch (v7.0.1090_win64) pipeline (Edgar, 2010). Taxonomy affiliation was done with the Greengenes database (http://greengenes.lbl.gov/) and the final nucleotide sequences obtained were deposited in the GenBank database (http://www.ncbi.nlm.nih.gov/genbank/) under accession numbers KR013301 to KR013741 for bacteria and KR013288 to KR013300 for archaea.

5.2.4. Data analysis and statistics

Microbial diversity was measured through the computation of three alpha diversity indices. Richness, reflecting the number of distinct T-RFs and OTUs, was calculated to assess the variety of taxa present in the microbial community. Evenness, describing how uniformly individuals are distributed among these taxa, was measured using the Pielou index (J) (Pielou, 1967). Overall community diversity, integrating both richness and evenness, was quantified using the Shannon-Weaver index (H′) (Shannon, 1948). To assess the diversity indices (J, richness, H′) over time, linear mixed-effect models (LMM) were calibrated for each reactor, considering time (the different sampling points) as fixed factor and the replicates as random factor. Post hoc tests (Tukey's honest significant difference test) were applied to further compare pairwise sampling points for significant LMM. To compare, respectively, the bacterial and archaeal community results from the two molecular techniques (T-RFLP and HTS) used in this study, pairwise Bray-Curtis (Bray & Curtis, 1957) distance matrices were calculated using Mothur (Schloss et al., 2009) and represented using non-metric multidimensional scaling (NMDS) diagrams. The average pairwise Bray-Curtis distance for each microbial community between results from T-RFLP and HTS were then compared statistically using Wilcoxon signed-rank test. Differences were considered statistically significant at a p-value < 0.05. The influence of process parameters on the microbial community diversity, assessed by HTS, was analysed using canonical correspondence analysis (CCA) with the CANOCO software (version 4.5) (Ter Braak, 1987) and a correlation analysis (Spearman). The significance test for CCAs was carried out by Monte Carlo permutation (499 times) and correlations were considered significant at a p-value < 0.05. All statistical and correlation analyses were performed using the freeware R version 3.1.0 (R Core Team, 2013).

5.3. Results and discussion

5.3.1. Operational parameters and anaerobic digestion process performance

The reactors were previously acclimated for 16 months to adapt to a mono-feedstock, sugar beet pulp, and to reach a steady-state with a final HRT of 28 days (**Figure 5.1**). The steady-state reactor SSR was constantly and cautiously fed with

sugar beet pulp at an OLR of 1.6 $gVS.L_{slurry}^{-1}.day^{-1}$, ensuring a stable process with slurry parameters in the following ranges: 7.1 < pH < 7.6, TIC = 8.825 ± 0.003 $gCaCO_3.L_{slurry}^{-1}$ (average ± standard deviation (n-1)), TAN < 1.5 $gN\text{-}NH_4.L_{slurry}^{-1}$ (**Figure 5.2**a,b), 0.019 < TS < 0.024 $gTS.gFM^{-1}$ and 0.60 < VS < 0.67 $gVS.gTS^{-1}$.

For the three test reactors ORs and from the beginning of the OLR increase (sampling period P1), a substantially low TS content in the slurry, between 0.025 and 0.041 $gTS.gFM^{-1}$, resulted in high sensitivity to VFA accumulation. At P1, acetate was the dominant VFA in the test reactors and its concentration was only 0.409 ± 0.026 $g.kg_{slurry}^{-1}$. Then, progressive overfeeding of the ORs during sampling periods P2 (late OLR increase) and P3 (early FVFA intoxication) led the total VFA concentration to reach the value of 10.6 ± 2.7 $g.kg_{slurry}^{-1}$, for an OLR of 4.4 $gVS.L_{slurry}^{-1}.day^{-1}$ (**Figure 5.3**, **Figure 5.4** and **Figure 5.5**). This VFA accumulation led the slurry pH to decrease to reach the value of 5.2 ± 0.4 at P3. During the late OLR increase (P2), the TIC content of the slurry decreased from ~10.13 $gCaCO_3.L_{slurry}^{-1}$ at P1 to reach ~1.47, ~5.39 and ~2.94 $gCaCO_3.L_{slurry}^{-1}$ at P2 for OR1, OR2 and OR3, respectively. During the late FVFA intoxication phase (P4), the concentration in total VFAs continued to increase to reach a maximal value of ~12 $g.kg_{slurry}^{-1}$ for OR1 and OR3, and ~8 $g.kg_{slurry}^{-1}$ for OR2. At this stage, acetate, propionate, and isobutyrate were the dominant VFAs and accounted for 70 ± 6 %, 11 ± 1 % and 3 ± 1 % of total VFAs, respectively. Even though a propionate/acetate ratio above 1.4 is considered as one of the most appropriate indicators of process imbalance (Hill et al., 1987), for the three test reactors, it did not exceed 0.17 ± 0.0, which could prevent the right diagnosis of the reactor state if only relying on VFAs measurement. Indeed, it was previously reported that different reactors could have their own specific VFAs levels at steady-state because the conditions that are considered stable for one reactor may not be optimal for another (Angelidaki & Ahring, 1993; Franke-Whittle et al., 2014; Murto et al., 2004). Therefore, VFAs concentrations should be used carefully as AD process stability indicators since VFA toxicity thresholds are reactor-dependant.

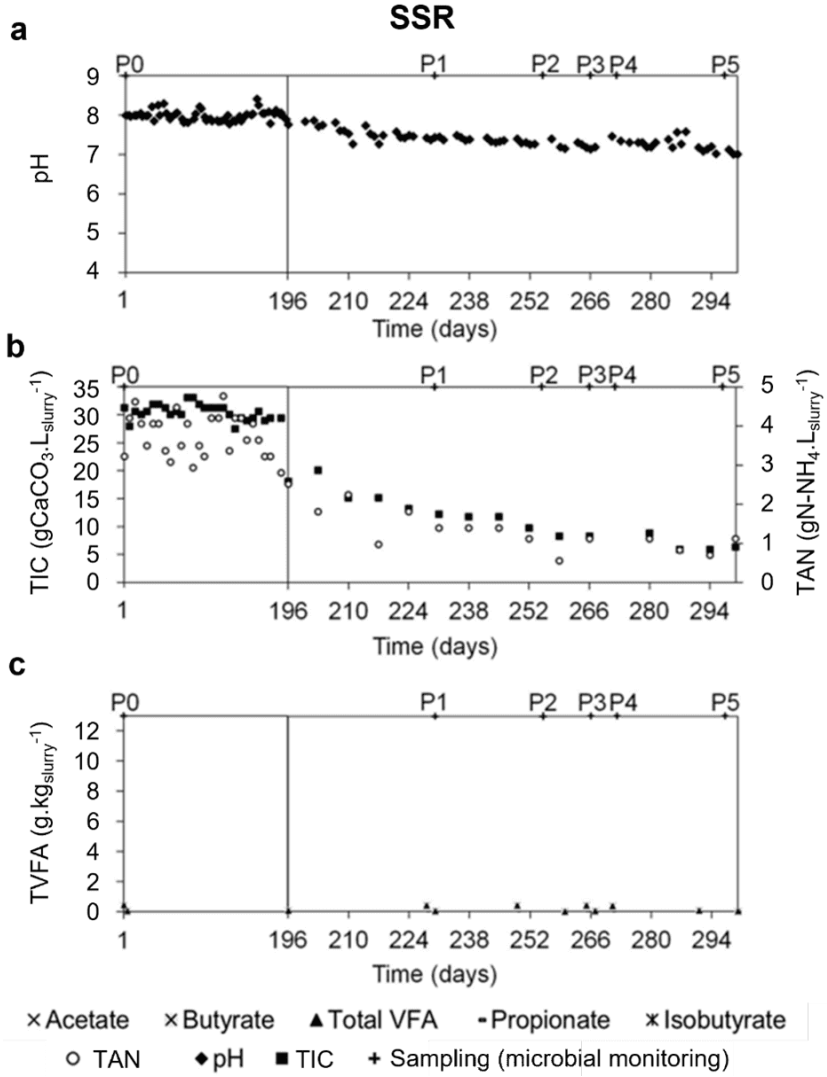

Figure 5.2. Progress over time of the characteristics of the slurry for the steady-state reactor (SSR) used as a control: (a) pH; (b) total inorganic carbon (TIC) and total ammonia nitrogen (TAN) contents; (c) total concentration of volatile fatty acids (TVFA). P1-P5: sampling periods for microbiome analyses, defined in **Figure 5.1**.

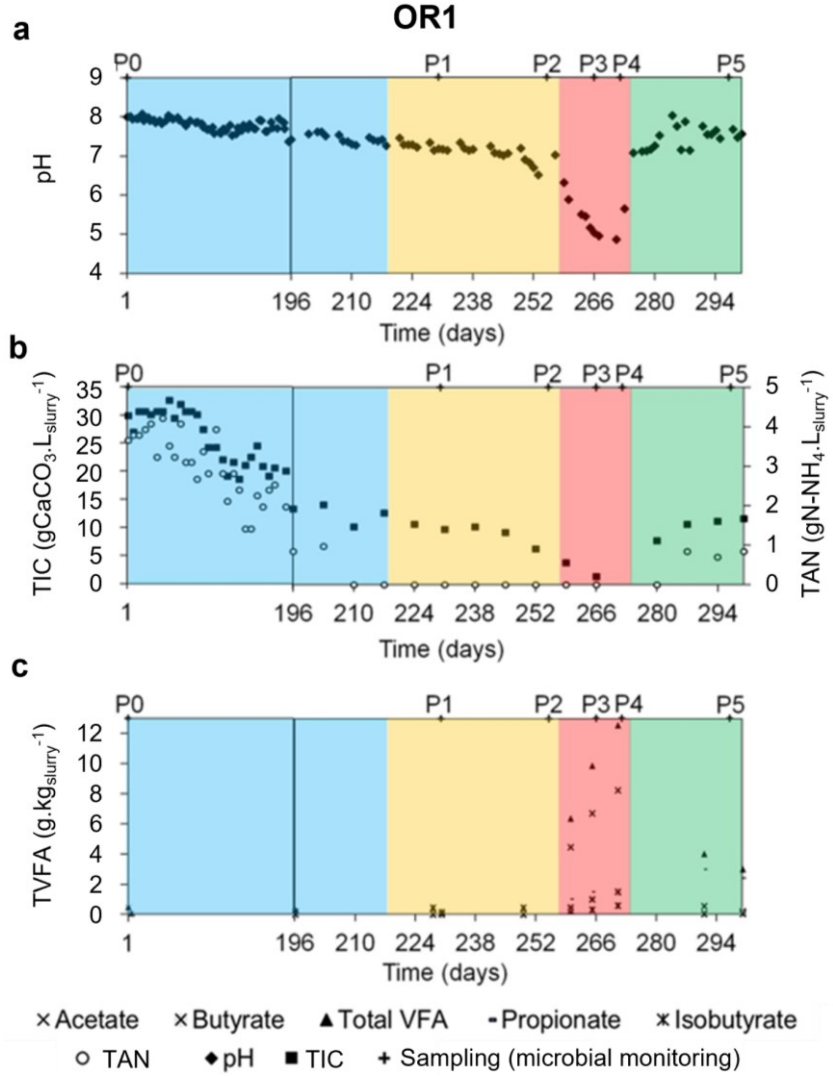

Figure 5.3. Progress over time of the characteristics of the slurry for the test reactor 1 (OR1): (a) pH; (b) total inorganic carbon (TIC) and total ammonia nitrogen (TAN) contents; (c) total concentration of volatile fatty acids (TVFA). P1-P5: sampling periods for microbiome analyses, defined in **Figure 5.1**.

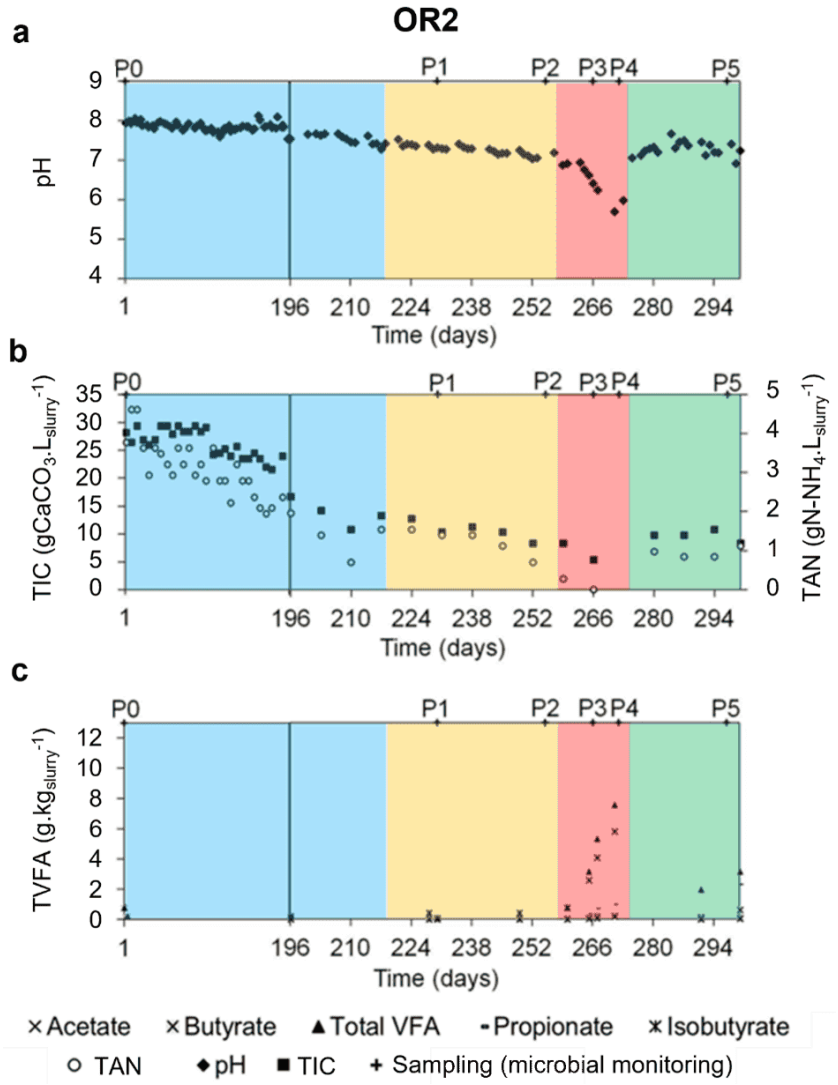

Figure 5.4. Progress over time of the characteristics of the slurry for the test reactor 2 (OR2): (a) pH; (b) total inorganic carbon (TIC) and total ammonia nitrogen (TAN) contents; (c) total concentration of volatile fatty acids (TVFA). P1-P5: sampling periods for microbiome analyses, defined in **Figure 5.1**.

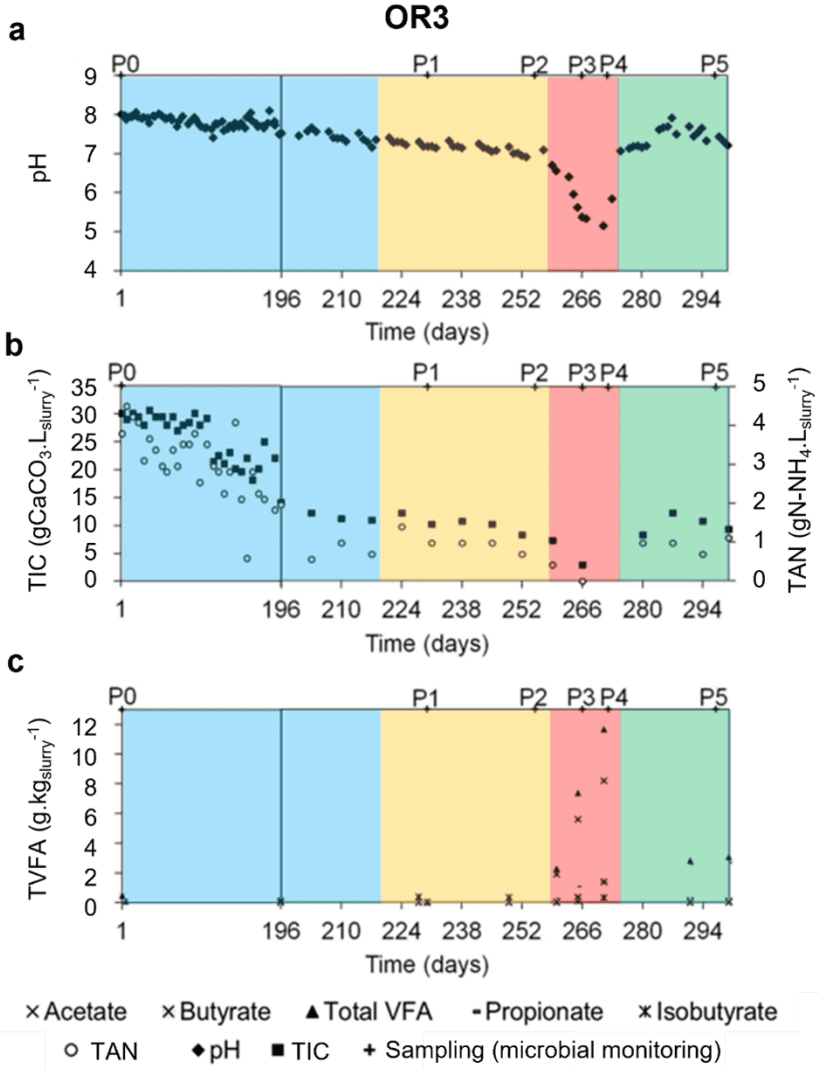

Figure 5.5. Progress over time of the characteristics of the slurry for the test reactor 3 (OR3): (a) pH; (b) total inorganic carbon (TIC) and total ammonia nitrogen (TAN) contents; (c) total concentration of volatile fatty acids (TVFA). P1-P5: sampling periods for microbiome analyses, defined in **Figure 5.1**.

During the late FVFA intoxication phase (P4), large differences in biogas production and composition were observed between the reactors (**Figure 5.6**). The CH_4 content of the biogas released by the ORs abruptly decreased to reach minimal values of 9, 25, and 32 %v/v for OR1, OR2 and OR3, respectively. In comparison, the CH_4 content in the biogas released by the SSR remained higher than 55%v during the same period. Moreover, H_2 production peaks (> 2000 ppmv) were detected for the ORs indicating a decoupling between the H_2-producing and H_2-consuming microorganisms (**Figure 5.6**d-f).

Following the FVFA intoxication, a process recovery (restoration of biogas production with average methane content above 50%v; P5) was promoted by an artificial pH increase, which led the total VFAs concentration to decrease to the level of ~4.0, ~2.0 and ~2.8 $g.kg_{slurry}^{-1}$ for OR1, OR2 and OR3, respectively (P5; **Figure 5.3**c, **Figure 5.4**c and **Figure 5.5**c, respectively). A significant increase in methane content in the biogas was concomitant with acetate consumption, what could indicate the re-establishment of the acetoclastic methanogenesis. However, at the same time, propionate was the dominant VFA (75 and 90 % of total VFAs for OR1 and OR2-OR3, respectively) and the propionate/acetate ratio was above 12.5 ± 6.4 during the recovery stage. Incapacity to quickly re-consume propionate might point to the fact that acetogenic bacteria were the one the most affected by the experimental conditions examined in this study. Propionate oxidation is a thermodynamically unfavourable reaction ($\Delta G0'$ equals +72 $kJ.mol_{propionate}^{-1}$) that occurs only if H_2-producing (propionate oxidising acetogens) and H_2-consuming (mostly hydrogenotrophic methanogens and homo-acetogens) microbial populations are balanced, which allows syntrophic propionate oxidation (Gallert & Winter, 2005).

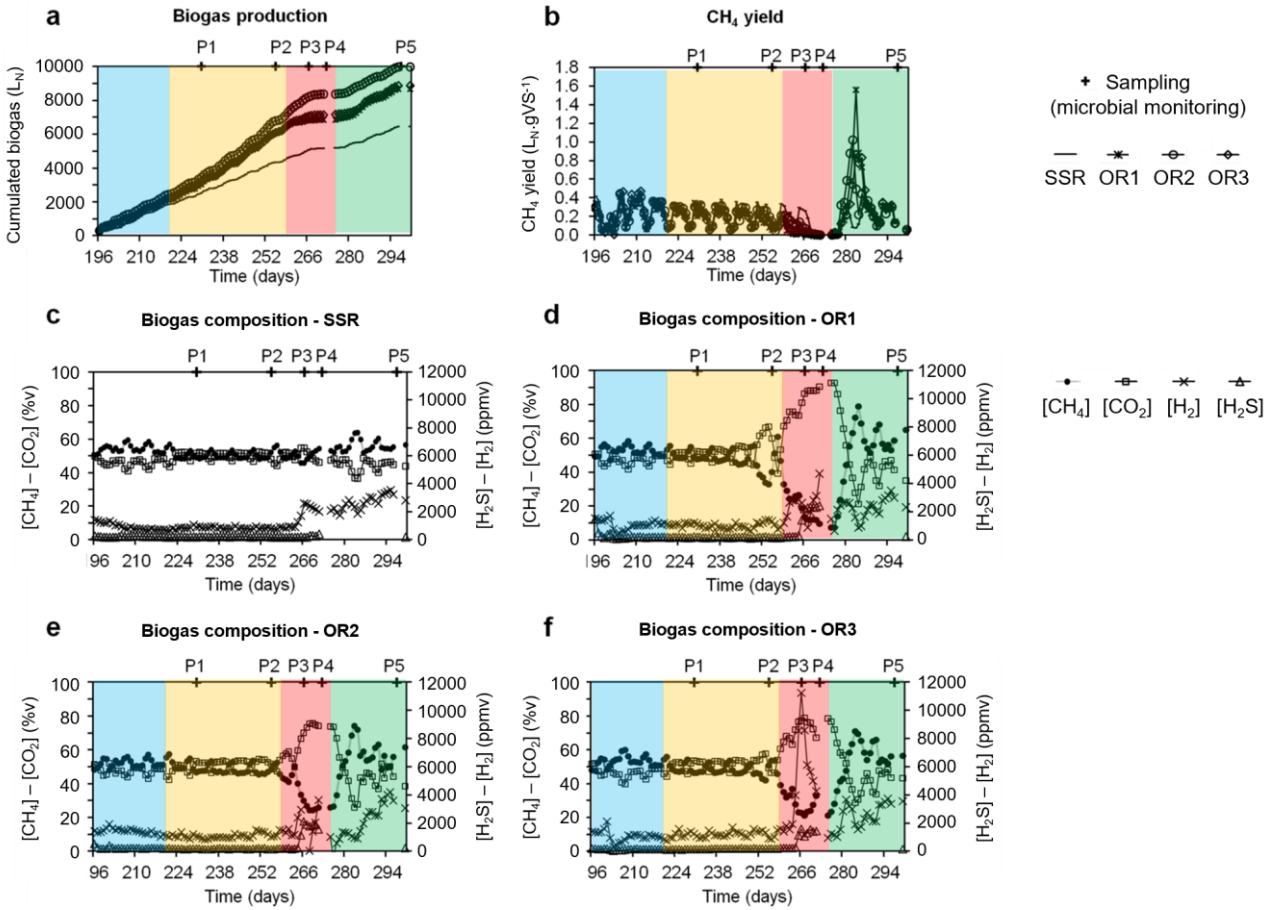
a
Biogas production
Cumulated biogas (L_N)
Time (days)
b
CH_4 yield
CH_4 yield (L_N.gVS^{-1})
Time (days)
Sampling
(microbial monitoring)
SSR OR1 OR2 OR3
c
Biogas composition - SSR
d
Biogas composition - OR1
e
Biogas composition - OR2
f
Biogas composition - OR3
P1 P2 P3 P4 P5
[CH_4] – [CO_2] (%v)
[H_2S] – [H_2] (ppmv)
Time (days)
[CH_4] [CO_2] [H_2] [H_2S]

Figure 5.6. Progress over time of the production and the composition of the biogas released by the reactors: cumulated biogas production of the four reactors (a); CH_4 yield of the four reactors (b); composition of the biogas released by the SSR (c), the OR1 (d), the OR2 (e) and the OR3 (f). SSR: steady-state reactor used as a control; OR1-OR3: test reactors exposed to increasing organic loading rate, free volatile fatty acids intoxication, and process recovery; P1-P5: sampling periods chosen for microbial community analyses (see **Figure 5.1**); gaps in the curves indicate missing data due to measurement failure.

5.3.2. Comparison of the 16S rRNA gene-based T-RFLP and high-throughput 16S rRNA amplicon sequencing results.

Microbial communities were monitored in the four studied reactors by means of 16S rRNA gene-based T-RFLP (**Figure 5.7**) and high-throughput amplicon sequencing (HTS) (**Figure 5.8**). It is well known that while the T-RFLP allows for the detection and semi-quantification of only the most abundant species in a sample (Bent & Forney, 2008; Liu et al., 1997; Osborn et al., 2000), taxon-specific resolution of the HTS is much higher (Pilloni et al., 2012). Therefore, knowing this limitation the calculated species richness based on the T-RFLP results was consistently relatively lower compared to the amplicon sequencing (**Chapter 10**: Annex 3 - **Table Ch5_S1**). Also, the total terminal restriction fragments (T-RF) diversity was only around 50% of that resulting from the HTS. Similar differences between the two molecular approaches were previously observed for AD reactors (Pilloni et al., 2012) as well as for other studied environments, e.g., human anterior nares (Camarinha-Silva et al., 2012). These differences can result from the use of different primers pairs for T-RFLP and HTS (Berry et al., 2011). Due to the length limitation of the HTS technology, longer amplicons required for T-RFLP were too large for HTS. However, the calculated average pairwise Bray-Curtis distances reflecting the dissimilarities in community structures between the four reactors at the different sampling points were not significantly different between T-RFLP and HTS results (**Figure 5.9**c,f). This observation suggests that both techniques accurately characterised the species dynamics over time in the four reactors, even though HTS was superior to T-RFLP regarding its sensitivity to detect minority species and the direct taxonomic affiliation of resulting sequencing reads. Interestingly, based on the HTS results, the ten most abundant bacterial operational taxonomic units (OTUs) at the sampling period P0 (steady-state process) accounted for an average of 52.0 ± 7.9 % of the population in the studied reactors. At the same time, the average bacterial richness calculated based

on the T-RFLP was 8.7 ± 1.3, suggesting that indeed the T-RFLP approach could be sufficient to characterise at least the dominant part of the bacterial community in the reactor. Nevertheless, the attempts to taxonomically assign in silico the obtained T-RFs failed to provide unequivocal results due to a difference of a few base pairs. This discrepancy is often found between T-RFs predicted in silico and T-RFs measured in vivo (Pilloni et al., 2012; Winded et al., 2008). It usually results from the presence of unknown species in analysed environmental samples, thus the adequate 16S rRNA gene sequences lack in required databases used to assign in silico the generated T-RFLP results.

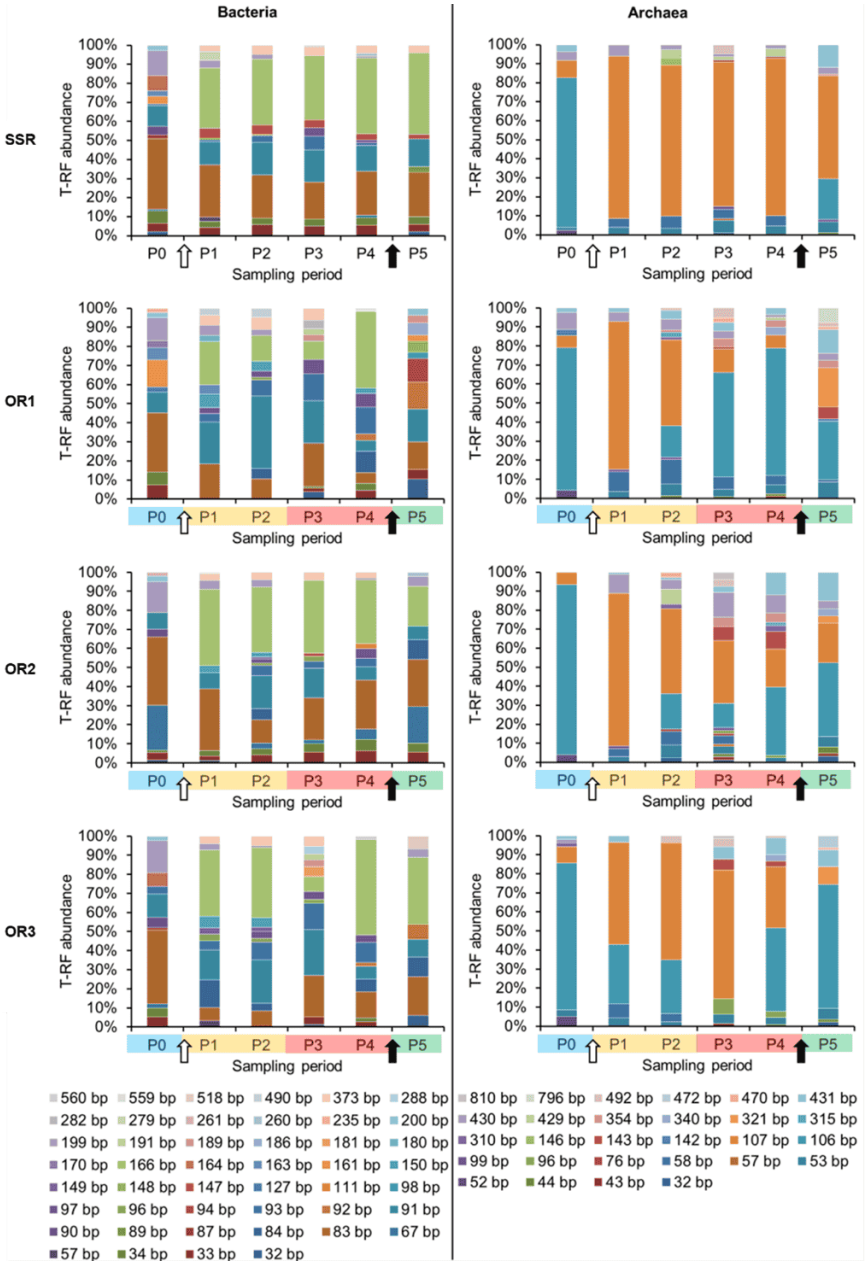

Figure 5.7. Dynamics of the bacterial and archaeal community structure as assessed by 16S rRNA gene-based T-RFLP analysis SSR: steady-state reactor used as a control; OR1-OR3: test reactors exposed to increasing organic loading rate, free volatile fatty acids intoxication, and process recovery; P1-P5: sampling periods chosen for microbial community analyses (defined in **Figure 5.1**); T-RFs are characterized by their length in base pairs (bp); the *white arrow* represents the initiation of the hydraulic retention time decrease; the *black arrow* represents the onset of the starving period.

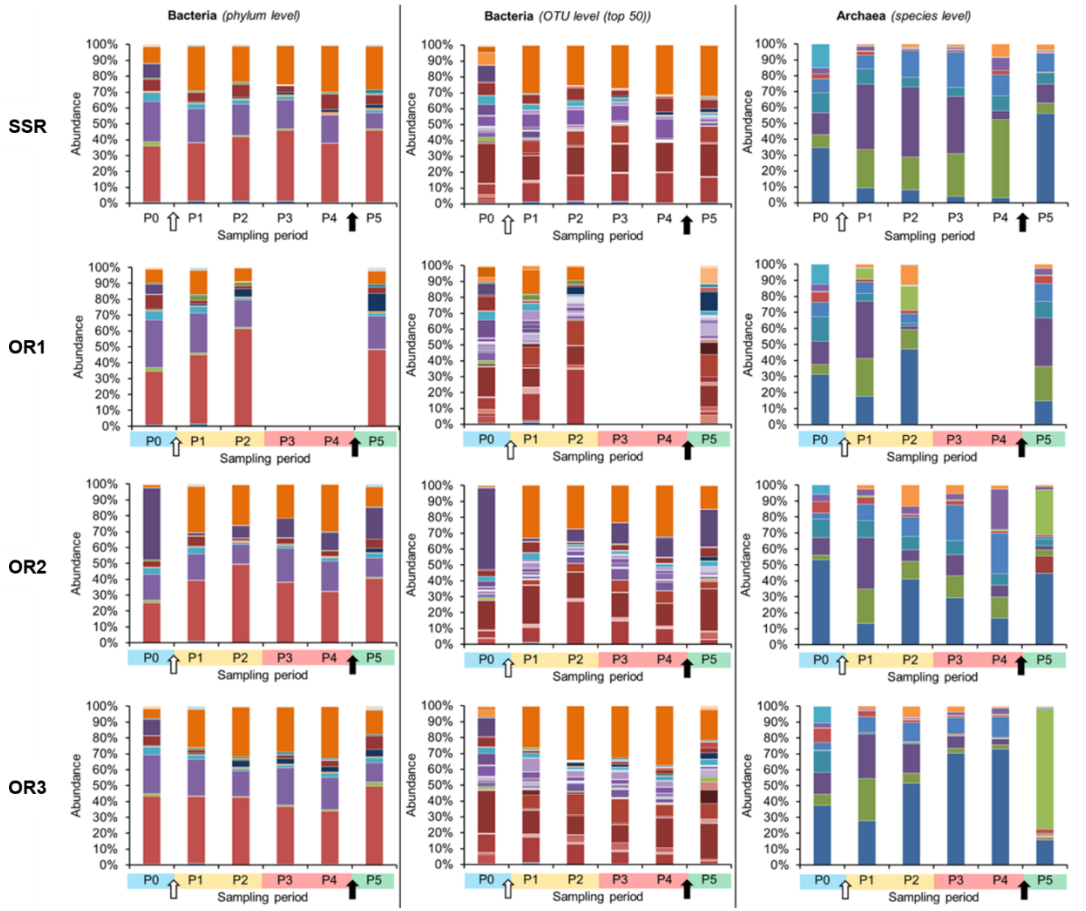
Bacteria (phylum level)
Bacteria (OTU level (top 50))
Archaea (species level)
SSR
OR1
OR2
OR3
Abundance
100%
90%
80%
70%
60%
50%
40%
30%
20%
10%
0%
P0
P1
P2
P3
P4
P5
Sampling period

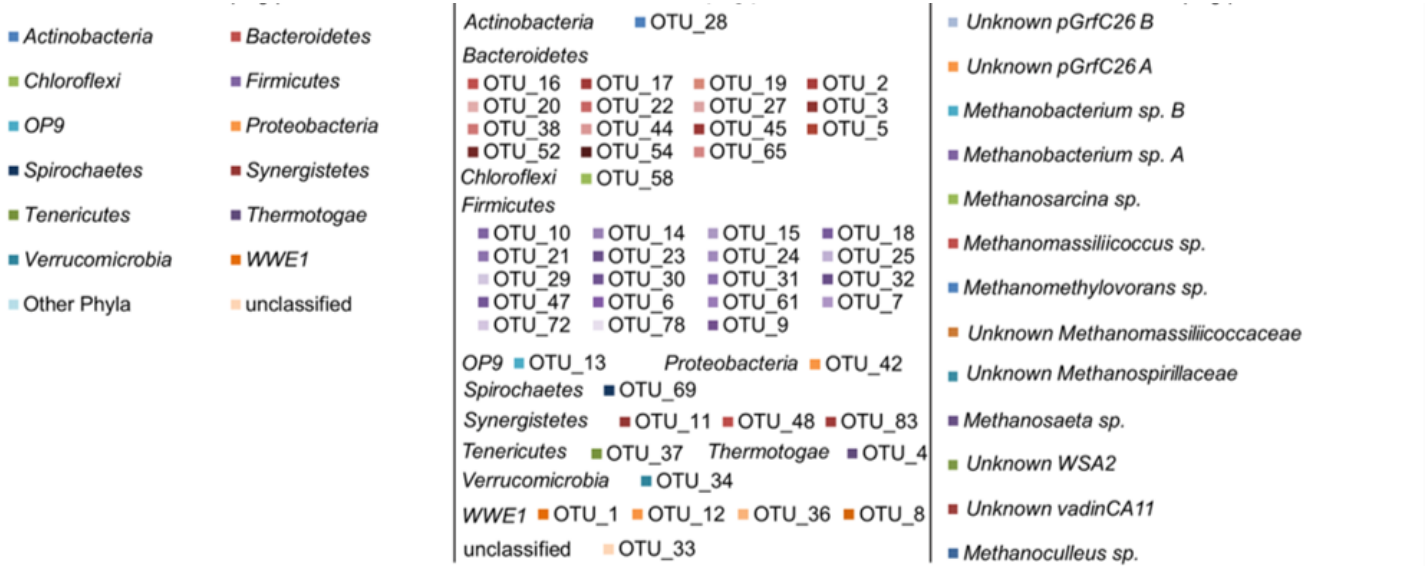

Figure 5.8. Dynamics of the bacterial[12] and archaeal diversity assessed by high-throughput 16S rRNA amplicon sequencing (HTS) Results are presented at the phylum level and the OTU level (top 50) for bacteria and at the species level for archaea. SSR: steady-state reactor used as a control; OR1-OR3: test reactors exposed to increasing organic loading rate, free volatile fatty acids (FVFA) intoxication and process recovery; P1-P5: sampling periods chosen for microbial community analyses; gaps for OR1 at sampling periods P3 and P4 were due to the poor quality of extracted DNA during severe FVFA intoxication; the *white arrow* represents the initiation of the hydraulic retention time decrease; the *black arrow* represents the onset of the starving period.

[12] The bacterial taxonomy reflects the nomenclature in use at the time the study was conducted. The correspondence with the most recent taxonomic classification is provided in **Table 1.1** of the general introduction.

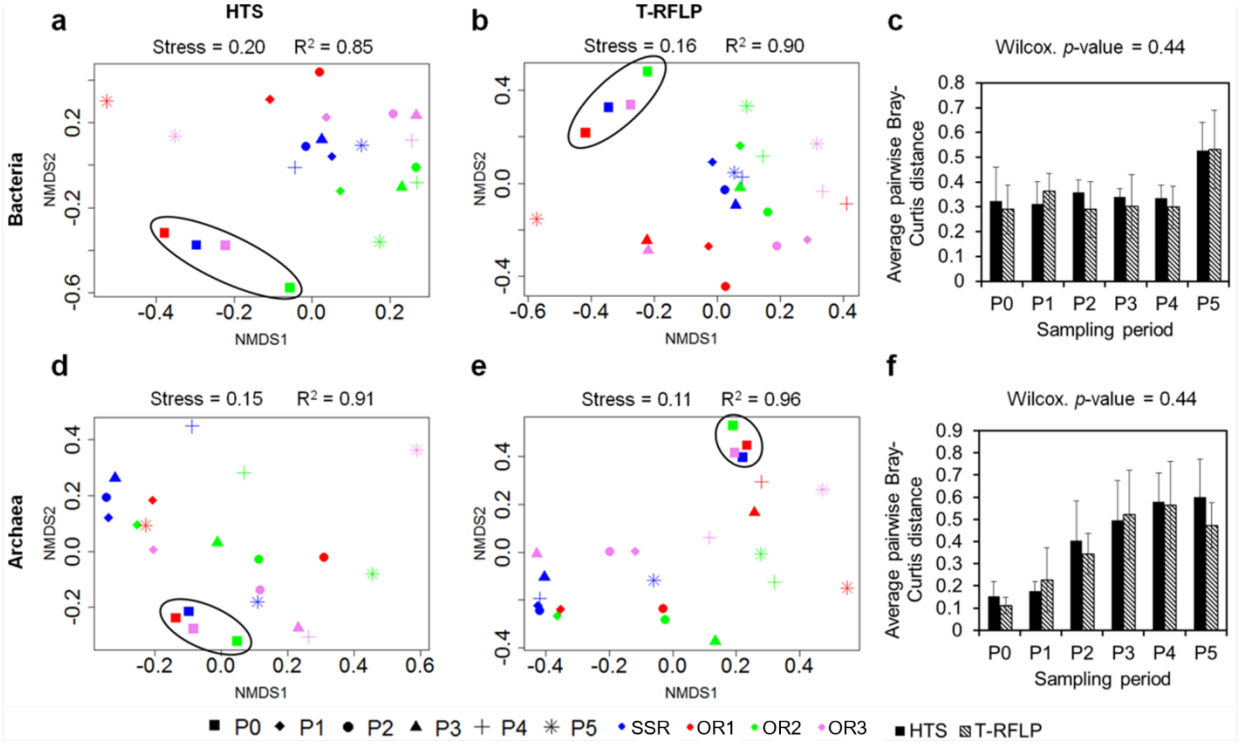

Figure 5.9. Non-metric multidimensional scaling (NMDS) ordination diagrams of temporal variations in bacterial and archaeal community structures. The ordination is based on Bray-Curtis similarity matrices of the relative abundance data obtained from high-throughput amplicon sequencing (a and d) and T-RFLP (b and e) for the bacterial and archaeal community, respectively; (c) and (f) show the average pairwise Bray-Curtis distance for the four reactors at the different sampling periods based on the high-throughput amplicon sequencing and T-RFLP results for the bacterial and archaeal community, respectively; the black ellipses group sampling period P0 (steady-state process) for each reactor.

5.3.3. Microbial communities in replicate reactors at steady state

At P0 (steady-state process), on average, 22.8 ± 5.7 % and 63.3 ± 13.8 % of bacterial and below 1.0 ± 0.0 % and 19.6 ± 3.3 % of archaeal 16S rRNA amplicon reads could not be classified at the family and genus levels, respectively, confirming that bacterial and to a lesser extent archaeal communities in AD reactors remain largely uncharacterized. Both at the OTUs and T-RFs levels, bacterial and archaeal communities from replicate reactors (except for OR2) clustered together at P0 based on NMDS analyses (**Figure 5.9**). This indicates that stable operational conditions during the acclimation period led to similar microbial populations in replicate AD reactors. In general, archaeal communities were much less diverse than bacterial ones (**Chapter 10**: Annex 3 - **Table Ch5_S1**). In SSR, OR1 and OR3, *Methanomicrobiaceae*, *Methanobacteriaceae* and *Methanosaetaceae* were the dominant families at P0 (**Figure 5.8**). In these three reactors, bacterial communities were dominated by representatives of the phyla *Bacteroidetes*, *Firmicutes* and candidate phylum *WWE1*, with respectively *Porphyromonadaceae*, *Lachnospiraceae* and *Cloacamonaceaea* being the dominant families. The prevalence of *Bacteroidetes* and *Firmicutes* is not surprising and has been frequently reported for different AD reactors treating agricultural and agro-food residues (Sundberg et al., 2013). The other bacterial phyla, including *Chloroflexi* and *Synergistetes* were only detected with low abundance. Concerning OR2, the unexpected failure of the heating system during the acclimation period (239 days before P0; **Figure 5.1**) led to a temperature drop to 30°C for less than 24h, which most probably explains the more dissimilar microbiome, with *Thermotogae* and *Bacteroidetes* being the dominant bacterial phyla at P0. The archaeal community in OR2 at P0 was dominated by *Methanoculleus* sp. (over 50 % of all 16S rRNA reads) and to a lesser extent by *Methanosaeta* sp. and unknown *Methanospirillaceae*.

Towards the end of the acclimation period, the HRT was gradually decreased in the four CSTRs (**Figure 5.1**), from more than 300 days at P0 to 28 days at P1 (data not shown), which influenced the shift of microbial diversity between the two sampling periods (**Figure 5.7** and **Figure 5.8**). At day 221, while the OLR started to be gradually increased for the test reactors ORs, it remained unchanged for the SSR, which resulted in a relatively stable bacterial community between P1 and P5 for this control reactor (**Figure 5.7** and **Figure 5.8**). The six prevalent bacterial T-RFs (T-RFs

33, 83, 91, 147, 166 and 373 bp), with high relative abundance at P1, were also detected for the other sampling points (**Figure 5.7**). Similarly, the archaeal community remained stable in the SSR between the sampling periods P1 and P4, with the T-RF 107 bp representing more than 80 % of the total T-RF abundance (**Figure 5.7**). At P5, its abundance decreased, and another T-RF (106 bp) started to emerge. By correlating 16S rRNA gene-based T-RFLP and 16S rRNA amplicon sequencing results, we could relate T-RF 107 bp to *Methanosaeta* sp., and T-RF 106 bp to *Methanoculleus* sp. The apparent redirection from acetoclastic towards hydrogenotrophic methanogenesis, as could be concluded based on the increased abundance of *Methanoculleus* sp. at P5, is most probably attributable to the depleting source of acetate during the 11-day-long starving regime applied to the SSR (which corresponds to the late FVFA intoxication and partially to the recovery period applied to the ORs).

5.3.4. Bacterial community dynamics in replicate reactors exposed to increasing OLR and FVFA intoxication

As the selection pressure increased, due to the increased OLR applied to the test reactors, the environment turned from a steady-state to a selective one and distinct microbes begun to dominate in each OR (**Figure 5.7** and **Figure 5.8**). Therefore, the replicate test reactors developed their own bacterial populations, with community structures that were more similar between the different sampling points for the same reactor, than between the different reactors for the same sampling point (**Figure 5.9**a,b). At the same time, these communities were functionally redundant, since all reactors operated stably and showed similar global characteristics (**Figure 5.2** to **Figure 5.5**; **Figure 5.6**). Similarly to SSR, the three dominant phyla, namely *Bacteroidetes*, *Firmicutes* and candidate phylum *WWE1* also dominated in OR2 and OR3 (**Figure 5.8**). No data for OR1 could be recorded during the FVFA intoxication phase due to poor quality of extracted DNA for these sampling periods (harsh acidic environment). While in total 441 OTUs were characterized for bacteria, roughly 50 top OTUs represented on average 88.1 ± 4.4 % of the whole bacterial populations in the studied reactors, and they were assigned to 12 different phyla (**Figure 5.8**). The top 10 OTUs accounted for 70.8 ± 14.9 % of all sequenced 16S rRNA reads for the sampling periods P1-P5 for the four reactors, with the dominating OTUs representing

the candidate phylum *WWE1* (OTU_1), *Bacteroidetes* (OTU_ 2, 3 and 5), *Firmicutes* (OTU_6, 7 and 18), the candidate phylum *OP9* (OTU_13) and *Synergistetes* (OTU_11). *Thermotogae* (OTU_4) was also dominant in the case of OR2.

In general, the diversity of *Firmicutes* with a total of 231 different OTUs (223 assigned to *Clostridia*) was much higher than *Bacteroidetes* with only 59 OTUs. While the dominant *Bacteroidetes* OTUs (accounting for an average of 31.6 % ± 8.8 of the total bacterial 16S rRNA reads for the ORs) appeared resistant to the increasing OLR and the FVFA intoxication, *Firmicutes* (accounting for an average of 6.1 % ± 3.6 of total 16S rRNA reads for the ORs) were much more sensitive (**Chapter 10**: Annex 3 - **Table Ch5_S2**). Several dominant *Firmicutes* OTUs disappeared (e.g., OTU_7, 15 and 32 unclassified bacteria of the order MBA08, OTU_14, an unclassified bacterium of the order SHA-98), and other new OTUs appeared during the FVFA intoxication. These new OTUs, e.g., OTU_18, 31, 78, 101 and 103, were classified as *Clostridiales*, including families of *Ruminococcaceae* and *Lachnospiraceae* (**Chapter 10**: Annex 3 - **Table Ch5_S2**). Whether this functional redundancy of *Firmicutes* explains their much higher diversity than *Bacteroidetes* is not clear at this stage and needs further investigation. Interestingly, it is well recognised that more diverse microbial communities provide a wider range of parallel pathways, what in principle should ensure their overall functional stability when confronted with an environmental stress (Carballa et al., 2015). For this reason, decrease of the diversity index is often proposed as warning indicator for AD process disturbances (see below). However, the fact that our reactors were dominated by a few resistant *Bacteroidetes* OTUs, suggests that each of these microbes must have a suite of parallel pathways encoded on its genome to allow to quickly adapt to the changing environment. Therefore, further metagenomic studies should show whether these yet uncharacterised *Bacteroidetes* are indeed broad-specificity bacteria.

The remaining phyla detected in our test reactors were much less diverse, with a candidate phylum *WWE1* being represented by five OTUs and *Thermotogae* by two OTUs only. The most abundant OTU_1, in terms of total 16S rRNA reads, was assigned to the candidate phylum *WWE1* and constituted a fourth part of the whole bacterial community in OR2 and OR3 between P1 and P4 (on average 27.6 % ± 3.9), and it only decreased during the recovery stage (13.6 % ± 1.5). For OR1, its abundance varied depending on the experimental stage. Interestingly, this OTU_1 was

below the detection limit for all reactors at the beginning of the experiment (P0). *Candidatus* Cloacimonas, belonging to candidate division *WWE1*, was previously shown to be the most dominant genus in an AD reactor co-digesting fish-waste and cow manure (Solli et al., 2014). The reconstructed genome of a representative bacterium from the same division suggested that it could be a hydrogen-producing syntroph (Pelletier et al., 2008). Other authors demonstrated the involvement of the *WWE1* candidate bacteria to cellulose fermentation, from its incubation with ^{13}C-cellulose and observation with a high-resolution nanometer-scale secondary ion mass spectrometer (nano SIMS)(Limam et al., 2014). With regards to *Thermotogae*, members of this phylum have been previously detected in mesophilic anaerobic reactors (Nesbø et al., 2006) and their presence could not be clearly linked to process parameters such as HRT or OLR (Krakat et al., 2011). Surprisingly, the high abundance of OTU_4 (*Thermotogae*) in OR2 coincided with the higher pH reached in this reactor compared to the other test reactors during the late FVFA intoxication (P4, pH 5.7, **Figure 5.4**a vs **Figure 5.3**a and **Figure 5.5**a). Moreover, members of *Thermotogae* have been characterised for complex polysaccharide fermentation and hydrogen production (Conners et al., 2006), what might promote beneficial associations with hydrogenotrophic methanogens (Muralidharan et al., 1997).

5.3.5. Bacterial diversity

Although alpha diversity indices are often used to interpret the behaviour of AD reactors according to their microbial community dynamics (Carballa et al., 2011; De Vrieze et al., 2013; Hailu et al., 2021; Heeg et al., 2014; Talbot et al., 2008), the use of these indices as warning indicators remains questionable (Carballa et al., 2015). In principle, functionally diverse microbial communities provide a better suite of resistant, redundant and resilient pathways[13], and a higher microbial diversity is usually correlated with well-performing AD reactors. However, exposing microbial

[13] This concept, known as functional redundancy (C. Li et al., 2024), suggests that a more diverse community can better buffer against shocks. However, research increasingly shows that the functionality of an AD system is often driven by the microbial composition and interactions within a "core microbiome" (Blasco et al., 2022; Calusinska et al., 2018) hosting key syntrophic partnerships. Therefore, while a diverse microbial consortium provides robustness, optimal performance may rely on the presence and activity of specific, well-adapted functional groups rather than just the total number of species.

communities to environmental changes causes high selection pressure, which is usually reflected by a decreased diversity (Nguyen et al., 2019). Indeed, between the early and the late FVFA intoxication periods (P3 and P4), the bacterial richness and diversity indices decreased for OR1 and OR3 (based on T-RFLP and HTS; **Chapter 10**: Annex 3 - **Table Ch5_S1**). In contrast, for OR2, these indices either increased (T-RFLP) or remained unchanged (HTS). Interestingly, while in general OR2 was characterised by a lower species diversity during the FVFA intoxication period than OR3 (no HTS data for OR1; **Chapter 10**: Annex 3 - **Table Ch5_S1**), this test reactor maintained the highest pH at P4 (5.7 versus 4.9 and 5.2 for OR1 and OR3, respectively), and produced significantly more biogas than OR1 and OR3, with the most favourable CH_4/CO_2 ratio (**Figure 5.4** and **Figure 5.6**).

While the use of alpha diversity indices as process disturbance indicators has still to be carefully considered, a decrease of microbial community evenness has been shown to be a good candidate for such an application (Werner et al., 2011, 2014). Nevertheless, in our study, evenness measured for the ORs at the different sampling periods, using the Pielou index (**Chapter 10**: Annex 3 - **Table Ch5_S1**), did not show any uniform patterns, based on both T-RFLP and HTS results. This observation suggests that evenness indices should be carefully interpreted when used as warning indicators. The overall functional redundancy demonstrated for the microbial communities of our replicate overfed reactors, and the absence of uniform patterns in terms of microbial ecology indices raise the question whether the conclusions of studies that investigated a unique reactor (no replicate) are meaningful. Indeed, similarly to our observations, recent studies that assessed parallel reactors treating beet silage (Krakat et al., 2011) or co-digesting fish waste and cow manure (Solli et al., 2014), showed as well that different microbial communities can establish in distinct reactors although these reactors are exposed to the same treatment.

5.3.6. Adaptation of archaeal communities to FVFA intoxication and correlation with reactor´s parameters

Following the VFA accumulation in the slurry and the simultaneous pH drop (P3 and P4; FVFA intoxication), the diversity of the archaeal community was in general higher in the ORs than at the beginning of their overfeeding (P1), which is in contradiction with another report (Kundu et al., 2013). The evenness (Pielou index)

calculated for the archaeal population showed a trend similar to the one calculated for the bacterial community (**Chapter 10**: Annex 3 - **Table Ch5_S1**), providing no evidence that a lower evenness can be associated with a process imbalance. In continuation, canonical correspondence analysis (CCA) was used to highlight the influence of the changing process parameters on the archaeal community (the CCA performed for bacteria was not statistically significant, most probably due to the differential answer of the different communities that established in replicate reactors; p-value of the Monte Carlo test was > 0.05; therefore, these results are not discussed here). As shown in **Figure 5.10**, 65 % of the total species variance could be explained by the first two axes of the CCA ordination diplot. While the slurry pH showed a strong positive correlation with the TIC content of the slurry ($r = 0.94$, p-value < 0.001) and a negative correlation with the VS content of the slurry ($r = -0.89$, p-value < 0.001), it was not correlated with the total biogas production (p-value = 0.34). Indeed, total biogas production was not strongly reduced during the FVFA intoxication, due to the increased production of CO_2 (**Figure 5.6**) by hydrolytic and fermentative bacteria and the conversion of HCO_3- to CO_2 caused by acidic conditions. This is well reflected by a strong negative correlation between the slurry pH and the CO_2 content in the biogas ($r = -0.80$, p-value < 0.001). At the same time, the slurry pH also showed a high positive correlation with the CH_4 content in the biogas ($r = 0.80$, p-value > 0.001), which was strongly reduced during the FVFA intoxication (**Figure 5.6**d-f). Interestingly, higher biogas production was also correlated with the abundance of *Methanosaeta* sp. ($r = 0.48$, p-value = 0.025). Moreover, the presence of *Methanosaeta* sp. was negatively correlated with the total VFAs content in the slurry of the reactors ($r = -0.72$, p-value < 0.001) and with the abundance of *Methanoculleus* sp. ($r = -0.49$, p-value = 0.022). Indeed, in the test reactors ORs, the relative abundance of T-RFs 107 bp, assigned to *Methanosaeta* sp., was dominant at the beginning of the OLR increase (P1), then decreased during FVFA intoxication to be replaced by T-RFs 106 pb, related to *Methanoculleus* sp. (**Figure 5.7** and **Figure 5.8**). This suggests an overall redundancy of the archaeal population in sub-optimal conditions. Similarly, a transition from acetoclastic (*Methanosaeta* sp.-dominated) to hydrogenotrophic (*Methanoculleus* sp.-dominated) methanogenesis has been previously reported for low pH and high VFAs concentration in the slurry, for an anaerobic membrane bioreactor treating swine

manure and exposed to high shear condition (Padmasiri et al., 2007), and for a hybrid anaerobic reactor exposed to changing OLR (Kundu et al., 2013). Although in the absence of *Methanosaetaceae*, syntrophic acetate oxidation (SAO) and hydrogenotrophic methanogenesis were proposed to be the dominant CH_4 production pathways from acetate (Karakashev et al., 2006), we did not detect any of a few known SAO[14] bacteria in our test reactors (Werner et al., 2014) (**Chapter 10**: Annex 3 - **Table Ch5_S2**). This might indicate either the presence of previously unknown SAO bacteria, which could be expected regarding the relatively high number of taxonomically unassigned 16S rRNA sequences generated in this study, or the existence of new metabolic pathways leading to VFAs conversion and subsequent CH_4 production.

[14] The Acetobase database (A. Singh & Schnürer, 2022) was not available at the time this study was conducted.

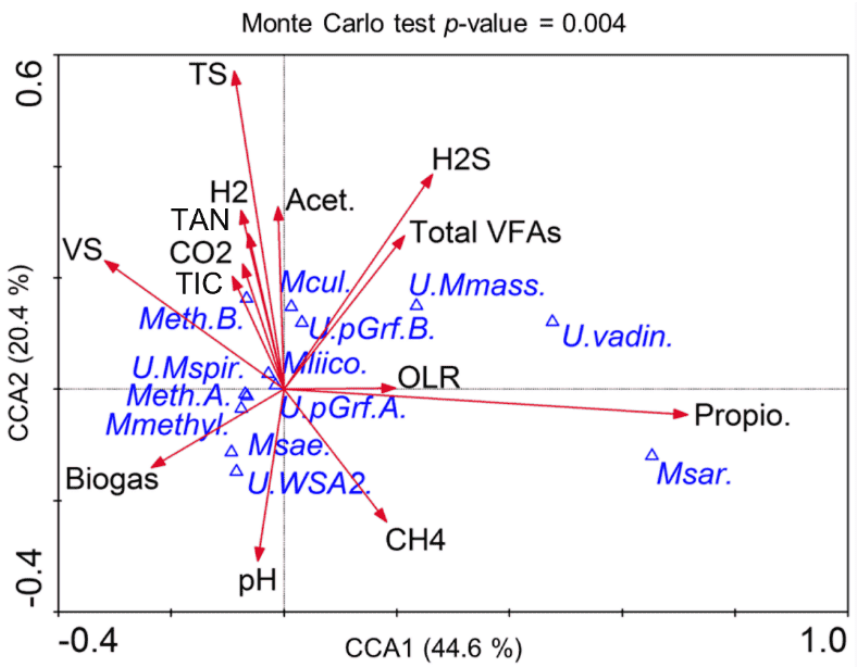

Figure 5.10. Canonical correspondence analysis (CCA) ordination diplot for the archaeal community. *Red vectors* represent the influence of the process parameters such as pH (pH), organic loading rate (OLR), biogas production (Biogas), methane (CH_4), carbon dioxide (CO_2) and hydrogen sulfide (H_2S) contents in the biogas, total solids (TS), volatile solids (VS), total inorganic carbon (TIC), total ammonia nitrogen (TAN), total volatile fatty acids (Total VFAs), acetate (Acet.) and propionate (Propio.) contents in the slurry; blue triangles represent archaeal taxa derived from the high-throughput 16S rRNA amplicon sequencing at the species level: unknown *Methanomassiliicoccaceae* (*U.Mmass.*), unknown *Methanospirillaceae* (*U.Mspir*.), unknown *WSA2* (*U.WSA2.*), unknown *vadinCA11* (*U.vadin*.), *Methanobacterium* sp. A (*Meth.A*.), *Methanobacterium* sp. B (*Meth.B.*), *Methanoculleus* sp. (*Mcul*.), *Methanomassiliicoccus* sp. (*Mliico.*), *Methanomethylovorans* sp. (*Mmethyl.*), *Methanosaeta* sp. (*Msae.*), *Methanosarcina* sp. (*Msar.*), unknown *pGrfC26* sp. A (*U.pGrf.A*), unknown *pGrfC26* sp. B (*U.pGrf.B*). A detailed correlation matrix including all process parameters and the archaeal community diversity is provided as Annex 3 - **Table Ch5_S1** (**Chapter 10**).

Methanosaeta sp. is regarded as a functionally redundant archaeon and a decrease in its abundance has been proposed as an early warning indicator of AD process disturbances (Carballa et al., 2015). Here, by correlating the 16S rRNA amplicon sequencing with the changes observed at macroscopic level, we could indeed observe that *Methanosaeta* sp. started to decrease in abundance in the test reactors at the sampling period P2, to be substituted by *Methanoculleus* sp. At this moment, the pH was still above 7, no accumulation of VFAs was observed, and the

methane yield was not yet affected (**Figure 5.3**, **Figure 5.4**, **Figure 5.5** and **Figure 5.6**).

Although the dominance of *Methanoculleus* was documented for many well-performing agricultural digesters (Nettmann et al., 2010), the presence of this species (already present at P0 in our studied reactors) can not point to the approaching process disturbance; instead the sudden shift of the dominant archaeal population, while the test reactors were still performing efficiently, is significant. Therefore, in accordance with other authors (Carballa et al., 2015), we tentatively propose that the substitution of a dominant archaeal population (*Methanosaeta* sp. is often dominant in reactors inoculated with slurry from a wastewater treatment plant and operated at low acetate and free ammonia concentrations (De Vrieze et al., 2012; Karakashev et al., 2005; Nettmann et al., 2010; Zheng & Raskin, 2000) by another archaeal population (*Methanoculleus* sp. emerged at the onset of VFAs accumulation) could be regarded as an early warning indicator of FVFA intoxication. Nevertheless, other authors proposed other species, especially related to *Methanosarcina thermophilia,* qualified as heavy-duty methanogens (De Vrieze et al., 2012), to be the earliest indicators of acidification in overloaded fed-batch reactors digesting maize silage (Kampmann et al., 2014). In our study, *Methanosarcina* sp. was detected neither before nor during the FVFA intoxication (**Figure 5.8**). Therefore, we suggest conducting further large-scale microbial monitoring of different well-performing as well as failed AD reactors fed with diverse feedstocks before a microbial species can univocally be proposed as a good and universal indicator of any process disturbance.

5.3.7. Restoration of the biogas production with NaOH and $NaHCO_3$ addition

During the FVFA intoxication, the test reactors ORs almost stopped producing CH_4 from the fed sugar beet pulp. On the last feeding day of the overfeeding campaign (day 266, P3), the CH_4 yield of the ORs (0.04 ± 0.03 $L_N.gVS.day^{-1}$), was much lower than the one measured for the cautiously fed SSR (0.26 $L_N.gVS.day^{-1}$). After the FVFA intoxication, a starving period followed by the progressive introduction of NaOH and $NaHCO_3$ in the ORs, resulted in a pH increase to a neutral level after 3 days only. The complete process recovery and restoration of biogas production with methane content exceeding 50%v, occurred after 9 days following

the beginning of the alkali addition. In comparison, bioaugmentation of overfed acidic reactors (pH decreased from around 7.0 to 6.8 only), has been shown to decrease the recovery time by a maximum of 37 days, compared to about 180 days for non-bioaugmented ones (Tale et al., 2015)!

Interestingly, the archaeal population in the test reactors ORs, although affected in terms of community structure, was not eradicated by the relatively low pH (5.2 ± 0.4) reached during the FVFA intoxication. Following the pH increase, and probably due to the influence of the starvation and the NaOH introduction, *Methanosarcina* sp., which was previously described as a fast-growing archaeon resistant to high concentrations of acetate and sodium salts (De Vrieze et al., 2012), started to outcompete *Methanoculleus* sp. in OR2 and OR3 (**Figure 5.8**). Additionally, a new archaeal OTU_15, classified as a candidate genus *vadinCA11*, emerged in OR1 and OR2 during the recovery phase (P5) (**Figure 5.8**, **Chapter 10**: Annex 3 - **Table Ch5_S3**). This genus has been reported as potentially halophilic (Durbin & Teske, 2012). The increased concentration of sodium ion due to the addition of alkali probably favoured the outbreak of these microbes during the recovery phase.

The drastic increase of pH also influenced the structure of the bacterial community in the ORs. While the three *Bacteroidetes* OTUs (OTU_2, 3 and 5) that dominated at P1-P4 were still detected at P5 (with lower abundance), new *Bacteroidetes* OTUs (OTU_19, 45, 65 and 74, **Chapter 10**: Annex 3 - **Table Ch5_S2**), also representing families of *Porphyromonadaceae* and *Bacteroidaceae*, became clearly detectable during the recovery phase. *Firmicutes* also responded with a functional redundancy to the pH increase. Three OTUs (OTU_25, 68 and 72, **Chapter 10**: Annex 3 - **Table Ch5_S2**) emerged and became dominant (OTU_25 assigned as unclassified *Sedimentibacter*, OTU_68 potentially assigned as *Clostridium bolteae* and OTU_72 assigned as unclassified *Epulopiscium*). At P5, based on the HTS results, OTU_68 constituted 10.6, 0.5 and 7.6 % of the whole bacterial population, for OR1, OR2 and OR3, respectively. *C. bolteae*, which is a spore-forming propionate producer (Pequegnat et al., 2013; Song et al., 2003), was only detected for OR3 at P0, at a very low abundance level (around 0.01 % of the whole bacterial community). As one could expect, an increased propionate concentration at P5 was linked to an increased abundance of a propionate-producing

bacteria (*C. bolteae*) and a decreased abundance of a potentially propionate-consuming bacteria (candidate phylum *WWE1*) (Pelletier et al., 2008).

Although the bacterial and archaeal community structures of the three ORs strongly changed following the alkali addition (**Figure 5.7** and **Figure 5.8**), the microbial population successfully self-optimized to the new environmental conditions, as the biogas and methane production restarted quickly (**Figure 5.6**). On the one hand, we showed that the addition of NaOH and $NaHCO_3$ to raise the pH and the TIC content of the slurry represents an efficient treatment for AD reactors that faced FVFA intoxication. On the other hand, the drastically changing environmental conditions influenced the structure of the prevailing microbial communities in a way that a favourable niche was created for other species to emerge.

5.4. Conclusions

The impact of increasing OLR of sugar beet pulp, FVFA intoxication and finally process recovery on microbial community richness and diversity in three mesophilic CSTR reactors (OR1-OR3) were compared with a cautiously fed reactor (SSR). Although the overfed reactors responded rather similarly in terms of process performance to the OLR increase, each reactor established its own microbial community structure over time, dominated by only a few OTUs. Our results showed that traditional microbial parameters such as richness, diversity and evenness are not effective to detect process imbalances, as the microbial consortia behaved differentially in the replicated reactors. Moreover, the reactor with the least diverse microbial community (OR2) was the most resistant to FVFA intoxication and the best performing one in terms of methane production. The shift from *Methanosaeta* sp. to *Methanoculleus* sp. in *Methanosaeta* sp.-dominated reactor could be an interesting and promising warning indicator of an approaching FVFA intoxication since this shift occurred before the pH started to decrease. The combination of the reactor starvation and the pH adjustment with NaOH and $NaHCO_3$ demonstrated a good potential for process recovery after FVFA intoxication, as reflected by a quick restart of the methane production, even if a new microbial community has established. Nevertheless, longer monitoring periods of microbial communities after man-induced process recovery are necessary to evaluate if the newly established microbial populations are stable over time and if they are better adapted to high VFAs

concentrations. Relying on the results of this study, alkali-mediated AD process recovery from FVFA intoxication was successfully applied to a full-scale anaerobic reactor in Germany (data not shown).

Acknowledgements

We thank Bénédicte De Vos and Anaïs Noo for their valuable technical support and Laurent Solinhac, Sylvain Legay, Beate Kröck and Ingo Bergmann for their help to set up the T-RFLP method. This work was supported by the Fonds National de la Recherche, Luxembourg (FNR CORE 2011 project GASPOP, CO11/SR/1280949: Influence of the Reactor Design and the Operational Parameters on the Dynamics of the Microbial Consortia Involved in the Biomethanation Process) and co-financed by the European Fund for Regional Development (ERDF) through the INTERREG IV A program 2007–2013 «Greater Region» for the OPTIBIOGAZ project.

Chapter 6

Potential of acetic acid to restore methane production in anaerobic reactors critically intoxicated by ammonia as evidenced by metabolic and microbial monitoring

Adapted[15] from:

Lemaigre, S., Gerin, P. A., Adam, G., Klimek, D., Goux, X., Herold, M., Frkova, Z., Calusinska, M., & Delfosse, P. (2023). Potential of acetic acid to restore methane production in anaerobic reactors critically intoxicated by ammonia as evidenced by metabolic and microbial monitoring. *Biotechnology for Biofuels and Bioproducts*, *16*(1), 1–20. doi:10.1186/s13068-023-02438-5

[15] In § 6.2.3 and § 6.2.5, the methods already described in previous chapters were not repeated. **Figure 6.4** has been slightly restructured for improved readability in the thesis format.

Context and contribution to the thesis

In **Chapter 5**, we showed that chemical adjustment of pH and buffer capacity could restore CH_4 production in AD reactors suffering from critical free VFA intoxication, by re-establishing environmental conditions favourable to microbial activity. A similar approach may also be effective for reactors exposed to critical FAN intoxication. In this chapter, we evaluate such a recovery strategy aimed at restoring AD functionality in the three FAN-intoxicated reactors that had ceased CH_4 production following the treatment described in **Chapter 4**.

In this context, **Chapter 6** of this thesis utilises results from AD experiment **Exp2_FAN_intoxication**[16] to address the research question **Q3 Recovery from FAN intoxication** (*Can the AD process be recovered after a critical FAN intoxication without supplementing the intoxicated reactors with inocula acclimatised to ammonia?*).

Personal Contribution:

- Equipped four 100-L reactors with components for heating, temperature regulation, and stirring (**Chapter 10**; Annex 1).
- Developed and assembled equipment for automatic sampling and analysis of the biogas produced by the reactors (**Chapter 10**; Annex 1).
- Developed software for acquiring the biogas datasets.
- Contributed to defining the process recovery strategy assessed in the study.
- Conducted the AD experiment in the laboratory.

[16] AD reactors exposed to increased nitrogen input until critical FAN intoxication + Assessment of a process recovery strategy.

Highlights

- pH correction with acetic acid and water dilution were insufficient to restore methane production in three pilot-scale AD reactors previously exposed to critical FAN intoxication (max. FAN content ~ 5.0 g_N L^{-1}), despite the availability of direct CH_4 precursors.
- Resuming feeding with sugar beet pulp, alongside re-inoculation with effluents from a low-nitrogen input reactor, triggered the restoration of biogas production.
- Acetic acid supplementation reduced FAN toxicity and enabled substantial CH_4 production during the recovery phase.
- All reactors fully recovered within 11 weeks and efficiently converted feedstock to CH_4 without further re-inoculation.
- Re-inoculation proved essential to stabilise the process and could be effectively achieved using effluents from a reactor not acclimatised to ammonia.
- Re-inoculation had little impact on the archaeal community, which remained dominated by a *Methanosarcina* sp., despite the transient proliferation of a methylotrophic methanogen (*Candidatus* Methanoplasma).

Abstract

Background: Biogas and biomethane production from the agricultural anaerobic digestion (AD) of animal manure and agri-food wastes could play a key role in transforming Europe's energy system by mitigating its dependence on fossil fuels and tackling the climate crisis. Although ammonia is essential for microbial growth, it inhibits the AD process if present in high concentrations, especially under its free form, thus leading to economic losses. In this study, a recovery strategy was applied to restore feedstock conversion to methane in AD reactors facing critical free ammonia intoxication, with monitoring of the metabolic and microbial evolution.

Results: The AD process of three mesophilic semi-continuous 100L reactors critically intoxicated by free ammonia (max. 5 g_FAN L^{-1}; inhibited hydrolysis and heterotrophic acetogenesis; interrupted methanogenesis) was restored by applying a strategy that included reducing pH using acetic acid, washing out total ammonia with water, re-inoculation with active microbial flora and progressively re-introducing sugar beet pulp as a feedstock. After five weeks, two reactors restarted to hydrolyse the pulp and produced CH_4 from the methylotrophic methanogenesis pathway. The acetoclastic pathway remained inhibited due to the transient dominance of a strictly methylotrophic methanogen (genus *Candidatus* Methanoplasma) to the detriment of *Methanosarcina*. Concomitantly, the third reactor, in which *Methanosarcina* remained dominant, produced CH_4 from the acetoclastic pathway but faced hydrolysis inhibition. After eleven weeks, the hydrolysis, the acetoclastic pathway and possibly the hydrogenotrophic pathway were functional in all reactors. The methylotrophic pathway was no longer favoured. Although syntrophic propionate oxidation remained suboptimal, the final pulp to CH_4 conversion ratio (0.41 ± 0.10 L_N_CH_4 g_VS^{-1}) was analogous to the pulp biochemical methane potential (0.38 ± 0.03 L_N_CH_4 g_VS^{-1}).

Conclusions: Despite an extreme free ammonia intoxication, the proposed process recovery strategy allowed CH_4 production to be restored in three intoxicated reactors within eight weeks, a period during which re-inoculation appeared to be crucial to sustain the process. Introducing acetic acid allowed substantial CH_4 production during the recovery period. Furthermore, the initial pH reduction promoted ammonium capture in the slurry, which could allow the application on crops of the effluents produced by full-scale digesters recovering from ammonia intoxication.

6.1. Background

The European Union (EU) is currently proposing to increase the 2030 target for renewable energy source consumption to 45% (Bórawski et al., 2022). In this context, biogas production from the on-farm anaerobic digestion (AD) of animal manure and agri-food residues can play a key role in increasing the contribution of alternative energy sources. AD can help accelerate the transition towards net-zero global greenhouse gas emissions by 2050 while valorizing carbon and nitrogen from biodegradable waste resources (IPCC, 2022). Moreover, biogas production increases European energy security by reducing dependence on imported fossil fuels and can alleviate the burden of energy costs on households and industries (Xue et al., 2022).

Biogas production through AD has increased almost fivefold in the last two decades in the EU (Pavičić et al., 2022), especially in Germany, where national subsidies promoted biogas production relying on the use of energy crops as the main reactor feedstocks (Theuerl et al., 2019). However, competition for land between energy and food markets resulted in food versus fuel debates (Ackrill & Kay, 2014). A comparative assessment, employing parameters such as fossil fuel consumption, greenhouse gas emissions, fertilizer application, electricity consumption and transportation - as provided by the EU document on the sustainability of solid and gaseous biomass used for bioenergy production (DG Energy, 2014) - revealed that biogas production from agri-food wastes could generate ~30% less CO_2 emissions than biogas production from energy crops (Lijó et al., 2017). Therefore, the replacement of energy crops with agri-food wastes in biogas production through AD is both environmentally sustainable and economically profitable in the long-term. However, changing the feedstock in AD to nitrogen-rich feedstocks (manure, organic fraction of municipal solid wastes or waste from slaughterhouses) could result in both acute and chronic ammonia toxicities for the reactors' microbial communities (Bellucci et al., 2022; Yenigün & Demirel, 2013).

Total ammonia nitrogen (TAN) exists in two forms in aqueous environments such as AD slurries: ionized ammonium nitrogen (NH_4^+-N) and un-ionized "free" ammonia nitrogen (FAN, i.e., NH_3–N). The concentration ratio of these two forms is driven by pH and temperature (Jiang et al., 2019). FAN is generally regarded as the main inhibition cause of the methanogenesis (Wijesinghe et al., 2021) of nitrogen-rich

feedstocks due to its high diffusion rate through membranes of microbial cells (Jiang et al., 2019). Methanogenic archaea are especially vulnerable to ammonia intoxication compared to the other AD microbes because of their cell wall composition, which lacks peptidoglycans (Capson-Tojo et al., 2017; Yan et al., 2020). At an equivalent pH, the FAN proportion is higher in thermophilic temperature conditions that in mesophilic conditions. Therefore, thermophilic archaea were reported to have developed a higher tolerance to FAN than the mesophilic ones (Capson-Tojo et al., 2020). Indeed, the former are more likely to grow at higher FAN concentrations than the latter. In non-inhibited AD reactors, about 70% of methanogenesis is generally attributed to the acetoclastic pathway and ~30% to the hydrogenotrophic pathway (Conrad, 2006; Polag et al., 2013), while only a minimal amount of CH_4 (<1%) is produced from methyl compounds via methylotrophic methanogenesis (Ferry, 1993). Under a high FAN concentration in the slurry, hydrogenotrophic methanogens were reported to become predominant and accordingly, the major methanogenesis pathway shifted to hydrogenotrophy (Calli et al., 2005; Westerholm et al., 2022). The same authors also reported the presence of bacterial syntrophic acetate oxidizers (SAO) in association with these hydrogenotrophic archaea. In FAN-intoxicated reactors relying mostly on the hydrogenotrophic pathway, any disturbance to methanogenesis would cause an accumulation of hydrogen in the slurry, resulting in a thermodynamic blockage of propionate degradation (Koch et al., 1983). This phenomenon can explain why AD reactors treating nitrogen-rich feedstocks are subject to a quick and often irreversible process failure (Jiang et al., 2019). Excessive FAN content in the slurry strongly affects the performance of AD reactors, causing significant economic losses for biogas plants. The ideal way to address these economic losses is to ensure a careful feedstock management including balanced nitrogen availability within the reactors. However, this is difficult to put into practice on farms, as the feedstock composition varies on a daily/weekly basis, and quantities are fed arbitrarily. Therefore, it is necessary to detect the risk of process disturbance and put prevention systems in place (Lemaigre et al., 2016). However, preventive measures are challenging to implement as the FAN toxicity depends on the complexity of the AD process where mechanisms such as antagonism, synergism and acclimatization can significantly affect the inhibition phenomenon (Jiang et al., 2019; Jo et al., 2022).

Various management methods have been investigated in order to avoid or mitigate FAN intoxication in AD reactors, including pH alteration with hydrochloric or humic acid, the adjustment of the feedstock C/N ratio, slurry dilution and microbial immobilization (Y. Chen et al., 2008; Khalil et al., 2017; Yenigün & Demirel, 2013). Besides these potential solutions, a few strategies have also recently been investigated, including the gradual acclimation of the microorganisms to high nitrogen conditions (Jo et al., 2022) and lignite addition for ammonium adsorption (Wijesinghe et al., 2021). However, these methods aim either at preventing ammonia inhibition or at optimizing biogas production after a moderate ammonia intoxication, and studies proposing recovery strategies after critical FAN-intoxication of the AD process are scarce (Nielsen & Angelidaki, 2008; Niu et al., 2013).

This paper complements our previous work on the assessment of a multivariate statistical process control model exploiting biogas composition to predict the process status of AD reactors that were intentionally driven to critical FAN intoxication (**Chapter 4**; Lemaigre et al., 2018). In the previous study, three mesophilic pilot-scale continuous stirred tank reactors (referred to as the high nitrogen input reactors HNR1, HNR2 and HNR3) were fed with a sugar beet pulp basal diet complemented with increasing amounts of urea until the complete interruption of their biogas production due to FAN toxicity [FAN ~ 5 grams of nitrogen per litre of slurry (i.e., g_N L^{-1}) ; TAN ~ 17.5 g_N L^{-1}]. In parallel, a fourth reactor (referred to as the low nitrogen input reactor, LNR), was fed with the sugar beet pulp basal diet only (no urea supplied) and was used as a reference reactor. We showed that the first warning signal delivered by our model was synchronous to a shift in the microbiome structure of the three HNRs, which announced the upcoming process collapse. In the present study, we further test a specifically designed process recovery strategy (**Table 6.1** and **Figure 6.1**), which was applied to these three critically FAN-intoxicated reactors (here still referred to as HNRs). The aim was to assess whether this process recovery strategy could restore the main AD process pathways in our HNRs, in which prolonged and excessive FAN exposure made the hydrolysis, heterotrophic acetogenesis and methanogenesis unfunctional. The process status of the HNRs was assessed by monitoring key abiotic process stability indicators and comparing them to those measured for the LNR as a reference for optimal process performance. A particular focus was placed on tracing the microbial communities due to their ability

to convert the introduced feedstocks (sugar beet pulp and acetic acid) to CH_4. Bacteria and archaea were monitored (separately) using 16S rRNA gene amplicon high-throughput sequencing, allowing us to link changes in the ecological richness, evenness and diversity of the microbial communities to the recovery strategy applied and the final process stability assessment.

Table 6.1. Treatments applied to the free ammonia intoxicated reactors HNR1, HNR2 and HNR3.

Stage	Phase	Weeks	Treatment
Process reconditioning	I	0 (day 0-1)	*pH reduction to 7.7 with pure acetic acid* (15 g L^{-1} in total)
	II	0 (days 2-5) and 1	*Dilution with tap water at 37°C* (25 mL L^{-1} d_feed^{-1})
	III	2 to 3	*Re-inoculation with LNR effluents* (6.5 mL L^{-1} d_feed^{-1})*; Water dilution**
Process recovery	/	4 to 7	*Re-inoculation with LNR effluents* (6.5 mL L^{-1} d_feed^{-1}); *Feeding with sugar beet pulp* (0.5→2 $g\_VS\ L^{-1}$ d_feed^{-1})*; Water dilution**
Process stability test	/	8 to 11	*Feeding with sugar beet pulp* (2 $g\_VS\ L^{-1}$ d_feed^{-1})*; Water dilution**

The reactors were fed on working days, usually five consecutive days (i.e., d_feed) per week; * inputs suspended in tap water at 37°C to reach a hydraulic retention time of 56 days (total fed volume: 25 mL L^{-1} d_feed^{-1}); LNR: low nitrogen input reactor used as a reference reactor; VS: volatile solids.

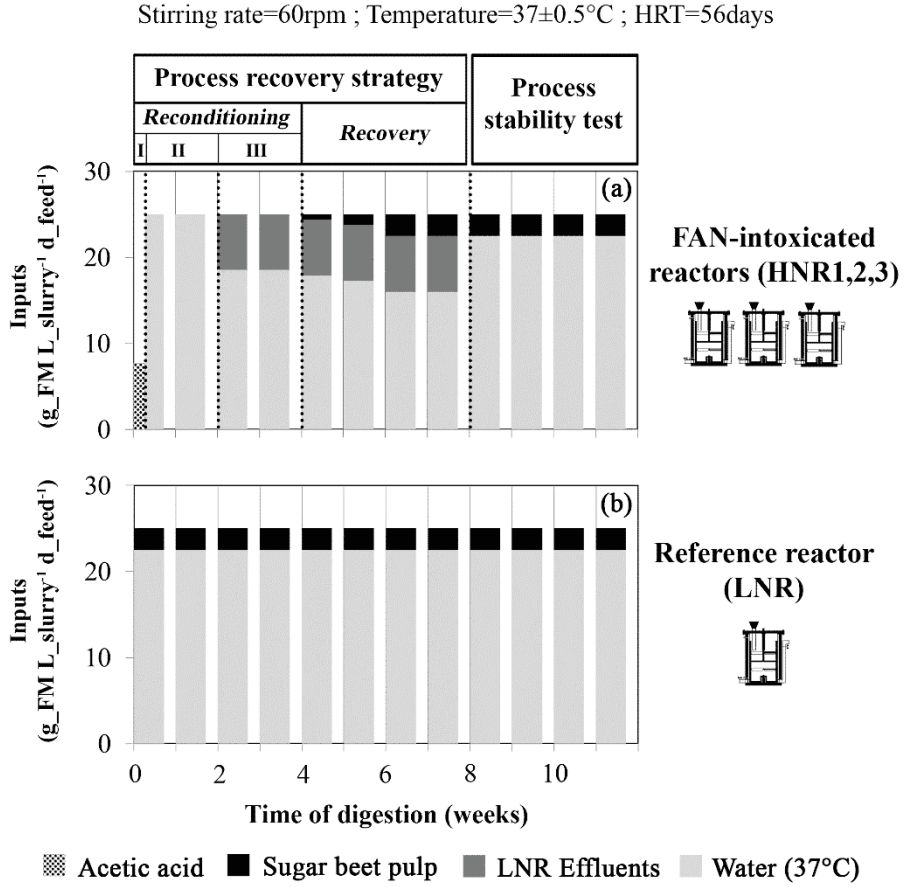

Figure 6.1. Mass of inputs (expressed in fresh matter, FM) introduced per litre of slurry and per feeding day (i.e., d_feed) in (a) the free ammonia intoxicated reactors, HNRs and (b) the reference reactor, LNR. "Process reconditioning I, II, III", "Process recovery" and "Process stability test" refer to the stages and phases described in **Table 6.1**.

6.2. Material and methods

6.2.1. FAN intoxication

The method used to generate severe FAN intoxication in the reactors is described in detail in **Chapter 4** (Lemaigre et al., 2018). Briefly, the experiment was performed in mesophilic temperature conditions (37 ± 0.5 °C), using four stainless steel tank reactors of 100L working volume, continuously stirred at 60 rotations per minute (rpm) with a central anchor-type stirrer and presenting an additional 25L headspace volume. All four reactors were initially and simultaneously inoculated with

anaerobic sludge from a mesophilic anaerobic reactor at a wastewater treatment plant (Schifflange, Luxembourg). Then, the reactors were manually fed on working days, usually 5 consecutive days (d_feed) per week, with commercial dried sugar beet pulp pellets (**Table 3.1**) used as the basal diet, following a semi-continuous scheme. The pulp contained 0.012 grams of nitrogen per gram of volatile solids (g_N g_VS^{-1}) and its biochemical methane potential (BMP) was measured to be 0.38 normal litres of CH_4 per gram of VS (L_N CH_4 g_VS^{-1}) according to standard BMP assessment methods (Mayer et al., 2014). The pulp organic loading rate (OLR) was 2 grams of VS per litre of slurry and per feeding day (g_VS L^{-1} d_feed^{-1}), i.e., 1.4 g_VS L^{-1} day^{-1} on a weekly average, while the hydraulic retention time (HRT) was adjusted at 56 days by adding tap water at 37°C to the pulp feed. The four reactors were initially acclimatized to the feedstock for 8 weeks, then three reactors (referred to as high nitrogen input reactors, with the respective acronyms HNR1, HNR2 and HNR3) underwent identical exposure to increasing nitrogen input by adding urea to the basal sugar beet pulp diet (maximal nitrogen supply of 0.95 g_N L^{-1} d_feed^{-1}). After 23 weeks, this treatment led to severely FAN-intoxicated reactors, with a process collapse marked by the complete interruption of biogas production due to high pH and FAN content (pH > 8.3 and FAN ~ 5.0 g_N L^{-1}). The fourth reactor, utilized as a reference (low nitrogen input reactor, LNR), was maintained in steady state during the whole experimental period with a low nitrogen supply using the abovementioned feeding regime based only on sugar beet pulp pellets. Following its inoculation, the LNR efficiently converted the feedstock to CH_4 with a yield of 0.33 ± 0.03 L_N CH_4 g_VS^{-1}, which remained close to the pulp BMP.

After 23 weeks of progressive intoxication, the feeding of the three FAN-intoxicated reactors (HNRs) was stopped, and these reactors were left to rest for three days before initiating the process recovery strategy described below. During this resting period, no biogas production was detected for the HNRs.

6.2.2. Process recovery strategy and assessment of the process stability during post-intoxication recovery

The process recovery strategy involved a process reconditioning stage followed by a process recovery stage (**Table 6.1** and **Figure 6.1**) and was applied in an identical way to the three FAN-intoxicated reactors HNRs, while the management

of the reference reactor LNR was left unchanged following the FAN-intoxication period applied to the HNRs (i.e., sugar beet pulp as the unique feedstock; OLR and HRT set to 2 g_VS L^{-1} d_$feed^{-1}$ and 56 days, respectively). As a follow-up, a process stability test stage was performed to assess the process recovery of the HNRs. The treatments applied to the HNRs during these stages are detailed hereafter:

- *Process reconditioning stage - Phase I: pH neutralization with acetic acid* (day 0). First, a composite sample (1:1:1) of slurries from the three HNRs was titrated against pure acetic acid (Sigma-Aldrich, USA) until the pH was reduced from 8.3 to 7.7, which required the injection of 15 g_VS of acetic acid per litre of slurry (0.25 M). Then, this amount of pure acetic acid was injected into the slurry of the HNRs at a flow rate of 0.03 g_VS per litre of slurry and per minute using a peristaltic pump (IPC 8, Ismatec, Germany).
- *Process reconditioning stage - Phase II: Water dilution* (end of week 0 and week 1). For each HNR, 25 mL of tap water at 37°C was introduced per litre of slurry and per feeding day (mL L^{-1} d_$feed^{-1}$), according to a 56-day HRT.
- *Process reconditioning stage - Phase III: Water dilution and re-inoculation* (week 2 to week 3). Each HNR was fed with 6.5 mL LNR effluents per litre of slurry and per feeding day. The LNR effluents were supplemented with tap water at 37°C to reach a total volume of 25 mL L^{-1} d_$feed^{-1}$, corresponding to a 56-day HRT.
- *Process recovery stage: Water dilution, re-inoculation and feeding* (week 4 to week 7). For each HNR, sugar beet pulp was introduced following a progressively increasing OLR to reach a value of 2 g_VS L^{-1} d_$feed^{-1}$ (from week 6 onwards), identical to the steady OLR applied to the LNR. The introduction of effluents produced by the LNR into the three HNRs was maintained (6.5 mL L^{-1} d_$feed^{-1}$). The feed was supplemented with tap water at 37°C to reach a total volume of 25 mL L^{-1} d_$feed^{-1}$, corresponding to a 56-day HRT.
- *Process stability test stage: Feeding and water dilution* (from week 8 onwards). To assess the process stability after the recovery strategy, the three HNRs were fed in the same manner as the LNR, i.e., 2 g_VS sugar beet pulp L^{-1} d_$feed^{-1}$ as

the sole feedstock, supplemented with tap water at 37°C to reach a total volume load of 25 mL L^{-1} d_feed^{-1}, corresponding to a 56-day HRT.

6.2.3. Slurry monitoring

Every Monday, the total ammonia nitrogen content (TAN, $g\_N\ L^{-1}$), the total inorganic carbon content (TIC, $g\_CaCO_3\ L^{-1}$), the individual VFA concentrations (C2 to C5, g kg^{-1}), the total solids content (TS, g kg^{-1}) and the pH were measured in the slurry. The TAN and the TIC contents were measured using the BiogasPro system (RIMU, Königsbrunn, Germany) in conformity with the manufacturer's protocol and as performed in **Chapter 5** (Goux et al., 2015). For the TAN content measurement, the BiogasPro method is equivalent to the Quantofix N-Volumeter method (Terraflor, Iserlohn, Germany) that was previously described (Van Kessel & Reeves, 2000). For the TIC content measurement, the BiogasPro method consists in acidifying 200 mL slurry with 150 mL HCl 5%v/v and to measure the volume of the released CO_2, visualized by the displacement of a water column in a graduated cylinder (Adam et al., 2015; Hecht et al., 2007). The individual VFA concentrations, the TS content and the pH of the slurry were measured according to the methods exposed in **Chapter 5** (Goux et al., 2015). The total VFA concentration (TVFA, g kg^{-1}) was expressed as the sum of the individual VFA concentrations, measured for acetate, propionate, iso-butyrate, butyrate, iso-valerate and valerate. The FAN content in the slurry ($g\_N\ L^{-1}$) was calculated on the basis of the TAN content and the pH (Calli et al., 2005), with a temperature of 37°C and a pKa of 8.89.

To assess the fate of the acetic acid provided for process recovery, for each HNR, the concentration of acetate measured in the slurry was compared with the concentration that could be expected in the absence of microbial activity, i.e., if the variation of the acetate concentration was only due to the dilution and wash-out (**Figure 6.7**).

6.2.4. Bacterial and archaeal community monitoring

Aliquots of about 200 µL of slurry were sampled once per week (on Mondays) throughout the experiment and for each studied reactor. Aliquots were immediately snap frozen in liquid nitrogen and stored at -80°C prior to further analysis. Total DNA was extracted using the DNeasy PowerSoil Kit from Qiagen

(Carlsbad, CA) according to the manufacturer's protocol. The 16S rRNA gene amplicon libraries were then prepared, sequenced, de-multiplexed, quality trimmed, clustered into operational taxonomic units (OTUs) at 97% similarity and taxonomically assigned using the Silva 138 database as previously explained (Calusinska et al., 2018). Briefly, separate primer pairs targeting the V6-V8 and V4-V6 regions, respectively, of 16SrRNA were used to assess the bacterial and archaeal communities. All the bioinformatic processing steps were done using usearch v11 (Edgar, 2010). On average, 65.5% of reads passed the quality control thresholds and the resulting read counts were normalized to 10000 reads per sample for further comparative analyses. Syntrophic acetate oxidisers (SAO) and syntrophic propionate oxidizers (SPO) were identified using blast against the Acetobase database (A. Singh & Schnürer, 2022) and using the 16S rRNA gene signatures of known SPOs (Westerholm et al., 2022), respectively. Matches with a sequence similarity of over 97% were retained as positive for both SAOs and SPOs. The alpha diversity of the bacterial and archaeal communities was assessed using the sobs and invsimpson calculators in mothur (v.1.34.4 or later ; Schloss et al., 2009), respectively. The higher these indices, the higher the richness and diversity of the community studied, respectively. Community evenness was measured via the Simpson coefficient ranging from 0 (uneven community; one or several dominant OTUs and many singlets) to 1 (perfectly even community; all OTUs present at the same relative abundance). The influence of process parameters on the archaeal community composition was analysed using canonical correspondence analysis (CCA) with R and the Vegan package (Dixon, 2003) (**Chapter 8**; Annex 4 - **Figure Ch6_S1** and **Figure Ch6_S2**). The nucleotide sequences obtained from sequencing were deposited in the GenBank database (http://www.ncbi.nlm.nih.gov/genbank/) and are part of a bigger submission with accession numbers from OQ217616 to OQ219830 for bacteria and from OQ220520 to OQ220896 for archaea.

6.2.5. Biogas monitoring

For the four reactors, the biogas was monitored every 2h for production and composition (CH_4, CO_2, H_2, H_2S, N_2 and O_2) as detailed in **Chapter 4**. The biogas composition measurements could not be taken from week 1 to week 3 for the HNRs, due to the absence of detectable biogas production.

6.3. Results and discussion

6.3.1. Process stability and microbiome of the reference reactor

In the LNR reference reactor, the fed sugar beet pulp was efficiently and continuously converted to methane, with a CH_4 yield of 0.32 ± 0.1 normalized litres (L_N) of CH_4 per gram of volatile solids (VS) added (i.e., L_N_CH_4 g_VS^{-1}). This value remained close to the pulp biochemical methane potential (BMP, 0.38 ± 0.03 L_N_CH_4 g_VS^{-1}), which is in accordance with the continuous but careful feeding regime of this reactor [OLR = 2 g of VS per litre of slurry and per feeding day (i.e., g_VS L^{-1} d_$feed^{-1}$)] (**Chapter 4**; Lemaigre et al., 2018). The biogas production was ~6 L_N L^{-1} $week^{-1}$ (**Figure 6.2**g) and was characterized by a [CH_4]/[CO_2] ratio close to 1 (**Figure 6.3**a) and an H_2 concentration lower than 100 parts per million by volume (ppmv) (**Figure 6.3**b). The total volatile fatty acid (TVFA) concentration remained below 0.04 grams per kilogram of slurry (i.e., g kg^{-1}).

Bacteroidota phylum dominated the bacterial[17] community of the LNR throughout the experiment (relative abundance 34.0 ± 4.4%; **Figure 6.4**a). The other phyla, including *Spirochaetota*, *Cloacimonadota* and *Desulfobacterota* were less abundant, representing 14.8 ± 2.9%, 10.7 ± 1.8%, 7.1 ± 0.6% of the community, respectively. The archaeal community was dominated at the genus level by *Methanomassiliicoccus* (31.2 ± 6.3%), *Candidatus* Methanofastidiosum, *Methanosaeta* and members of the *Bathyarchaeia* family (**Figure 6.4**c). The ecological indices, including richness, diversity and evenness remained quite stable over time for the bacterial community (**Figure 6.5**a,b,c). Evenness and diversity increased over time for archaea (**Figure 6.5**d,e,f), most probably due to a decrease in the abundance of *Methanomassiliicoccus* after week 6 (**Figure 6.4**c). The dominant bacterial and archaeal groups present in the LNR are typically found in uninhibited AD microbiomes (M. S. Rahman et al., 2021) and were identified in our laboratory reactors during previous experiments performed with a similar inoculum (**Chapter 5**; Goux et al., 2015).

[17] The bacterial taxonomy reflects the nomenclature in use at the time the study was conducted. The correspondence with the most recent taxonomic classification is provided in **Table 1.1** of the general introduction.

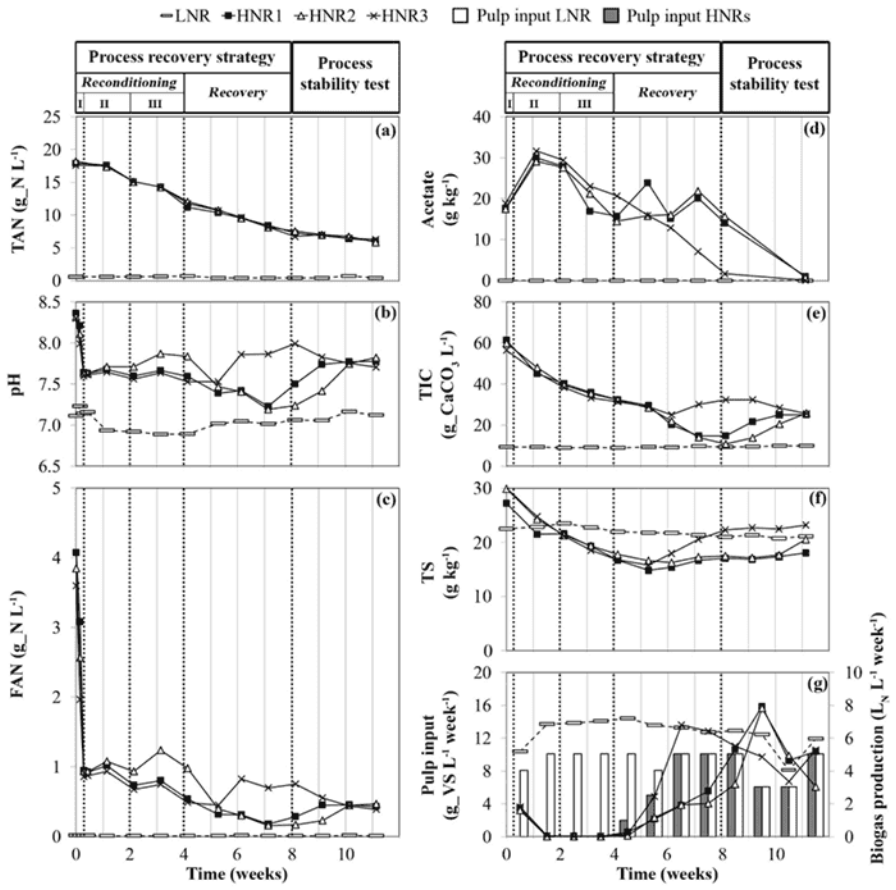

Figure 6.2. Progress over time of: (a) total ammonia nitrogen (TAN) measured; (b) pH; (c) free ammonia nitrogen (FAN) calculated; (d) acetate; (e) total inorganic carbon (TIC); (f) total solid (TS) content in the slurry of the reactors; (g) mass of sugar beet pulp (expressed in volatile solids, VS) introduced weekly into the reactors and their weekly biogas production. The decrease in biogas production observed during week 10 for the LNR reference reactor is due to a reduced pulp input in weeks 9 and 10 (only three feeding days per week). "Process reconditioning I, II, III", "Process recovery" and "Process stability test" refer to the stages and phases described in **Table 6.1**. HNR: free ammonia intoxicated reactor.

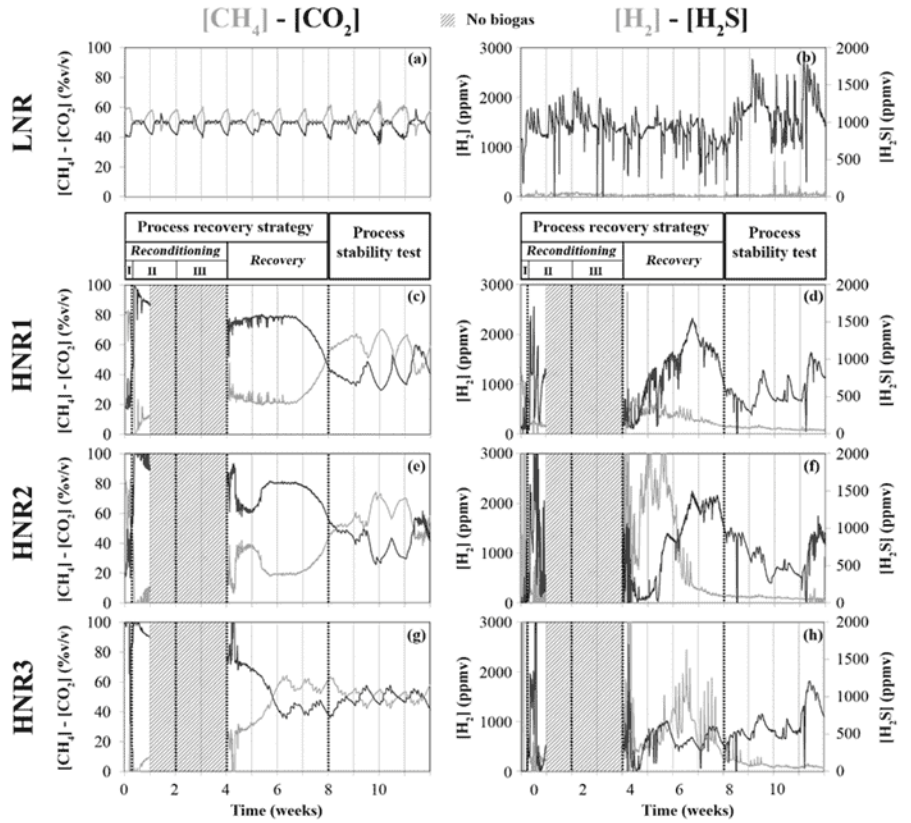

Figure 6.3. Progress over time of the biogas concentrations in CH_4, CO_2, H_2 and H_2S for: (a, b) the LNR reference reactor, (c, d) the free ammonia intoxicated reactor, HNR1, (e, f) HNR2 and (g, h) HNR3. CH_4 and CO_2 concentrations are expressed in volume/volume percents (%v/v). H_2 and H_2S concentrations are expressed in parts per million by volume (ppmv). Measurements could not be performed from week 1 to week 3 due to the interruption of the biogas production (hatched grey area). "Process reconditioning I, II, III", "Process recovery" and "Process stability test" refer to the stages and phases described in **Table 6.1**.

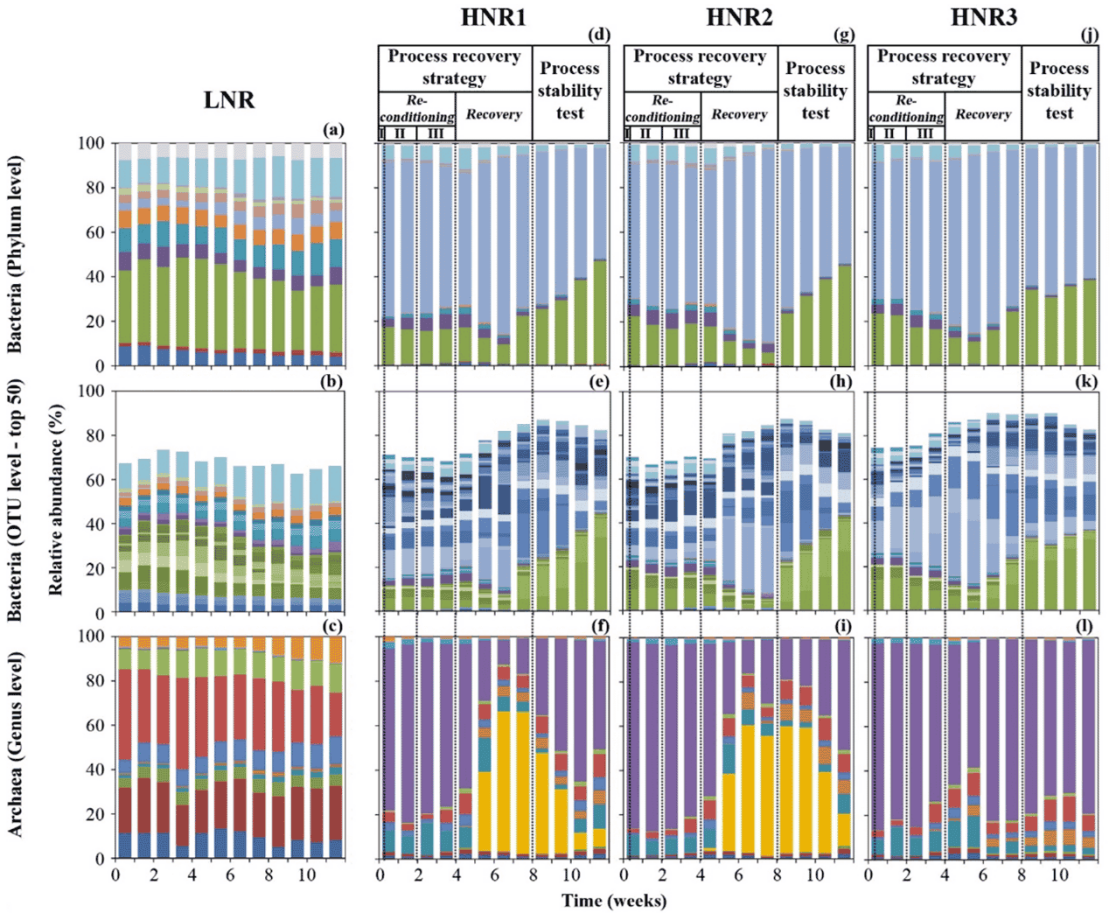
LNR
HNR1
HNR2
HNR3
Process recovery strategy
Re-conditioning
Recovery
Process stability test
I
II
III
(a)
(b)
(c)
(d)
(e)
(f)
(g)
(h)
(i)
(j)
(k)
(l)
Bacteria (Phylum level)
Bacteria (OTU level - top 50)
Archaea (Genus level)
Relative abundance (%)
Time (weeks)
0
20
40
60
80
100
0
2
4
6
8
10

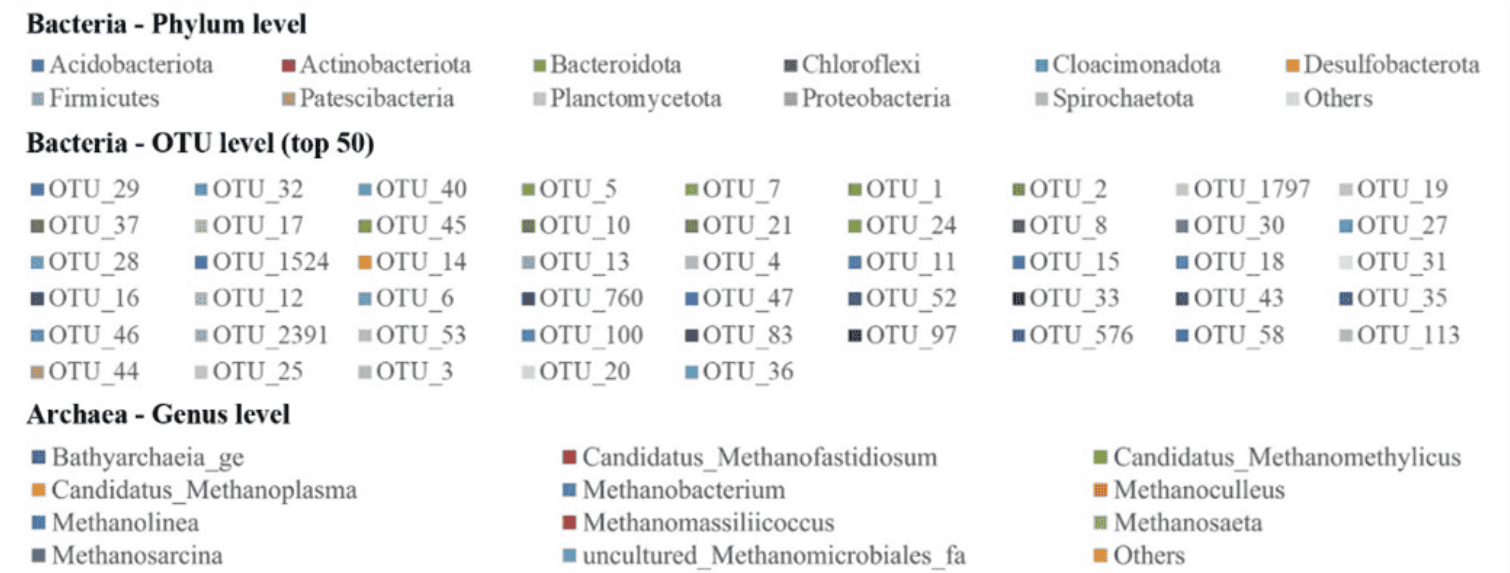

Figure 6.4. Bacterial (phylum level and top 50 OTUs level) and archaeal (genus level) structure dynamics over time as assessed by high-throughput 16S rRNA amplicon sequencing for: (a, b, c) the LNR reference reactor, (d, e, f) the free ammonia intoxicated reactor, HNR1, (g, h, i) HNR2 and (j, k, l) HNR3. The data presented correspond to slurry samples collected on Mondays. "Process reconditioning I, II, III", "Process recovery" and "Process stability test" refer to the stages and phases described in **Table 6.1** The taxonomic affiliation of the bacterial OTUs can be found in the **Table Ch6_S1** (**Chapter 10**; Annex 4).

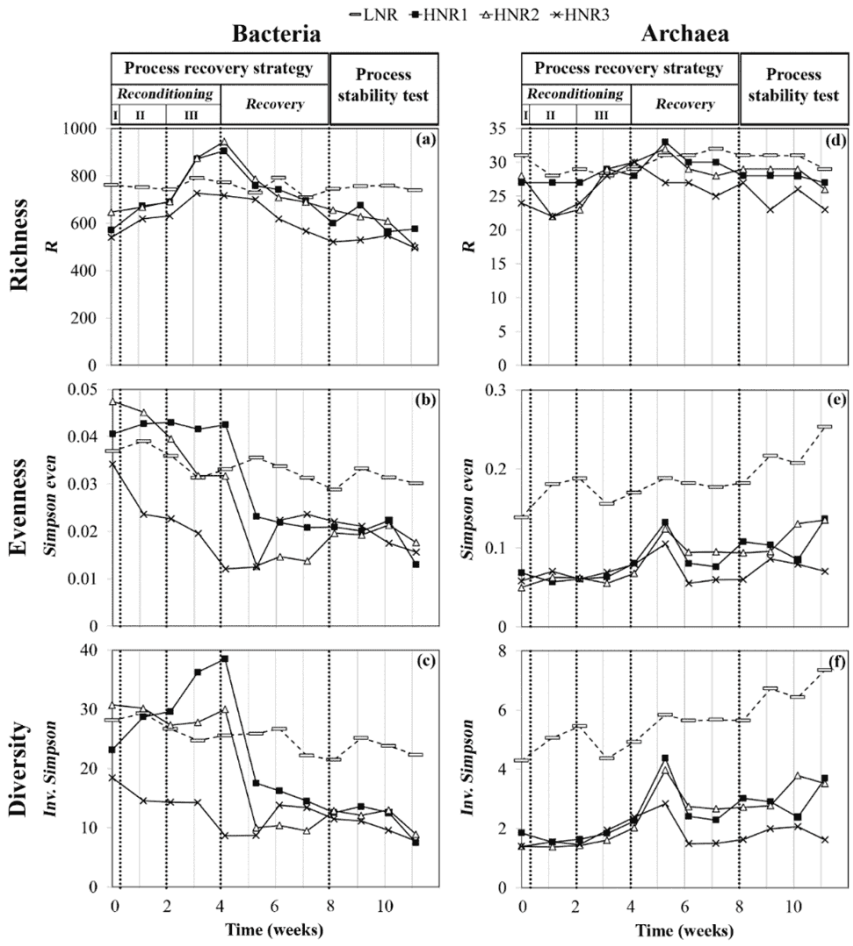

Figure 6.5. Progress over time of the ecological richness, evenness and diversity calculated at the OTU level for bacteria (a, b ,c) and archaea (d, e, f) for the LNR reference reactor and the free ammonia intoxicated reactors, HNR1, HNR2 and HNR3. For the (observed) richness (R) and diversity (Inv. Simpson), increased values indicate a higher richness and diversity of species, respectively. For the evenness (Simpson even), values range from 0 (uneven community; one or several dominant OTUs and many singlets) to 1 (perfectly even community, all OTUs present at the same relative abundance). "Process reconditioning I, II, III", "Process recovery" and "Process stability test" refer to the stages and phases described in **Table 6.1**.

6.3.2. Initial process status and microbiome of the FAN-intoxicated reactors

The initial process status of the reactors is presented in **Table 6.2**. At day 0, crucial AD metabolic pathways were inhibited in all HNRs. Firstly, hydrolysis was inefficient as attested both visually by the accumulation of raw sugar beet pulp residue

in the slurry, and analytically by the high total solid (TS) content (**Figure 6.2**f and **Table 6.2**) and the absence of detectable CO_2 production (**Table 6.2**). However, products of hydrolysis were still being generated from sugar beet pulp degradation, probably at a suboptimal rate. Indeed, acidogenesis remained active, as indicated by the TVFA accumulation observed in all HNRs during the last week of the FAN intoxication experiment (**Chapter 4**; Lemaigre et al., 2018). Secondly, the syntrophic oxidation of propionate and butyrate to acetate (i.e. heterotrophic acetogenesis) was inhibited, as these VFAs largely accumulated in the slurry. Thirdly, acetoclastic methanogenesis pathway was also inhibited, as suggested by the absence of CH_4 production (**Table 6.2**), and the high acetate concentration in the slurry. Fourthly, hydrogenotrophic methanogenesis pathway was halted since both total inorganic carbon (TIC) (**Figure 6.2**e) and H_2 (**Figure 6.3**c,e,g) were available in the slurry while no CH_4 was produced.

An acute inhibition of the AD process was promoted by the extremely high FAN and the TVFA concentrations in the slurry of the HNRs at the end of the FAN intoxication period (**Figure 6.2**). The phenomenon of a critical FAN intoxication has not been previously examined and in general, mostly reports on moderated FAN concentration can be found in the literature. For example, Fernandes et al. (2014) observed that ammonia did not significantly affect the hydrolysis rate in mesophilic reactors exposed to FAN concentrations ranging from 0.28 to 0.96 g_N L^{-1}. In contrast, our study indicates that a hydrolysis inhibition will occur under mesophilic conditions when the reactors are exposed to FAN concentration of ~5.0 g_N L^{-1} (**Chapter 4**).

Table 6.2. Process status of the reactors before initiating the process recovery strategy (day 0).

Process stability indicator	LNR	HNR1	HNR2	HNR3
pH	7.11	8.36	8.32	8.30
TAN (g_N L^{-1})	0.56	17.92	18.20	17.64
FAN (g_N L^{-1})	0.01	4.07	3.84	3.59
TS (g kg^{-1})	22.5	27.2	29.90	30.00
TVFA (g kg^{-1})	0.03	21.99	21.99	23.63
Acetate (g kg^{-1})	0.02	17.68	17.49	18.91
Propionate (g kg^{-1})	0.01	3.34	3.46	3.73
Biogas production (L_N L^{-1} $week^{-1}$)	6.52	ND	ND	ND

FAN: free ammonia nitrogen; HNR1,2,3: free ammonia intoxicated reactors; LNR: low nitrogen input reactor used as a reference reactor; L_N: normalized litre of gas; ND: not detected; TAN: total ammonia nitrogen; TS: total solids; TVFA: total volatile fatty acids.

The initial abiotic parameters of the HNRs differed from those of the reference LNR (**Figure 6.2** and **Figure 6.3**). Accordingly, the initial microbiome structure of the HNRs varied substantially (**Figure 6.4**). The overall bacterial richness was lower than in the control LNR, while diversity and evenness differed greatly between the HNRs and were in the range of the LNR (**Figure 6.5**). Members of the *Firmicutes* phylum, especially those belonging to the *Clostridia* order, largely dominated the HNRs. In line with our observations, high FAN contents have previously been shown to select *Firmicutes* in full-scale anaerobic digesters treating cattle or swine manure (J. Li et al., 2015). At day 0, the archaeal operational taxonomic unit (OTU) 1, assigned to the *Methanosarcina* genus (100% sequence identity, **Chapter 10**; Annex 3 – **Table Ch6_S3**), accounted on average for 80.4 ± 6.6% of the relative archaeal community abundance for the HNRs (**Figure 6.4**f,i,l). *Methanosarcina* species are versatile methanogens that can produce CH_4 through acetoclastic, hydrogenotrophic and methylotrophic pathways (De Vrieze et al., 2012; Lambie et al., 2015). Lü et al. (2013) observed that *Methanosarcinaceae* might shift their methanogenic pathway from acetoclastic to hydrogenotrophic as the concentrations of TAN and acetate increase. However, these authors reported that, when facing extreme concentrations of these molecules, *Methanosarcinaceae* could not survive even functioning by hydrogenotrophic methanogenesis and would then be replaced by other hydrogenotrophic methanogens. At day 0, strictly hydrogenotrophic archaeal genera (*Methanobacterium*, *Methanoculleus*) were minimal in the HNRs,

which suggests that this phenomenon did not occur during the intoxication experiment. Interestingly, De Vrieze et al. (2012) linked the resistance of *Methanosarcina* spp. to high TAN concentrations to their ability to grow in clusters, contrarily to other methanogens. At day 0, strictly acetoclastic methanogens of the *Methanosaeta* genus were almost absent in the microbiome of the HNRs (**Figure 6.4**f,i,l) while they were abundant in the LNR (**Figure 6.4**c).

6.3.3. Impact of the reconditioning stage on the FAN-intoxicated reactors

The initial 3-phases reconditioning stage (**Table 6.1**) had a major impact on both the TAN and the FAN content in the slurry. During the process reconditioning stage - phase I (pH neutralization with acetate), the supplementation of acetic acid increased the acetate concentration in all HNRs (**Figure 6.2**d) and caused their slurry pH to drop to 7.6 ± 0.0 (**Figure 6.2**b). This pH value remained higher than the one measured for the LNR (pH ~7.2). However, since our process recovery strategy aimed at re-establishing both acetoclastic and hydrogenotrophic methanogenesis in our HNRs, we chose to limit the initial acetate introduction to a reasonable amount. Indeed, when combined to high TAN concentration, high acetate concentration was previously identified as a factor promoting syntrophic acetate oxidation coupled to hydrogenotrophic methanogenesis in AD reactors (Lü et al., 2013). Nevertheless, such a limited pH drop was sufficient to cause a sharp reduction in the average FAN content in the HNRs (**Figure 6.2**c), from 3.8 ± 0.2 to 0.9 ± 0.1 g_N L^{-1}, respectively. Subsequently, during the process reconditioning stage - phase II (water dilution only) and the process reconditioning stage - phase III (water dilution and re-inoculation with the LNR effluents), the average TAN content in the HNRs decreased from 17.9 ± 0.3 (week 1) to 11.7 ± 0.4 g_N L^{-1} (week 4), corresponding to an average concentration drop of 35%. During these two dilution phases, the FAN content did not undergo any further changes for HNR2 (**Figure 6.2**c), due to a pH increase (**Figure 6.2**b). In contrast, the FAN content clearly dropped for HNRs 1 and 3 (**Figure 6.2**c). Overall, the reconditioning stage allowed the average FAN content in the HNRs to be reduced to 0.67 ± 0.27 g_N L^{-1} (week 4), corresponding to a total concentration drop of ~82%. It has been reported that a similar final value of the FAN content (~ 1 g_N L^{-1}) allowed the biogas production to restart in a mesophilic continuously stirred tank reactor

(CSTR) fed with chicken manure recovering from critical FAN intoxication (Niu et al., 2013).

At the phylum level for bacteria and at the genus level for archaea, the reconditioning stage did not drastically alter the microbial composition of the HNRs (**Figure 6.4**), which remained very different from the LNR. *Methanosarcina* and *Firmicutes* remained dominant in the archaeal and bacterial communities, respectively. However, clearer changes in the microbiome of the HNRs were detected at the OTU level (**Figure 6.4**e,h,k), as attested by the dynamics of the ecological indices (**Figure 6.5**). During the reconditioning stage – phases II and III, a potential washout of the microbial community was expected with the addition of water. However, the bacterial evenness and diversity indices did not change significantly in HNRs 1 and 2 and remained similar to those determined for the LNR; they decreased only for HNR3 (**Figure 6.5**b,c). During the reconditioning stage – phase III, supplying the HNRs with LNR effluents increased the archaeal richness for all the HNRs, indicating that the number of distinct archaeal OTUs increased in the slurry of the HNRs. The archaeal community of the HNRs also became slightly more even (**Figure 6.5**e), mostly due to the increased abundance of OTU_2, assigned to the *Methanomassiliicoccus* genus (100% sequence identity, **Chapter 10**; Annex 3 – **Table Ch6_S3**) and the progressive disappearance of OTU_1, assigned to *Methanosarcina*. Although the resilience of an AD microbiome cannot be assessed solely on the basis of ecological parameters (Goux et al., 2015; L. Li et al., 2018), we interpret the increase of the archaeal richness and evenness as a sign that the reconditioning stage of our strategy made the environmental conditions in the HNRs more favourable to the re-establishment of a functional methanogenesis. Similarly, the bacterial richness increased in all HNRs during the reconditioning stage – phase III (**Figure 6.5**a), however, this trend was slightly less marked for HNR3. This observation may indicate that bacterial OTUs from the LNR established in the microbiome of the HNRs, certain potentially capable of hydrolysis. However, the reconditioning stage mostly resulted in the increased abundance of the bacterial OTU_13, especially in HNRs 2 and 3 (**Figure 6.4**h,k). This microbe, assigned to the *Caldicoprobacter* genus (80% sequence identity; **Chapter 10**: Annex 3 – **Table Ch6_S3**), was not abundant in the LNR slurry (maximal relative abundance of 0.01%). *Caldicoprobacter* were shown to dominate the bacterial community of

mesophilic AD reactors at TAN concentrations higher than 10 g_N L^{-1} (Poirier et al., 2016), which is similar to the TAN content remaining in slurry at the end of the reconditioning stage. This means that these bacteria are well adapted to high TAN concentrations and might thus be good indicators of increasing N content in the reactor's slurry.

During the process reconditioning stage – Phase I, the three HNRs temporarily released high volumes of CO_2 and H_2S (**Figure 6.3**), probably due to the pH drop caused by the addition of acetic acid. However, none of the HNRs produced biogas during the process reconditioning stage – Phases II and III (**Figure 6.2**g), despite the high carbon content potentially convertible to CH_4 and CO_2 and available in their slurry in the form of acetate and TIC (**Figure 6.2**d,e). Therefore, such an absence of biogas production suggests that both the acetoclastic and the hydrogenotrophic methanogenesis pathways remained inhibited in the HNRs at the end of the reconditioning stage, despite the reduction of the FAN and TAN content and the reactor re-inoculation with LNR effluents. Nielsen & Angelidaki (2008) compared different dilution strategies to restore the AD process in the FAN-intoxicated thermophilic reactors that stopped producing CH_4. In their study, the reactors were exposed to a FAN concentration of 1.2 g_N L^{-1} for only 5 days before the dilution strategies were applied. In contrast, our HNRs were exposed to FAN concentrations higher than 2 g_N L^{-1} for more than 2 weeks (maximal FAN concentration > 3.5 g_N L^{-1}) in a phase preceding our process recovery strategy (**Chapter 4**; Lemaigre et al., 2018). Therefore, these extreme FAN concentrations could explain the prolonged inhibition of the AD process observed in our HNRs during the reconditioning stage of our recovery strategy.

6.3.4. Restoration of CH_4 production for the FAN-intoxicated reactors

To verify whether hydrolysis remained inhibited and to re-initiate the acetoclastic and hydrogenotrophic methanogenesis pathways, the HNRs were subsequently supplied with a complex feedstock in the form of sugar beet pulp (process recovery stage, **Table 6.1**). The OLR of the HNRs was progressively increased (**Figure 6.2**g), while the introduction of water and effluent from the LNR reference reactor remained the same. During the first week of this treatment (OLR_{HNRs} = 0.5 g_VS L^{-1} d_feed^{-1}), the TAN and FAN contents further decreased in the slurry

(**Figure 6.4**a,c). Interestingly, the biogas production restarted in the HNRs (**Figure 6.2**g), although it remained very low during week 4. This observation became much clearer for all HNRs during week 5 (OLR_{HNRs} = 1 g_VS L^{-1} d_$feed^{-1}$). From week 5 onwards, the behaviour of HNR3 diverged from that of HNRs 1 and 2. HNRs 1 and 2 initially produced little biogas (**Figure 6.2**g) (weeks 5-6) but with a high CO_2 content, which finally decreased during week 7 in favour of CH_4 (**Figure 6.3**c,e). For these two reactors, the pH of the slurry slightly decreased (**Figure 6.2**b), while H_2S was released into the biogas (**Figure 6.3**d,f). Concomitantly, the TS content in the slurry stopped decreasing compared to the process reconditioning stage and subsequently did not progress much despite the daily supply of sugar beet pulp (**Figure 6.2**f), suggesting a progressive improvement of the hydrolysis for HNRs 1 and 2. The faster synthesis of acetate (**Figure 6.2**d), butyrate and propionate (**Figure 6.6**a,b) in the slurry also confirms that products of hydrolysis (i.e,, substrates of the acidogenesis stage) were synthesised at a higher rate than previously. During weeks 5-6, the H_2 concentration in the biogas decreased (**Figure 6.3**d,f), suggesting microbial consumption of H_2. This could indicate the progressive restoration of the hydrogenotrophic pathway and/or a potential contribution of the H_2-dependent methylotrophic pathway to CH_4 production, which is consistent with the microbiome dynamics in the HNRs (see below). Indeed, the archaea involved in both pathways compete for H_2 as a common substrate (Christou et al., 2021). On the other hand, the net synthesis of acetate (**Figure 6.7**) and the low CH_4 production compared to HNR3 (**Figure 6.2**g and **Figure 6.3**c,e), while acetate was abundant in the slurry (**Figure 6.2**d), suggest that the acetoclastic pathway remained inhibited. In contrast, for HNR3, CH_4 was produced massively from week 5 to week 7 (**Figure 6.2**g and **Figure 6.3**g) while the acetate concentration in the slurry decreased from 15.9 to 1.7 g kg^{-1} (**Figure 6.2**d). The dilution rate of the slurry cannot explain such a fast concentration drop (**Figure 6.7**c), which suggests the microbial consumption of acetate and advocates for the restoration of the acetoclastic pathway in HNR3. However, the TS accumulated concomitantly in the slurry (**Figure 6.2**f), suggesting that the hydrolysis remained suboptimal in HNR3 at the end of the process recovery stage. We attributed this prolonged inhibition of the hydrolysis to the pH increase (pH range of 7.7-8.0; **Figure 6.2**b) that was caused by the microbial consumption of acetate. Indeed, Romsaiyud et

al. (2009) showed that the pH range required to optimize both cellulase synthesis and cellulose hydrolysis was between 5.3 and 7.5 at 37°C.

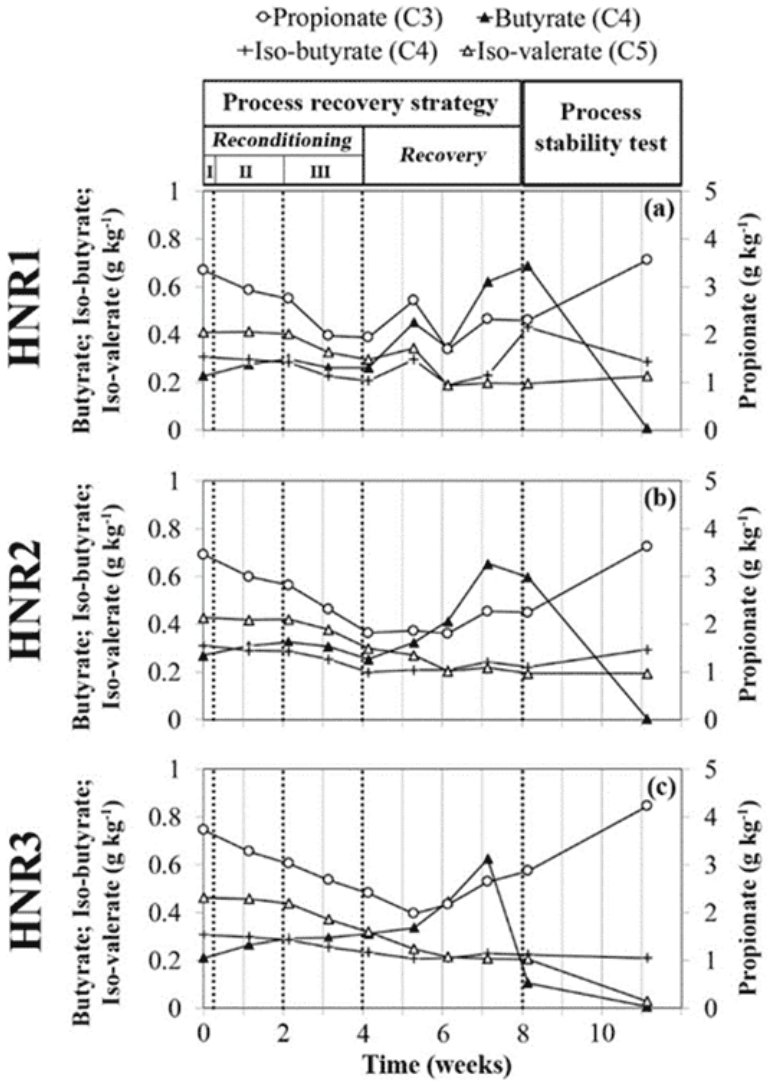

Figure 6.6. Progress over time of the concentration of C3 to C5 volatile fatty acids in the slurry for: (a) the free ammonia intoxicated reactor, HNR1, (b) HNR2 and (c) HNR3. The valerate (C5) concentration was below the detection limit of the analytical method during the whole experiment. "Process reconditioning I, II, III", "Process recovery" and "Process stability test" refer to the stages and phases described in **Table 6.1**.

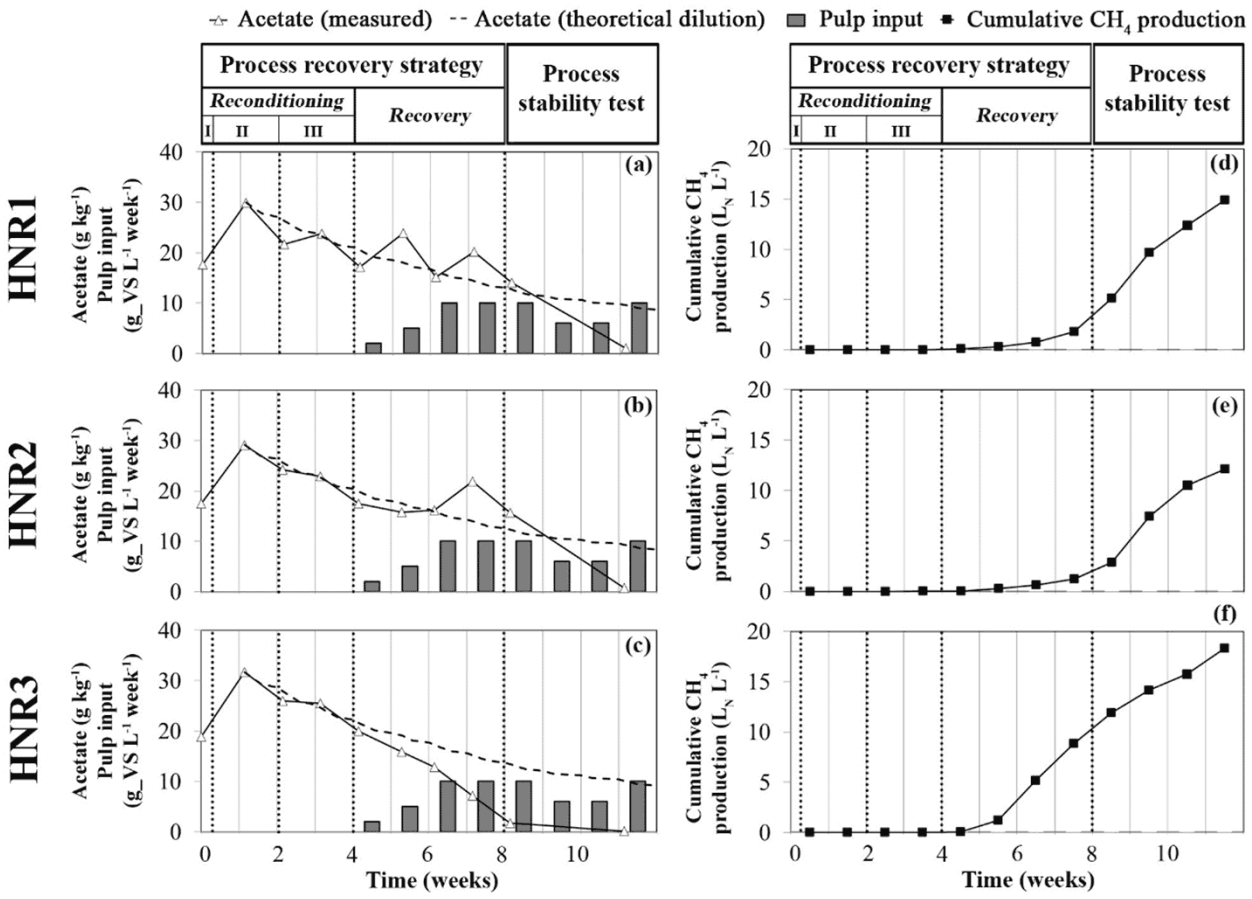
Acetate (measured)
Acetate (theoretical dilution)
Pulp input
Cumulative CH4 production
Process recovery strategy
Reconditioning
Recovery
Process stability test
I
II
III
HNR1
HNR2
HNR3
(a)
(b)
(c)
(d)
(e)
(f)
Acetate (g kg-1)
Pulp input
(g_VS L-1 week-1)
Cumulative CH4 production (LN L-1)
Time (weeks)

Figure 6.7. Comparison of the acetate concentration measured in the slurry and the acetate concentration expected when considering that wash-out is the only mechanism of removal (absence of microbial synthesis or degradation) for: (a) the free ammonia intoxicated reactor, HNR1, (b) HNR2 and (c) HNR3. The weekly pulp input is also presented for each HNR. Cumulative CH_4 production for: (d) HNR1, (e) HNR2 and (f) HNR3. "Process reconditioning I, II, III", "Process recovery" and "Process stability test" refer to the stages and phases described in **Table 6.1**.

6.3.5. Microbial community dynamics in the FAN-intoxicated reactors during the restoration of the CH_4 production

Improved hydrolysis for HNRs 1 and 2 (week 5) coincided with an abrupt decrease of the bacterial richness, evenness and diversity (**Figure 6.5**a,b,c), while the archaeal ecological indices transiently increased (**Figure 6.5**d,e,f). The same indices remained relatively stable for HNR3. The change in the bacterial community structure was related to an increased relative abundance of the *Firmicutes* phylum and a decreased relative abundance of the *Bacteroidota* and *Spirochaetes* phyla (**Figure 6.4**d,g). Commonly described butyrate-producing bacteria belong to the *Firmicutes* phylum and the *Clostridia* order (Fu et al., 2019), which could explain the rising butyrate concentration in all HNRs (**Figure 6.6**). The change in the archaeal richness, evenness and diversity reflected a drastic reshaping of the community structure, due to the replacement of the formerly dominant archaeal OTU_1 (assigned to the *Methanosarcina* genus; **Chapter 10**; Annex 4 - **Table Ch6_S3**) by OTU_4 (assigned to the *Candidatus* Methanoplasma genus) in HNRs 1 and 2. The latter OTU reached more than 50% of the relative archaeal abundance (weeks 5-6, **Figure 6.4**f,i). In contrast to HNRs 1 and 2, the dominance of a versatile *Methanosarcina* coincided with an increased acetate consumption in HNR3, which may indicate the restoration of the acetoclastic pathway in this reactor.

Members of the *Candidatus* Methanoplasma genus are strictly methylotrophic methanogens that can only produce CH_4 from the hydrogen-dependent reduction of methanol or methylamines (Lang et al., 2015). In a recent study (Christou et al., 2021), *Candidatus* Methanoplasma were shown to play a key role in the successful bio-augmentation of mesophilic reactors operating at high FAN concentrations. Therefore, their rise in abundance suggests that the methylotrophic pathway could have contributed to the restoration of the CH_4 production in HNRs 1

and 2, possibly in combination with the hydrogenotrophic pathway, while the acetoclastic pathways were of minor importance at that stage.

We can further link the progressive dominance of *Candidatus* Methanoplasma and the improvement of the hydrolysis in HNRs 1 and 2 via the canonical correspondence analysis (CCA) computed for the archaeal genera (**Chapter 10**: Annex 4 - **Figure Ch6_S2**). It highlights a negative corelation between the relative abundance of *Candidatus* Methanoplasma and the TS content in the slurry of the HNRs. Tian et al. (2019) also observed the appearance of strictly methylotrophic methanogens in exposing mesophilic inocula at increasing FAN concentrations (up to ~1 g_N L^{-1}). The authors linked this phenomenon to the presence of bacteria assigned to the *Tissierella* genus. Indeed, these microbes can produce methylamine from different amino acids and could therefore provide methylotrophic methanogens with substrate. In our reactors, only the bacterial OTU_47 was assigned to an unclassified member of the *Peptostreptococcales-Tissierellales* family (100% sequence identity; **Chapter 10**; Annex 4 - **Table Ch6_S1**). Interestingly, in week 5, the relative abundance of this bacteria was higher in HNR1 (1.31%) and HNR2 (1.61%) than in HNR3 (0.67%). Therefore, the improvement of the sugar beet pulp hydrolysis in HNRs 1 and 2 may have induced the release of amino acids in the slurry, which in turn were converted to methylamines by this *Peptostreptococcales-Tissierellales* member, generating favourable conditions for the preferential growth of *Candidatus* Methanoplasma.

Feeding sugar beet pulp also resulted in the increased abundance of *Methanoculleus* in all HNRs (**Figure 6.4**f,i,l). *Methanoculleus* spp. are strictly hydrogenotrophic methanogens (Lv, Leite, et al., 2014) and were reported to outcompete *Methanosaeta* spp. at higher OLR (>1 g_COD L^{-1} day^{-1}) (Lebiocka et al., 2018; Zielińska et al., 2013), which would explain their sudden appearance. This can indicate a progressive restoration of the hydrogenotrophic methanogenesis pathway in the HNRs. It should be noted that the contribution of putative syntrophic acetate oxidizers (SAO) to the CH_4 production of the HNRs was most likely very low. Their total relative abundance in the slurry of the HNRs remained <2% during the whole experiment. Such low abundance is in line with the fact that acetoclastic methanogenesis has a thermodynamic advantage over SAO-induced

hydrogenotrophic methanogenesis at mesophilic temperatures (Nie et al., 2021). Nevertheless, the presence of other as yet unknown SAO cannot be excluded.

6.3.6. Testing the process stability in the FAN-intoxicated reactors after the process recovery strategy

To assess the operational stability of the recovered HNRs, the re-inoculation was interrupted from week 8 onwards while sugar beet pulp feeding was maintained according to the feeding scheme applied to the LNR (process stability test stage, **Table 6.1**). For all HNRs, propionate started to accumulate in the slurry after the re-inoculation was interrupted (**Figure 6.6**, weeks 8-11). In our reactors, only *Cloacimonadota* members were identified as potential SPOs (Calusinska et al., 2018) and they were more abundant in the LNR effluents (**Figure 6.4**a) than in the slurry of the HNRs (**Figure 6.4**d,g,j). However, they continuously decreased in abundance in the HNRs all along the experiment, which indicates that SPO from the LNR could not establish in the HNRs. However, re-inoculation was a key element of our process recovery strategy in stabilizing the AD process of the HNRs during the restoration of their CH_4 production.

During the process stability test, the biogas production dynamics of the HNRs resembled those of the LNR, except during the last week of the experiment for HNR2 (**Figure 6.2**g), where a slight decrease in biogas production was accompanied by the accumulation of TS in the slurry (**Figure 6.2**f). Otherwise, the TS content in the slurry of HNRs 1 and 2 remained constant, suggesting that the hydrolysis of the fed sugar beet pulp was preserved in these reactors. HNRs 1 and 2 maintained a similar $[CH_4]/[CO_2]$ ratio until the end of the experiment (**Figure 6.3**c,e), which was substantially higher during weeks 8-9 (**Figure 6.2**g) possibly due to a rise in pH (**Figure 6.2**b) that favoured the CO_2 capture in the slurry. This pH rise was probably caused by the depletion of acetate that reached a negligible concentration at the end of the experiment (**Figure 6.2**d). The dilution rate of the slurry could not explain such an important acetate concentration drop (**Figure 6.7**c), and therefore suggests its microbial consumption and advocates for the restoration of the acetoclastic methanogenesis in HNRs 1 and 2. During the last week of the experiment, the CO_2 content in the biogas produced by HNRs 1 and 2 transiently increased (**Figure 6.3**c,e). However, as CH_4 production continued, we attributed this phenomenon to the final

depletion of acetate, followed by a fluent transition to CH_4 production from the fed sugar beet pulp only. For HNR3, the $[CH_4]/[CO_2]$ ratio in the biogas remained close to 1 and its dynamics adopted a weekly pattern analogous to that of the LNR (**Figure 6.3**g). Concomitantly, TS stopped to accumulate in the slurry (**Figure 6.2**f), suggesting an improvement of the pulp hydrolysis. In HNR3, CH_4 was continuously produced (**Figure 6.7**f) while the residual acetate concentration in the slurry was negligible (**Figure 6.7**c), suggesting that the sugar beet pulp degradation was the main source of CH_4 production. During the last week of the experiment, the average pulp to CH_4 conversion ratio was 0.41 ± 0.10 L_N_CH_4 g_VS^{-1} for the HNRs, which is analogous to the pulp BMP (0.38 ± 0.03 L_N_CH_4 g_VS^{-1}). Therefore, we conclude that the AD process was successfully restored for the three HNRs. The pH of the slurry as well as its TAN and FAN content were similar for all HNRs (**Figure 6.2**a,b,c) and approached the values observed for the LNR. However, the AD process remained slightly disturbed in the HNRs as evidenced by propionate accumulation, which is attributable to the fact that re-inoculation was interrupted too early to ensure the long-term process stability of the HNRs.

6.3.7. Final microbiome structure of the recovered reactors

The final microbiome of the HNRs remained different from that of the LNR (**Figure 6.4**). In particular, strictly acetoclastic methanogens of the *Methanosaeta* genus remained much less abundant in the HNRs (**Figure 6.4**f,i,l) compared to the LNR (**Figure 6.4**c). Also, the final values of the richness, evenness and diversity indices were lower for the HNRs than for the LNR (**Figure 6.5**), both for bacteria and archaea. Indeed, the microbial communities of the HNRs were exposed to high selection pressure due to environmental changes, which is usually reflected by a decreased richness and diversity (**Chapter 5**; Goux et al., 2015).

At the end of the experiment, *Firmicutes* still dominated the bacterial microbiome of the HNRs, but the relative abundance of *Bacteroidota* had clearly increased (**Figure 6.4**d,g,j). A recent meta-regression study (Ma et al., 2021) comprising 846 mesophilic and 246 thermophilic AD processes revealed that these two phyla significantly determined the CH_4 yield in both stable and unstable process conditions. Towards the end of the experiment in HNRs 1 and 2, the relative abundance of the archaeal OTU_4, assigned to the strictly methylotrophic genus

Candidatus Methanoplasma, was decreasing in favour of OTU_1, assigned to *Methanosarcina* (**Figure 6.4**f,i). This suggests an increasing contribution of the acetoclastic and hydrogenotrophic pathways to CH_4 production, and the minor importance of methylotrophic methanogenesis in the recovered reactors. For HNR3, no large changes were observed at the archaea genus level during the stability test (**Figure 6.4**l), and the final archaeal community remained dominated by OTU_1. In other words, the final archaeal microbiome was dominated by the same *Methanosarcina* member as on day 0 despite the re-inoculation of the HNRs with LNR effluents. Previously, efficient CH_4 production has been achieved in *Methanosarcina*-dominated AD reactors operating at FAN concentrations up to 0.6 g_N L^{-1} (Capson-Tojo et al., 2020). The persistence of this versatile methanogen in the HNRs after the restoration of a functional AD process confirms our assumption that microbes capable of acetoclastic and/or hydrogenotrophic methanogenesis remained present in the slurry after the intoxication experiment and shows that our process recovery strategy allowed environmental conditions favourable to their activity to be restored.

6.3.8. Perspectives for process recovery in real-scale biogas production plants

Due to the current price of acetic acid on the European market (December 2022), applying our strategy to ammonia intoxicated real-scale digesters of the size of several thousand m^3 could represent a significant cost for plant managers. Indeed, it would cost US $17.5 to treat 1 m^3 of slurry (CHEMANALYST, 2022). However, **Figure 6.7** shows that CH_4 production from the added acetic acid could partially compensate the cost of its addition to real-scale FAN-intoxicated digesters. Indeed, the potential CH_4 production from acetoclastic methanogenesis in HNRs 1 and 2 during the process recovery stage accounted for 34.4 and 48.7% of their CH_4 production, respectively. For HNR3, the potential CH_4 production from acetoclastic methanogenesis during the process stability test stage accounted for 77.6% of its CH_4 production.

The initial pH drop due to the introduction of acetic acid in the slurry of the HNRs induced a quick conversion of free ammonia, a highly volatile compound causing threats to the environment and human health (Ni et al., 2015), to ammonium,

a non-volatile form of nitrogen that could be used as an interesting fertilizer (N. Rahman & Forrestal, 2021). In addition, acetic acid has recently been proposed as a low-cost biostimulant under drought stress for a range of major crops, such as maize (Kim et al., 2017), cassava (Utsumi et al., 2019) and mung bean (M. M. Rahman et al., 2019). Therefore, our process recovery strategy could allow the open-air storage and field application of the effluents produced by real-scale digesters recovering from FAN intoxication. Such agronomic valorization of the reactor's effluents would be more problematic with alternative dilution strategies that do not involve an initial pH adjustment of the slurry (Nielsen & Angelidaki, 2008; Niu et al., 2013). These benefits are an additional compensation for the high cost of acetic acid and relativize the long duration required to reach full process recovery after applying our strategy.

Re-inoculating real-scale digesters exposed to ammonia intoxication can be regarded as challenging, in the sense that it would require the provision of large quantities of "healthy" digestate. We would not advise biogas plant managers to use a post-digester as a source of uninhibited biomass as it is most likely exposed to the same TAN concentration as the intoxicated main digester. Therefore, daily transportation of fresh digestate from the closest non-inhibited biogas plant could be necessary to ensure the stability of the process during the process recovery period. Applying our strategy to a typical farm-scale digester of 1000 m^3 working volume would require transporting 6.5 m^3 of fresh digestate per day during the re-inoculation period, which is feasible with a slurry tanker. In our opinion, applying such a complex strategy could be justified compared to a complete restart of the process. Indeed, we showed in a previous work (Goux et al., 2016) that establishing a functional AD process during the start-up phase of a full-scale mesophilic digester fed with psychrophilic feedstocks requires >120 days. In addition, the microbiome resulting from such a start-up phase was not acclimatized to high FAN concentrations, whereas the microbiome of a digester that has recovered from ammonia intoxication could appear more resilient to future intoxication events.

6.4. Conclusions

This study assesses an AD process recovery strategy that we applied to three anaerobic reactors that were previously exposed to a complete process collapse caused by extreme free ammonia intoxication. The initial reconditioning stage of the process

recovery strategy includes (i) pH reduction by acetic acid, (ii) water dilution and (iii) re-inoculation combined with moderate water dilution. These reconditioning steps did not allow the biogas production to be re-established. Restoring the feedstock supply after the reconditioning stage appeared to be decisive for the re-establishment of biogas production, while re-inoculating the reactors appeared to be essential to maintain process stability during the process recovery period. Overall, the proposed process recovery strategy was successful in restoring an efficient conversion of the feedstock to CH_4 for the three intoxicated reactors within eleven weeks. The initial introduction of acetic acid allowed substantial CH_4 production during the recovery period. Introducing acetic acid in the intoxicated reactors promoted ammonium sequestration in the slurry. This would enable the open-air storage and field application of the effluents produced by full-scale biogas production digesters recovering from FAN intoxication. However, to ensure the long-lasting process recovery of such digesters, we recommend prolongating the re-inoculation over a longer period than assessed here. Additional lab-scale experiments integrating reactors that are not re-inoculated could allow to be better assess the impact of re-inoculation on process stability. Lastly, the present study highlights the importance of replicates when working with (semi-)continuously fed AD reactors exposed to stress. Indeed, although the three intoxicated reactors had been exposed to the same treatment from their inoculation, they showed contrasting behaviours and distinct microbiome dynamics during the experiment.

Acknowledgements

We thank Bénédicte De Vos and Anaïs Noo for their valuable technical support and Lindsey Stokes for proofreading the manuscript. This work was supported by the Fonds National de la Recherche, Luxembourg (FNR CORE 2011 project GASPOP, CO11/SR/1280949: Influence of the Reactor Design and the Operational Parameters on the Dynamics of the Microbial Consortia Involved in the Biomethanation Process) and by LIST core funding.

Chapter 7

General discussion

7.1. Biogas-based PCA-MSPC presents potential to detect the two main disturbances of the AD process

7.1.1. Static PCA-MSPC integrating the biogas composition is suitable for monitoring AD reactors using data from independent steady-state reactors to define in-control conditions

A static PCA-MSPC model coupling biogas composition (CH_4, CO_2, H_2) and slurry parameters (TIC, TAN) delivered early warning of free VFA intoxication in overfed reactors while using data of an independent steady-state reactor for in-control process baseline definition (**Chapter 3**). Notably, we found that biogas-measured IPVs were key in detecting early symptoms of FVFA intoxication. Interestingly, our findings contradict a previous study (Boe et al., 2010), where biogas parameters provided delayed information on the AD process compared to slurry parameters. However, in that study, parameters were compared over time in a univariate manner. Our results suggest that PCA-MSPC can leverage the correlation between individual process variables (IPVs) to extract early warning signals from the dynamics of CH_4, CO_2, and H_2 in biogas. In contrast, microbial ecological indices monitored during the FVFA intoxication experiment (**Chapter 5**) failed to detect the disturbance. While these results highlight the potential of biogas composition dynamics for monitoring the AD process, the online analysis of slurry IPVs remains challenging. Moreover, operating an additional reactor solely to generate in-control process data is impractical for full-scale biogas plants.

To address these limitations, we attempted to monitor high-nitrogen input reactors (HNRs) using only biogas-measured IPVs (CH_4, CO_2, H_2, H_2S) to build static PCA-MSPC models from initial steady-state data of the monitored reactors (**Chapter 4)**. However, these models were unable to reliably discriminate true out-of-control observations from baseline drift. Persistent false alarms were triggered by a progressive, expected increase in H_2S concentration in the biogas. As a result, the statistical indices failed to accurately represent the reactors' process status. Extending the model-building period to capture greater in-control variability could potentially improve the reliability of such models. However, we were unable to verify this hypothesis, raising doubts on the suitability of this approach for real-time AD process monitoring. Furthermore, applying this method in agricultural biogas plants would

prevent monitoring during the critical start-up phase of the primary digester (Goux et al., 2016).

Therefore, we do not recommend pursuing further assessment of static models PCA-MSPC models built from an initial steady-state period of the monitored reactor. However, static models integrating biogas-measured IPVs and developed from in-control data of independent steady-state reactors warrant further evaluation under real-time monitoring conditions.

7.1.2. Recursively updated PCA-MSPC should be considered for biogas-based monitoring of the AD process, using data from independent steady-state reactors to calibrate the effective memory length

While static PCA-MSPC models were shown to detect early signs of FVFA intoxication without incorporating the H_2S concentration in biogas as an IPV (**Chapter 3**), capturing rapid H_2S fluctuations could enhance these models, as such fluctuations often reflect changes in slurry pH. As an attempt to prevent false alarms due to H_2S low-frequency dynamics in biogas, we assessed recursively updated PCA-MSPC (RU-PCA-MSPC) models to monitor three HNRs (**Chapter 4**). Solely by analysing the biogas composition (CH_4, CO_2, H_2, H_2S), mixing failures and early signs of FAN intoxication, which heralded drastic changes in reactor microbiomes, were detected in three HNRs, suggesting good replicability and potential for broader application. These findings support our earlier assumption (**Chapter 3**) that the AD process can be monitored using PCA-MSPC models based solely on biogas composition dynamics, eliminating the technical and analytical challenges associated with slurry monitoring. Using only biogas compounds as IPVs also avoided modelling issues caused by the lack of correlation between biogas and slurry-measured IPVs (**Chapter 3**). Unlike static models built from an initial steady-state period (**Chapter 4**), recursively updated models were not impacted by a drift in the in-control process baseline, provided that the model effective memory length was correctly calibrated.

Despite using data from the monitored reactors to build these models, an additional steady-state reactor was still needed to calibrate the model updates. Additionally, after the first FAN intoxication symptoms, the models gave erratic signals for the HNRs, coinciding with major microbiome shifts. This loss of reliability could hinder full-scale process monitoring. However, in practice, early warnings

would likely prompt a stop in nitrogen input, preventing the microbiome shift and maintaining model reliability. Unfortunately, this hypothesis remains speculative due to the post-experimental modelling approach used in this thesis, as the PCA-MSPC model warning signals were not available when the first symptoms of disturbance appeared in the reactors.

Despite these limitations, RU-PCA-MSPC models based solely on biogas composition should be further assessed for AD process monitoring, in-real time monitoring conditions.

7.1.3. The potential for low-cost and practical online monitoring of the AD process justifies further assessment of biogas-based MSPC.

In this thesis, each type of process disturbance was investigated in a dedicated experiment, whereas agricultural digesters may encounter a sequence of different disturbances. Additionally, while agricultural digesters experience regular fluctuations in feeding regimes, our reactors were consistently fed with sugar beet pulp as the sole feedstock (with urea added for the FAN intoxication experiment).

In a review of recent advances and major challenges in AD process monitoring (Wu et al., 2019), the authors summarised early-warning indicators identified from experiments conducted over the past decade. Of the eleven studies focused on detecting FVFA or FAN intoxication, all addressed only one type of disturbance, and none included feeding schemes with alternating feedstocks. This likely highlights the challenge of developing universal techniques that can reliably detect the two major AD process disturbances while distinguishing true process imbalances from false alarms caused by normal feeding fluctuations. Although such scope limitations are common in AD experimentation, the range of conditions under which we assessed our MSPC models is too narrow to conclusively prove their suitability for AD process monitoring. Therefore, before considering full-scale application, further lab-scale experimentation is necessary to assess how (1) feedstock composition and (2) other disturbances (e.g. heavy metals and salt intoxication, micro-nutrient deficiencies) can impact the reliability of MSPC models based on biogas composition.

In the aforementioned review (Wu et al., 2019), six studies proposed slurry-measured parameters as early indicators of FVFA intoxication (Boe et al., 2010;

Kleyböcker et al., 2012, 2014; L. Li et al., 2014; Martín-González et al., 2013) or FAN intoxication (Bruni et al., 2013), while only four studies proposed biogas-measured parameters to detect these disturbances (D. Li et al., 2018; Lv, Hu, et al., 2014; Polag et al., 2015). However, the major components of biogas were monitored in all studies. This suggests that biogas composition dynamics remain underutilised for disturbance detection in AD reactors, despite our demonstration of its potential for online process monitoring using multivariate statistical approaches.

Two studies identified the $[CH_4]/[CO_2]$ ratio in biogas as early indicator of FVFA intoxication, proposing values below 1.2 mol/mol as an instability threshold for both mesophilic (D. Li et al., 2017) and thermophilic (D. Li et al., 2018) temperature conditions. However, AD process monitoring approaches based on threshold values of single indicators are now considered outdated (Wu et al., 2021), as each reactor has its own unique configuration of operational parameters, microbial composition, and adaptability (Drosg, 2013). In comparison, our PCA-MSPC models also detected out-of-control observations linked to early shifts in the $[CH_4]/[CO_2]$ ratio, signalling the onset of both FVFA (**Chapter 3**) and FAN intoxication (**Chapter 4**). These warning signals reflected process deviations from in-control periods specific to either the monitored reactor (with recursively updated models, **Chapter 4**) or an independent steady-state reactor inoculated with the same microbial consortium (static model, **Chapter 3**). For full-scale implementation, our multivariate monitoring approaches could thus be tailored to each plant's specific profile, in contrast to methods that rely on commonly accepted toxicity thresholds.

The remaining two studies (Lv, Hu, et al., 2014; Polag et al., 2015) focused on CH_4 and/or CO_2 isotope fingerprinting for AD process monitoring. These methods aim to detect shifts between dominant methanogenic pathways, leveraging the fact that CH_4 and CO_2 produced from acetoclastic and hydrogenotrophic methanogenesis exhibit different isotope fractionation patterns (Conrad, 2005). By following this approach, changes in methane's stable isotope composition (measured online using a portable high-precision laser absorption spectrometer) correctly detected early signs of FVFA intoxication in a full-scale digester (Polag et al., 2015). Similarly, Lv et al. (2014) detected early symptoms of FAN intoxication in lab-scale reactors by measuring changes in the stable isotope composition of biogas, using offline gas chromatography combined with isotope-ratio mass spectrometry (GC-IRMS). While

these results are promising, the equipment required for high-precision isotope ratio monitoring is costly, involves complex gas pre-treatment methods (Lv, Hu, et al., 2014), requires specialised training for operation and maintenance, and needs frequent calibration with gas standards (eight times per day) to mitigate the effects of temperature and instrument drift (Polag et al., 2015).

In contrast, the monitoring approaches we propose can be implemented with gas sensors based on well-established, user-friendly technologies that have low requirements for sample pre-treatment. Low-cost sensors based on non-dispersive infrared (NDIR) technology allow for the accurate and stable detection of CH_4 and CO_2 in biogas with minimal maintenance and calibration needs (Basyooni et al., 2024). However, low-cost technologies for detecting H_2 and H_2S with adequate sensitivity still face limitations. Although electrochemical sensors commonly used in biogas analysers are inexpensive, they suffer from short life-time (usually lower than 1 year) and frequent calibration requirements (Redondo et al., 2008). Therefore, conventional biogas analysers could be used for multivariate monitoring of the AD process in full-scale biogas plants, provided that a strict maintenance and calibration plan for the gas sensors is in place. Alternatively, a compact gas chromatograph (CompactGC, Interscience, NL) can be used as an online biogas analyser, as was done in the FAN intoxication experiment. This equipment provides highly selective, multicomponent gas analysis in a compact, portable, and low-maintenance system (as compared to traditional gas chromatography), making it suitable for online AD process monitoring. However, CompactGCs are more expensive than conventional biogas analysers and require regular quality control checks by trained personnel.

In a limited range of experimental conditions (inherent to many studies), we showed that biogas composition dynamics can be utilised to detect the two main disturbances in the AD process through adequate use of MSPC techniques. Such findings are particularly relevant because biogas composition is generally underutilised for AD process monitoring.

7.2. Limitations of our PCA-MSPC approaches and directions for future research

7.2.1. Limitations

In this work, we did not assess the existence of *linear* relationships between our IPVs prior to PCA. However, the strong dimensionality reduction observed during model development (**Chapter 3** and **Chapter 4**) is itself evidence of significant linear correlation within our datasets. This is further supported by the fact that the PCs retained in our models had markedly higher eigenvalues than the remaining components, a pattern characteristic of multicollinearity (Gwelo, 2019). Part of the observed multicollinearity is likely attributable to the inclusion of IPVs representing the main components of biogas, which are compositional in nature and constrained to sum nearly 100%. If we had used MSPC models based directly on the original IPVs, this multicollinearity could have rendered the covariance matrix ill-conditioned, potentially compromising the stability and interpretability of the T^2 index. Using PCA-MSPC, such correlations were effectively addressed through the orthogonalisation of variables, thereby justifying the omission of prior collinearity checks. Although log-ratio transformations (Greenacre, 2021) are theoretically recommended when applying PCA to compositional data, they were not employed in this work. This choice is justified by the practical objective of process monitoring, for which PCA-MSPC has demonstrated sufficient robustness and sensitivity to detect deviations even when directly applied to raw compositional variables (Nijhuis et al., 1997). However, it would be insightful to apply such transformations to our biogas datasets and compare the results with those presented here.

While our results suggest that using a linear method like PCA was appropriate, it does not exclude the possibility of *nonlinear* relationships within our datasets. With no prior reason to suspect quadratic, exponential, or any other complex nonlinear relationship between our IPVs, we did not verify their existence. Importantly, the SPE control chart enables the detection of deviations from a (linear) PCA model, which can happen if a nonlinear behaviour appears. For processes characterised by IPVs that are expected to follow nonlinear relationships, nonlinear extensions of PCA-MSPC, such as kernel PCA-MSPC (Pani, 2022), are justified. However, the applicability of these methods is limited by the complex and subjective

process of selecting an appropriate kernel function and tuning its parameters, a step not required for the simpler, non-parametric PCA-MSPC.

Our model building methods benefited from the post-experimental approach adopted in this work. For static models, post-experimental modelling allowed the integration of in-control baseline data from the steady-state reactor recorded after early disturbance symptoms were detected in the overfed reactor (**Chapter 3**). For recursively updated models, we calibrated the effective memory length using steady-state data from the LNR collected throughout the experiment, including after the first signs of FAN intoxication appeared in the HNRs (**Chapter 4**). Therefore, static and recursively updated models should further be assessed for real-time AD process monitoring, while trying to overcome their main limitation: the need to operate an additional steady-state reactor for the sole purpose of in-control process data generation.

7.2.2. Directions for future research

7.2.2.1. Strategy for real-time implementation of biogas-based AD process monitoring

Real-time biogas-based MSPC could potentially be achieved in multi-stage AD plants by using a post-digester (rarely exposed to process disturbance) for continuous generation of in-control process data. Using only biogas composition as input, both static and recursively updated PCA-MSPC should be assessed for monitoring the primary digester, according to the following approaches

- **Static PCA-MSPC Models:** a dynamic in-control baseline would be built from post-digester biogas data and continuously updated to differentiate between process drift and relevant warnings.
- **Recursively updated PCA-MSPC models:** an algorithm would dynamically adjust the model's effective memory length to minimise the number of out-of-control observations detected for the post-digester.

Although the use of post-digesters as in-control process references requires validation through further pilot-scale experiments, positive outcomes would represent a significant step toward robust, reliable, and cost-effective online monitoring of the AD process.

Alternatively, other process monitoring techniques could be assessed to discriminate true faults from baseline drift without critical tuning of memory parameters. The most direct and interpretable method is *dynamic* PCA-MSPC (DPCA-MSPC), which incorporates process dynamics into a static model (Ku et al., 1995). While this avoids sensitive tuning, its main drawback is the assumption that these dynamics remain stationary after the model development period. For more complex, nonlinear processes, deep learning offers a state-of-the-art solution by learning memory structures directly from the data (Ahmed et al., 2023). However, this comes at a significant cost (Sarker, 2021): models are "black boxes" that hinder fault diagnosis, and their implementation requires very large datasets, substantial expertise and computational power.

7.2.2.2. Monitoring of trace biogas compounds, especially VFAs, could enhance disturbance detection with MSPC models

Monitoring short-chain VFAs in reactor slurry presents well-known technical and analytical challenges. However, the opportunity of analysing these compounds in biogas could offer a promising solution for online monitoring of the AD process. The primary challenge is detecting molecules at very low concentrations (parts per billion) within a gaseous background dominated by a few major compounds. In this context, conventional gas chromatography techniques often fail to detect VFAs in biogas (Arnold & Kajolinna, 2010; Kymäläinen et al., 2012; Rasi et al., 2011). During my thesis, I became familiar with an experimental analytical technique that combines gas chromatography (GC) for analyte separation with differential mobility spectrometry (DMS). DMS first ionises the analytes, then separates and characterises ions based on the nonlinear relationship between ion velocity and the strength of an electric field (Nazarov, 2012). Compared to conventional chromatography detectors, DMS detectors enhances selectivity, allowing for the separation of complex mixtures and the identification of specific compounds.

Applied to biogas-based monitoring of the AD process, this technique was detailed in a patent application (Orlewski et al., 2013) and has been shown to provide immediate results without the need for complex gas sample pretreatment. The patent application demonstrates successful monitoring of short-chain VFAs in biogas produced by a reactor experiencing progressive organic overload, with several VFAs

showing significant correlations with slurry pH and the $[CH_4]/[CO_2]$ ratio in biogas. Using GC-DMS, increases in formic, propionic, and valeric acids concentrations in the biogas were identified as indicators of process shifts toward FVFA intoxication.

Formic acid, like hydrogen, is known to contribute to the energy balance of acetogenic bacteria and their methanogenic partners (Schink et al., 2017), yet its potential use for AD process monitoring has not, to our knowledge, been previously reported. In addition to VFAs, trace compounds in biogas can include a wide variety of families, such as alcohols, aldehydes, alkanes, alkenes, aromatics, esters, ethers, halogenated organics, ketones, terpenes, sulfur- and silicon-based compounds, and even metal(loid) species (Lecharlier et al., 2022). GC-DMS could potentially detect unknown volatile metabolites in biogas, further enhancing AD process monitoring. Indeed, our understanding of the full spectrum of microbiome metabolites involved in AD remains incomplete (Jones et al., 2016; Vanwonterghem et al., 2014).

When combined with conventional biogas analysers, innovative techniques like GC-DMS could help develop enhanced MSPC models, enabling reliable online process monitoring in agricultural biogas plants.

The answers brought to the scientific question **Q1 Disturbance detection** are graphically presented below (**Figure 7.1**).

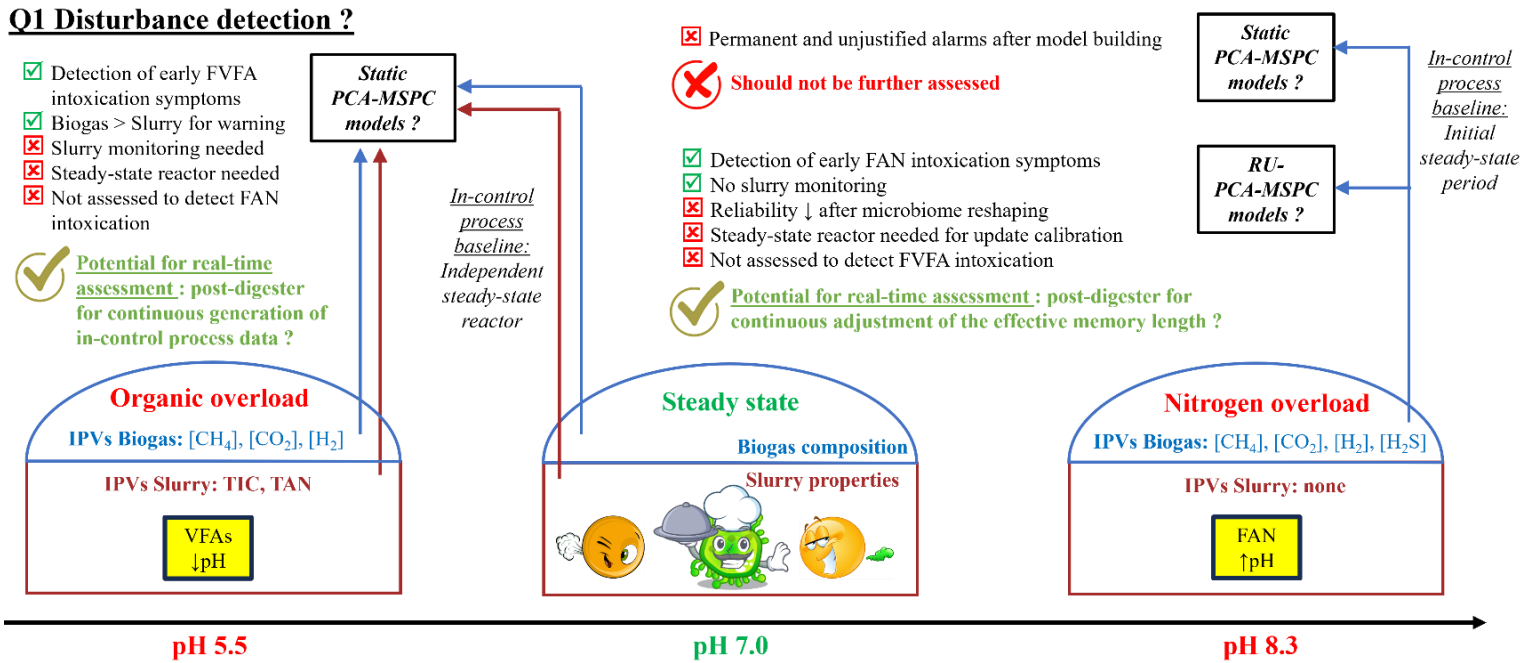

Figure 7.1. Answers brought to the research question **Q1 Disturbance detection** (*Is a multivariate statistical process control (MSPC) approach based on biogas composition useful to detect the two main disturbances of the AD process, FVFA and FAN intoxication?*). IPV: individual process variable, PCA-MSPC: MSPC based on principal component analysis, RU-PCA-MSPC: recursively updated PCA-MSPC, FAN: free ammonia nitrogen, FVFA: free volatile fatty acids, TAN: total ammonia nitrogen, TIC: total inorganic carbon.

7.3. Chemical pH correction enables recovery from critical FVFA intoxication but is insufficient to reverse critical FAN intoxication

Despite the extremely low pH reached in our overfed reactors exposed to critical FVFA intoxication (minimum pH: 5.2 ± 0.4), adjusting the pH to ~7.0 using 1 M NaOH, followed by buffering with $NaHCO_3$ to pH 7.5, enabled the restoration of efficient CH_4 production from a complex feedstock (**Chapter 5**). These results are in contradiction with findings by W. Zhang et al. (2018), who reported that correcting the pH to 7.5 with NaOH failed to restore methanogenic activity in mesophilic reactors at early (pH 6.9), moderate (pH 6.5), and advanced (pH 6.2) stages of VFA intoxication. While both experiments used inocula from wastewater treatment plants, differences in feedstock composition (food waste versus sugar beet pulp) could account for the discrepancy. Our results demonstrate that pH correction alone can be sufficient to re-establish methanogenic activity even after critical intoxication, likely by reducing the toxicity of FVFAs and recreating conditions favourable for microbial recovery.

In contrast, adjusting the pH from ~8.8 to ~7.6 using pure acetic acid did not restore CH_4 production in HNRs that had been exposed to extreme FAN concentrations exceeding $2.0\ g\ N\_L^{-1}$ for over two weeks and had ceased biogas production due to critical intoxication (**Chapter 4** and **Chapter 6**). Although pH adjustment promoted the conversion of cytotoxic FAN to the less inhibitory NH_4^+, it was insufficient on its own to recover AD process functionality, despite the availability of direct CH_4 precursors (acetate, CO_2 and H_2) in the slurry. In the case of our HNRs, the primary cause is most likely the high microbial death rate caused by extreme FAN intoxication (**Chapter 4**). However, divergent toxicity mechanisms could also have contributed.

Both VFAs and ammonia inhibit methanogens by passively diffusing into the cell in their uncharged “free” forms, but their intracellular effects differ. Once inside the cell, free VFAs typically encounter a higher pH than outside, causing them to dissociate and release protons, which acidifies the cytoplasm. In contrast, free ammonia enters a more acidic environment, where it becomes protonated into ammonium, leading to intracellular alkalinisation. To counter the increased H^+

demand caused by ammonia protonation, the cell activates its potassium (K^+) pump to expel K^+ (Jiang et al., 2019). While both stresses cost energy to the cell, intracellular K^+ depletion is particularly harmful, as potassium is a vital element allowing protein synthesis and a key cofactor for many enzymes (Sharma et al., 2013). This added toxicity may explain why process recovery from FAN intoxication requires measures such as dilution or re-inoculation, whereas FVFA intoxication can be reversed by pH correction alone.

7.4. Recovery from critical FAN intoxication can be long and complex

Unlike VFAs, TAN cannot be significantly removed from the slurry through microbial conversion into gaseous compounds. As a result, TAN elimination relies almost entirely on discharge with the liquid effluents (neglecting minor NH_3 emissions in biogas). In our experiment, TAN removal through effluent discharge was first promoted by water supplementation alone, followed by the combined addition of water and effluents from a low-nitrogen input reactor (containing negligible TAN). These two operations effectively reduced the TAN concentration from 17.9 ± 0.3 to 11.7 ± 0.4 g_N L^{-1} over a four-week period, under a HRT of eight weeks. While a more rapid TAN reduction could have been achieved by increasing the daily input of water and low-TAN effluents (thus lowering the HRT), we considered the practical constraints of full-scale application, where the sudden production of large volumes of ammonia-rich digestate could pose significant handling and disposal challenges.

After these dilution steps, the resumption of feeding with sugar beet pulp (while re-inoculation with effluents from the low-nitrogen input reactor was maintained) triggered the recovery of biogas production. However, a total of eleven weeks was required before hydrolysis, the acetoclastic pathway, and possibly the hydrogenotrophic pathway were fully functional in all reactors. By comparison, the recovery time of our reactors subjected to critical FVFA intoxication was only ~3 weeks (**Chapter 5**).

7.5. Re-inoculation is not required for recovery from critical FVFA intoxication, but supports process stability during critical FAN intoxication recovery, even with non-acclimatised microorganisms

We showed that process recovery from critical FVFA intoxication can be induced without any re-inoculation (**Chapter 5**). Interestingly, the recovery time of our reactors was 20 days, significantly shorter than the 80 to 120 days reported by Tale et al. (2015) when using propionate-exposed microbial cultures for bioaugmentation of reactors facing more moderate intoxication (minimum pH: 6.8 ± 0.05) than ours. Our recovered reactors still showed symptoms of process instability (propionate accumulation in the slurry) three weeks after initiating our process recovery strategy. However, our overfed reactors were exposed to a particularly severe intoxication, and we hypothesise that such residual process instability could be avoided in treating more moderately intoxicated reactors.

In contrast, the HNRs were re-inoculated with effluents from a LNR, as pH correction with acetic acid and water dilution proved insufficient in restoring CH_4 production. Ammonia is well known to impair syntrophic propionate oxidation in AD reactors (C. Zhang et al., 2018). Consistent with this, potential syntrophic propionate oxidisers belonging to the phylum *Cloacimonadota* (Westerholm et al., 2022) declined in abundance in the HNRs during the FAN intoxication phase of the experiment (**Chapter 4**). Consequently, during the process recovery phase, members of *Cloacimonadota* reached a relative abundance of approximately 10% in the low-nitrogen input reactor (LNR), compared to only 1–3% in the HNRs recovering from FAN intoxication (**Chapter 6**). It could be expected that re-inoculating HNRs with LNR effluents would support the restoration of syntrophic propionate oxidation. However, *Cloacimonadota* from the LNR did not establish significantly in the HNRs. After re-inoculation was discontinued, propionate accumulation was observed in all HNRs. Although this phenomenon could not be directly linked to changes in microbial community composition, it suggests that re-inoculation with effluents from a low-nitrogen reactor can contribute to maintaining process stability during recovery from critical FAN intoxication.

7.6. *Methanosarcina* as a potential driver of AD process recovery after critical disturbances

Methanosarcina species are fast-growing, robust, and versatile methanogens that can produce CH_4 from all known methanogenesis pathways in a wide range of environmental conditions, sometimes surprisingly extreme (De Vrieze et al., 2012). Due to such unique characteristics, these microbes, previously termed "heavy-duty methanogens", probably played a key role in the recovery of our reactors exposed to critical process disturbances.

7.6.1. Recovery from critical FVFA intoxication

Methanogens, like other archaea, are negatively affected by high salt concentrations. However, several *Methanosarcina* spp. tolerate these compounds, particularly sodium salts (Spanheimer & Müller, 2008; Vyrides et al., 2010), because of their rapid physiological response (Roeßler & Müller, 2001; Spanheimer & Müller, 2008).. Furthermore, members of *Methanosarcina* have high growth rates (doubling times around 1.0–1.2 days) and are tolerant to sudden pH drops of 0.8–1.0 units compared to other methanogens, which have minimum doubling times of 4–6 days and are affected by pH shocks of only 0.5 units (Conklin et al., 2006; Shin et al., 2011). These outstanding physiological traits likely allowed *Methanosarcina* spp. to quickly establish an ecological niche in our reactors recovering from acidic conditions and supplemented with sodium (**Chapter 5**). This is particularly noteworthy given the negligible abundance of these archaea when we initiated our process recovery strategy. We thus hypothesise that the presence of *Methanosarcina* was decisive in the fact that reinoculation was not required to restore a functional AD process in our reactors exposed to critical FVFA intoxication.

7.6.1. Recovery from critical FAN intoxication

Compared to other methanogens (e.g. *Methanosaeta* spp.), *Methanosarcina* spp. are reported to be exceptionally resistant to ammonia toxicity (De Vrieze et al., 2012). This resilience can be attributed to their ability to grow in clusters and their distinctive coccoid shape, which results in a low surface-to-volume ratio, thereby limiting the influx of NH_3 into the cells over time (Calli et al., 2005). These characteristics likely explains why a *Methanosarcina* sp. outcompeted other archaea

in all HNRs during the process collapse due to critical FAN intoxication (**Chapter 4**). During the process recovery (**Chapter 6**), the initial dominance of a FAN-acclimatised *Methanosarcina* sp. prevented suboptimal AD process-characterising archaea (genus *Candidatus* Methanoplasma) from establishing in the long-term in the HNRs. Once a functional process was restored, the final archaeal microbiome remained dominated by the same *Methanosarcina* sp. despite re-inoculating with LNR effluents. We thus hypothesise that *Methanosarcina* was the main driver of feedstock conversion to CH_4 during the recovery. By re-establishing environmental conditions favourable to AD, the combined effect of acetic acid supplementation and water dilution may have reactivated its metabolic activity.

Bio-augmentation with pure *Methanosarcina barkeri* strains has been shown to be effective to counteract ammonia inhibition in lab-scale reactors (Yang et al., 2019). However, it is doubtful that bio-augmenting our intoxicated reactors would have been useful, as the supplemented strains would likely have struggled to outcompete already established FAN-acclimatised *Methanosarcina* sp. This could also explain why archaeal strains originating from the LNR effluents did not significantly establish in the microbial communities of the recovering HNRs, indicating that re-inoculation was not a determining factor in the restoration of methanogenesis.

7.7. Could chemical-based process recovery strategies be upscaled to agricultural digesters?

For both types of process disturbance, our chemical-based strategies successfully restored the AD process in three reactors, demonstrating good repeatability of the results. The experiments were conducted in pilot-scale reactors (100 L), semi-continuously fed with unsterilised feedstocks, to replicate the conditions of full-scale anaerobic digesters. Additionally, agricultural digesters typically have a higher abundance of *Methanosarcina* spp. than those at wastewater treatment plants, which was the source of our inoculum (Calusinska et al., 2018). These factors suggest the potential for scaling up our chemical-based recovery approaches.

7.7.1. Recovery from critical FVFA intoxication

7.7.1.1. Inducing process recovery with NaOH and $NaHCO_3$ is straightforward and already implemented in biogas plants

We showed that successful recovery can be obtain without the need to re-inoculate the impaired digester. This could help avoid the impractical and risky slurry exchanges between impaired and functional digesters in full-scale applications. Since our first study's publication (Goux et al., 2015), our alkali-based recovery strategy has successfully restored efficient feedstock conversion to CH_4 in the 1500-m³ primary digester exposed to FVFA intoxication in a German biogas plant. Correcting pH and buffer capacity with NaOH and $NaHCO_3$ is easy to implement and requires only small amounts of chemicals. Ready-to-pump 50% NaOH solution is available for industrial application and $NaHCO_3$ is frequently stored on-farm to heal cattle from rumen acidosis. It is important to note that adding $NaHCO_3$ directly to severely intoxicated digesters with pH << 6.3 (pKa_1 of the carbonate system; $H_2CO_3 \rightleftharpoons H^+ + HCO_3^- \rightleftharpoons 2H^+ + CO_3^{2-}$) leads to CO_2 off-gassing, wasting the bicarbonate, offering no buffering effect, and potentially causing foaming. For more moderate acidification (pH > 6.3), prior pH correction with NaOH is unnecessary.

7.7.1.2. Potassium as a soil-friendly substitute for sodium?

Excessive concentration of sodium cations (Na^+) in the topsoil reduces crop productivity by dispersing clay particles, degrading soil structure, and impairing water infiltration and aeration, leading to poor drainage (Halliwell et al., 2001). Crop fertilisation with digestate resulting from digesters supplemented with sodium could thus be detrimental for agricultural soils.

In our pilot-scale reactors, restoring AD process functionality by adding NaOH and $NaHCO_3$ resulted in an average sodium concentration of 2.4 kg per m^3 of slurry in the reactors (**Chapter 5**). Applying such effluents to fields at a rate of 30 m^3 ha^{-1} $year^{-1}$ would correspond to a sodium input of approximately 72 kg ha^{-1} $year^{-1}$. In comparison, the average sodium deposition from precipitation in Europe was only about 5 kg ha^{-1} $year^{-1}$ between 2000 and 2017 (Keresztesi et al., 2019). Thus, soils fertilised with such digestate would be exposed to exceptionally high sodium inputs, potentially causing harmful effects and reducing crop yields.

To mitigate soil sodification risks, alkali-based recovery strategies should be explored using cations that are less harmful to soils than Na^+. Potassium cation (K^+) is an excellent candidate for such experiments. Potassium is one of the three essential nutrients required for plant growth and is included in the NPK value of fertilisers. Compared to sodium, potassium promotes soil structure stability (Y. Chen et al., 1983) by enhancing clay particle flocculation (Grasso et al., 2005) and favours soil drainage by maintaining larger pore spaces.

The chemical behaviour of potassium hydroxide (KOH) and sodium hydroxide (NaOH) is nearly identical, as both are strong alkalis that fully dissociate in aqueous solutions. The chemical behaviour of potassium bicarbonate ($KHCO_3$) and sodium bicarbonate ($NaHCO_3$) is quite similar, as both are alkaline bicarbonate salts that act as pH buffers, maintaining a mildly alkaline solution (with a pKa of approximately 10.3 for both). Therefore, introducing KOH and $KHCO_3$ into reactors exposed to FVFA intoxication would likely create similar chemical conditions in the slurry as introducing NaOH and $NaHCO_3$.

Like other light metal cations, Na^+ and K^+ are required for microbial growth (Y. Chen et al., 2008) but can inhibit the AD process when present at elevated concentrations. K^+ is a vital intracellular cation that microorganisms accumulate for osmoregulation (Pflüger et al., 2005); its toxicity arises primarily from the physical

effect of excessive osmotic pressure at high extracellular concentration. In contrast, the toxicity of Na^+ is more complex and primarily an intracellular issue. Na^+ is toxic at high intracellular levels due to electrochemical and osmotic interactions with nucleic acids and proteins (Valentine, 2007). Additionally, intracellular Na^+ accumulation collapses the sodium gradient used for ATP synthesis (Schlegel & Mller, 2011). This added layer of intracellular toxicity explains why Na^+ is fundamentally more inhibitory than K^+. To our knowledge, Fang et al. (2011) conducted the only study directly comparing Na^+ and K^+ toxicities in AD under identical conditions. Their results confirmed that the 50% inhibition threshold was indeed lower for Na^+ (0.48 $mol \cdot L^{-1}$) than for K^+ (0.72 $mol \cdot L^{-1}$) under thermophilic conditions.

Several studies have highlighted the greater Na^+ tolerance of *Methanosarcina* spp. compared to other methanogens (Saia et al., 2010; Spanheimer & Müller, 2008; Vyrides et al., 2010). However, no studies have reported a similar enhanced tolerance to K^+. Further research is needed to verify if potassium supplementation also selects *Methanosarcina* and if this response dictates the success or failure of the process recovery.

7.7.1.3. Cost of chemicals

Treating 1 m^3 of slurry from a digester exposed to a FVFA intoxication as severe as the one we induced (pH 5.5) would require the supplementation of 46.7 mol OH^- and 90.7 mol HCO_3^- (**Chapter 5**). European market prices (June 2025) are 0.008 €/mol and 0.041 €/mol for NaOH and $NaHCO_3$, respectively (Business Analytiq, 2025). However, potassium-based compounds are about three times more expensive than their sodium-based counterparts: current market prices are 0.033 €/mol and 0.126 €/mol for KOH and $KHCO_3$, respectively. Therefore, the cost in chemicals would be 4.1 €/m_{slurry}^3 and 13.0 €/m_{slurry}^3 using sodium-based and potassium-based alkali, respectively.

It should be noted that expenses related to NaOH or KOH can be avoided in digesters exposed to moderate FVFA intoxication.

7.7.2. Recovery from critical FAN intoxication

7.7.2.1. Counteracting critical FAN intoxication can be long and require slurry transfer between biogas plants

As demonstrated in our lab-scale experiment, TAN removal from the slurry typically results in longer recovery period from critical FAN intoxication (~11 weeks, **Chapter 6**) compared to recovery from critical FVFA intoxication (~3 weeks, **Chapter 5**). Re-inoculation being a complex operation to accomplish on-farm, it should only be considered if pH correction and water dilution techniques failed in restoring biogas production. We do not recommend re-inoculating a digester affected by FAN intoxication using effluents from its own post-digester. Since the post-digester processes the outflow from the primary digester, its TAN concentration cannot be lower than that of the primary digester, as TAN is only removed via liquid discharge. Furthermore, when the post-digester has a longer HRT and TAN synthesis continues, TAN levels may even accumulate to higher concentrations than in the primary digester. As a result, re-inoculation of agricultural digesters exposed to FAN intoxication using local slurry resources is not feasible, even in multi-stage biogas plants. Transferring digestate from a nearby biogas plant is therefore the only viable option for re-inoculation, which can be carried out with a slurry tanker (**Chapter 6**).

7.7.2.2. Methanosarcina could ease process recovery from FAN intoxication and make recovered digesters more resilient

Members of the *Methanosarcinaceae* family tend to increase in abundance under elevated ammonia concentrations, regardless the inoculum origin (De Vrieze et al., 2015). This suggests that bioaugmentation with FAN-acclimatised inocula may be unnecessary to restore functional AD processes in agricultural digesters facing FAN intoxication. Efficient CH_4 production has been achieved in *Methanosarcina*-dominated AD reactors operating at FAN concentrations up to 0.6 g_N L^{-1} (Capson-Tojo et al., 2020), potentially making digesters recovered from FAN intoxication using our strategy more resilient to future ammonia accumulation. However, additional lab-scale experimentation is required to verify this hypothesis.

7.7.2.3. Methane production resulting from acetic acid supplementation can recover up to 68% of the associated acetic acid cost

For a mesophilic digester exposed to FAN intoxication as severe as that induced in our HNRs (pH = 8.3, ~18 g_TAN L^{-1}), reducing the pH to 7.7 would require the addition of approximately 250 moles of pure acetic acid per m³ of slurry (**Chapter 6**). Based on the current European market price for acetic acid (0.030 €/mol in June 2025; Business Analytiq, 2025), this corresponds to a cost of 7.44 €/m³ of slurry.

Assuming an ideal scenario in which all supplemented acetic acid is converted to methane via acetoclastic methanogenesis (i.e. 1 mol acetic acid → 1 mol CH_4), the resulting methane production would be 5.6 Nm³/m³ of slurry. Given a methane selling price of 90 €/MWh and a lower heating value of 0.01 MWh/Nm³, the revenue from this methane would be 5.0 €/m³ of slurry.

This rough economic assessment shows that the cost of acetic acid can be substantially offset (by up to 68%) through the revenue generated from the resulting methane production.

7.7.2.4. Acetic acid supplementation provides environmental and agronomic benefits

The initial pH drop due to the introduction of acetic acid in the slurry of the HNRs induces a quick conversion of free ammonia, a highly volatile compound causing threats to the environment and human health (Ni et al., 2015), to ammonium, a non-volatile form of nitrogen that could be used as an interesting fertiliser (N. Rahman & Forrestal, 2021). In addition, acetic acid has recently been proposed as a low-cost bio-stimulant under drought stress for a range of major crops, such as maize (Kim et al., 2017), cassava (Utsumi et al., 2019) and mung bean (M. M. Rahman et al., 2019). Therefore, acetic acid supplementation could allow the open-air storage and field application of the effluents produced by real-scale digesters recovering from FAN intoxication.

7.7.2.5. Anaerobic biofilm reactors: A potential solution to eliminate slurry transfers between biogas plants?

Anaerobic biofilm reactors (ABRs) share a key feature: they promote high-density biomass immobilisation using microbial carriers with a large specific surface (Abera et al., 2024). A key benefit of ABRs is their ability to promote biofilm formation, which protects microbial communities from FAN toxicity (Poirier et al., 2016). Biofilms provide a stable environment, allowing acetogenesis and methanogenesis to continue even under high-FAN conditions. High biomass density enhances microbial interactions (Conrad et al., 1985; Schmidt & Ahring, 1993), which facilitates hydrogen and formate interspecies electron transfer (IET) (Poirier et al., 2017). When microbial carriers are made from conductive materials, ABRs can even promote direct IET (Park et al., 2018). Enhanced IET strengthens the syntrophic relationship between acetogenic bacteria and hydrogenotrophic methanogens, which are essential for the oxidation of VFAs longer than acetate (such as propionate).

In agricultural biogas plants treating nitrogen-rich feedstocks, installing ABRs in parallel with digesters could support the main digesters to assist them with functional acetogenesis. ABRs could continuously exchange slurry with digesters that are either experiencing or at risk of FAN intoxication. Under normal conditions, they would operate with moderate slurry recirculation, increasing the flow when FAN intoxication is detected. Although maintaining additional reactors on-site may present challenges, ABRs offer a higher biomass-to-volume ratio compared to continuously stirred tank reactors (CSTRs), which are commonly used for generating acclimated inocula. This makes ABRs a potentially more cost-effective solution for biogas plants. However, further research is needed to assess their effectiveness and operational feasibility.

7.7.3. Conclusions

Process recovery from critical FVFA intoxication is quick and straightforward but should be further assessed with potassium-based chemicals, more soil-friendly that their sodium-based counterparts. Process recovery from critical FAN intoxication can be long and require unpractical slurry transfers between biogas plants. However, environmental and agronomic benefits linked to acetic acid

supplementation and the valuable CH_4 production it provides compensates these drawbacks.

The answers brought to the scientific questions **Q2 Recovery from FVFA intoxication** and **Q3 Recovery from FAN intoxication** are graphically presented below (**Figure 7.2**).

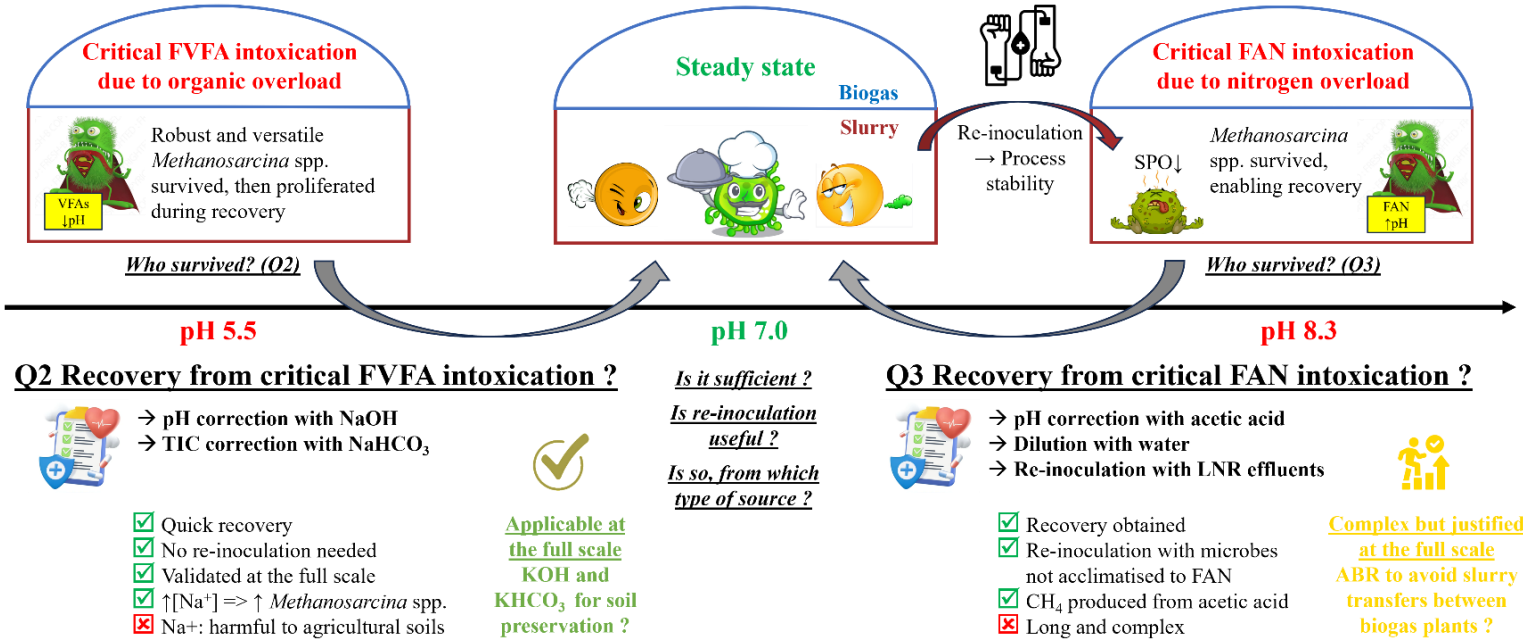

Figure 7.2. Answers brought to the research questions **Q2 Recovery from FVFA intoxication** (*Can the AD process be recovered after a critical FVFA intoxication without supplementing the intoxicated reactors with inocula acclimatised to VFAs?*) and **Q3 Recovery from FAN intoxication** (*Can the AD process be recovered after a critical FAN intoxication without supplementing the intoxicated reactors with inocula acclimatised to FAN?*). ABR: anaerobic biofilm reactor, FAN: free ammonia nitrogen, FVFA: free volatile fatty acids, SPO: syntrophic propionate oxidisers, TIC: total inorganic carbon.

Chapter 8

Conclusions and perspectives

8.1. Conclusions

By applying MSPC techniques to post-experimental data from pilot-scale AD reactors intentionally subjected to FVFA and FAN intoxication, we developed two biogas-based process monitoring methods using static and recursively updated models. Through out-of-control values of statistical indices, *static* PCA-MSPC models based primarily on biogas composition allowed to detect early symptoms of FVFA intoxication, while *recursively updated* PCA-MSPC models, relying on biogas composition only, allowed to detect early symptoms of FAN intoxication. Both approaches require parallel monitoring of a stable reference reactor to generate in-control process data, which could potentially be achieved at full scale using post-digesters (though this requires further validation). While biogas-based MSPC could allow online process monitoring in full-scale biogas plants, further evaluation under real-time monitoring conditions is needed to assess its effectiveness in detecting the two key process disturbances across a wide range of operating conditions.

FVFA and FAN intoxication, even in their most severe forms, can be counteracted without the need to supplement the impaired reactors with inocula acclimatised to the corresponding toxicants. Critical FVFA intoxication can be mitigated without re-inoculation, simply by adjusting the pH and buffer capacity of the slurry with sodium hydroxide and sodium bicarbonate, respectively. In our reactors recovering from critical FVFA intoxication, we attribute the successful restoration of the CH_4 production to the selective proliferation of *Methanosarcina* spp., robust and versatile methanogens known to thrive in sodium-rich environments.

Critical FAN intoxication can be addressed through a multi-step strategy consisting of:

- interrupting the nitrogen supply,
- neutralising pH with pure acetic acid,
- diluting the slurry to promote TAN removal through effluent discharge,
- re-inoculating with effluents from a low-nitrogen input reactor.

Acetic acid supplementation alone was insufficient to fully restore CH_4 production in FAN-intoxicated reactors that had ceased methanogenesis. However, it effectively converted cytotoxic FAN into ammonium, thereby re-establishing conditions favourable to microbial activity. Methane production ultimately resumed,

likely driven by the high resilience of *Methanosarcina* spp. in ammonia-rich environments.

The widespread presence of *Methanosarcina* spp. in agricultural biogas digesters suggests that such process recovery strategies could be applied on a larger scale. Our method for mitigating critical FVFA intoxication is straightforward and has already been successfully implemented in full-scale digesters. Although recovery from critical FAN intoxication requires longer durations and involves impractical slurry exchanges between biogas plants, these drawbacks can be partially offset by the ability to sustain CH_4 production through acetic acid methanogenesis during the recovery period.

8.2. Perspectives

8.2.1. Process monitoring

Further lab-scale experiments should assess whether static PCA-MSPC can detect disturbances beyond FVFA intoxication, and whether RU-PCA-MSPC can detect disturbances other than FAN intoxication. Further research is also needed to assess biogas-based PCA-MSPC models under real-time monitoring conditions, using post-digesters as a stable, in-control reference. Initially, real-time AD process monitoring should be tested using a pilot-scale setup that simulates a two-stage biogas plant, as inducing process disturbances at full scale would be impractical. Both static and recursively updated models should be evaluated for their ability to detect the two process disturbances studied, with the goal of identifying versatile approaches for AD process monitoring. Specifically, it would be valuable to verify whether a post-digester remains a reliable in-control process reference during FAN intoxication in the primary digester. Alternatives to RU-PCA-MSPC that rely less on the critical tuning of memory parameters, such as dynamic PCA-MSPC, should also be evaluated.

It would also be valuable to evaluate how the biogas renewal rate in the reactor headspace affects the response time of MSPC models based on biogas composition. At fixed OLR and feedstock composition, this renewal rate is directly proportional to the ratio of working volume to headspace volume in the reactor (V_{work}:$V_{headspace}$). In our experiments (with V_{work}:$V_{headspace}$ = 5), biogas composition varied quickly enough to allow for fast-response process monitoring (with a biogas

renewal rate of 5 times per day for typical biogas production of 1 $L_{biogas}.L_{work}^{-1}.day^{-1}$). However, the flexible membrane gas holder in agricultural digesters is designed for gas storage and typically has the capacity to store a volume equivalent to one day of biogas production. Therefore, reactors with a higher V_{head}:V_{work} ratio (1:1) than those used in our experiments should be preferred for this pilot-scale experimentation phase to determine if the models can maintain low response times under such conditions. A full-scale assessment should be considered as a second step, contingent on pilot-scale validation. While implementing this research strategy may require substantial effort, successful outcomes could enable low-cost, online, and rapid-response AD process monitoring in biogas plants equipped with biogas analysers.

Incorporating new sensors into biogas analysers could enhance data quality and improve the accuracy of MSPC models. Early research could focus on developing advanced sensor technologies for robust and accurate detection of H_2S and H_2 in biogas. Looking further ahead, innovative analytical techniques, such as coupling gas chromatography with differential mobility spectrometry (GC-DMS), should be explored to monitor VFAs (including formic acid) and other trace compounds (such ammonia) in biogas. Incorporating trace compounds as individual variables into biogas-based MSPC models could significantly enhance AD process monitoring. These new analytical techniques could lead to the development of advanced biogas-based MSPC models, enabling more reliable, real-time process monitoring in agricultural biogas plants.

Finally, the rapid development of artificial intelligence (AI), especially machine learning, presents an exciting opportunity to revolutionise AD process monitoring. AI could enable more precise and efficient optimisation and prediction of biogas production in agricultural biogas plants (T. Singh et al., 2023). Recent studies have demonstrated AI's potential in optimising operational parameters during anaerobic co-digestion, improving biogas yields, and enhancing the stability and efficiency of the AD process (Ling et al., 2024). Integrating machine learning techniques into the biogas-based multivariate monitoring approach presented in this thesis could lead to low-cost, robust, and reliable monitoring systems for agricultural biogas plants.

8.2.2. Process recovery

Further research is needed to assess the feasibility of using potassium-based chemicals instead of sodium to counteract FVFA intoxication, which could help mitigate potential adverse effects on agricultural soils fertilised with digestates derived from this treatment. No studies have specifically compared the effects of Na^+ and K^+ on the recovery of reactors exposed to FVFA intoxication. It would be insightful to determine whether the rapid recovery times observed with our sodium-based strategy can be replicated using the potassium-based chemicals. Especially, it would be useful to investigate whether the success of alkali-based strategies is linked to the proliferation of *Methanosarcina* spp. during recovery, or if their low abundance in cases of failure is a contributing factor.

Additional lab-scale experiments including reactors that are not re-inoculated would help better assess the specific contribution of re-inoculation to process stability during recovery from critical FAN intoxication. Ultimately, recovered reactors should be compared with reference low-nitrogen input reactors during a post-recovery phase in which all reactors are fed nitrogen-rich feedstocks. This phase could determine whether the recovered reactors developed increased FAN tolerance. Throughout these experiments, it would be valuable to test our hypothesis regarding the key role of *Methanosarcina* spp. in process recovery, and to investigate whether reactors exhibiting enhanced FAN tolerance are characterised by a higher abundance of *Methanosarcina* spp.

Finally, further research is needed to evaluate whether anaerobic biofilm reactors (ABRs), operated in parallel with digesters, could eliminate the need for slurry transfers between biogas plants to manage FAN intoxication. Pilot-scale experimentation is necessary to assess their effectiveness and operational feasibility under realistic conditions. A key area of investigation will be ensuring that the promotion of VFA degradation in these systems does not inadvertently raise the slurry pH in reactors fed with nitrogen-rich feedstocks, as this could exacerbate FAN toxicity.

Final words…

Addressing the research questions that shaped this PhD thesis was at times challenging but always an exciting journey. This lengthy yet rewarding process allowed me to develop scientific skills, appreciate the value of interdisciplinary teamwork, and build relationships with inspiring individuals.

Moreover, this journey reinforced my belief that advancing the biogas production sector can help address the complex challenges of our changing world, including conflicts, climate change, and economic uncertainties. Optimising biogas production not only supports sustainable agricultural practices but also enhances energy resilience, resource efficiency, and environmental protection. By leveraging local resources and reducing dependence on external energy and nutrient sources, agricultural biogas production offers a practical means of mitigating the impacts of global disruptions.

Therefore, fostering the biogas production sector should be seen not only as an environmental necessity but also as a strategic priority for ensuring the stability and sustainability of rural economies in an increasingly volatile global landscape.

Chapter 9

Bibliography

Abera, G. B., Trømborg, E., Solli, L., Walter, J. M., Wahid, R., Govasmark, E., Horn, S. J., Aryal, N., & Feng, L. (2024). Biofilm application for anaerobic digestion: a systematic review and an industrial scale case. *Biotechnology for Biofuels and Bioproducts*, *17*(1), 145. doi:10.1186/S13068-024-02592-4

Ackrill, R., & Kay, A. (2014). *The growth of biofuels in the 21st century: Policy drivers and market challenges* (1st ed.). Palgrave Macmillan.

Adam, G., Lemaigre, S., Goux, X., Delfosse, P., & Romain, A. C. (2015). Upscaling of an electronic nose for completely stirred tank reactor stability monitoring from pilot-scale to real-scale agricultural co-digestion biogas plant. *Bioresource Technology*, *178*, 285–296. doi:10.1016/j.biortech.2014.09.106

Adam, G., Lemaigre, S., Romain, A. C., Nicolas, J., & Delfosse, P. (2013). Evaluation of an electronic nose for the early detection of organic overload of anaerobic digesters. *Bioprocess and Biosystems Engineering*, *36*(1), 23–33. doi:10.1007/s00449-012-0757-6

Adelt, M., Wolf, D., & Vogel, A. (2011). LCA of biomethane. *Journal of Natural Gas Science and Engineering*, *3*(5), 646–650. doi:10.1016/j.jngse.2011.07.003

Ahmed, S. F., Alam, M. S. Bin, Hassan, M., Rozbu, M. R., Ishtiak, T., Rafa, N., Mofijur, M., Shawkat Ali, A. B. M., & Gandomi, A. H. (2023). Deep learning modelling techniques: current progress, applications, advantages, and challenges. *Artificial Intelligence Review*, *56*(11), 13521–13617. doi:10.1007/s10462-023-10466-8

Ahring, B. K. (2003). Perspectives for anaerobic digestion. In *Biomethanation I* (Vol. 81, pp. 1–30). Springer, Berlin, Heidelberg. doi:10.1007/3-540-45839-5_1

Ahring, B. K., Sandberg, M., & Angelidaki, I. (1995). Volatile fatty acids as indicators of process imbalance in anaerobic digestors. *Applied Microbiology and Biotechnology*, *43*(3), 559–565. doi:10.1007/BF00218466

Akuzawa, M., Hori, T., Haruta, S., Ueno, Y., Ishii, M., & Igarashi, Y. (2011). Distinctive Responses of Metabolically Active Microbiota to Acidification in a Thermophilic Anaerobic Digester. *Microbial Ecology*, *61*(3), 595–605. doi:10.1007/s00248-010-9788-1

Al Rawashdeh, R. (2020). World peak potash: An analytical study. *Resources Policy*, *69*, 101834. doi:10.1016/J.RESOURPOL.2020.101834

Alin, A. (2010). Multicollinearity. *Wiley Interdisciplinary Reviews: Computational Statistics*, *2*(3), 370–374. doi:10.1002/wics.84

Angelidaki, I., & Ahring, B. K. (1993). Thermophilic anaerobic digestion of livestock waste: the effect of ammonia. *Applied Microbiology and Biotechnology*, *38*(4), 560–564. doi:10.1007/BF00242955

Arshak, K., Moore, E., Lyons, G. M., Harris, J., & Clifford, S. (2004). A review of gas sensors employed in electronic nose applications. *Sensor Review*, *24*(2), 181–198. doi:10.1108/02602280410525977/FULL/HTML

Aven, T., & Krohn, B. S. (2014). A new perspective on how to understand, assess and manage risk and the unforeseen. *Reliability Engineering & System Safety*, *121*, 1–10. doi:10.1016/J.RESS.2013.07.005

Baek, G., Kim, J., Kim, J., & Lee, C. (2018). Role and Potential of Direct Interspecies Electron Transfer in Anaerobic Digestion. *Energies 2018, Vol. 11, Page 107*, *11*(1), 107. doi:10.3390/EN11010107

Baraldi, A. N., & Enders, C. K. (2010). An introduction to modern missing data analyses. *Journal of School Psychology*, *48*(1), 5–37. doi:10.1016/j.jsp.2009.10.001

Basak, B., Patil, S. M., Saha, S., Kurade, M. B., Ha, G. S., Govindwar, S. P., Lee, S. S., Chang, S. W., Chung, W. J., & Jeon, B. H. (2021). Rapid recovery of methane yield in organic overloaded-failed anaerobic digesters through bioaugmentation with acclimatized microbial consortium. *Science of the Total Environment*, *764*, 144219. doi:10.1016/j.scitotenv.2020.144219

Basyooni, M. A., Zaki, S. E., Tihtih, M., Boukhoubza, I., En-nadir, R., & Attia, G. F. (2024). Fundamentals and Classifications of CO2 Sensors. In *Handbook of Nanosensors* (pp. 1–36). doi:10.1007/978-3-031-16338-8_22-1

Batstone, D. J., & Virdis, B. (2016). The role of anaerobic digestion in the emerging energy economy. *Current Opinion in Biotechnology*, *27*, 142–149. doi:10.1016/j.copbio.2014.01.013

Bellucci, M., Borruso, L., Piergiacomo, F., Brusetti, L., & Beneduce, L. (2022). The effect of substituting energy crop with agricultural waste on the dynamics of bacterial communities in a two-stage anaerobic digester. *Chemosphere*, *294*, 133776. doi:10.1016/j.chemosphere.2022.133776

Bent, S. J., & Forney, L. J. (2008). The tragedy of the uncommon: Understanding limitations in the analysis of microbial diversity. *ISME Journal*, *2*(7), 689–695. doi:10.1038/ismej.2008.44

Beraud-Martínez, L. K., Betancourt-Lozano, M., Gómez-Gil, B., Asaff-Torres, A., Monroy-Hermosillo, O. A., & Franco-Nava, M. Á. (2024). Methylotrophic methanogenesis induced by ammonia nitrogen in an anaerobic digestion system. *Anaerobe*, *88*, 102877. doi:10.1016/j.anaerobe.2024.102877

Berg, G., Rybakova, D., Fischer, D., Cernava, T., Vergès, M. C. C., Charles, T., Chen, X., Cocolin, L., Eversole, K., Corral, G. H., Kazou, M., Kinkel, L., Lange, L., Lima, N., Loy, A., Macklin, J. A., Maguin, E., Mauchline, T., McClure, R., Mitter, B., Ryan, M., Sarand, I., Smidt, H., Schelkle, B., Roume, H., Kiran, G. S., Selvin, J., Souza, R. S. C. de, Van Overbeek, L., Singh, B. K., Wagner, M., Walsh, A., Sessitsch, A., & Schloter, M. (2020). Microbiome definition re-visited: old concepts and new challenges. In *Microbiome* (Vol. 8, Issue 1, pp. 1–22). BioMed Central Ltd. doi:10.1186/s40168-020-00875-0

Berry, D., Mahfoudh, K. Ben, Wagner, M., & Loy, A. (2011). Barcoded primers used in multiplex amplicon pyrosequencing bias amplification. *Applied and Environmental Microbiology*, *77*(21), 7846–7849. doi:10.1128/AEM.05220-11

Björnsson, L., Murto, M., & Mattiasson, B. (2000). Evaluation of parameters for monitoring an anaerobic co-digestion process. *Applied Microbiology and Biotechnology*, *54*(6), 844–849. doi:10.1007/s002530000471

Blasco, L., Kahala, M., Ervasti, S., & Tampio, E. (2022). Dynamics of microbial community in response to co-feedstock composition in anaerobic digestion. *Bioresource Technology*, *364*, 128039. doi:10.1016/j.biortech.2022.128039

Blaut, M. (1994). Metabolism of methanogens. *Antonie van Leeuwenhoek*, *66*(1–3), 187–208. doi:10.1007/BF00871639

Blume, F., Bergmann, I., Nettmann, E., Schelle, H., Rehde, G., Mundt, K., & Klocke, M. (2010). Methanogenic population dynamics during semi-continuous biogas fermentation and acidification by overloading. *Journal of Applied Microbiology*, *109*(2), 441–450. doi:10.1111/j.1365-2672.2010.04682.x

Boe, K., Batstone, D. J., & Angelidaki, I. (2007). An innovative online VFA monitoring system for the anaerobic process, based on headspace gas

chromatography. *Biotechnology and Bioengineering*, *96*(4), 712–721. doi:10.1002/bit.21131

Boe, K., Batstone, D. J., Steyer, J. P., & Angelidaki, I. (2010). State indicators for monitoring the anaerobic digestion process. *Water Research*, *44*(20), 5973–5980. doi:10.1016/J.WATRES.2010.07.043

Bórawski, P., Wyszomierski, R., Bełdycka-Bórawska, A., Mickiewicz, B., Kalinowska, B., Dunn, J. W., & Rokicki, T. (2022). Development of Renewable Energy Sources in the European Union in the Context of Sustainable Development Policy. *Energies*, *15*(4). doi:10.3390/en15041545

Bray, J. R., & Curtis, J. T. (1957). An Ordination of the Upland Forest Communities of Southern Wisconsin. *Ecological Monographs*, *27*(4), 325–349. doi:10.2307/1942268

Bruni, E., Ward, A. J., Køcks, M., Feilberg, A., Adamsen, A. P. S., Jensen, A. P., & Poulsen, A. K. (2013). Comprehensive monitoring of a biogas process during pulse loads with ammonia. *Biomass and Bioenergy*, *56*, 211–220. doi:10.1016/j.biombioe.2013.05.002

Buczkowska, A., Witkowska, E., Górski, Ł., Zamojska, A., Szewczyk, K. W., Wróblewski, W., & Ciosek, P. (2010). The monitoring of methane fermentation in sequencing batch bioreactor with flow-through array of miniaturized solid state electrodes. *Talanta*, *81*(4–5), 1387–1392. doi:10.1016/j.talanta.2010.02.039

Business Analytiq. **(2025)**. *Price trend data & tools to create benchmarks and leading indicators*. 2025, June 14. https://businessanalytiq.com/

Calli, B., Mertoglu, B., Inanc, B., & Yenigun, O. (2005). Effects of high free ammonia concentrations on the performances of anaerobic bioreactors. *Process Biochemistry*, *40*, 1285–1292. doi:10.1016/j.procbio.2004.05.008

Calusinska, M., Goux, X., Fossépré, M., Muller, E. E. L., Wilmes, P., & Delfosse, P. (2018). A year of monitoring 20 mesophilic full-scale bioreactors reveals the existence of stable but different core microbiomes in bio-waste and wastewater anaerobic digestion systems. *Biotechnology for Biofuels*, *11*(1), 196. doi:10.1186/s13068-018-1195-8

Camarinha-Silva, A., Wos-Oxley, M. L., Jáuregui, R., Becker, K., & Pieper, D. H. (2012). Validating T-RFLP as a sensitive and high-throughput approach to assess

bacterial diversity patterns in human anterior nares. *FEMS Microbiology Ecology*, *79*(1), 98–108. doi:10.1111/j.1574-6941.2011.01197.x

Capson-Tojo, G., Moscoviz, R., Astals, S., Robles, & Steyer, J. P. (2020). Unraveling the literature chaos around free ammonia inhibition in anaerobic digestion. *Renewable and Sustainable Energy Reviews*, *117*, 109487. doi:10.1016/j.rser.2019.109487

Capson-Tojo, G., Rouez, M., Crest, M., Trably, E., Steyer, J. P., Bernet, N., Delgenès, J. P., & Escudié, R. (2017). Kinetic study of dry anaerobic co-digestion of food waste and cardboard for methane production. *Waste Management*, *69*, 470–479. doi:10.1016/j.wasman.2017.09.002

Carballa, M., Regueiro, L., & Lema, J. M. (2015). Microbial management of anaerobic digestion: Exploiting the microbiome-functionality nexus. *Current Opinion in Biotechnology*, *33*, 103–111. doi:10.1016/j.copbio.2015.01.008

Carballa, M., Smits, M., Etchebehere, C., Boon, N., & Verstraete, W. (2011). Correlations between molecular and operational parameters in continuous lab-scale anaerobic reactors. *Applied Microbiology and Biotechnology*, *89*(2), 303–314. doi:10.1007/s00253-010-2858-y

CHEMANALYST. **(2022)**. Real-time price movement of 200+ chemical and petrochemical products for informed purchase decisions. *Market Overview*, 38.

Chen, J. L., Ortiz, R., Steele, T. W. J., & Stuckey, D. C. (2014). Toxicants inhibiting anaerobic digestion: A review. In *Biotechnology Advances* (Vol. 32, Issue 8, pp. 1523–1534). Elsevier. doi:10.1016/j.biotechadv.2014.10.005

Chen, Y., Banin, A., & Borochovitch, A. (1983). Effect of Potassium on Soil Structure in Relation to Hydraulic Conductivity. *Developments in Soil Science*, *12*(C), 135–147. doi:10.1016/s0166-2481(08)70289-7

Chen, Y., Cheng, J. J., & Creamer, K. S. (2008). Inhibition of anaerobic digestion process: A review. *Bioresource Technology*, *99*(10), 4044–4064. doi:10.1016/j.biortech.2007.01.057

Cholewińska, P., Górniak, W., & Wojnarowski, K. (2021). Impact of selected environmental factors on microbiome of the digestive tract of ruminants. *BMC Veterinary Research*, *17*(1), 1–10. doi:10.1186/S12917-021-02742-Y/FIGURES/1

Christou, M. L., Vasileiadis, S., Karpouzas, D. G., Angelidaki, I., & Kotsopoulos, T. A. (2021). Effects of organic loading rate and hydraulic retention time on

bioaugmentation performance to tackle ammonia inhibition in anaerobic digestion. *Bioresource Technology*, *334*, 124323. doi:10.1016/j.biortech.2021.125246

Cioabla, A. E., Ionel, I., Dumitrel, G. A., & Popescu, F. (2012). Comparative study on factors affecting anaerobic digestion of agricultural vegetal residues. *Biotechnology for Biofuels*, *5*, 39. doi:10.1186/1754-6834-5-39

Conklin, A., Stensel, H. D., & Ferguson, J. (2006). Growth Kinetics and Competition Between Methanosarcina and Methanosaeta in Mesophilic Anaerobic Digestion. *Water Environment Research*, *78*(5), 486–496. doi:10.2175/106143006X95393

Conners, S. B., Mongodin, E. F., Johnson, M. R., Montero, C. I., Nelson, K. E., & Kelly, R. M. (2006). Microbial biochemistry, physiology, and biotechnology of hyperthermophilic Thermotoga species. In *FEMS Microbiology Reviews* (Vol. 30, Issue 6, pp. 872–905). doi:10.1111/j.1574-6976.2006.00039.x

Conrad, R. (2005). Quantification of methanogenic pathways using stable carbon isotopic signatures: A review and a proposal. *Organic Geochemistry*, *36*(5), 739–752. doi:10.1016/j.orggeochem.2004.09.006

Conrad, R. (2006). Contribution of hydrogen to methane production and control of hydrogen concentrations in methanogenic soils and sediments. *FEMS Microbiology Ecology*, *28*(3), 193–202. doi:10.1111/j.1574-6941.1999.tb00575.x

Conrad, R., Phelps, T. J., & Zeikus, J. G. (1985). Gas metabolism evidence in support of the juxtaposition of hydrogen-producing and methanogenic bacteria in sewage sludge and lake sediments. *Applied and Environmental Microbiology*, *50*(3), 595–601. doi:10.1128/AEM.50.3.595-601.1985

Culman, S. W., Bukowski, R., Gauch, H. G., Cadillo-Quiroz, H., & Buckley, D. H. (2009). T-REX: Software for the processing and analysis of T-RFLP data. *BMC Bioinformatics*, *10*. doi:10.1186/1471-2105-10-171

De Bok, F. A. M., Plugge, C. M., & Stams, A. J. M. (2004). Interspecies electron transfer in methanogenic propionate degrading consortia. *Water Research*, *38*(6), 1368–1375. doi:10.1016/J.WATRES.2003.11.028

De Vrieze, J., Gildemyn, S., Vilchez-Vargas, R., Jáuregui, R., Pieper, D. H., Verstraete, W., & Boon, N. (2015). Inoculum selection is crucial to ensure operational stability in anaerobic digestion. *Applied Microbiology and Biotechnology*, *99*(1), 189–199. doi:10.1007/S00253-014-6046-3/METRICS

De Vrieze, J., Hennebel, T., Boon, N., & Verstraete, W. (2012). Methanosarcina: The rediscovered methanogen for heavy duty biomethanation. *Bioresource Technology*, *112*, 1–9. doi:10.1016/j.biortech.2012.02.079

De Vrieze, J., Verstraete, W., & Boon, N. (2013). Repeated pulse feeding induces functional stability in anaerobic digestion. *Microbial Biotechnology*, *6*(4), 414–424. doi:10.1111/1751-7915.12025

Delbès, C., Moletta, R., & Godon, J.-J. (2006). Bacterial and archaeal 16S rDNA and 16S rRNA dynamics during an acetate crisis in an anaerobic digestor ecosystem. *FEMS Microbiology Ecology*, *35*(1), 19–26. doi:10.1111/j.1574-6941.2001.tb00784.x

Demirel, B., & Scherer, P. (2008). The roles of acetotrophic and hydrogenotrophic methanogens during anaerobic conversion of biomass to methane: A review. *Reviews in Environmental Science and Biotechnology*, *7*(2), 173–190. doi:10.1007/s11157-008-9131-1

DG Energy. **(2014)**. *State of play on the sustainability of solid and gaseous biomass used for electricity, heating and cooling in the EU (SWD 259 Final)*. https://ec.europa.eu/energy/en/topics/renewable-energy/biomass

Dixon, P. (2003). VEGAN, a package of R functions for community ecology. *Journal of Vegetation Science*, *14*(6), 927–930. doi:10.1111/J.1654-1103.2003.TB02228.X

Drosg, B. (2013). Process monitoring in biogas plants. *IEA Bioenergy Task*, *37*, 1–38.

Dunbar, J., Ticknor, L. O., & Kuske, C. R. (2001). Phylogenetic specificity and reproducibility and new method for analysis of terminal restriction fragment profiles of 16S rRNA genes from bacterial communities. *Applied and Environmental Microbiology*, *67*(1), 190–197. doi:10.1128/AEM.67.1.190-197.2001

Durbin, A. M., & Teske, A. (2012). Archaea in organic-lean and organic-rich marine subsurface sediments: An environmental gradient reflected in distinct phylogenetic lineages. *Frontiers in Microbiology*, *3*(MAY). doi:10.3389/fmicb.2012.00168

EBA. **(2022)**. *EBA Statistical Report 2022.* Brussels, Belgium, November 2022.

Edgar, R. C. (2010). Search and clustering orders of magnitude faster than BLAST. *Bioinformatics*, *26*(19), 2460–2461. doi:10.1093/bioinformatics/btq461

Fang, C., Boe, K., & Angelidaki, I. (2011). Anaerobic co-digestion of desugared molasses with cow manure; focusing on sodium and potassium inhibition.

Bioresource Technology, *102*(2), 1005–1011. doi:10.1016/J.BIORTECH.2010.09.077

Feldewert, C., Lang, K., & Brune, A. (2021). The hydrogen threshold of obligately methyl-reducing methanogens. *FEMS Microbiology Letters*, *367*(17), 137. doi:10.1093/femsle/fnaa137

Fernandes, T. V., Keesman, K. J., Zeeman, G., & van Lier, J. B. (2014). Effect of ammonia on the anaerobic hydrolysis of cellulose and tributyrin. *Biomass and Bioenergy*, *47*, 316–323. doi:10.1016/j.biombioe.2012.09.029

Ferrer, A. (2007). Multivariate Statistical Process Control Based on Principal Component Analysis (MSPC-PCA): Some Reflections and a Case Study in an Autobody Assembly Process. *Quality Engineering*, *19*(4), 311–325. doi:10.1080/08982110701621304

Ferry, J. G. (1993). *Methanogenesis: Ecology, Physiology, Biochemistry & Genetics (Chapman & Hall Microbiology Series)* (C. A. Reddy, A. M. Chakrabarty, A. L. Demain, & J. M. Tiedje, Eds.; 3rd ed.). SpringerScience + Business Media.

Fotidis, I. A., Karakashev, D., & Angelidaki, I. (2014). The dominant acetate degradation pathway/methanogenic composition in full-scale anaerobic digesters operating under different ammonia levels. *International Journal of Environmental Science and Technology*, *11*(7), 2087–2094. doi:10.1007/s13762-013-0407-9

Fotidis, I. A., Karakashev, D., Kotsopoulos, T. A., Martzopoulos, G. G., & Angelidaki, I. (2013). Effect of ammonium and acetate on methanogenic pathway and methanogenic community composition. *FEMS Microbiology*, *83*(1), 38–48. doi:10.1111/j.1574-6941.2012.01456.x

Franke-Whittle, I. H., Walter, A., Ebner, C., & Insam, H. (2014). Investigation into the effect of high concentrations of volatile fatty acids in anaerobic digestion on methanogenic communities. *Waste Management*, *34*(11), 2080–2089. doi:10.1016/j.wasman.2014.07.020

Fu, X., Liu, Z., Zhu, C., Mou, H., & Kong, Q. (2019). Nondigestible carbohydrates, butyrate, and butyrate-producing bacteria. In *Critical Reviews in Food Science and Nutrition* (Vol. 59, Issue S1, pp. S130–S152). Taylor & Francis. doi:10.1080/10408398.2018.1542587

Gallert, C., & Winter, J. (2005). Bacterial Metabolism in Wastewater Treatment Systems. In *Environmental Biotechnology: Concepts and Applications* (pp. 1–48). doi:10.1002/3527604286.ch1

Godon, J.-J. (1998). Aspects biochimiques et microbiologiques de la méthanisation. In *La méthanisation* (pp. 62–83). Moletta, R.

González-Fernández, C., & García-Encina, P. A. (2009). Impact of substrate to inoculum ratio in anaerobic digestion of swine slurry. *Biomass and Bioenergy*, *33*(8), 1065–1069. doi:10.1016/j.biombioe.2009.03.008

Görish, Uwe., & Helm, M. (2008). *La production de biogaz*. Ulmer.

Goux, X., Calusinska, M., Fossépré, M., Benizri, E., & Delfosse, P. (2016). Start-up phase of an anaerobic full-scale farm reactor – Appearance of mesophilic anaerobic conditions and establishment of the methanogenic microbial community. *Bioresource Technology*, *212*, 217–226. doi:10.1016/J.BIORTECH.2016.04.040

Goux, X., Calusinska, M., Lemaigre, S., Marynowska, M., Klocke, M., Udelhoven, T., Benizri, E., & Delfosse, P. (2015). Microbial community dynamics in replicate anaerobic digesters exposed sequentially to increasing organic loading rate, acidosis, and process recovery. *Biotechnology for Biofuels*, *8*(1), 122. doi:10.1186/s13068-015-0309-9

Grasso, D., Strevett, K., & Pesari, H. (2005). Impact of Sodium and Potassium on Environmental Systems. *Journal of Environmental Systems*, *22*(4), 297–323. doi:10.2190/rrnd-6y9q-jn16-06nd

Greenacre, M. (2021). Compositional data analysis. In *Annual Review of Statistics and Its Application* (Vol. 8, Issue Volume 8, 2021, pp. 271–299). Annual Reviews Inc. doi:10.1146/annurev-statistics-042720-124436

Großkopf, R., Janssen, P. H., & Liesack, W. (1998). Diversity and structure of the methanogenic community in anoxic rice paddy soil microcosms as examined by cultivation and direct 16S rRNA gene sequence retrieval. *Applied and Environmental Microbiology*, *64*(3), 960–969. doi:10.1128/AEM.64.3.960-969.1998

Gunther, J. C., Conner, J. S., & Seborg, D. E. (2007). Fault detection and diagnosis in an industrial fed-batch cell culture process. *Biotechnology Progress*, *23*(4), 851–857. doi:10.1021/BP070063M

Gwelo, A. S. (2019). Principal components to overcome multicollinearity problem. *Oradea Journal of Business and Economics*, *4*(1), 79–91. doi:10.47535/1991ojbe062

Hailu, A. M., Palani, S. G., Asfaw, S. L., & Tegaye, T. A. (2021). Insight into microbial community diversity and composition of two-stage anaerobic digestion: Focusing methanogenic stage. *Bioresource Technology Reports*, *15*. doi:10.1016/j.biteb.2021.100764

Halliwell, D. J., Barlow, K. M., & Nash, D. M. (2001). A review of the effects of wastewater sodium on soil physical properties and their implications for irrigation systems. *Soil Research*, *39*(6), 1259–1267. doi:10.1071/SR00047

Hao, L. P., Mazéas, L., Lü, F., Grossin-Debattista, J., He, P. J., & Bouchez, T. (2017). Effect of ammonia on methane production pathways and reaction rates in acetate-fed biogas processes. *Water Science and Technology*, *75*(8), 1839–1848. doi:10.2166/wst.2017.032

Harirchi, S., Wainaina, S., Sar, T., Nojoumi, S. A., Parchami, M., Parchami, M., Varjani, S., Khanal, S. K., Wong, J., Awasthi, M. K., & Taherzadeh, M. J. (2022). Microbiological insights into anaerobic digestion for biogas, hydrogen or volatile fatty acids (VFAs): a review. *Bioengineered*, *13*(3), 6521–6557. doi:10.1080/21655979.2022.2035986

Hecht, M., Clemens, P., & Wulf, S. (2007). Entwicklung eines einfachen und für den Landwirt durchführbaren Verfahrens zur Überwachung der Prozessstabilität in landwirtschaftlichen Biogasanlagen. *Schriftenreihe Des Lehr- Und Forschungsschwerpunktes USL*, *Nr. 151*, 51.

Heeg, K., Pohl, M., Sontag, M., Mumme, J., Klocke, M., & Nettmann, E. (2014). Microbial communities involved in biogas production from wheat straw as the sole substrate within a two-phase solid-state anaerobic digestion. *Systematic and Applied Microbiology*, *37*(8), 590–600. doi:10.1016/j.syapm.2014.10.002

Helm, D. (2014). The European framework for energy and climate policies. *Energy Policy*, *64*, 29–35. doi:10.1016/j.enpol.2013.05.063

Hill, D. T., Cobb, S. A., & Bolte, J. P. (1987). Using volatile fatty acid relationship to predic anaerobic digester failure. *Transactions of the American Society of Agricultural Engineers*, *30*(2), 496–501. doi:10.13031/2013.31978

Huang, T.-C., & Chen, D.-H. (2007). Kinetic study of urease-catalysed urea hydrolysis. *Journal of Chemical Technology & Biotechnology*, *52*(4), 433–444. doi:10.1002/jctb.280520402

IPCC. **(2022)**. Working Group III contribution to the Sixth Assessment Report of the Intergovernmental Panel on Climate Change, Mitigation of Climate Change Summary for Policymakers (SPM). In A. Core Writing Team, Jager-Waldau & T. Sapkota (Eds.), *Cambridge University Press* (Issue 1). IPCC.

Jacobi, H. F., Moschner, C. R., & Hartung, E. (2009). Use of near infrared spectroscopy in monitoring of volatile fatty acids in anaerobic digestion. *Water Science and Technology*, *60*(2), 339–346. doi:10.2166/wst.2009.345

Ji, J. Y., Xing, Y. J., Ma, Z. T., Cai, J., Zheng, P., & Lu, H. F. (2013). Toxicity assessment of anaerobic digestion intermediates and antibiotics in pharmaceutical wastewater by luminescent bacterium. *Journal of Hazardous Materials*, *246–247*, 319–323. doi:10.1016/j.jhazmat.2012.12.025

Jiang, Y., McAdam, E., Zhang, Y., Heaven, S., Banks, C., & Longhurst, P. (2019). Ammonia inhibition and toxicity in anaerobic digestion: A critical review. *Journal of Water Process Engineering*, *32*, 100899. doi:10.1016/j.jwpe.2019.100899

Jin, X., Li, X., Zhao, N., Angelidaki, I., & Zhang, Y. (2017). Bio-electrolytic sensor for rapid monitoring of volatile fatty acids in anaerobic digestion process. *Water Research*, *111*, 74–80. doi:10.1016/j.watres.2016.12.045

Jo, Y., Cayetano, R. D. A., Kim, G.-B. B., Park, J., & Kim, S.-H. H. (2022). The effects of ammonia acclimation on biogas recovery and the microbial population in continuous anaerobic digestion of swine manure. *Environmental Research*, *212*, 113483. doi:10.1016/j.envres.2022.113483

Jones, O. A. H., Lear, G., Welji, A. M., Collins, G., & Quince, C. (2016). Community metabolomics in environmental microbiology. In *Microbial Metabolomics: Applications in Clinical, Environmental, and Industrial Microbiology* (pp. 199–224). Springer International Publishing. doi:10.1007/978-3-319-46326-1_7

Kaiser, H. F. (1960). The Application of Electronic Computers to Factor Analysis. *Educational and Psychological Measurement*, *20*(1), 141–151. doi:10.1177/001316446002000116

Kaltschmitt, M., Friedmann, H., & Goertz, G. (2005). *Fermentation of organic materials-VDI guideline 4630; Vergaerung organischer Stoffe-VDI-Richtlinie 4630*. https://www.osti.gov/etdeweb/biblio/20682804

Kampmann, K., Ratering, S., Geißler-Plaum, R., Schmidt, M., Zerr, W., & Schnell, S. (2014). Changes of the microbial population structure in an overloaded

fed-batch biogas reactor digesting maize silage. *Bioresource Technology*, *174*, 108–117. doi:10.1016/j.biortech.2014.09.150

Karakashev, D., Batstone, D. J., & Angelidaki, I. (2005). Influence of environmental conditions on methanogenic compositions in anaerobic biogas reactors. *Applied and Environmental Microbiology*, *71*(1), 331–338. doi:10.1128/AEM.71.1.331-338.2005

Karakashev, D., Batstone, D. J., Trably, E., & Angelidaki, I. (2006). Acetate oxidation is the dominant methanogenic pathway from acetate in the absence of Methanosaetaceae. *Applied and Environmental Microbiology*, *72*(7), 5138–5141. doi:10.1128/AEM.00489-06

Karekar, S., Stefanini, R., & Ahring, B. (2022). Homo-Acetogens: Their Metabolism and Competitive Relationship with Hydrogenotrophic Methanogens. In *Microorganisms* (Vol. 10, Issue 2). doi:10.3390/microorganisms10020397

Keresztesi, Á., Birsan, M. V., Nita, I. A., Bodor, Z., & Szép, R. (2019). Assessing the neutralisation, wet deposition and source contributions of the precipitation chemistry over Europe during 2000–2017. *Environmental Sciences Europe*, *31*(1), 1–15. doi:10.1186/S12302-019-0234-9/TABLES/2

Khalil, C. A., Ghanimeh, S., & Medawar, Y. (2017). Ammonia inhibition and recovery potential in anaerobic digesters: A review. *Proceedings of the Air and Waste Management Association's Annual Conference and Exhibition, AWMA*, 275193.

Kim, J. M., To, T. K., Matsui, A., Tanoi, K., Kobayashi, N. I., Matsuda, F., Habu, Y., Ogawa, D., Sakamoto, T., Matsunaga, S., Bashir, K., Rasheed, S., Ando, M., Takeda, H., Kawaura, K., Kusano, M., Fukushima, A., Endo, T. A., Kuromori, T., Ishida, J., Morosawa, T., Tanaka, M., Torii, C., Takebayashi, Y., Sakakibara, H., Ogihara, Y., Saito, K., Shinozaki, K., Devoto, A., & Seki, M. (2017). Acetate-mediated novel survival strategy against drought in plants. *Nature Plants*, *3*, 17097. doi:10.1038/nplants.2017.97

Kleyböcker, A., Liebrich, M., Verstraete, W., Kraume, M., & Würdemann, H. (2012). Early warning indicators for process failure due to organic overloading by rapeseed oil in one-stage continuously stirred tank reactor, sewage sludge and waste digesters. *Bioresource Technology*, *123*, 534–541. doi:10.1016/j.biortech.2012.07.089

Kleyböcker, A., Lienen, T., Liebrich, M., Kasina, M., Kraume, M., & Würdemann, H. (2014). Application of an early warning indicator and CaO to maximize the time–space-yield of an completely mixed waste digester using rape seed oil as co-substrate. *Waste Management*, *34*(3), 661–668. doi:10.1016/J.WASMAN.2013.11.011

Klindworth, A., Pruesse, E., Schweer, T., Peplies, J., Quast, C., Horn, M., & Glöckner, F. O. (2013). Evaluation of general 16S ribosomal RNA gene PCR primers for classical and next-generation sequencing-based diversity studies. *Nucleic Acids Research*, *41*(1). doi:10.1093/nar/gks808

Klocke, M., Mähnert, P., Mundt, K., Souidi, K., & Linke, B. (2007). Microbial community analysis of a biogas-producing completely stirred tank reactor fed continuously with fodder beet silage as mono-substrate. *Systematic and Applied Microbiology*, *30*(2), 139–151. doi:10.1016/j.syapm.2006.03.007

Klocke, M., Nettmann, E., Bergmann, I., Mundt, K., Souidi, K., Mumme, J., & Linke, B. (2008). Characterization of the methanogenic Archaea within two-phase biogas reactor systems operated with plant biomass. *Systematic and Applied Microbiology*, *31*(3), 190–205. doi:10.1016/j.syapm.2008.02.003

Koch, M., Dolfing, J., Wuhrmann, K., & Zehnder, A. J. B. (1983). Pathways of propionate degradation by enriched methanogenic cultures. *Applied and Environmental Microbiology*, *45*(4), 1411–1414. doi:10.1128/aem.45.4.1411-1414.1983

Kourti, T. (2005). Application of Latent Variable Methods to Process Control and Multivariate Statistical Process Control in Industry. *International Journal of Adaptive Control and Signal Processing*, *19*, 213–246. doi:10.1002/acs.859

Kourti, T., & MacGregor, J. F. (1995). Process analysis, monitoring and diagnosis, using multivariate projection methods. *Chemometrics and Intelligent Laboratory Systems*, *28*, 3–21. doi:10.1016/0169-7439(95)80036-9

Krakat, N., Schmidt, S., & Scherer, P. (2011). Potential impact of process parameters upon the bacterial diversity in the mesophilic anaerobic digestion of beet silage. *Bioresource Technology*, *102*(10), 5692–5701. doi:10.1016/j.biortech.2011.02.108

Krapf, L. C., Nast, D., Gronauer, A., Schmidhalter, U., & Heuwinkel, H. (2013). Transfer of a near infrared spectroscopy laboratory application to an online process

analyser for in situ monitoring of anaerobic digestion. *Bioresource Technology*, *129*, 39–50. doi:10.1016/j.biortech.2012.11.027

Kroeker, E. J., Schulte, D. D., Sparling, A. B., & Lapp, H. M. (1979). Anaerobic treatment process stability. *Journal of the Water Pollution Control Federation*, *51*(4), 718–727.

Ku, W., Storer, R. H., & Georgakis, C. (1995). Disturbance detection and isolation by dynamic principal component analysis. *Chemometrics and Intelligent Laboratory Systems*, *30*(1), 179–196. doi:10.1016/0169-7439(95)00076-3

Kundu, K., Sharma, S., & Sreekrishnan, T. R. (2013). Changes in microbial communities in a hybrid anaerobic reactor with organic loading rate and temperature. *Bioresource Technology*, *129*, 538–547. doi:10.1016/j.biortech.2012.11.118

Lambie, S. C., Kelly, W. J., Leahy, S. C., Li, D., Reilly, K., McAllister, T. A., Valle, E. R., Attwood, G. T., & Altermann, E. (2015). The complete genome sequence of the rumen methanogen Methanosarcina barkeri CM1. *Standards in Genomic Sciences*, *10*(1), 1–8. doi:10.1186/s40793-015-0038-5

Lane, D. J. (1991). 16S/23S rRNA Sequencing. *Nucleic Acid Techniques in Bacterial Systematics*, 115–175.

Lang, K., Schuldes, J., Klingl, A., Poehlein, A., Daniel, R., & Brune, A. (2015). New Mode of Energy Metabolism in the Seventh Order of Methanogens as Revealed by Comparative Genome Analysis of "Candidatus Methanoplasma termitum." *Applied and Environmental Microbiology*, *81*(4), 1338–1352. doi:10.1128/AEM.03389-14

Lay, J., Li, Y., & Noike, T. (1998). The influence of pH and ammonia concentration on the methane production in high-solids digestion processes. *Water Environment Research*, *70*(5), 1075–1082. doi:10.2175/106143098X123426

Lebiocka, M., Montusiewicz, A., & Cydzik-Kwiatkowska, A. (2018). Effect of Bioaugmentation on Biogas Yields and Kinetics in Anaerobic Digestion of Sewage Sludge. In *International Journal of Environmental Research and Public Health* (Vol. 15, Issue 8). doi:10.3390/ijerph15081717

Lecharlier, A., Carrier, H., & Le Hécho, I. (2022). Characterization of biogas and biomethane trace compounds: A critical review of advances in in situ sampling and preconcentration techniques. In *Analytica Chimica Acta* (Vol. 1229, p. 340174). Elsevier. doi:10.1016/j.aca.2022.340174

Lee, D. S., Lee, M. W., Woo, S. H., Kim, Y. J., & Park, J. M. (2006). Multivariate online monitoring of a full-scale biological anaerobic filter process using kernel-based algorithms. *Industrial and Engineering Chemistry Research*, *45*(12), 4335–4344. doi:10.1021/ie050916k

Lee, D. S., Park, J. M., & Vanrolleghem, P. A. (2005). Adaptive multiscale principal component analysis for on-line monitoring of a sequencing batch reactor. *Journal of Biotechnology*, *116*(2), 195–210. doi:10.1016/j.jbiotec.2004.10.012

Lee, J. M., Yoo, C. K., & Lee, I. B. (2004). Statistical process monitoring with independent component analysis. *Journal of Process Control*, *14*(5), 467–485. doi:10.1016/J.JPROCONT.2003.09.004

Lemaigre, S., Adam, G., Gerin, P. A., Noo, A., De Vos, B., Klimek, D., Goux, X., Calusinska, M., & Delfosse, P. (2018). Potential of multivariate statistical process monitoring based on the biogas composition to detect free ammonia intoxication in anaerobic reactors. *Biochemical Engineering Journal*, *140*, 17–28. doi:10.1016/j.bej.2018.08.018

Lemaigre, S., Adam, G., Goux, X., Noo, A., De Vos, B., Gerin, P. A., & Delfosse, P. (2016). Transfer of a static PCA-MSPC model from a steady-state anaerobic reactor to an independent anaerobic reactor exposed to organic overload. *Chemometrics and Intelligent Laboratory Systems*, *159*, 20–30. doi:10.1016/j.chemolab.2016.09.010

Lerm, S., Kleyböcker, A., Miethling-Graff, R., Alawi, M., Kasina, M., Liebrich, M., & Würdemann, H. (2012). Archaeal community composition affects the function of anaerobic co-digesters in response to organic overload. *Waste Management*, *32*(3), 389–399. doi:10.1016/j.wasman.2011.11.013

Li, C., Lü, F., Peng, W., He, P. J., & Zhang, H. (2024). Functional Redundant Microbiome Enhanced Anaerobic Digestion Efficiency under Ammonium Inhibition Conditions. *Environmental Science and Technology*, *58*(15), 6659–6669. doi:10.1021/acs.est.4c01227

Li, D., Chen, L., Liu, X., Mei, Z., Ren, H., Cao, Q., & Yan, Z. (2017). Instability mechanisms and early warning indicators for mesophilic anaerobic digestion of vegetable waste. *Bioresource Technology*, *245*, 90–97. doi:10.1016/j.biortech.2017.07.098

Li, D., Ran, Y., Chen, L., Cao, Q., Li, Z., & Liu, X. (2018). Instability diagnosis and syntrophic acetate oxidation during thermophilic digestion of vegetable waste. *Water Research*, *139*, 263–271. doi:10.1016/j.watres.2018.04.019

Li, J., Rui, J., Yao, M., Zhang, S., Yan, X., Wang, Y., Yan, Z., & Li, X. (2015). Substrate type and free ammonia determine bacterial community structure in full-scale mesophilic anaerobic digesters treating cattle or swine manure. *Frontiers in Microbiology*, *6*, 1337. doi:10.3389/fmicb.2015.01337

Li, L., He, Q., Wei, Y., He, Q., & Peng, X. (2014). Early warning indicators for monitoring the process failure of anaerobic digestion system of food waste. *Bioresource Technology*, *171*, 491–494. doi:10.1016/j.biortech.2014.08.089

Li, L., Peng, X., Wang, X., & Wu, D. (2018). Anaerobic digestion of food waste: A review focusing on process stability. *Bioresource Technology*, *248*, 20–28. doi:10.1016/J.BIORTECH.2017.07.012

Li, W., Yue, H., Valle-Cervantes, S., & Qin, S. J. (2000). Recursive PCA for adaptive process monitoring. *Journal of Process Control*, *10*, 471–486. doi:10.1016/S0959-1524(00)00022-6

Li, Y., Yang, G., Li, L., & Sun, Y. (2018). Bioaugmentation for overloaded anaerobic digestion recovery with acid-tolerant methanogenic enrichment. *Waste Management*, *79*, 744–751. doi:10.1016/j.wasman.2018.08.043

Li, Y., Zhang, Y., Sun, Y., Wu, S., Kong, X., Yuan, Z., & Dong, R. (2017). The performance efficiency of bioaugmentation to prevent anaerobic digestion failure from ammonia and propionate inhibition. *Bioresource Technology*, *231*, 94–100. doi:10.1016/j.biortech.2017.01.068

Li, Z. Y., Inoue, D., & Ike, M. (2023). Mitigating ammonia-inhibition in anaerobic digestion by bioaugmentation: A review. *Journal of Water Process Engineering*, *52*. doi:10.1016/j.jwpe.2023.103506

Lijó, L., González-García, S., Bacenetti, J., & Moreira, M. T. (2017). The environmental effect of substituting energy crops for food waste as feedstock for biogas production. *Energy*, *137*, 1130–1143. doi:10.1016/j.energy.2017.04.137

Lim, J. W., Park, T., Tong, Y. W., & Yu, Z. (2020). The microbiome driving anaerobic digestion and microbial analysis. *Advances in Bioenergy*, *5*, 1. doi:10.1016/BS.AIBE.2020.04.001

Limam, R. D., Chouari, R., Mazéas, L., Wu, T. Di, Li, T., Grossin-Debattista, J., Guerquin-Kern, J. L., Saidi, M., Landoulsi, A., Sghir, A., & Bouchez, T. (2014). Members of the uncultured bacterial candidate division WWE1 are implicated in anaerobic digestion of cellulose. *MicrobiologyOpen*, *3*(2), 157–167. doi:10.1002/mbo3.144

Ling, J. Y. X., Chan, Y. J., Chen, J. W., Chong, D. J. S., Tan, A. L. L., Arumugasamy, S. K., & Lau, P. L. (2024). Machine learning methods for the modelling and optimisation of biogas production from anaerobic digestion: a review. *Environmental Science and Pollution Research*, *31*(13), 19085–19104. doi:10.1007/S11356-024-32435-6/TABLES/6

Liu, W. T., Marsh, T. L., Cheng, H., & Forney, L. J. (1997). Characterization of microbial diversity by determining terminal restriction fragment length polymorphisms of genes encoding 16S rRNA. *Applied and Environmental Microbiology*, *63*(11), 4516–4522. doi:10.1128/aem.63.11.4516-4522.1997

Lomborg, C. J., Holm-Nielsen, J. B., Oleskowicz-Popiel, P., & Esbensen, K. H. (2009). Near infrared and acoustic chemometrics monitoring of volatile fatty acids and dry matter during co-digestion of manure and maize silage. *Bioresource Technology*, *100*(5), 1711–1719. doi:10.1016/j.biortech.2008.09.043

Lü, F., Hao, L., Guan, D., Qi, Y., Shao, L., & He, P. (2013). Synergetic stress of acids and ammonium on the shift in the methanogenic pathways during thermophilic anaerobic digestion of organics. *Water Research*, *47*(7), 2297–2306. doi:10.1016/j.watres.2013.01.049

Lueders, T., & Friedrich, M. (2000). Archaeal population dynamics during sequential reduction processes in rice field soil. *Applied and Environmental Microbiology*, *66*(7), 2732–2742. doi:10.1128/AEM.66.7.2732-2742.2000

Lv, Z., Hu, M., Harms, H., Richnow, H. H., Liebetrau, J., & Nikolausz, M. (2014). Stable isotope composition of biogas allows early warning of complete process failure as a result of ammonia inhibition in anaerobic digesters. *Bioresource Technology*, *167*, 251–259. doi:10.1016/j.biortech.2014.06.029

Lv, Z., Leite, A. F., Harms, H., Richnow, H. H., Liebetrau, J., & Nikolausz, M. (2014). Influences of the substrate feeding regime on methanogenic activity in biogas reactors approached by molecular and stable isotope methods. *Anaerobe*, *29*, 91–99. doi:10.1016/j.anaerobe.2013.11.005

Lyu, Z., & Liu, Y. (2018). Diversity and Taxonomy of Methanogens. In *Biogenesis of Hydrocarbons* (pp. 1–59). Springer International Publishing. doi:10.1007/978-3-319-53114-4_5-2

Ma, G., Chen, Y., & Ndegwa, P. (2021). Association between methane yield and microbiota abundance in the anaerobic digestion process: A meta-regression. In *Renewable and Sustainable Energy Reviews* (Vol. 135, p. 110212). Pergamon. doi:10.1016/j.rser.2020.110212

MacGregor, J. (1995). Statistical process control of multivariate processes. *Control Engineering Practice*, *3*(3), 403–414. doi:10.1016/0967-0661(95)00014-L

Madsen, M., Holm-Nielsen, J. B., & Esbensen, K. H. (2011). Monitoring of anaerobic digestion processes: A review perspective. *Renewable and Sustainable Energy Reviews*, *15*(6), 3141–3155. doi:10.1016/j.rser.2011.04.026

Martín-González, L., Font, X., & Vicent, T. (2013). Alkalinity ratios to identify process imbalances in anaerobic digesters treating source-sorted organic fraction of municipal wastes. *Biochemical Engineering Journal*, *76*, 1–5. doi:10.1016/j.bej.2013.03.016

Mason, R. L., & Young, J. C. (2002). *Multivariate Statistical Process Control with Industrial Applications*. Society for Industrial and Applied Mathematics. doi:10.1137/1.9780898718461

Mayer, F., Gerin, P. A., Noo, A., Foucart, G., Flammang, J., Lemaigre, S., Sinnaeve, G., Dardenne, P., & Delfosse, P. (2014). Assessment of factors influencing the biomethane yield of maize silages. *Bioresource Technology*, *153*, 260–268. doi:10.1016/j.biortech.2013.11.081

Mizuno, O., Li, Y. Y., & Noike, T. (1998). The behavior of sulfate-reducing bacteria in acidogenic phase. *Water Research*, *32*(5), 1626–1634.

Moestedt, J., Müller, B., Westerholm, M., & Schnürer, A. (2016). Ammonia threshold for inhibition of anaerobic digestion of thin stillage and the importance of organic loading rate. *Microbial Biotechnology*, *9*(2), 180–194. doi:10.1111/1751-7915.12330

Möller, K., & Müller, T. (2012). Effects of anaerobic digestion on digestate nutrient availability and crop growth: A review. *Engineering in Life Sciences*, *12*(3), 242–257. doi:10.1002/elsc.201100085

Möller, K., & Stinner, W. (2009). Effects of different manuring systems with and without biogas digestion on soil mineral nitrogen content and on gaseous nitrogen losses (ammonia, nitrous oxides). *European Journal of Agronomy*, *30*(1), 1–16. doi:10.1016/j.eja.2008.06.003

Munisamy, P., Ravichandran, M., Natarajan, S. D., & Varadhaaraju, C. (2017). Biological aspects of anaerobic digestion and its kinetics: An overview. *Journal of Microbiology, Biotechnology and Food Sciences*, *6*(4), 1090–1097. doi:10.15414/jmbfs.2017.6.4.1090-1097

Muralidharan, V., Rinker, K. D., Hirsh, I. S., Bouwer, E. J., & Kelly, R. M. (1997). Hydrogen transfer between methanogens and fermentative heterotrophs in hyperthermophilic cocultures. *Biotechnology and Bioengineering*, *56*(3), 268–278. doi:10.1002/(SICI)1097-0290(19971105)56:3<268::AID-BIT4>3.0.CO;2-H

Murphy, J. D., & Thanasit Thamsiriroj. **(2013)**. Fundamental science and engineering of the anaerobic digestion process for biogas production. In *The Biogas Handbook* (pp. 104–130). doi:10.1533/9780857097415.1.104

Murto, M., Björnsson, L., & Mattiasson, B. (2004). Impact of food industrial waste on anaerobic co-digestion of sewage sludge and pig manure. *Journal of Environmental Management*, *70*(2), 101–107. doi:10.1016/j.jenvman.2003.11.001

Nativ, P., Gräber, Y., Aviezer, Y., & Lahav, O. (2021). A simple and accurate approach for determining the vfa concentration in anaerobic digestion liquors, relying on two titration points and an external inorganic carbon analysis. *ChemEngineering*, *5*(2). doi:10.3390/chemengineering5020015

Nazarov, E. G. (2012). A journey into DMS/FAIMS technology. *International Journal for Ion Mobility Spectrometry*, *15*(3), 83–84. doi:10.1007/S12127-012-0112-2/METRICS

Nesbø, C. L., Dlutek, M., Zhaxybayeva, O., & Doolittle, W. F. (2006). Evidence for existence of "mesotogas," members of the order Thermotogales adapted to low-temperature environments. *Applied and Environmental Microbiology*, *72*(7), 5061–5068. doi:10.1128/AEM.00342-06

Nettmann, E., Bergmann, I., Mundt, K., Linke, B., & Klocke, M. (2008). Archaea diversity within a commercial biogas plant utilizing herbal biomass determined by 16S rDNA and mcrA analysis. *Journal of Applied Microbiology*, *105*(6), 1835–1850. doi:10.1111/j.1365-2672.2008.03949.x

Nettmann, E., Bergmann, I., Pramschüfer, S., Mundt, K., Plogsties, V., Herrmann, C., & Klocke, M. (2010). Polyphasic analyses of methanogenic archaeal communities in agricultural biogas plants. *Applied and Environmental Microbiology*, *76*(8), 2540–2548. doi:10.1128/AEM.01423-09

Nguyen, L. N., Nguyen, A. Q., & Nghiem, L. D. (2019). Microbial Community in Anaerobic Digestion System: Progression in Microbial Ecology. In *Energy, Environment, and Sustainability* (pp. 331–355). Springer Nature. doi:10.1007/978-981-13-3259-3_15

Ni, K., Köster, J. R., Seidel, A., & Pacholski, A. (2015). Field measurement of ammonia emissions after nitrogen fertilization-A comparison between micrometeorological and chamber methods. *European Journal of Agronomy*, *71*, 115–122. doi:10.1016/j.eja.2015.09.004

Nie, E., He, P., Zhang, H., Hao, L., Shao, L., & Lü, F. (2021). How does temperature regulate anaerobic digestion? *Renewable and Sustainable Energy Reviews*, *150*, 111453. doi:10.1016/j.rser.2021.111453

Nielsen, H. B., & Angelidaki, I. (2008). Strategies for optimizing recovery of the biogas process following ammonia inhibition. *Bioresource Technology*, *99*(17), 7995–8001. doi:10.1016/j.biortech.2008.03.049

Nijhuis, A., De Jong, S., & Vandeginste, B. G. M. (1997). Multivariate statistical process control in chromatography. *Chemometrics and Intelligent Laboratory Systems*, *38*(1), 51–62. doi:10.1016/S0169-7439(97)00054-3

Niu, Q., Qiao, W., Qiang, H., Hojo, T., & Li, Y. Y. (2013). Mesophilic methane fermentation of chicken manure at a wide range of ammonia concentration: Stability, inhibition and recovery. *Bioresource Technology*, *137*, 358–367. doi:10.1016/j.biortech.2013.03.080

Nordberg, A., Hansson, M., Sundh, I., Nordkvist, E., Carisson, H., & Mathisen, B. (2000). Monitoring of a biogas process using electronic gas sensors and near-infrared spectroscopy (NIR). *Water Science and Technology : A Journal of the International Association on Water Pollution Research*, *41*(3), 1–8. doi:10.2166/wst.2000.0049

Orlewski, P., Delfosse, P., & Camara, M. (2013). Process for controlling and monitoring the production of biogas. *Google Patents*, *1*(19), Art. US20130022959A1.

https://patentimages.storage.googleapis.com/4a/a2/92/34b6319dd78fb7/EP2548849A1.pdf

Osborn, A. M., Moore, E. R. B., & Timmis, K. N. (2000). An evaluation of terminal-restriction fragment length polymorphism (T-RFLP) analysis for the study of microbial community structure and dynamics. *Environmental Microbiology*, *2*(1), 39–50. doi:10.1046/j.1462-2920.2000.00081.x

Padmasiri, S. I., Zhang, J., Fitch, M., Norddahl, B., Morgenroth, E., & Raskin, L. (2007). Methanogenic population dynamics and performance of an anaerobic membrane bioreactor (AnMBR) treating swine manure under high shear conditions. *Water Research*, *41*(1), 134–144. doi:10.1016/J.WATRES.2006.09.021

Pan, X., Zhao, L., Li, C., Angelidaki, I., Lv, N., Ning, J., Cai, G., & Zhu, G. (2021). Deep insights into the network of acetate metabolism in anaerobic digestion: focusing on syntrophic acetate oxidation and homoacetogenesis. *Water Research*, *190*, 116774. doi:10.1016/j.watres.2020.116774

Pani, A. K. (2022). Non-linear process monitoring using kernel principal component analysis: A review of the basic and modified techniques with industrial applications. In *Brazilian Journal of Chemical Engineering* (Vol. 39, Issue 2, pp. 327–344). Springer Science and Business Media Deutschland GmbH. doi:10.1007/s43153-021-00125-2

Pavičić, J., Mavar, K. N., Brkić, V., & Simon, K. (2022). Biogas and Biomethane Production and Usage: Technology Development, Advantages and Challenges in Europe. In *Energies* (Vol. 15, Issue 8, p. 2940). MDPI. doi:10.3390/en15082940

Pelletier, E., Kreimeyer, A., Bocs, S., Rouy, Z., Gyapay, G., Chouari, R., Rivière, D., Ganesan, A., Daegelen, P., Sghir, A., Cohen, G. N., Médigue, C., Weissenbach, J., & Le Paslier, D. (2008). "Candidatus Cloacamonas acidaminovorans": Genome sequence reconstruction provides a first glimpse of a new bacterial division. *Journal of Bacteriology*, *190*(7), 2572–2579. doi:10.1128/JB.01248-07

Pequegnat, B., Sagermann, M., Valliani, M., Toh, M., Chow, H., Allen-Vercoe, E., & Monteiro, M. A. (2013). A vaccine and diagnostic target for Clostridium bolteae, an autism-associated bacterium. *Vaccine*, *31*(26), 2787–2790. doi:10.1016/j.vaccine.2013.04.018

Pflüger, K., Wieland, H., & Müller, V. (2005). Osmoadaptation in Methanogenic Archaea: Recent Insights from a Genomic Perspective. In *Adaptation to Life at High*

Salt Concentrations in Archaea, Bacteria, and Eukarya (pp. 239–251). Springer-Verlag. doi:10.1007/1-4020-3633-7_16

Pielou, E. C. (1967). The measurement of diversity in different types of biological collections. *Journal of Theoretical Biology*, *15*(1), 177. doi:10.1016/0022-5193(67)90048-3

Pilloni, G., Granitsiotis, M. S., Engel, M., & Lueders, T. (2012). Testing the limits of 454 pyrotag sequencing: Reproducibility, quantitative assessment and comparison to T-RFLP fingerprinting of aquifer microbes. *PLoS ONE*, *7*(7). doi:10.1371/journal.pone.0040467

Pind, P., Angelidaki, I., Ahring, B., & Stamatelatou, K. (2003). Monitoring and control of anaerobic reactors. In T. Scheper (Ed.), *Biomethanation II* (pp. 135–182).

Poirier, S., Desmond-Le Quéméner, E., Madigou, C., Bouchez, T., & Chapleur, O. (2016). Anaerobic digestion of biowaste under extreme ammonia concentration: Identification of key microbial phylotypes. *Bioresource Technology*, *207*, 92–101. doi:10.1016/j.biortech.2016.01.124

Polag, D., Heuwinkel, H., Laukenmann, S., Greule, M., & Keppler, F. (2013). Evidence of anaerobic syntrophic acetate oxidation in biogas batch reactors by analysis of 13C carbon isotopes. *Isotopes in Environmental and Health Studies*, *49*(3), 365–377. doi:10.1080/10256016.2013.805758

Polag, D., May, T., Müller, L., König, H., Jacobi, F., Laukenmann, S., & Keppler, F. (2015). Online monitoring of stable carbon isotopes of methane in anaerobic digestion as a new tool for early warning of process instability. *Bioresource Technology*, *197*, 161–170. doi:10.1016/j.biortech.2015.08.058

R Core Team. **(2013)**. *R: A language and environment for statistical computing [v3.0.1]*.

Rahman, M. M., Mostofa, M. G., Rahman, M. A., Islam, M. R., Keya, S. S., Das, A. K., Miah, M. G., Kawser, A. Q. M. R., Ahsan, S. M., Hashem, A., Tabassum, B., Abd_Allah, E. F., & Tran, L. S. P. (2019). Acetic acid: a cost-effective agent for mitigation of seawater-induced salt toxicity in mung bean. *Scientific Reports*, *9*(1), 11. doi:10.1038/s41598-019-51178-w

Rahman, M. S., Hoque, M. N., Puspo, J. A., Islam, M. R., Das, N., Siddique, M. A., Hossain, M. A., & Sultana, M. (2021). Microbiome signature and diversity

regulates the level of energy production under anaerobic condition. *Scientific Reports*, *11*(1), 19777. doi:10.1038/s41598-021-99104-3

Rahman, N., & Forrestal, P. J. (2021). Ammonium fertilizer reduces nitrous oxide emission compared to nitrate fertilizer while yielding equally in a temperate grassland. *Agriculture (Switzerland)*, *11*(11), 1141. doi:10.3390/agriculture11111141

Rajagopal, R., Massé, D. I., & Singh, G. (2013). A critical review on inhibition of anaerobic digestion process by excess ammonia. *Bioresource Technology*, *143*, 632–641. doi:10.1016/j.biortech.2013.06.030

Rato, T. J., & Reis, M. S. (2013a). Advantage of using decorrelated residuals in dynamic principal component analysis for monitoring large-scale systems. *Industrial and Engineering Chemistry Research*, *52*(38), 13685–13698. doi:10.1021/IE3035306/ASSET/IMAGES/IE-2012-035306_M032.GIF

Rato, T. J., & Reis, M. S. (2013b). Fault detection in the Tennessee Eastman benchmark process using dynamic principal components analysis based on decorrelated residuals (DPCA-DR). *Chemometrics and Intelligent Laboratory Systems*, *125*, 101–108. doi:10.1016/j.chemolab.2013.04.002

Razon, L. F. (2014). Life cycle analysis of an alternative to the haber-bosch process: Non-renewable energy usage and global warming potential of liquid ammonia from cyanobacteria. *Environmental Progress & Sustainable Energy*, *33*(2), 618–624. doi:10.1002/EP.11817

Redondo, R., MacHado, V. C., Baeza, M., Lafuente, J., & Gabriel, D. (2008). On-line monitoring of gas-phase bioreactors for biogas treatment: Hydrogen sulfide and sulfide analysis by automated flow systems. *Analytical and Bioanalytical Chemistry*, *391*(3), 789–798. doi:10.1007/s00216-008-1891-5

Reed, J. P., Devlin, D., Esteves, S. R. R., Dinsdale, R., & Guwy, A. J. (2013). Integration of NIRS and PCA techniques for the process monitoring of a sewage sludge anaerobic digester. *Bioresource Technology*, *133*, 398–404. doi:10.1016/j.biortech.2013.01.083

Reguera, G., McCarthy, K. D., Mehta, T., Nicoll, J. S., Tuominen, M. T., & Lovley, D. R. (2005). Extracellular electron transfer via microbial nanowires. *Nature*, *435*(7045), 1098–1101. doi:10.1038/NATURE03661

Reijnders, L. (2014). Phosphorus resources, their depletion and conservation, a review. *Resources, Conservation and Recycling*, *93*, 32–49. doi:10.1016/J.RESCONREC.2014.09.006

Resch, C., Wörl, A., Waltenberger, R., Braun, R., & Kirchmayr, R. (2011). Enhancement options for the utilisation of nitrogen rich animal by-products in anaerobic digestion. *Bioresource Technology*, *102*(3), 2503–2510. doi:10.1016/j.biortech.2010.11.044

Roeßler, M., & Müller, V. (2001). Osmoadaptation in bacteria and archaea: common principles and differences. *Environmental Microbiology*, *3*(12), 743–754. doi:10.1046/J.1462-2920.2001.00252.X

Romain, A.-C., & Nicolas, J. (2010). Sensors and Actuators B : Chemical Long term stability of metal oxide-based gas sensors for e-nose environmental applications : An overview. *Sensors & Actuators: B. Chemical*, *146*(2), 502–506. doi:10.1016/j.snb.2009.12.027

Romsaiyud, A., Songkasiri, W., Nopharatana, A., & Chaiprasaert, P. (2009). Combination effect of pH and acetate on enzymatic cellulose hydrolysis. *Journal of Environmental Sciences*, *21*(7), 965–970. doi:10.1016/S1001-0742(08)62369-4

Saia, F., Domingues, M., Pellizari, V., & Vazoller, R. (2010). Occurrence of methanogenic archaea in highly polluted sediments of tropical Santos-São Vicente Estuary (São Paulo, Brazil). *Current Microbiology*, *60*(1), 66–70. doi:10.1007/S00284-009-9503-Y

Santos-Fernández, E. (2012). *Multivariate statistical quality control using R*. https://books.google.fr/books?hl=fr&lr=&id=SZfRrDr7VHYC&oi=fnd&pg=PR5&dq=Santos-Fernandez+E+(2013).+Multivariate+Statistical+Quality+Control+Using+R&ots=YjYljSc-uc&sig=V4cBx3rdvLArdQuVO_6pT7E2wwE

Sarker, I. H. (2021). Deep Learning: A Comprehensive Overview on Techniques, Taxonomy, Applications and Research Directions. In *SN Computer Science* (Vol. 2, Issue 6, pp. 1–20). Springer. doi:10.1007/s42979-021-00815-1

Schink, B., Montag, D., Keller, A., & Müller, N. (2017). Hydrogen or formate: Alternative key players in methanogenic degradation. *Environmental Microbiology Reports*, *9*(3), 189–202. doi:10.1111/1758-2229.12524

Schlegel, K., & Mller, V. (2011). Sodium ion translocation and ATP synthesis in methanogens. In *Methods in Enzymology* (Vol. 494, pp. 233–255). Academic Press. doi:10.1016/B978-0-12-385112-3.00012-3

Schloss, P. D., Westcott, S. L., Ryabin, T., Hall, J. R., Hartmann, M., Hollister, E. B., Lesniewski, R. A., Oakley, B. B., Parks, D. H., Robinson, C. J., Sahl, J. W., Stres, B., Thallinger, G. G., Van Horn, D. J., & Weber, C. F. (2009). Introducing mothur: Open-source, platform-independent, community-supported software for describing and comparing microbial communities. *Applied and Environmental Microbiology*, *75*(23), 7537–7541. doi:10.1128/AEM.01541-09

Schmidt, J. E., & Ahring, B. K. (1993). Effects of hydrogen and formate on the degradation of propionate and butyrate in thermophilic granules from an upflow anaerobic sludge blanket reactor. *Applied and Environmental Microbiology*, *59*(8), 2546–2551. doi:10.1128/AEM.59.8.2546-2551.1993

Scilab Enterprises. **(2012)**. *Scilab: Free and Open Source software for numerical computation*.

Shannon, C. E. (1948). A Mathematical Theory of Communication. *Bell System Technical Journal*, *27*(3), 379–423. doi:10.1002/j.1538-7305.1948.tb01338.x

Sharma, T., Dreyer, I., & Riedelsberger, J. (2013). The role of K+ channels in uptake and redistribution of potassium in the model plant Arabidopsis thaliana. In *Frontiers in Plant Science* (Vol. 4, Issue JUN, p. 50009). Frontiers Research Foundation. doi:10.3389/fpls.2013.00224

Shewhart, W. A. (1926). Quality Control Charts. *Bell System Technical Journal*, *5*(4), 593–603. doi:10.1002/j.1538-7305.1926.tb00125.x

Shin, S. G., Zhou, B. W., Lee, S., Kim, W., & Hwang, S. (2011). Variations in methanogenic population structure under overloading of pre-acidified high-strength organic wastewaters. *Process Biochemistry*, *46*(4), 1035–1038. doi:10.1016/J.PROCBIO.2011.01.009

Sieber, J. R., McInerney, M. J., Müller, N., Schink, B., Gunsalus, R. P., & Plugge, C. M. (2018). Methanogens: Syntrophic Metabolism. *Biogenesis of Hydrocarbons*, 1–31. doi:10.1007/978-3-319-53114-4_2-1

Sikora, A., Detman, A., Mielecki, D., Chojnacka, A., & Błaszczyk, M. (2019). Searching for Metabolic Pathways of Anaerobic Digestion: A Useful List of the Key Enzymes. In *Anaerobic Digestion*. doi:10.5772/intechopen.81256

Singh, A., Moestedt, J., Berg, A., & Schnürer, A. (2021). Microbiological Surveillance of Biogas Plants: Targeting Acetogenic Community. *Frontiers in Microbiology*, *12*, 700256. doi:10.3389/fmicb.2021.700256

Singh, A., & Schnürer, A. (2022). AcetoBase Version 2: a database update and re-analysis of formyltetrahydrofolate synthetase amplicon sequencing data from anaerobic digesters. *Database*, *2022*. doi:10.1093/database/baac041

Singh, T., Ramagopal, ·, & Uppaluri, V. S. (2023). Optimizing biogas production: a novel hybrid approach using anaerobic digestion calculator and machine learning techniques on Indian biogas plant Graphical abstract. *Clean Technologies and Environmental Policy*, *25*, 3319–3343. doi:10.1007/s10098-023-02584-2

Solli, L., Håvelsrud, O. E., Horn, S. J., & Rike, A. G. (2014). A metagenomic study of the microbial communities in four parallel biogas reactors. *Biotechnology for Biofuels*, *7*(1). doi:10.1186/s13068-014-0146-2

Song, Y., Liu, C., Molitoris, D. R., Tomzynski, T. J., Lawson, P. A., Collins, M. D., & Finegold, S. M. (2003). Clostridium bolteae sp. nov., isolated from human sources. *Systematic and Applied Microbiology*, *26*(1), 84–89. doi:10.1078/072320203322337353

Spanheimer, R., & Müller, V. (2008). The molecular basis of salt adaptation in Methanosarcina mazei Gö1. *Archives of Microbiology*, *190*(3), 271–279. doi:10.1007/S00203-008-0363-9

Spanjers, H., & van Lier, J. B. (2006). Instrumentation in anaerobic treatment - Research and practice. *Water Science and Technology*, *53*(4–5), 63–76. doi:10.2166/wst.2006.111

Stams, A. J. M., De Bok, F. A. M., Plugge, C. M., Van Eekert, M. H. A., Dolfing, J., & Schraa, G. (2006). Exocellular electron transfer in anaerobic microbial communities. In *Environmental Microbiology* (Vol. 8, Issue 3, pp. 371–382). John Wiley & Sons, Ltd. doi:10.1111/j.1462-2920.2006.00989.x

Sterling, M. C., Lacey, R. E., Engler, C. R., & Ricke, S. C. (2001). Effects of ammonia nitrogen on H2 and CH4 production during anaerobic digestion of dairy cattle manure. *Bioresource Technology*, *77*(1), 9–18. doi:10.1016/S0960-8524(00)00138-3

Sundberg, C., Al-Soud, W. A., Larsson, M., Alm, E., Yekta, S. S., Svensson, B. H., Sørensen, S. J., & Karlsson, A. (2013). 454 pyrosequencing analyses of bacterial

and archaeal richness in 21 full-scale biogas digesters. *FEMS Microbiology Ecology*, *85*(3), 612–626. doi:10.1111/1574-6941.12148

Talbot, G., Topp, E., Palin, M. F., & Massé, D. I. (2008). Evaluation of molecular methods used for establishing the interactions and functions of microorganisms in anaerobic bioreactors. *Water Research*, *42*(3), 513–537. doi:10.1016/j.watres.2007.08.003

Tale, V. P., Maki, J. S., & Zitomer, D. H. (2015). Bioaugmentation of overloaded anaerobic digesters restores function and archaeal community. *Water Research*, *70*, 138–147. doi:10.1016/j.watres.2014.11.037

Ter Braak, C. J. F. (1987). The analysis of vegetation-environment relationships by canonical correspondence analysis. *Vegetatio*, *69*(1–3), 69–77. doi:10.1007/BF00038688

Thauer, R. K., Jungermann, K., & Decker, K. (1977). Energy conservation in chemotrophic anaerobic bacteria. *Bacteriological Reviews*, *41*(1), 100–180. doi:10.1128/br.41.1.100-180.1977

Theuerl, S., Herrmann, C., Heiermann, M., Grundmann, P., Landwehr, N., Kreidenweis, U., & Prochnow, A. (2019). The future agricultural biogas plant in Germany: A vision. *Energies*, *12*(3), 396. doi:10.3390/en12030396

Thiele, J. H., & Zeikus, J. G. (1988). Control of Interspecies Electron Flow during Anaerobic Digestion: Significance of Formate Transfer versus Hydrogen Transfer during Syntrophic Methanogenesis in Flocs. *Applied and Environmental Microbiology*, *54*(1), 20–29. doi:10.1128/AEM.54.1.20-29.1988

Tian, H., Treu, L., Konstantopoulos, K., Fotidis, I. A., & Angelidaki, I. (2019). 16s rRNA gene sequencing and radioisotopic analysis reveal the composition of ammonia acclimatized methanogenic consortia. *Bioresource Technology*, *272*, 54–62. doi:10.1016/j.biortech.2018.09.128

Tracy, N. D., Young, J. C., & Mason, R. L. (1992). Multivariate Control Charts for Individual Observations. *Journal of Quality Technology*, *24*(2), 88–95. doi:10.1080/00224065.1992.12015232

Utsumi, Y., Utsumi, C., Tanaka, M., Ha, C. Van, Takahashi, S., Matsui, A., Matsunaga, T. M., Matsunaga, S., Kanno, Y., Seo, M., Okamoto, Y., Moriya, E., & Seki, M. (2019). Acetic acid treatment enhances drought avoidance in cassava

(Manihot esculenta crantz). *Frontiers in Plant Science*, *10*, 521. doi:10.3389/fpls.2019.00521

Valentine, D. L. (2007). Adaptations to energy stress dictate the ecology and evolution of the Archaea. *Nature Reviews Microbiology*, *5*(4), 316–323. doi:10.1038/nrmicro1619

Valle, S., Li, W., & Qin, S. J. (1999). Selection of the number of principal components: The variance of the reconstruction error criterion with a comparison to other methods. *Industrial and Engineering Chemistry Research*, *38*(11), 4389–4401. doi:10.1021/IE990110I

Van Kessel, J. S., & Reeves, J. B. (2000). On-Farm Quick Tests for Estimating Nitrogen in Dairy Manure. *Journal of Dairy Science*, *83*(8), 1837–1844. doi:10.3168/JDS.S0022-0302(00)75054-5

Vanwonterghem, I., Jensen, P. D., Ho, D. P., Batstone, D. J., & Tyson, G. W. (2014). Linking microbial community structure, interactions and function in anaerobic digesters using new molecular techniques. *Current Opinion in Biotechnology*, *27*, 55–64. doi:10.1016/j.copbio.2013.11.004

Vyrides, I., Santos, H., Mingote, A., Ray, M. J., & Stuckey, D. C. (2010). Are Compatible Solutes Compatible with Biological Treatment of Saline Wastewater? Batch and Continuous Studies Using Submerged Anaerobic Membrane Bioreactors (SAMBRs). *Environmental Science and Technology*, *44*(19), 7437–7442. doi:10.1021/ES903981K

Wang, X., Kruger, U., Irwin, G. W., McCullough, G., & McDowell, N. (2008). Nonlinear PCA with the local approach for diesel engine fault detection and diagnosis. *IEEE Transactions on Control Systems Technology*, *16*(1), 122–129. doi:10.1109/TCST.2007.899744

Ward, A. J., Hobbs, P. J., Holliman, P. J., & Jones, D. L. (2008). Optimisation of the anaerobic digestion of agricultural resources. In *Bioresource Technology* (Vol. 99, Issue 17, pp. 7928–7940). Elsevier. doi:10.1016/j.biortech.2008.02.044

Weiland, P. (2006). Biomass Digestion in Agriculture: A Successful Pathway for the Energy Production and Waste Treatment in Germany. *Engineering in Life Sciences*, *6*(3), 302–309. doi:10.1002/elsc.200620128

Weiland, P. (2010). Biogas production: current state and perspectives. *Applied Microbiology and Biotechnology*, *85*(4), 849–860. doi:10.1007/s00253-009-2246-7

Weisburg, W. G., Barns, S. M., Pelletier, D. A., & Lane, D. J. (1991). 16S ribosomal DNA amplification for phylogenetic study. *Journal of Bacteriology*, *173*(2), 697–703. doi:10.1128/JB.173.2.697-703.1991

Werner, J. J., Garcia, M. L., Perkins, S. D., Yarasheski, K. E., Smith, S. R., Muegge, B. D., Stadermann, F. J., Derito, C. M., Floss, C., Madsen, E. L., Gordon, J. I., & Angenent, L. T. (2014). Microbial community dynamics and stability during an ammonia-induced shift to syntrophic acetate oxidation. *Applied and Environmental Microbiology*, *80*(11), 3375–3383. doi:10.1128/AEM.00166-14

Werner, J. J., Knights, D., Garcia, M. L., Scalfone, N. B., Smith, S., Yarasheski, K., Cummings, T. A., Beers, A. R., Knight, R., & Angenent, L. T. (2011). Bacterial community structures are unique and resilient in full-scale bioenergy systems. *Proceedings of the National Academy of Sciences of the United States of America*, *108*(10), 4158–4163. doi:10.1073/pnas.1015676108

Westerholm, M., Calusinska, M., & Dolfing, J. (2022). Syntrophic propionate-oxidizing bacteria in methanogenic systems. *FEMS Microbiology Reviews*, *46*(2), 1–26. doi:10.1093/FEMSRE/FUAB057

Westerhuis, J. A., Gurden, S. P., & Smilde, A. K. (2000). Generalized contribution plots in multivariate statistical process monitoring. *Chemometrics and Intelligent Laboratory Systems*, *51*(1), 95–114. doi:10.1016/S0169-7439(00)00062-9

Whitford, W., & Julien, C. (2007). Analytical Technology and PAT. *Bioprocess International*, *Jan*, 32–41.

Wijesinghe, D. T. N., Suter, H. C., Scales, P. J., & Chen, D. (2021). Lignite addition during anaerobic digestion of ammonium rich swine manure enhances biogas production. *Journal of Environmental Chemical Engineering*, *9*(1), 104669. doi:10.1016/j.jece.2020.104669

Wilkie, A. C. (2014). Biomethane from Biomass, Biowaste, and Biofuels. In *Bioenergy* (pp. 195–205). doi:10.1128/9781555815547.ch16

Winded, C., Anneser, B., Griebler, C., Meckenstock, R. U., & Lueders, T. (2008). Depth-resolved quantification of anaerobic toluene degraders and aquifer microbial community patterns in distinct redox zones of a tar oil contaminant plume. *Applied and Environmental Microbiology*, *74*(3), 792–801. doi:10.1128/AEM.01951-07

Wu, D., Li, L., Peng, Y., Yang, P., Peng, X., Sun, Y., & Wang, X. (2021). State indicators of anaerobic digestion: A critical review on process monitoring and

diagnosis. *Renewable and Sustainable Energy Reviews*, *148*, 111260. doi:10.1016/J.RSER.2021.111260

Wu, D., Li, L., Zhao, X., Peng, Y., Yang, P., & Peng, X. (2019). Anaerobic digestion: A review on process monitoring. *Renewable and Sustainable Energy Reviews*, *103*, 1–12. doi:10.1016/J.RSER.2018.12.039

Xue, S., Zhang, S., Wang, Y., Wang, Y., Song, J., Lyu, X., Wang, X., & Yang, G. (2022). What can we learn from the experience of European countries in biomethane industry: Taking China as an example? *Renewable and Sustainable Energy Reviews*, *157*, 112049. doi:10.1016/j.rser.2021.112049

Yan, M., Treu, L., Zhu, X., Tian, H., Basile, A., Fotidis, I. A., Campanaro, S., & Angelidaki, I. (2020). Insights into Ammonia Adaptation and Methanogenic Precursor Oxidation by Genome-Centric Analysis. *Environmental Science & Technology*, *54*(19), 12568–12582. doi:10.1021/acs.est.0c01945

Yang, Z., Wang, W., He, Y., Zhang, R., & Liu, G. (2018). Effect of ammonia on methane production, methanogenesis pathway, microbial community and reactor performance under mesophilic and thermophilic conditions. *Renewable Energy*, *125*, 915–925. doi:10.1016/j.renene.2018.03.032

Yang, Z., Wang, W., Liu, C., Zhang, R., & Liu, G. (2019). Mitigation of ammonia inhibition through bioaugmentation with different microorganisms during anaerobic digestion: Selection of strains and reactor performance evaluation. *Water Research*, *155*, 214–224. doi:10.1016/j.watres.2019.02.048

Yenigün, O., & Demirel, B. (2013). Ammonia inhibition in anaerobic digestion: A review. *Process Biochemistry*, *48*(5–6), 901–911. doi:10.1016/j.procbio.2013.04.012

Yiridoe, E. K., Gordon, R., & Brown, B. B. (2009). Nonmarket cobenefits and economic feasibility of on-farm biogas energy production. *Energy Policy*, *37*(3), 1170–1179. doi:10.1016/j.enpol.2008.11.018

Zhang, C., Yuan, Q., & Lu, Y. (2018). Inhibitory effects of ammonia on syntrophic propionate oxidation in anaerobic digester sludge. *Water Research*, *146*, 275–287. doi:10.1016/j.watres.2018.09.046

Zhang, L., & Zhang, D. (2015). Domain adaptation extreme learning machines for drift compensation in E-nose systems. *IEEE Transactions on Instrumentation And*, *64*(7), 1790–1801. doi:10.1109/TIM.2014.2367775

Zhang, W., Xing, W., & Li, R. (2018). Real-time recovery strategies for volatile fatty acid-inhibited anaerobic digestion of food waste for methane production. *Bioresource Technology*, *265*, 82–92. doi:10.1016/j.biortech.2018.05.098

Zhang, X., Wang, Y., Jiao, P., Zhang, M., Deng, Y., Jiang, C., Liu, X. W., Lou, L., Li, Y., Zhang, X. X., & Ma, L. (2024). Microbiome-functionality in anaerobic digesters: A critical review. In *Water Research* (Vol. 249). doi:10.1016/j.watres.2023.120891

Zhao, N., Li, X., Jin, X., Angelidaki, I., & Zhang, Y. (2018). Integrated electrochemical-biological process as an alternative mean for ammonia monitoring during anaerobic digestion of organic wastes. *Chemosphere*, *195*, 735–741. doi:10.1016/j.chemosphere.2017.12.139

Zheng, D., & Raskin, L. (2000). Quantification of Methanosaeta species in anaerobic bioreactors using genus- and species-specific hybridization probes. *Microbial Ecology*, *39*(3), 246–262. doi:10.1007/s002480000003

Zhou, H., & Qiu, G. (2006). Inhibitory effect of ammonia nitrogen on specific methanogenic activity of anaerobic granular sludge. *Journal of Central South University of Technology*, *13*(1), 63–67. doi:10.1007/s11771-006-0108-3

Zielińska, M., Cydzik-Kwiatkowska, A., Zieliński, M., & Dębowski, M. (2013). Impact of temperature, microwave radiation and organic loading rate on methanogenic community and biogas production during fermentation of dairy wastewater. *Bioresource Technology*, *129*, 308–314. doi:10.1016/j.biortech.2012.11.093

Chapter 10

Annexes

Annex 1. Anaerobic reactors and biogas monitoring systems developed for the research

The aims of this thesis involved measuring the composition of the biogas produced by semi-continuously fed pilot-scale reactors and relating this dynamic to the AD process efficiency. This required analysing the biogas composition at a sufficient frequency to capture its dynamic (unknown a priori) while allowing an acceptable analytical precision. Additionally, the measurements had to be performed simultaneously for multiple reactors operated with different feedstock compositions or organic loading rates, leading to potentially highly contrasted biogas compositions. No ready-to-use commercial biogas analyser fulfils these requirements. Moreover, the norm describing the fermentation tests for organic materials (Kaltschmitt et al., 2005) does not provide accurate guidelines regarding biogas monitoring for multiple reactors. In this context, I developed four anaerobic pilot-scale reactors, four biogas drying units, and two automatic biogas monitoring systems to conduct this research. This appendix section describes these tools.

1.1. Pilot-scale continuously stirred tank reactors

Four pilot-scale continuously stirred tank reactors (CSTRs), illustrated in **Figure A 1** and **Figure A 2**, were used for both **Exp1_FVFA_intoxication** (**Chapter 3** and **Chapter 5**) and **Exp2_FAN_intoxication** (**Chapter 4** and **Chapter 6**).

These CSTRs were home-designed and fully manufactured in stainless steel. They offered a 100-L working volume with an additional headspace volume of 20L. The stirring of the slurry was ensured by an anchor-type central stirrer driven by a brushless-type electric engine allowing a 0-120 rpm stirring rate. The lid included a biogas outlet, two transparent Plexiglas portholes, a dip tube for reactor feeding and slurry sampling, and an immersion sleeve protecting a resistance temperature detector (RTD) from the harsh environment of the slurry. The slurry was heated by hot water circulating in a lateral double-wall jacket, externally insulated to limit calorific losses. The heating water, supplied by an electric boiler, was introduced into the double-wall jacket by a circulation pump controlled by a proportional–integral–derivative temperature controller using the temperature of the slurry as an input signal. The

reactor effluents were collected at the bottom of the tank and evacuated by a lateral overflow pipe that allowed adjustment of the reactor working volume.

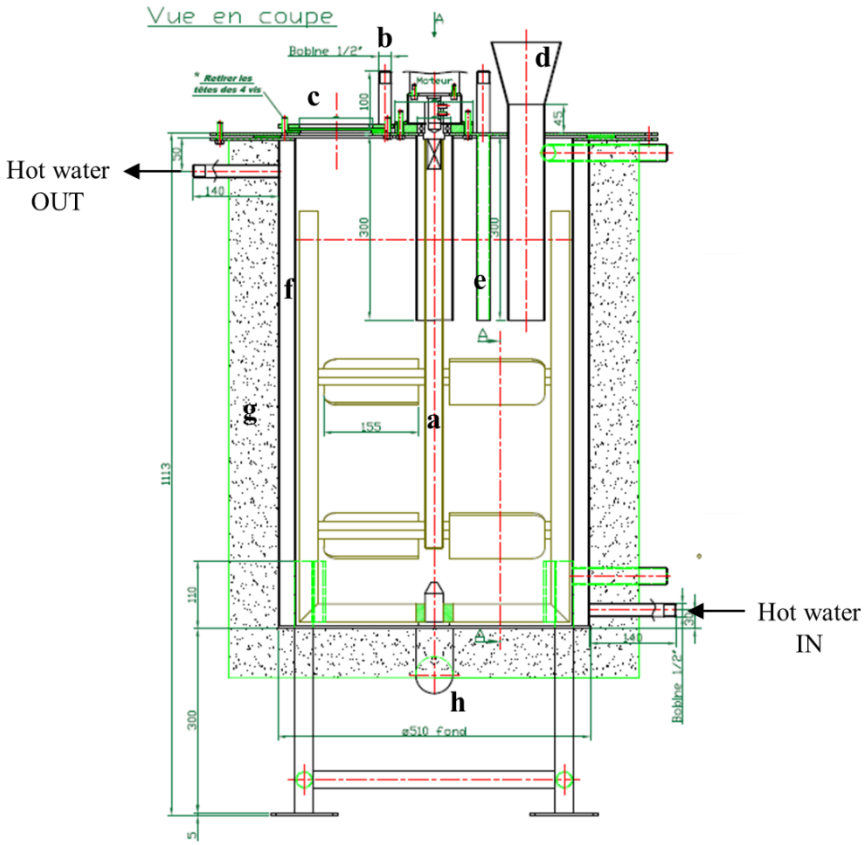

Figure A 1. 100-L continuously stirred tank reactor developed for this research: (a) anchor-type central stirrer; (b) biogas outlet; (c) transparent Plexiglas porthole; (d) dip tube used for reactor feeding and slurry sampling; (e) immersion sleeve protecting the temperature probe; (f) double-wall jacket; (g) thermal insulation; (h) effluents outlet. The dimensions are expressed in millimetres.

Figure A 2. One of the four 100-L continuously stirred tank reactor developed for this research: (a) lateral overflow pipe; (b) proportional-integrative-derivative temperature controller; (c) electric boiler; (d) circulation pump.

1.2. Biogas drying units

Before biogas composition analysis, the water content of the biogas was reduced to prevent liquid water from condensing in the tubing of the monitoring systems, especially at the level of the analytical equipment. For this purpose, four

biogas drying units were manufactured in stainless steel and placed vertically on the biogas outlet of each reactor. These drying units, illustrated in **Figure A 3**, were used for both **Exp1_FVFA_intoxication** (**Chapter 3** and **Chapter 5**) and **Exp2_FAN_intoxication** (**Chapter 4** and **Chapter 6**).

Each drying unit included a gas cooling chamber (containing a high-surface cold exchanger) and a gas sampling chamber of 600 mL. In each unit, the wet biogas first flowed through the cooling chamber, forcing the condensation of most of the water vapor content. The liquefied water was reintroduced into the reactor by gravity. Then, the dried biogas flowed through the sampling chamber, from which it was pumped for analysis. The cooling water was supplied and maintained at ~8°C by a beer cooling unit (Selbach, Germany). This type of equipment is highly robust and allows continuous production of cold water at a minor cost.

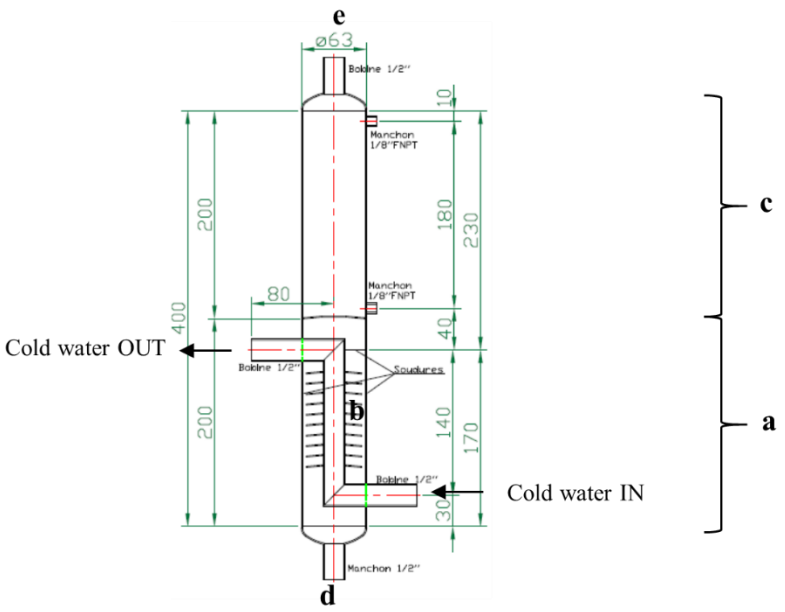

Figure A 3. Biogas drying units manufactured in stainless steel for the four continuously stirred tank reactors: (a) biogas cooling chamber; (b) high-surface cold exchanger; (c) biogas sampling chamber; (d) wet biogas inlet (reactor headspace); (e) dried biogas outlet. The dimensions are expressed in millimetres.

1.3. Biogas monitoring systems

For this research, I developed two biogas monitoring systems controlled by a personal computer equipped with a low-cost data acquisition card. For each system, I programmed a software interface that allowed control of data acquisition and storage of collected measurements in a database.

1.3.1. Biogas monitoring system N° 1

This first biogas monitoring system allowed automatic measurement of the production and composition (CH_4, CO_2, H_2S, and H_2) of the biogas released by up to four reactors operated simultaneously. This system, illustrated in **Figure A 4** and schematized in **Figure A 5**, was used to measure the biogas production and composition of the four CSTRs during **Exp1_FVFA_intoxication** (**Chapter 3** and **Chapter 5**).

Figure A 4. Biogas monitoring system N° 1 developed in the framework of this research (the system is placed in centred position among the four 100L continuously stirred tank reactors).

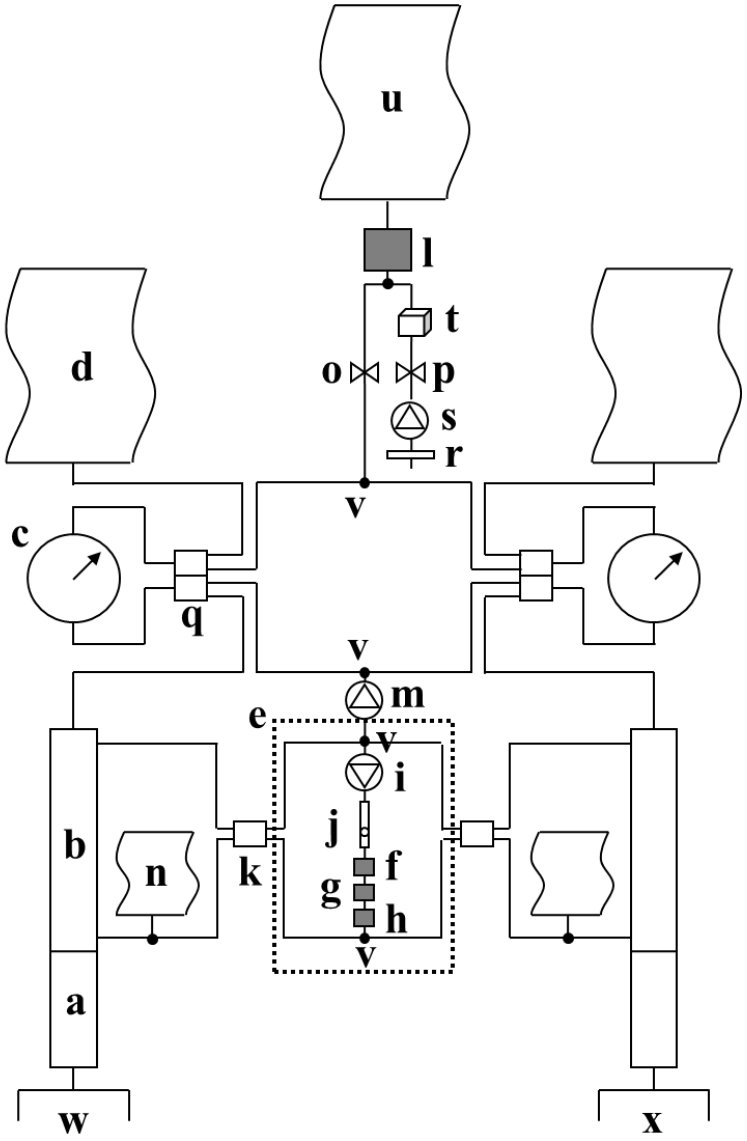

Figure A 5. Biogas monitoring system N° 1 developed in the framework of this research: (a) cooling chamber of the biogas drying unit; (b) sampling chamber of the biogas drying unit; (c) drum-type wet gas meter; (d) biogas storage bag; (e) recirculation loop; (f) CH_4 gas sensor; (g) CO_2 gas sensor; (h) H_2S gas sensor; (i) diaphragm pump; (j) rotameter with regulation valve; (k) pinch-type solenoid valve; (l) H_2 gas sensor; (m) diaphragm pump; (n) 10L gas buffer bag; (o,p) precision regulation valves; (q) pinch-type solenoid valve; (r) dust filter; (s) diaphragm pump; (t) thermal mass flow meter; (u) gas storage bag; (v) manifolds; (w) headspace reactor 1; (x) headspace reactor 2. For clarity, the system is presented for only two reactors, whereas it allowed biogas monitoring for up to four reactors.

1.3.1.1. Working principle and key components

The working principle of biogas monitoring system No. 1 is presented in **Figure A 6** and involves: (1) the online measurement of biogas production, which is continuously performed, and (2) regularly triggered measurement cycles during which the biogas composition is analyzed for each reactor.

*(a) Online measurement of the biogas production (***Figure A 6***a,d)*

The biogas produced by the reactors flows continuously through a gas drying unit, a drum-type wet gas meter (TG-0.5 Ritter, Germany) (**Figure A 5**c), and is finally collected in a 200-L gas storage bag (Tecobag, Tesseraux, Germany) (**Figure A 5**d). Each gas meter is equipped with a digital pulse generator allowing data acquisition.

*(b) Biogas composition analysis cycles (***Figure A 6***b,c)*

At regular intervals for each reactor successively, the produced biogas is sampled from the sampling chamber of the drying unit and injected into a recirculation loop (**Figure A 5**e). The recirculation loop includes gas sensors measuring the concentration of CH_4, CO_2, and H_2S in biogas. The concentrations of CH_4 and CO_2 are measured in the 0-100%v range using non-dispersive infrared (NDIR) gas sensors (Dynament, UK) (**Figure A 5**f,g). The concentration of H_2S is measured in the 0-10000 ppmv range using an electrochemical gas sensor (I-42, itg, Germany) (**Figure A 5**h). The connection between the biogas sources and the recirculation loop is controlled by pinch-type solenoid valves (Bio-Chem, Germany) (**Figure A 5**k).

The concentration of H_2 in the biogas is measured using a metal oxide semiconductor (MOS) sensor equipped with a molecular sieve to ensure selectivity to H_2 molecules (65-2442RK, RKI Instruments, USA) (**Figure A 5**l). This sensor requires the presence of oxygen in the gas sample. Since biogas is anoxic, the H_2 sensor is not included in the recirculation loop. Instead, biogas is pumped from the recirculation loop and mixed with ambient air; then the resulting gas mixture is supplied to the H_2 sensor cell. The volumetric mixing ratio between the biogas and the air is measured to calculate the H_2 concentration in the raw biogas. The biogas flow is volumetrically measured using the drum-type wet gas meter of the reactor. The air mass flow is measured by a thermal mass flow meter (AWM3100V,

Honeywell, USA) (**Figure A 5**t), and the corresponding volumetric flow is calculated using the conversion factor provided by the manufacturer. To prevent pressure drop in the reactor headspace due to biogas sampling, a 10-L buffer bag (Tecobag, Tesseraux, Germany) (**Figure A 5**n) is connected to the outlet of each biogas sampling chamber. At the outlet of the H_2 sensor cell, the gas mixture is finally collected in a 100-L storage bag (**Figure A 5**u) that is emptied manually when needed.

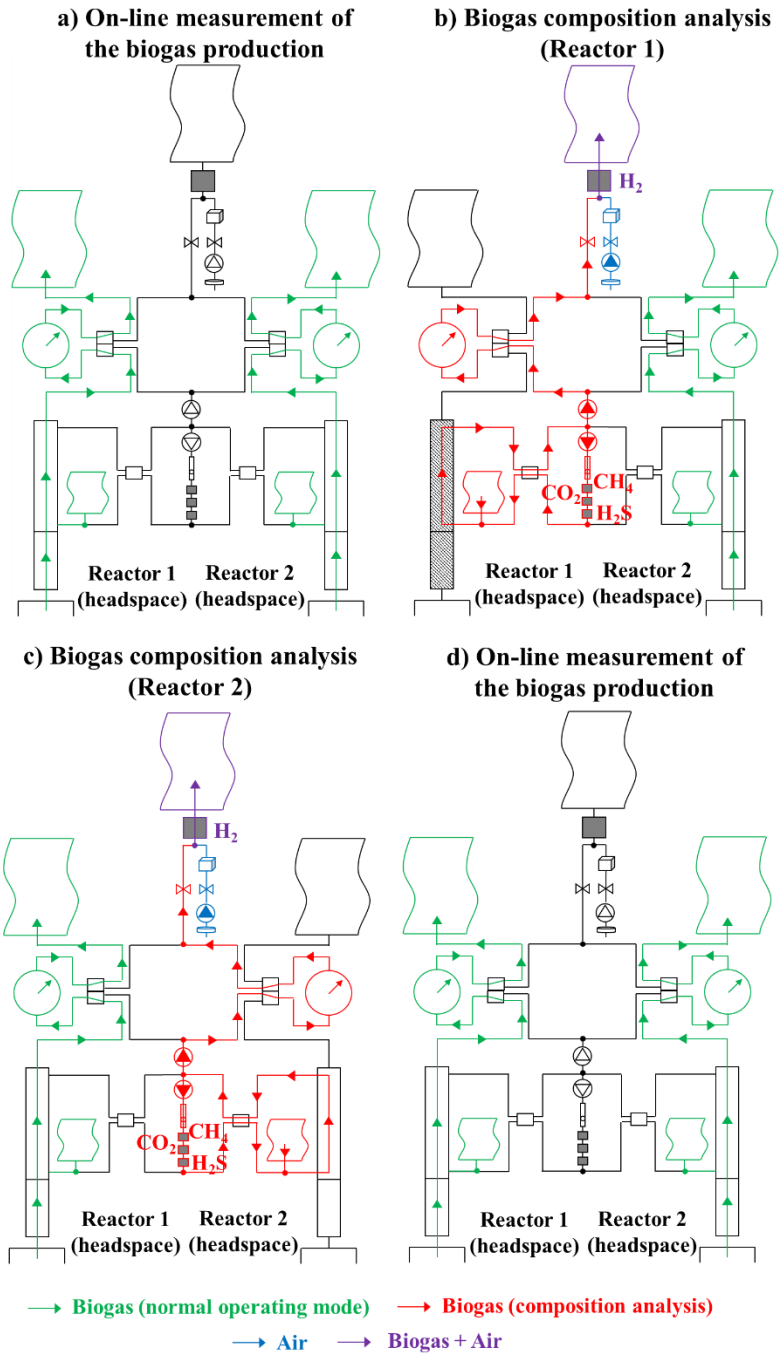

Figure A 6. Working principle of the biogas monitoring system N° 1 developed in the framework of this research. For clarity, the system is presented for only two reactors, whereas it allowed biogas monitoring for up to four reactors.

1.3.1.2. Limitations of the biogas monitoring system N° 1

- An independent drum-type wet gas meter is required to measure the biogas production of each reactor. Since these gas meters are highly expensive (~3000€/unit), the use of the biogas monitoring system No. 1 is limited to the simultaneous connection of a restricted number of reactors.
- The method used to normalize biogas production to normal conditions of temperature and pressure presents practical and analytical limitations. Indeed, the atmospheric pressure is not measured on-site but by a governmental meteorological station (Oberkorn, Luxembourg) located close to the laboratory (3 km).
- Mixing biogas with air for H_2 concentration analysis could generate explosive gas mixtures.
- The H_2S electrochemical sensor has a low response time compared to the CH_4 and CO_2 NDIR sensors and the MOS H_2 sensor used in the biogas analyzing system No. 1. Indeed, according to the sensor manufacturers, the response time at t90 (i.e. the time taken by a sensor to reach 90% of its final stable reading) of the H_2S electrochemical sensor is 90 seconds, whereas it is only 30 seconds for the CH_4 and CO_2 NDIR sensors and 20 seconds for the H_2 MOS sensor. Therefore, inaccurate H_2S measurements were observed during **Exp1_FVFA_intoxication** when the sensor cell was exposed to successive biogas samples presenting highly contrasted H_2S concentrations (**Figure A 7**). For this reason, the H_2S concentration in the biogas was not used as an individual process variable to build the MSPC models in **Chapter 3**.

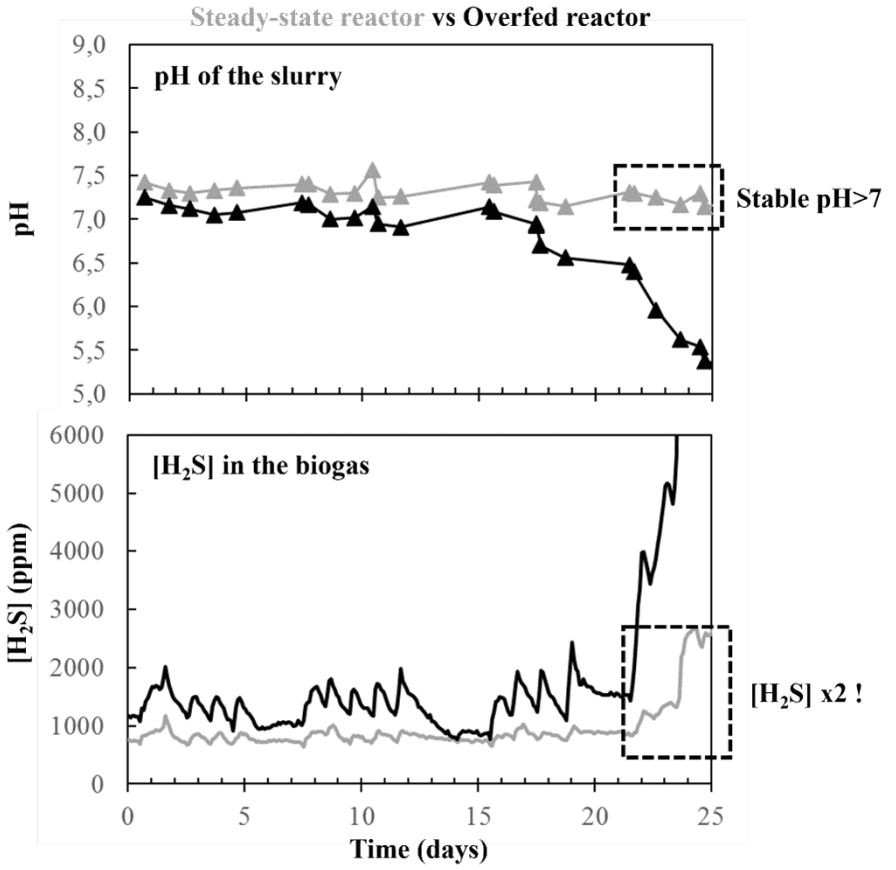

Figure A 7. During **Exp1_FVFA_intoxication**, the high difference of H_2S concentrations between the biogas produced by the steady-state reactor and the overfed reactor caused interferences in the measurements performed by the electro-chemical H_2S sensor.

1.3.2. Biogas monitoring system N° 2

Measuring online the biogas production of a high number of reactors using drum-type wet gas meters is highly expensive. However, an alternative consists of temporarily storing the biogas produced by each reactor and then measuring the volume of the stored biogas using a unique drum-type wet gas meter successively for each reactor. Following this approach, I developed the biogas monitoring system No. 2, which allowed automatic measurement of the biogas production and its composition (CH_4, CO_2, H_2S, and H_2) for up to 16 simultaneously operated reactors. I also integrated a gas chromatograph in this second biogas monitoring system to: (1)

improve the H_2S quantification when analysing successive biogas samples presenting highly different H_2S concentrations, and (2) avoid generating potentially explosive gas mixtures required for H_2 quantification with a MOS sensor. Finally, I integrated a digital barometer to make the normalization of biogas production more accurate, immediate, and less time-consuming.

This second biogas monitoring system, illustrated in illustrated in **Figure A 8**, **Figure A 9** and **Figure A 10**, was used to measure the biogas production and composition of the four CSTRs during **Exp2_FAN_intoxication** (**Chapters 4 and 6**). Simultaneously, four anaerobic baffled reactors, including three sections, were monitored using this system (data not presented), bringing the total number of simultaneously monitored biogas sources to 16.

Figure A 8. Main unit of the biogas monitoring system N° 2 developed in the framework of this research.

Figure A 9. Biogas monitoring system N° 2: gas bags used to store temporarily the biogas produced by the reactors.

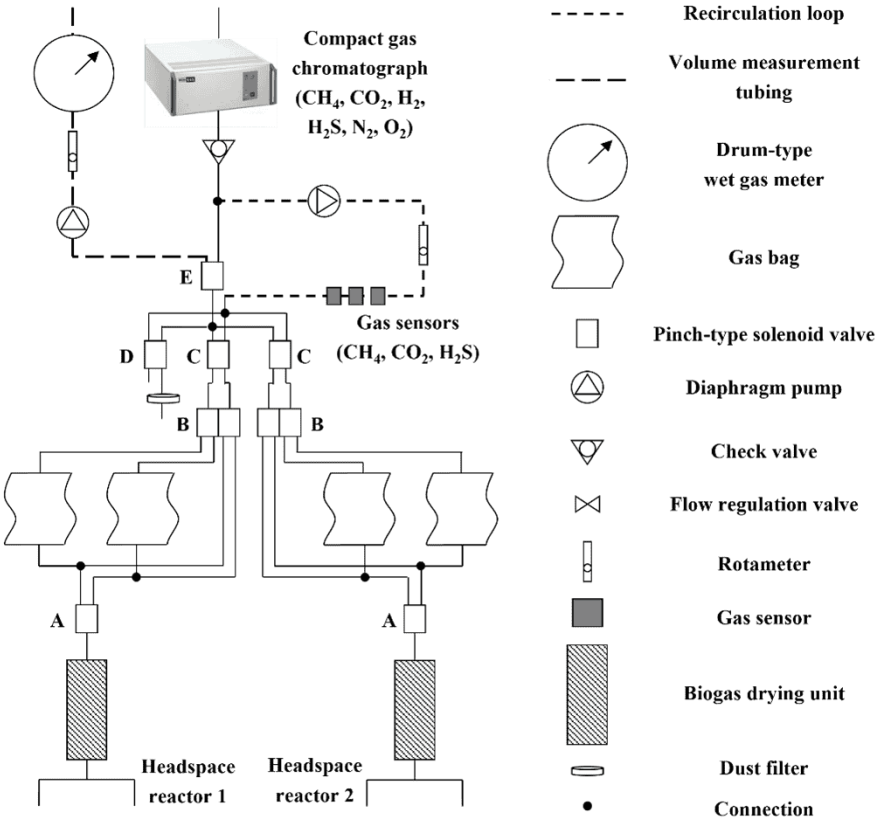

Figure A 10. Biogas monitoring system N° 2. The biogas produced by the reactors is continuously collected in gas bags that are put in connection with the analytic equipment during measurement cycles. The gas flows in the system are controlled by pinch-type solenoid valves that allow: (A) to select the gas bag collecting the biogas; (B) to select the gas bag connected to the analytic equipment; (C) to select the reactor for which the biogas is analysed; (D) to connect the recirculation loop to ambient air; (E) to switch between the biogas composition analysis and the volume measurement; (F) to close the recirculation loop during the volume measurement. For clarity, the system is presented for only two reactors, whereas it allowed biogas monitoring for up to 16 reactors.

1.3.2.1. Working principle and key components

The working principle of the biogas monitoring system No. 2 is presented in **Figure A 11** and **Figure A 12** and described hereafter.

1.3.2.2. Normal operating mode (Figure A 11a ; Figure A 12a)

In normal operating mode (a), the biogas produced by each reactor flows through a biogas drying unit, and the dried biogas is temporarily stored in an 80-L gas bag (Tecobag, Tesseraux, Germany). For each reactor, two gas bags are present and can be connected in turns to the reactor headspace. Doubling the gas bags allows storing the biogas produced by the reactors while the content of the other bag is analyzed for volume and composition.

1.3.2.3. Measurement cycles (Figure A 11b,c,d ; Figure A 12b,c,d)

At regular intervals, measurement cycles are automatically triggered during which successively for each reactor: (b) the biogas content of the bag is analyzed for concentrations in CH_4, CO_2, H_2S, and H_2; (c) ambient air is injected into the sensor cells to allow them to recover; (d) the biogas volume contained in the bag is measured:

(b) *Biogas composition analysis* (**Figure A 11**b; **Figure A 12**b)

First, the gas content of the bag is pumped through a recirculation loop using a diaphragm pump (Schego, Germany) until proper mixing in the sampling tubing. Then about 50 mL of biogas is pumped from the recirculation loop to a three-channel gas chromatograph (CompactGC global analyzer solutions™, Interscience, Belgium) to analyze the CH_4, CO_2, H_2, and H_2S concentrations. Specific gas sensors equivalent to those used in biogas monitoring system No. 1 are placed in the recirculation loop, allowing measurement of the CH_4, CO_2, and H_2S concentrations in the biogas during CompactGC maintenance. A rotameter (Cole-Parmer, USA) equipped with a regulation valve allows setting the biogas flow through the gas sensor cells. After the composition analysis, the gas concentrations measured by the GC and the specific sensors are stored in a database.

(c) *Purge of the recirculation loop* (**Figure A 11**c; **Figure A 12**c)

The recirculation loop is flushed with ambient air to allow the sensor cells to recover after being exposed to biogas.

(d) *Biogas production measurement* (**Figure A 11**d; **Figure A 12**d)

The gas stored in the bag is pumped using a high-flow (10 L min^{-1}) diaphragm pump (Secoh, Japan) and injected in a drum-type wet gas meter equipped with a digital pulse generator (TG-5, Ritter, Germany). The atmospheric pressure and the temperature of the water filling the gas meter are measured using a digital barometer (Dr.A.Müller, Germany) and a resistance temperature detector (RTD), respectively. The digital pulses generated by the gas meter are continuously sensed until the gas bag is empty, which is detected by a sharp decrease of the gas pulses frequency. This event triggers: (1) the numeric storage of the measurements corresponding to the gas volume, the gas temperature, and the atmospheric pressure; (2) the automatic normalization of the measured gas volume; (3) the repetition of the step (b), (c) and (d) for the next reactor.

The gas stored in the bag is pumped using a high-flow (10 L/min) diaphragm pump (Secoh, Japan) and injected into a drum-type wet gas meter equipped with a digital pulse generator (TG-5, Ritter, Germany). The atmospheric pressure and the temperature of the water filling the gas meter are measured using a digital barometer (Dr.A.Müller, Germany) and a resistance temperature detector (RTD), respectively. The digital pulses generated by the gas meter are continuously sensed until the gas bag is empty, which is detected by a sharp decrease in the gas pulse frequency. This event triggers: (1) the numeric storage of the measurements corresponding to the gas volume, gas temperature, and atmospheric pressure; (2) the automatic normalization of the measured gas volume; (3) the repetition of steps (b), (c), and (d) for the next reactor.

(e) *Purge of the GC* (**Figure A 12**e)

For the last monitored reactor, after the biogas production measurement, the GC is allowed to pump ambient air to preserve its internal parts from corrosion due to H_2S.

When a measurement cycle is completed, the biogas monitoring system switches back to the normal operating mode (a).

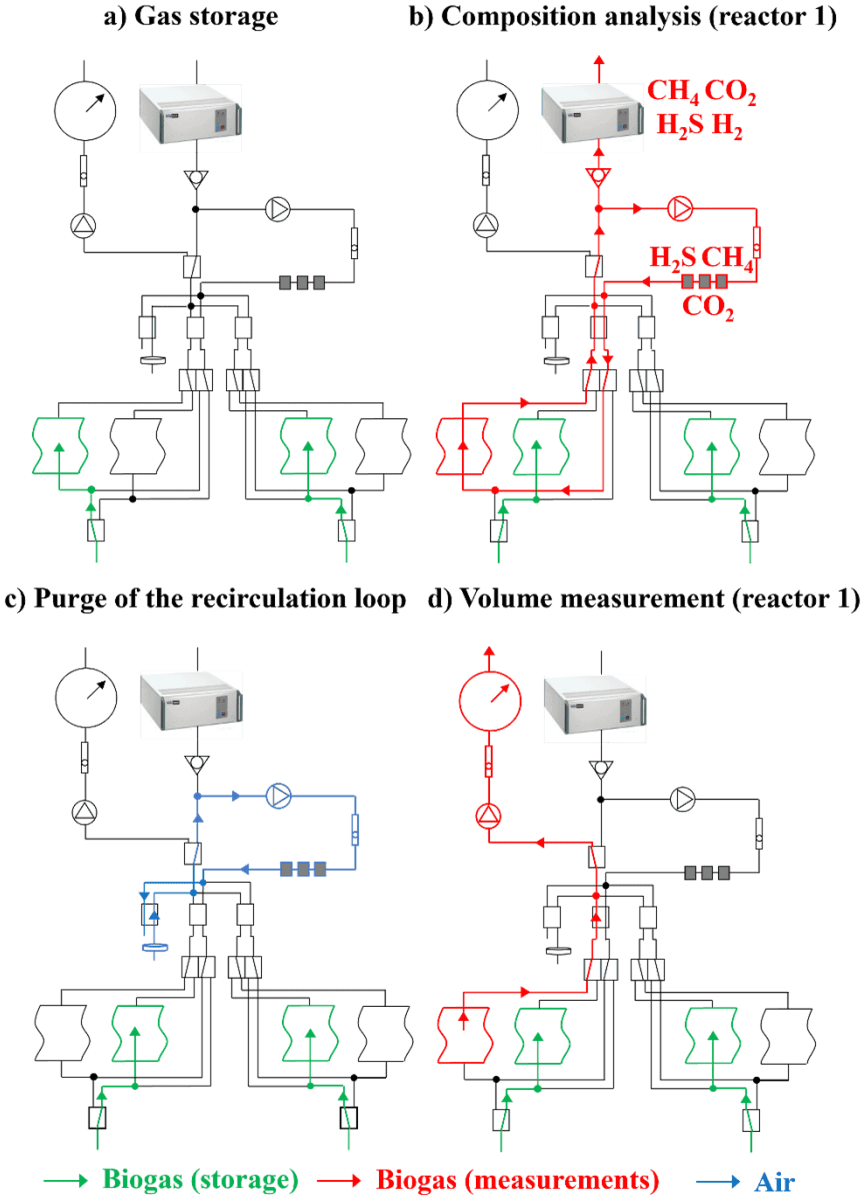

Figure A 11. Working principle of the biogas monitoring system N° 2 (1/2). For clarity, the system is presented for two reactors whereas it allowed biogas monitoring for up to 16 reactors.

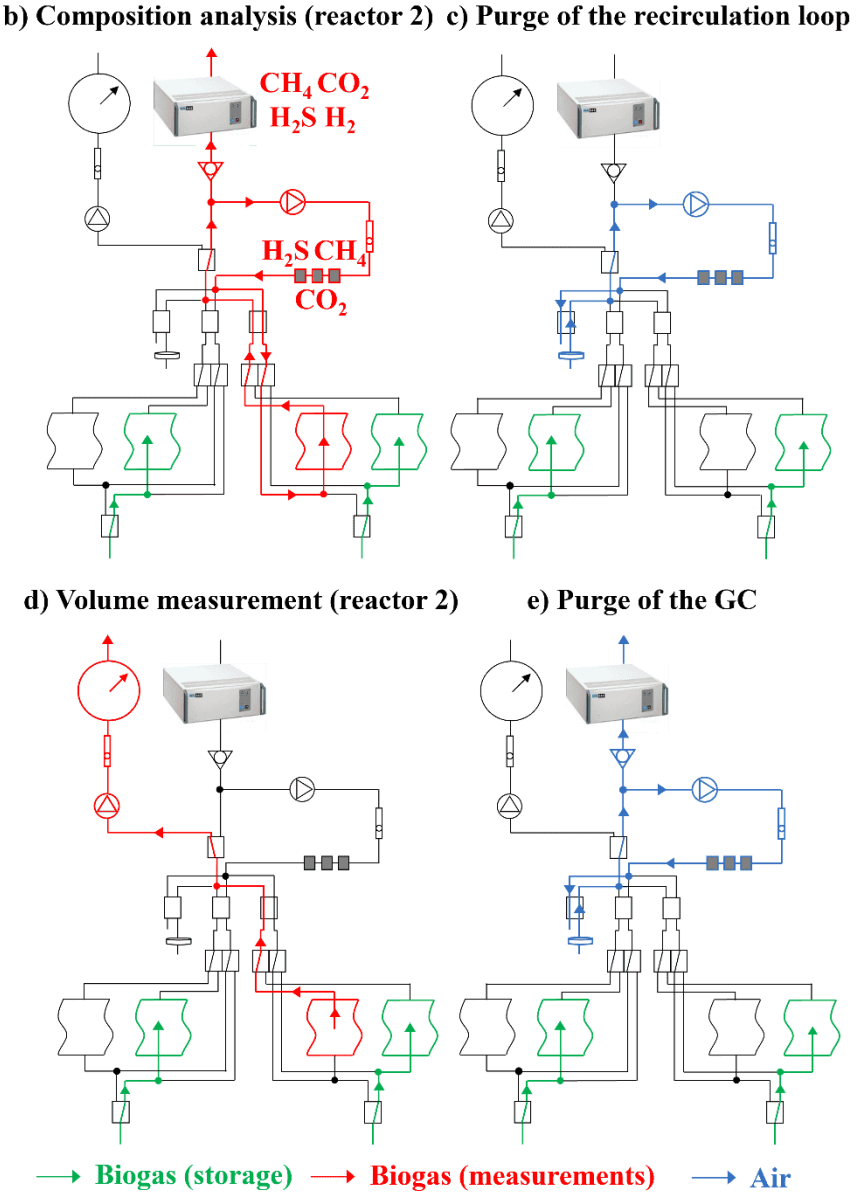

Figure A 12. Working principle of the biogas monitoring system N° 2 (2/2). For clarity, the system is presented for only two reactors whereas it allowed the biogas monitoring for up to 16 reactors.

Annex 2. Supplementary material of Chapter 4

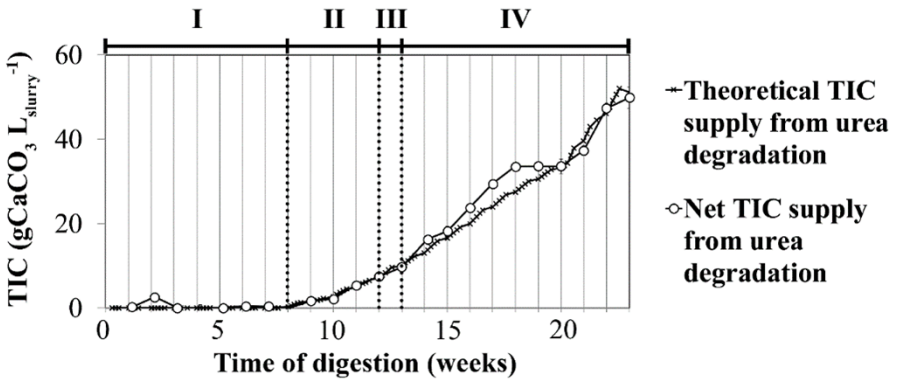

Figure Ch4_S 1. Comparison between the theoretical value of the supply of total inorganic carbon (TIC) due to urea degradation and the measured value of the net TIC supply from urea degradation in the slurry of the high nitrogen input reactors (TIC_{HNRS} minus TIC_{LNR}). I, II, III and IV correspond to the phases described in **Table 4.1**.

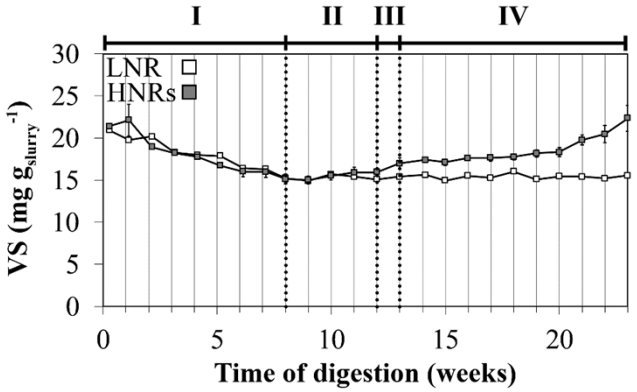

Figure Ch4_S 2. Progress over time of the volatile solids (VS) content in the slurry of the reactors. I, II, III and IV correspond to the phases described in **Table 4.1**. HNRs: high nitrogen input reactors; LNR: low nitrogen input reactor.

Annex 3. Supplementary material of Chapter 5

Table Ch5_S 1. Alpha diversity of the bacterial and archaeal communities in the four reactors.

		SSR			OR1			OR2			OR3		
	Sampling period	*H'*	*J*	*Richness*	*H'*	*J*	*Richness*	*H'*	*J*	*Richness*	*H'*	*J*	*Richness*
Bacteria T-RFLP	P0	2.71 ± 0.20 a	0.87 ± 0.04 c	8.7 ± 0.6 a	2.96 ± 0.13 b	0.89 ± 0.00 d	10.0 ± 1.0 ab	2.37 ± 0.10 ab	0.85 ± 0.03 b	7.0 ± 1.0 a	2.63 ± 0.07 c	0.83 ± 0.02 b	9.0 ± 0.0 b
	P1	2.74 ± 0.05 a	0.81 ± 0.00 ab	10.3 ± 0.6 a	3.04 ± 0.03 b	0.88 ± 0.01 c	11.0 ± 0.0 b	2.27 ± 0.06 a	0.74 ± 0.01 a	8.3 ± 0.6 b	2.62 ± 0.03 c	0.83 ± 0.01 b	9.0 ± 0.0 b
	P2	2.62 ± 0.08 a	0.81 ± 0.00 ab	9.3 ± 0.6 a	2.69 ± 0.01 a	0.85 ± 0.00 b	9.0 ± 0.0 a	2.83 ± 0.02 c	0.82 ± 0.01 b	11.0 ± 0.0 c	2.48 ± 0.07 bc	0.86 ± 0.01 cd	7.3 ± 0.6 a
	P3	2.73 ± 0.05 a	0.85 ± 0.01 bc	9.3 ± 0.6 a	3.01 ± 0.01 b	0.91 ± 0.00 e	10.0 ± 0.0 ab	2.47 ± 0.25 ab	0.83 ± 0.03 b	8.0 ± 1.0 ab	3.08 ± 0.00 d	0.89 ± 0.00 d	11.0 ± 0.0 c
	P4	2.45 ± 0.42 a	0.81 ± 0.03 ab	8.3 ± 2.3 a	2.65 ± 0.05 a	0.81 ± 0.01 a	9.7 ± 0.6 a	2.78 ± 0.08 c	0.82 ± 0.01 b	10.3 ± 0.6 c	2.16 ± 0.26 a	0.76 ± 0.02 a	7.3 ± 1.5 a
	P5	2.32 ± 0.01 a	0.77 ± 0.00 a	8.0 ± 0.0 a	3.21 ± 0.00 c	0.93 ± 0.00 f	11.0 ± 0.0 b	2.50 ± 0.05 b	0.85 ± 0.02 b	7.7 ± 0.6 ab	2.37 ± 0.02 ab	0.84 ± 0.00 bc	7.0 ± 0.0 a
Bacteria HTS	P0	4.74	0.6	242	4.97	0.62	263	3.54	0.46	216	4.52	0.57	247
	P1	4.09	0.52	246	4.96	0.57	239	4.08	0.51	268	4.35	0.55	248
	P2	4.22	0.53	245	4.06	0.53	203	3.54	0.47	193	3.9	0.5	216
	P3	4.04	0.51	239	-	-	-	4.04	0.53	194	4.37	0.57	212
	P4	3.42	0.44	209	-	-	-	3.9	0.51	194	4.19	0.55	205
	P5	4.06	0.51	239	5.16	0.65	249	4.24	0.55	199	4.97	0.63	229
Archaea T-RFLP	P0	1.09 ± 0.15 ac	0.52 ± 0.03 bc	4.3 ± 0.6 a	1.35 ± 0.00 ab	0.00 ± 0.00 a	6.0 ± 0.0 ab	0.58 ± 0.00 a	0.36 ± 0.00 a	3.0 ± 0.0 ab	1.21 ± 0.11 b	0.53 ± 0.05 bc	5.0 ± 1.4 ab
	P1	0.83 ± 0.07 a	0.41 ± 0.03 a	4.0 ± 0.0 a	1.17 ± 0.15 a	0.51 ± 0.00 b	5.0 ± 1.0 a	1.00 ± 0.07 a	0.50 ± 0.03 a	4.0 ± 0.0 b	0.84 ± 0.14 ab	0.42 ± 0.07 ab	4.0 ± 0.0 a
	P2	1.10 ± 0.18 ac	0.49 ± 0.04 ab	4.7 ± 0.6 a	1.87 ± 0.29 bc	0.68 ± 0.08 c	6.7 ± 0.6 ac	1.80 ± 0.08 b	0.66 ± 0.04 b	6.7 ± 0.6 bc	0.61 ± 0.19 a	0.32 ± 0.07 a	3.7 ± 0.6 a
	P3	1.31 ± 0.33 bc	0.53 ± 0.05 bc	5.7 ± 1.3 a	2.30 ± 0.33 cd	0.71 ± 0.05 c	9.3 ± 1.5 b	2.60 ± 0.64 c	0.80 ± 0.07 c	9.7 ± 3.2 c	1.72 ± 0.07 c	0.61 ± 0.02 cd	7.0 ± 0.0 cd
	P4	0.96 ± 0.11 ab	0.46 ± 0.03 ab	4.3 ± 0.6 a	1.80 ± 0.24 bc	0.61 ± 0.06 bc	7.7 ± 1.5 bc	2.31 ± 0.16 bc	0.79 ± 0.01 c	7.7 ± 1.2 ac	1.71 ± 0.22 c	0.59 ± 0.06 cd	7.3 ± 0.6 d
	P5	1.38 ± 0.21c	0.59 ± 0.09 c	5.0 ± 0.0 a	2.85 ± 0.08 d	0.87 ± 0.00 d	9.7 ± 0.6 b	1.94 ± 0.20 bc	0.68 ± 0.04 b	7.3 ± 0.6 bc	1.66 ± 0.15 c	0.67 ± 0.03 d	5.7 ± 0.6 bc
Archaea HTS	P0	2.66	0.8	10	2.77	0.77	12	2.25	0.65	11	2.66	0.77	11
	P1	2.38	0.72	10	2.48	0.69	12	2.66	0.84	9	2.3	0.69	10
	P2	2.22	0.67	11	2.35	0.66	12	2.53	0.76	10	2.14	0.6	12
	P3	2.28	0.66	11	-	-	-	2.69	0.75	12	1.64	0.46	12
	P4	2.37	0.68	11	-	-	-	2.67	0.8	10	1.49	0.4	13
	P5	2.11	0.59	12	2.67	0.84	9	2.24	0.65	11	1.29	0.35	13

H': Shannon-Weaver diversity index; J: Pielou evenness index; P0-P5: sampling periods; SSR: steady-state reactor used as control; OR1-OR3: test reactors exposed to increasing organic loading rate, FVFA intoxication and process recovery; T-RFLP: results from the 16S rRNA gene-based T-RFLP analysis; HTS: results from the high-throughput 16S rRNA amplicon sequencing. Statistical analyses were performed using linear mixed-effects models combined to a pairwise test (Tukey) for results of the 16S rRNA gene-based T-RFLP analysis; values holding the same letter in a column and for one taxonomic domain (Bacteria or Archaea) do not differ significantly ($p \leq 0.05$); there were no replicate for the HTS analysis.

Table Ch5_S2 (Abundance levels and taxonomic affiliation of the bacterial OTUs), **Table Ch5_S3** (Abundance levels and taxonomic affiliation of the archaeal OTUs) and **Table Ch5_S4** (Spearman correlation matrix for the relationships between the process parameters and the archaeal community diversity) are available in an excel file by following this link:
http://www.biotechnologyforbiofuels.com/content/supplementary/s13068-015-0309-9-s2.xlsx

Annex 4. Supplementary material of Chapter 6

Table Ch6_S 1. Taxonomic affiliation of the top 50 bacterial OTUs[18] presented in **Figure 6.4**.

OTUs	Phylum	Class	Order	Family	Genus
OTU_1	*Bacteroidota* (100)	*Bacteroidia* (100)	*Bacteroidales* (100)	*Paludibacteraceae* (100)	uncultured (100)
OTU_10	*Bacteroidota* (100)	*Bacteroidia* (100)	*Bacteroidales* (100)	*Bacteroidaceae* (100)	*Bacteroides* (100)
OTU_100	*Firmicutes* (100)	*Clostridia* (100)	*Oscillospirales* (99)	*Oscillospirales*_unclassified (99)	*Oscillospirales*_unclassified (99)
OTU_11	*Firmicutes* (100)	*Clostridia* (100)	*Lachnospirales* (100)	*Lachnospiraceae* (100)	*Lachnospiraceae*_unclassified (100)
OTU_113	*Firmicutes* (100)	*Clostridia* (100)	*Clostridia*_or (99)	*Hungateiclostridiaceae* (99)	*Hungateiclostridiaceae*_unclassified (99)
OTU_12	*Firmicutes* (100)	*Limnochordia* (100)	*MBA03* (100)	*MBA03*_fa (100)	*MBA03*_ge (100)
OTU_13	*Firmicutes* (100)	*Clostridia* (99)	*Caldicoprobacterales* (80)	*Caldico probacteraceae* (80)	*Caldicoprobacter* (80)
OTU_14	*Desulfobacterota* (100)	*Syntrophia* (100)	*Syntrophales* (100)	*Smithellaceae* (100)	*Smithella* (100)
OTU_15	*Firmicutes* (100)	*Clostridia* (100)	*Caldicoprobacterales* (100)	*Caldicoprobacteraceae* (100)	*Caldicoprobacter* (100)

[18] The numbers in brackets indicate the percentages of sequence identity.

OTU_1524	*Cloacimonadota* (100)	*Cloacimonadia* (100)	*Cloacimonadales* (100)	*Cloacimonadaceae* (100)	*Candidatus*_Cloacimonas (100)
OTU_16	*Firmicutes* (100)	*Clostridia* (100)	*Caldicoprobacterales* (100)	*Caldicoprobacteraceae* (100)	*Caldicoprobacter* (100)
OTU_17	*Bacteroidota* (100)	*Bacteroidia* (100)	*Bacteroidales* (100)	*Rikenellaceae* (100)	*DMER64* (100)
OTU_1797	*Bacteroidota* (100)	*Bacteroidia* (100)	*Bacteroidales* (100)	*Prolixibacteraceae* (100)	uncultured (99)
OTU_18	*Firmicutes* (100)	*Limnochordia* (100)	*Limnochordales* (100)	uncultured (100)	uncultured (100)
OTU_19	*Bacteroidota* (100)	*Bacteroidia* (100)	*Bacteroidales* (100)	*Paludibacteraceae* (100)	*Paludibacter* (100)
OTU_2	*Bacteroidota* (100)	*Bacteroidia* (100)	*Bacteroidales* (100)	*Prolixibacteraceae* (100)	uncultured (100)
OTU_20	*Spirochaetota* (99)	*Spirochaetia* (99)	*Spirochaetales* (99)	*Spirochaetaceae* (99)	*Sphaerochaeta* (97)
OTU_21	*Bacteroidota* (100)	*Bacteroidia* (100)	*Bacteroidales* (100)	*Bacteroidetes_vadinHA17* (100)	*Bacteroidetes_vadinHA17*_ge (100)
OTU_2391	*Firmicutes* (96)	*Limnochordia* (82)	*Limnochordia*_unclassified (82)	*Limnochordia*_unclassified (82)	*Limnochordia*_unclassified (82)
OTU_24	*Bacteroidota* (100)	*Bacteroidia* (100)	*Bacteroidales* (100)	*Prevotellaceae* (100)	*Prevotella* (99)
OTU_25	*Planctomycetota* (100)	*Phycisphaerae* (100)	*MSBL9* (100)	*SG8-4* (100)	*SG8-4*_ge (100)
OTU_27	*Cloacimonadota* (100)	*Cloacimonadia* (100)	*Cloacimonadales* (100)	*Cloacimonadaceae* (100)	*W5* (100)
OTU_28	*Cloacimonadota* (100)	*Cloacimonadia* (100)	*Cloacimonadales* (100)	*Cloacimonadaceae* (100)	*Candidatus*_Cloacimonas (98)

OTU_29	*Acidobacteriota* (100)	*Aminicenantia* (99)	*Aminicenantales* (99)	*Aminicenantales*_fa (99)	*Aminicenantales*_ge (99)
OTU_3	*Spirochaetota* (100)	*Spirochaetia* (100)	*Spirochaetales* (100)	*Spirochaetaceae* (100)	uncultured (100)
OTU_30	*Chloroflexi* (100)	*Anaerolineae* (100)	*SJA-15* (100)	*SJA-15*_fa (100)	*SJA-15*_ge (100)
OTU_31	*Firmicutes* (100)	*Limnochordia* (100)	*Limnochordales* (100)	uncultured (100)	uncultured (100)
OTU_32	*Acidobacteriota* (100)	*c5LKS83* (100)	*c5LKS83*_or (100)	*c5LKS83*_fa (100)	*c5LKS83*_ge (100)
OTU_33	*Firmicutes* (100)	*Clostridia* (100)	*Clostridia*_or (100)	*Hungateiclostridiaceae* (100)	*HN-HF0106* (100)
OTU_35	*Firmicutes* (100)	*Clostridia* (97)	*Lachnospirales* (97)	*Lachnospiraceae* (97)	*Lachnospiraceae*_unclassified (97)
OTU_36	*Spirochaetota* (98)	*Spirochaetia* (98)	*Spirochaetales* (98)	*Spirochaetaceae* (98)	*Sphaerochaeta* (93)
OTU_37	*Bacteroidota* (100)	*Bacteroidia* (100)	*Bacteroidales* (100)	*Dysgonomonadaceae* (100)	*Proteiniphilum* (100)
OTU_4	*Firmicutes* (100)	*Clostridia* (99)	*Lachnospirales* (99)	*Lachnospiraceae* (99)	*Lachnospiraceae*_unclassified (99)
OTU_40	*Actinobacteriota* (100)	*Actinobacteria* (100)	*Micrococcales* (98)	*Bogoriellaceae* (88)	*Georgenia* (88)
OTU_43	*Firmicutes* (100)	*Clostridia* (100)	*Lachnospirales* (100)	*Lachnospiraceae* (100)	*Lachnospiraceae*_unclassified (100)
OTU_44	*Patescibacteria* (100)	*ABY1* (100)	*Candidatus*_Falkowbacteria (100)	*Candidatus*_Falkowbacteria_fa (100)	*Candidatus*_Falkowbacteria_ge (100)

OTU_45	*Bacteroidota* (100)	*Bacteroidia* (100)	*Bacteroidales* (100)	*Dysgonomonadaceae* (100)	*Dysgonomonadaceae*_unclassified (100)
OTU_46	*Firmicutes* (100)	*Limnochordia* (100)	uncultured (100)	uncultured_fa (100)	uncultured_ge (100)
OTU_47	*Firmicutes* (100)	*Clostridia* (100)	*Peptostreptococcales-Tissierellales* (100)	*Peptostreptococcales-Tissierellales*_fa (100)	*Peptostreptococcales-Tissierellales*_fa_unclassified (100)
OTU_5	*Bacteroidota* (100)	*Bacteroidia* (100)	*Bacteroidales* (100)	*Dysgonomonadaceae* (100)	*Proteiniphilum* (100)
OTU_52	*Firmicutes* (100)	*Clostridia* (97)	*Lachnospirales* (97)	*Defluviitaleaceae* (88)	*Defluviitalea* (88)
OTU_53	*Firmicutes* (100)	*Clostridia* (100)	*Peptostreptococcales-Tissierellales* (100)	*Sedimentibacteraceae* (100)	*Sedimentibacter* (100)
OTU_576	*Firmicutes* (99)	*Clostridia* (99)	*Lachnospirales* (99)	*Lachnospiraceae* (99)	*Lachnospiraceae*_unclassified (99)
OTU_58	*Firmicutes* (100)	*Clostridia* (100)	*Clostridia*_or (97)	*Hungateiclostridiaceae* (97)	*Hungateiclostridiaceae*_unclassified (97)
OTU_6	*Firmicutes* (100)	*Limnochordia* (92)	*M55-D21* (84)	*M55-D21*_fa (84)	*M55-D21*_ge (84)
OTU_7	*Bacteroidota* (100)	*Bacteroidia* (100)	*Bacteroidales* (100)	*Dysgonomonadaceae* (100)	*Fermentimonas* (100)
OTU_760	*Firmicutes* (100)	*Limnochordia* (100)	*MBA03* (98)	*MBA03*_fa (98)	*MBA03*_ge (98)
OTU_8	*Chloroflexi* (100)	*Anaerolineae* (100)	*Anaerolineales* (100)	*Anaerolineaceae* (100)	uncultured (100)
OTU_83	*Firmicutes* (100)	*Clostridia* (100)	*Peptostreptococcales-Tissierellales* (100)	*Peptostreptococcales-Tissierellales*_fa (100)	*Tepidimicrobium* (99)

OTU_97	*Firmicutes* (100)	*Clostridia* (99)	*Caldicoprobacterales* (95)	*Caldicoprobacteraceae* (95)	*Caldicoprobacter* (95)

Table Ch6_S2 (Additional file 2 – Table S1: Relative abundance (%) and taxonomic affiliation according to Silva 138 database of 16S rRNA gene amplicon sequencing OTUs for bacteria) and **Table Ch6_S3** (Additional file 2 – Table S2: Relative abundance (%) and taxonomic affiliation according to Silva 138 database of 16S rRNA gene amplicon sequencing OTUs for bacteria) are available in an excel file by following this link:

https://link.springer.com/article/10.1186/s13068-023-02438-5

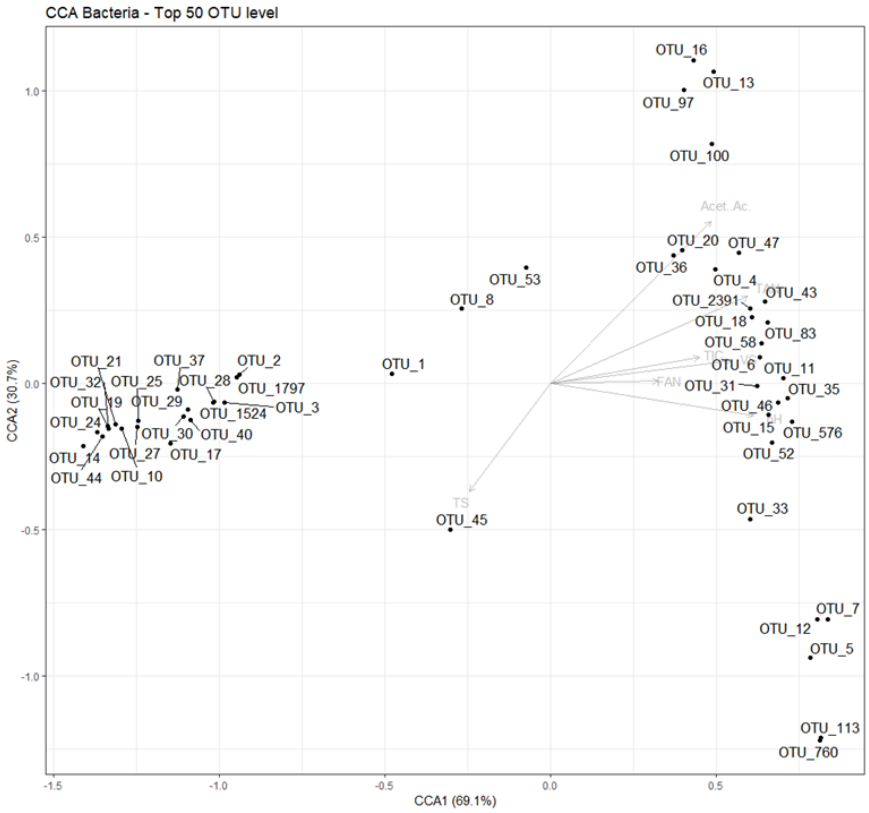

Figure Ch6_S 1. Canonical correspondence analysis (CCA) ordination diplot for the top 50 more abundant bacterial OTUs. Data from all the studied reactors (the LNR and the three HNRs, 12 time points for each of them) were used for this analysis. Light grey vectors represent process parameters influencing the microbial community such as the pH (pH), volatile solids (VS), total solids (TS), total ammonia nitrogen (TAN), free ammonia nitrogen (FAN), acetic acid concentration (Acet. Ac.), total inorganic carbon (TIC).

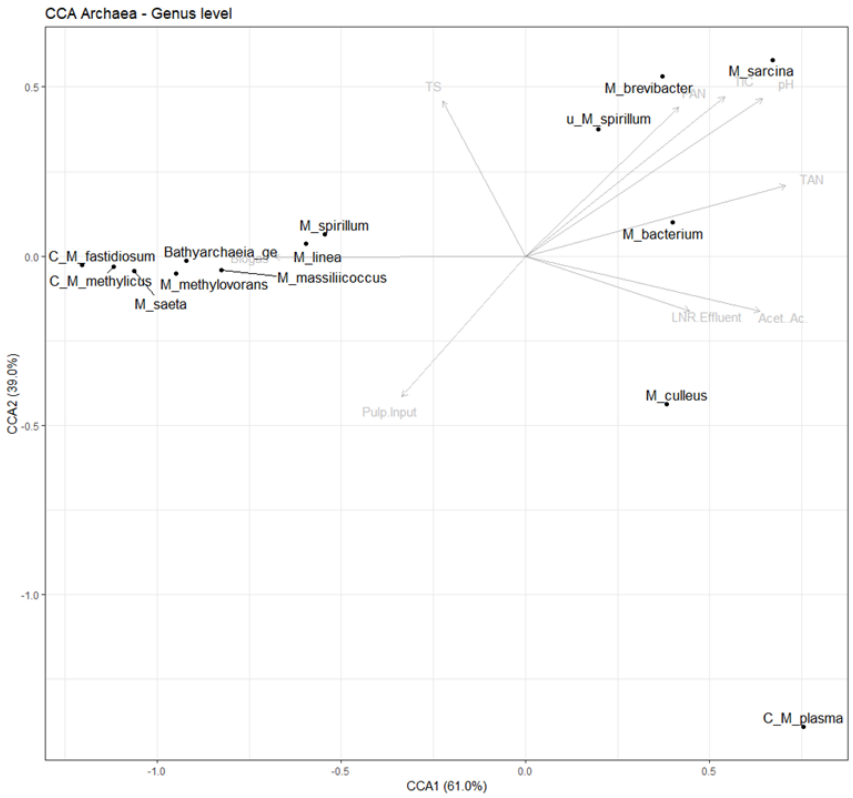

Figure Ch6_S 2. Canonical correspondence analysis (CCA) ordination diplot for the archaeal genera. Data from all the studied reactors (the LNR and the three HNRs, 12 time points for each of them) were used for this analysis. Light grey vectors represent process parameters influencing the microbial community such as the pH (pH), total solids (TS), total ammonia nitrogen (TAN), free ammonia nitrogen (FAN), total inorganic carbon (TIC), the recirculated low nitrogen reactor effluents (LNR Effluent), the sugar beet pulp organic loading rate (Pulp. Input), acetic acid concentration (Acet. Ac.), produced biogas volume (biogas).